Development of a Radiopharmaceutical Carrier for PET Lung Perfusion Studies

Sarwar Shabnam

THESE DE DOCTORAT DE

L'UNIVERSITE D'ANGERS, FRANCE

COMUE UNIVERSITE BRETAGNE LOIRE

ET DE

L'UNIVERSITE DE LIEGE, BELGIUM

ECOLE DOCTORALE N° 605
Biologie Santé
Spécialité : «*Sciences Pharmaceutiques*»

ECOLE DOCTORALE
Département De Médecine
«*Biomedical and pharmaceutical sciences*»

Par

Shabnam Sarwar

Development of a Radiopharmaceutical Carrier for PET Lung Perfusion Studies

Thèse présentée et soutenue à « " Université D'Angers" Angers 49100», le « 21/10/2020 »

Unité de recherche : CRCINA, Inserm UMR_S 1232, CRCINA, IRIS-CHU, 4 rue Larrey, Angers 49100, France

GIGA et Département De Médecine, CHU-De- Liège, 4000, Liège, Belgium

Thèse N° :

Rapporteurs avant soutenance:

Benjamin GUILLET	Dir. CERIMED, Univ Aix Marseille, Chef du APHM Et C2VN U1063, INSERM, INRA, Marseille, France
Isabelle QUELVEN-BERTIN	MCU-PH, Université Paul Sabatier, PUI - UF PHARE – CHU de Toulouse, Toulouse, France

Composition du Jury:

Nicolas NOIRET	Prof. Ecole Nationale Superieure de Chimie de Rennes, Dir. des relations Industrielles, Rennes, France
Benjamin GUILLET	Dir. CERIMED, Univ Aix Marseille, Chef du APHM Et C2VN U1063, INSERM, INRA, Marseille, France
Isabelle QUELVEN-BERTIN	MCU-PH, Université Paul Sabatier, PUI - UF PHARE – CHU de Toulouse, Toulouse, France
Emmanuel GARCION	Directeur d'équipe Inserm UMR_S 1232 (DR), Angers 49100 France
François HINDRÉ **(Directeur de thèse)**	AP. Université Angers, MCU CHU-d'Angers, Angers 49100, France
Franck LACOEUILLE **(Co-Directeur de thèse)**	AP. Et MCU-PH, Chef du Nucléaire Médicine Département CHU-d'Angers, Angers, 49100, France

Directeur & Co-Directeur de thèse:

Roland HUSTINX **(**Directeur de thèse)	Prof. ULG**,** Chef du Médecine Nucléaire et d'Imagerie Oncologique, CHU-De-Liège, Liège 4000, Belgium
Nadia WITHOFS (Co-Directeur de thèse)	MD PhD, Médecine Nucléaire et d'Imagerie Oncologique, CHU-De-Liège, Liège 4000, Belgium

RÉSUMÉ

La scintigraphie de ventilation/perfusion pulmonaire (V/Q), par le biais de la tomographie par émission monophotonique (TEMP/CT) et des macroagrégats d'albumine (MAA) marqués au ^{99m}Tc (^{99m}Tc-MAA) comme agent de perfusion pulmonaire, est toujours considérée comme une modalité d'imagerie de choix pour le diagnostic de l'embolie pulmonaire. Cependant, la technique TEMP/TDM présente certaines limites, comme une résolution spatiale ou une sensibilité plus faible que la tomographie par émission de positons (TEP/TDM). Avec la disponibilité récente des générateurs ^{68}Ge/^{68}Ga et le développement de produits radiopharmaceutiques marqués au ^{68}Ga qui peuvent être produits sur place et à la demande, la TEP/TDM V/Q semble désormais réalisable. Ainsi, différents groupes ont mis au point des procédures de radiomarquage des MAA pour substituer le ^{99m}Tc par du ^{68}Ga et réalisent avec succès des études de perfusion pulmonaire par TEP/CT. Cependant, les MAA, comme d'autres dérivés sanguins, comporte un risque théorique de transmission d'agents pathogènes infectieux. Pour relever ce défi, notre équipe a mis au point, il y a quelques années, un nouveau vecteur microparticulaire, d'origine végétale, sans albumine, capable de former des complexes stables avec les radiométaux pour des applications de médecine nucléaire (notamment la scintigraphie de perfusion pulmonaire). Ces microparticules à base d'amidon (SBMP) présentent des caractéristiques favorables telles qu'une taille de particule appropriée, une disponibilité sous forme de kits lyophilisés et un radiomarquage facile avec divers isotopes tels que le ^{99m}Tc, ^{68}Ga ou ^{188}Re.

Sur la base de ces résultats prometteurs, l'objectif du présent travail était d'évaluer, pour la première fois, la performance des microparticules 68Ga-SBMP comme radiopharmaceutique pour des études de TEP de perfusion pulmonaire. À cette fin, un radiomarquage, des études précliniques en TEP/CT et une estimation dosimétrique basée sur l'imagerie après injection intraveineuse de ^{68}Ga-SBMP ont été réalisés. Le ^{68}Ga étiqueté SBMP a été développé à température ambiante par la méthode simple et robuste sans conditions qui impliquent de sévères réactions produisant une pureté radiochimique très élevée (>99%) après 10 minutes d'incubation à température ambiante avec l'éluat gallium-68 ($^{68}GaCl_3$). Le radiopharmaceutique présenté visualisait clairement la zone pulmonaire et générait des images affinées de la vascularisation pulmonaire en peu de temps. Les estimations de dosimétrie basées sur l'image ont montré pour l'homme des valeurs plus faibles que la norme disponible de ^{99m}Tc-MAA (ICRP 80). D'autres études cliniques sont recommandées pour évaluer le potentiel de ^{68}Ga-SBMP dans les cliniques humaines

mots-clés: Microparticules à base d'amidon (SBMP), Gallium-68 (^{68}Ga), Perfusion pulmonaire, PET/CT, Dosimétrie

ABSTRACT

The lungs ventilation/perfusion (V/Q) scintigraphy, by the mean of Single Photon Emission Computed Tomography (SPECT/CT) and macroaggregates of albumin (MAA) labelled with ^{99m}Tc (^{99m}Tc-MAA) as lung perfusion agent, is still considered as an imaging modality of choice for the diagnosis of pulmonary embolism. However, SPECT/CT technique has some limitations such as lower spatial resolution or poor sensitivity compared to Positron Emission Tomography (PET/CT). With the recent availability of ^{68}Ge/^{68}Ga generator and the development of ^{68}Ga-labeled radiopharmaceuticals that can be produced on site and on demand, V/Q PET/CT appears now feasible. Thus, different groups have developed radiolabeling procedures of MAA with ^{68}Ga instead of ^{99m}Tc and successfully perform PET/CT lung perfusion studies. However, MAA, like other blood-derivatives, carries a theoretical risk of disease transmission. To address this challenge, few years ago, our team has developed a new microparticulate albumin-free carrier from vegetal origin, able to form complex with radiometals for nuclear medicine applications and especially for lung perfusion scintigraphy. These starch-based microparticles (SBMP) exhibit favorable characteristics such as suitable particle size, availability as freeze-dried kits and easy radiolabeling with various isotopes such as ^{99m}Tc, ^{68}Ga or ^{188}Re.

Based on those promising results, the objective of the present work was to evaluate, for the first time, the performance of the ^{68}Ga-SBMP microparticles as radiotracer for lung perfusion PET studies. To this end, radiolabeling, preclinical PET/CT studies and imaging-based dosimetry estimation following intravenous injection of ^{68}Ga-SBMP were realized. The ^{68}Ga labeled SBM has been developed at room temperature through simple, and robust method without the involvement of any severe reaction conditions producing very high radiochemical purity (>99%) after 10 minutes of room temperature incubation with gallium-68 eluate ($^{68}GaCl_3$). The presented radiopharmaceutical visualized the lungs fields clearly and generated fine-tuned images of pulmonary vasculature in a small time. Image based dosimetry estimates for humans indicated lower values than the available standard of ^{99m}Tc-MAA (ICRP 80). Further clinical studies are recommended to assess the potential of ^{68}Ga-SBMP in human clinics.

keywords: Starch based microparticles (SBMP), Gallium-68 (^{68}Ga), Lung Perfusion, PET/CT, Dosimetry

Acknowledgements

In the name of Allah the most beneficent and merciful and countless darood on his prophets (PBUH). The work presented here is an achievement of my family especially Ahsan Bilal, friends, coworkers and mentors whose vast, selfless support kept my hand steady in the most difficult times. No words can fully express the gratitude I feel towards this amazing group of people that I am proud to call my own.

I would like to express my sincere gratitude to my directors, Prof. Roland HUSTINX (Head of the Division of Nuclear Medicine and oncological Imaging; Department of Medical physics CHU of Liege, Belgium, Dr. François HINDRE (Associate Professor, University of Angers, France) and co-directors Dr. Franck LACOEUILLE (Assistant professor (MCU-PH) in nuclear medicine and biophysics, Head of NMD CHU Angers France) and Dr. Nadia WITHOFS (MD PhD Division of Nuclear Medicine and oncological Imaging; Department of Medical physics CHU of Liege, Belgium for their continuous support for my PhD study and related research, their motivation and immense knowledge. Their guidance helped me in all the time of research and writing of thesis.

Besides my advisors I would like to thank Prof. Frank Boury, as the coordinator of the European Doctorate in Nanomedicine and Pharmaceutical Innovation (NanoFar) that made possible the realization of this PhD research.

My sincere gratitude to Noiret NICOLAS, Prof Ecole Nationale Superieure de chimie de Rennes, Rennes and Benjamin GUILLET, Chef du NMD CHU-de Marseille, Prof. Aix Marseille University, (AMU), Head of radiopharmacy department, CHU de la Timone, Marseille and Quelven ISABELLE, MCU-PH University Paul Sabatier, Toulouse for giving me the honor of being reviewers for this PhD; and Prof. Emmanuel GARCION (Director of Research at Inserm, Angers, France) for the time dedicated to evaluate and examine this work.

Acknowledgements

Special thanks, humble appreciation to Francis BOUCHET for his extremely valuable PET/CT technical support, dosimetry, IMALYTICS and a kind attitude.

During the last years, I was fortunate to work in two different countries and two different laboratories. I am grateful to Luc DUWEZ, GIGA Technicien de recherché, Animal Facility of the University of Liege and Clément TETAUD, CRCINA-Technicien de recherché, GLIAD team, CHU d' Angers for their invaluable experience in the laboratory and help during the animal experimentation.

I would also like to thank Claire BERNARD and Geneviève MEFFRE Division of Nuclear Medicine and oncological Imaging; Department of Medical physics CHU of Liege, Belgium for their very important radioprotection training and technical support, during the preparation of radiopharmaceutical and in vivo work.

At the end I like to express deep appreciation again to my supervisor Franck LACOEUILLE for the opportunity to work with his team and benefit from their knowledge, experience and leadership. Their persistent confidence in me, along with the support in all professional and personal affairs, made all the difference.

Last but not the least many thanks to Marion TOUCHETEAU (responsible for Erasmus Mundus and communication at the University of Angers), Nicole LOTODE (registration department at University of Angers), Mylene DEFENGE (CHU-De-Liege) for their valuable help with the administrative procedures, during this joint PhD program, both in France and Belgium. I would like to thank all of my colleagues, especially Bilal LATIF, Rana MUHAMMAD GULFAM, Jérémie ZAPPIA, and Ouassim MEDHIOUB who in one way or another helped me during this PhD. This brief acknowledgement is not enough to thank all of them. Thank you for making these last four years such a memorable time.

Dedicated to my great parents, Mufti Muhammad Irfan

Ahsan Bilal and my beautiful kids!

Table of Contents

List of Figures

List of Tables

Abbreviations and Acronyms

CHSg	Chitosan Glycol
CI-AKI	Contrast induced acute kidney injury
CIN	Contrast induced nephropathy
CKD	Chronic kidney disease
CT	Computed tomography
CTPA	Computed tomography pulmonary embolism
COPD	Chronic obstruction pulmonary disease
DC	Decay Corrected
DC-ID/organ	Decay Corrected Injected Dose per organ
DOTA	1,4,7,10-tetraazacyclododecane-1,4,7,10-tetraaceticacid
DP	Deflector plate
DTPA	Diethylene triamine pentaacetic acid
EANM	European Association of Nuclear Medicine
ESC	European Society of Cardiology
ECG	Electrocardiographic
ECM	Extracellular sub-endothelial Matrix
EDE	Efficient dose equivalent
EDTA	Ethylene diamine tetra acetic acid
FDA	U.S. Food and Drug Administration
FDG	[18F] fluoro-2-deoxy-2-glucose
Gp	Glycoprotein
HAM	Human Albumin Microspheres
HAS	High Authority of Health
HSA	Human Serum of Albumin
^{123}I,^{125}I, ^{131}I	Iodine-123, Iodine-125, Iodine-131
IA (%)	percentage of injected activity
ICRP	International commission radiological protection
ID (%)	Percent injected Dose
IV	Intravenous

LEHR	Lower energy high resolution
LLS	Liver lung shunt
LMWH	Low molecular weight Heparin
LV	Left ventricle
MAA	Macroaggregates of Albumin
mCT	Micro Computes Tomography
MIRD	Medical internal radiation dose
MMAD	Mass median aerodynamic diameter
MRI	Magnetic resonance imaging
NIRF	Near Infra-red fluorescence
NOTA	1.4.7-triazacyclononane-1.4.7-triaceticacid
PAH	Pulmonary arterial hypertension
PAP	Pulmonary artery pressure
PE	Pulmonary embolism
PECAN	Diagnosing Pulmonary Embolism in the context of Common Alternative diagnoses in Primary care
PEG-PLGA	Methoxy polytheylne glycol PLGA
PERC	Pulmonary embolism rule out parameters
PET	Positron Emission Tomography
PET/CT	Positron Emission Tomography with low dose of CT
PFH	Perflurohexane
PGCD	poly (glycerol-citric-dodecanedioate)
PIOPED	Prospective Investigation of Pulmonary Embolism Diagnosis Study
PLA	Poly lactic acid microparticles
PLGA	Ploy Lactic glycolic acid
p-SCN-Bn-NOTA	S-2-(4-Isothiocyanatobenzyl)-1,4,7-triazacyclononane-1,4,7-triacetic acid
rHSA	Recombinant Human Serum of Albumin
rMAA	Recombinant macroaggregates of albumin
ROI	Region of interest
rt-PA	Recombinant tissue plasminogen activator
RV	Right ventricle
SBMP	Starch Based Microparticles

SD	Standard deviation
SPECT	Single Photon Computed Tomography
SPECT/CT	Single Photon Computed Tomography with low dose of CT
SUV	Standardized uptake value
TAC	Time activity curve
UFH	Unfractionated Heparin
US	Ultrasonography
VD	Volume of Distribution
VOI	Volume of interest
vWF	Von Willebrand factor
WHO	World Health Organization
WRIGHT	WHO research into global hazard of travel
Wt	Weighting factor

SECTION-I

Management of Pulmonary Embolism

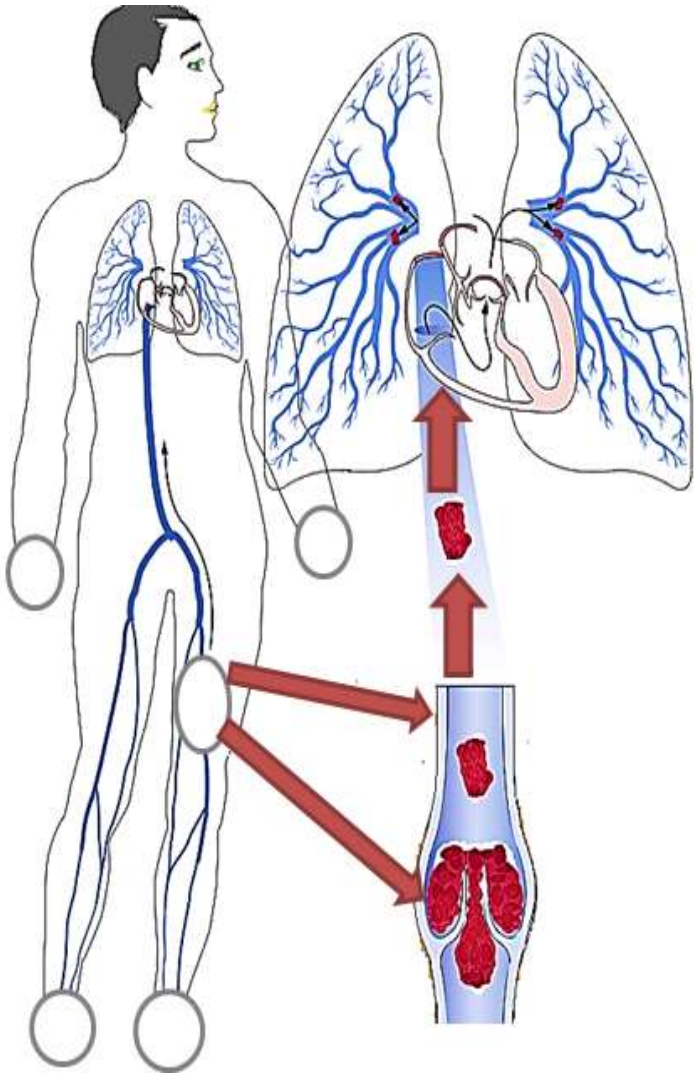

1. General Introduction

This dissertation is addressing the radio-synthesis of ^{68}Ga- labeled starch based microparticles, a new radiopharmaceutical and then characterization of the starch based microparticles for their size and formulation for radiochemical purity (RCP), *in-vitro* stability, lung perfusion scanning, biodistribution and pharmacokinetics in healthy rats, and dosimetry estimation for human organs. The radiotracer is developed from biodegradable, biosynthetic polymer fabricated from starch microparticles hence called starch based microparticulate system (SBMP).

Pulmonary embolism (PE) is a life-threatening disease which is a clinical and medical challenge. Accurate diagnosis is needed in all patients with suspected PE, although anticoagulant therapy is successful; but it is costly and correlated with the risk of bleeding. Despite all the progress in the field of medical imaging and nuclear medicine in particular, the diagnosis of pulmonary embolism is still challenging therefore accurate and robust diagnostic paradigms are important. Computed tomography PA (CTPA), and ventilation perfusion scintigraphy (V/Q) using single photon emission computed tomography with or without CT (SPECT or SPECT/CT) are playing a good role in the diagnosis of PE and especially SPECT in patients showing contraindication such as pregnant females and renal failure patients. V/Q imaging requires the injection of radiopharmaceutical based on microparticles, and ^{99m}Tc labeled macroaggregates of albumin (MAA) are considered as the gold standard in this field. Since MAA is derived from human serum albumin (HSA) and carry's a risk of potential diseases transfer. To address this issues of commercially available radiopharmaceuticals (^{99m}Tc-MAA, ^{99m}Tc-HSA microspheres), a variety of microparticulate systems are developed, radiolabeled, and evaluated for lung perfusion scintigraphy in animal models. Yet no particulate system is succeeded in the human clinic hence MAA successor is still anticipated. In this scenario our group has introduced starch based

microparticulate system (SBMB), labeled with ^{99m}Tc and evaluated for the successful diagnosis of pulmonary embolism in artificially embolized lungs of rats. Keeping in mind the promising results of ^{99m}Tc-labeled starch based microparticles (SBMP), and to utilize the superior and robust imaging through an emerging imaging modality for ventilation perfusion scintigraphy i.e. positron emission tomography (PET/CT), have led us to propose ^{68}Gallium labeled starch based microparticles: a new radiopharmaceutical.

Thesis is organized according to the following structure. 1st chapter is about the introduction of the dissertation which includes five subsections, (1.1) nuclear medical imaging; (1.2) pulmonary embolism; (1.3) imaging modalities used for PE diagnosis; (1.4) History of radiopharmaceuticals developed for pulmonary embolism diagnosis, concluding remarks, our project glimpses and lastly objectives of this research will close the introduction.

2ndchapter explains the experimental work. This chapter includes the development of radiopharmaceutical, and its *in-vitro* and *in-vivo* evaluation and lung perfusion studies in rats.

3rd chapter includes the general discussion on the experimental results, 4th chapter includes important conclusions derived from the experimental work, future perspectives, funding source and acknowledgement, lastly 5th chapter includes bibliography and annex.

1.1 Nuclear Medical Imaging

There are three basic nuclear medical imaging techniques: i) planar scintigraphy, ii) single photon emission computed tomography (SPECT), iii) positron emission tomography (PET). These modalities can be characterized as functional medical imaging techniques. They work in close proximity with anatomical imaging techniques (CT and NMR). The current thesis is focused on functional imaging combined with anatomical imaging because of their importance of attenuation correction and purpose of anatomical registration.

1.1.1 Planar Scintigraphy

The term radiotracer was devised by George de Hevesy in 1920. The radiotracer is injected in a small quantity to see the internal system without any disturbance. The first camera for nuclear imaging was designed by Hal Anger 1957 called Scintigraphy Camera (Figure 1). It is composed of sodium iodide crystal activated with thallium NaI (Tl). For the detection and amplification a number of photomultipliers are present. Crystal thickness varies from 6mm to 25 mm and optimum size of 10 mm to detect gamma energy of 120-200 keV collimator is present at the scintillation crystal front in order to permit near perpendicular or perpendicular photons for striking on the crystal. Gamma quantum interaction with crystal causes excitation following light emission. The light interaction with photocathode releasing electrons, that later amplifies in photomultipliers. In the crystal, only perpendicular rays are permitted to pass, so the amplification and emission locations are aligned in patients. All intensities and coordinates form a planar image.

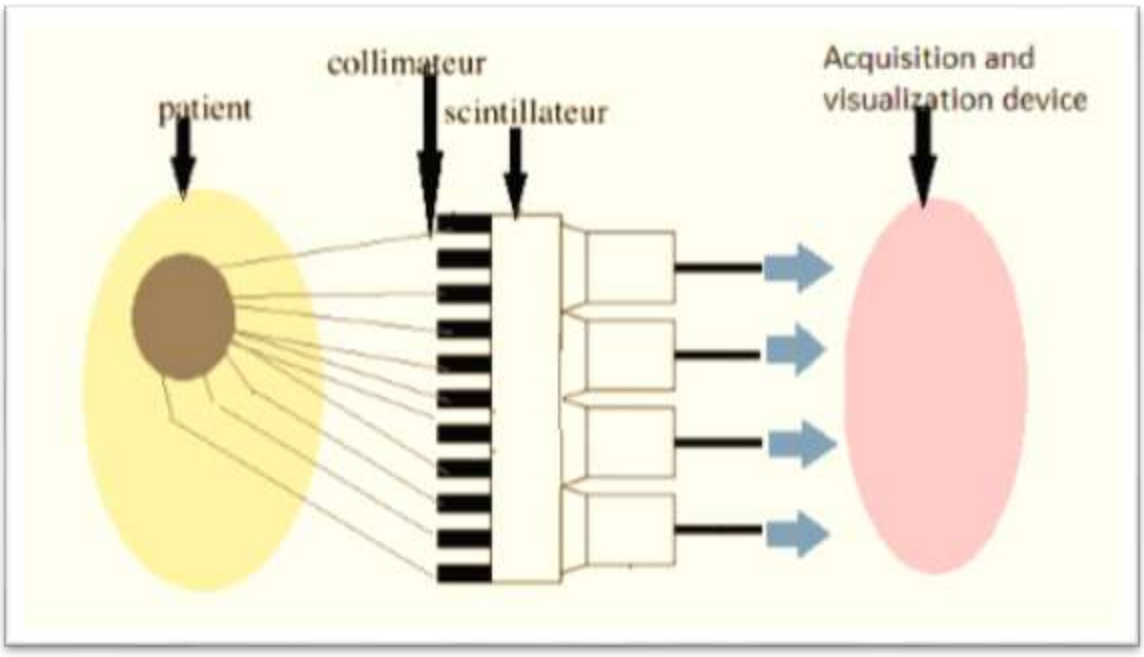

Figure 1 Constitution of Angers Camera

1.1.2 Single Photon Emission Tomography (SPECT)

An application of the Anger camera is called Single Photon Emission Tomography (SPECT). It is used to acquire 3D (three dimensional) images of radioisotopes.

Gamma photons are indirect ionizing radiations; they use three different way to interact with matter: i) Compton Effect ii) Photoelectric effect, iii) production of electronic pairs or simply pass through matter completely without interacting. The challenge of imaging used in nuclear medicine is to detect the photons emitted that do not interact with the material after injection of a radioactive tracer.

A gamma camera consists of a photomultiplier, a scintillator and a collimator. Different collimators come in different geometry (parallel, fan-shaped, conical channels) and with different sizes of septa and different holes. It allows selecting the direction of the incident

photons. After passing this first obstacle, each photon will interact with the scintillator in order to convert the radiation into a light signal. In theory, the number of photons emitted is proportional to the energy of the incident photon. The crystal (scintillator) is coupled to a photomultiplier in order to amplify the signal which will be collected by a photo detector. The signals are then processed to build an image.

Single Photon Emission CT (SPECT) cameras in clinics are constituted of dual planar camera head which can rotate on an axis around the patient to attain different projections to reconstruct an image. Each head works independently of the others and is identical to those used in scintigraphy. The contribution of the SPECT is the acquisition in 3 dimensions, thanks to the rotating system of the cameras. Image acquisition techniques associated with powerful computer tools have enabled scintigraphy (2-dimensional planar image) to evolve towards 3-dimensional tomographic images. SPECT Attenuation effects are severe and not uniform through the body, thus attenuation correction is the major limitation of the SPECT, therefore tracer quantification is difficult. Many approaches are taken to improve this defect and also got some success.

^{153}Gd (Gadolinium-153) source is used sometimes for transmission generation, or CT scans combined for correction. However SPECT is an excellent diagnostic technique in medical imaging study. A gamma camera present in the Nuclear Medicine Department is presented in (Figure 2).

Figure 2 Gamma Camera Present In the Nuclear Medicine Department Of CHU-De-Angers, France

1.1.3 Positron Emission Tomography (PET)

PET is a technique of medical imaging which is based on the annihilation of positron rather on the emission of positron (as indicated by name). As illustrated in (Figure 10), positron travels a distance prior to annihilation, which is directly proportional to beta disintegration energy. The two photons are emitted simultaneously in opposite directions (180° apart) and identified by opposite detectors that are arranged circularly in coincidence mode. Photons detection is registered and the intercepted with the detected path and imaged. PET detectors should be thick as compared to SPECT. Energy of annihilation is 511 keV while SPECT regular energy is 100-200 keV and hence detectors need great stop power. PET composed of crystals are fabricated from Lutetium oxy ortho silicate (LSO) with Cerium-dopping, Bismuth Germanate: $Bi_4Ge_3O_{12}$

and Bismuth Germanium Oxide: BGO. These crystals pssess good output of light as well as >80 percent time constant which is quite less compared to NaI (Tl) of 511 keV energy. Camera resolution has been increasing with time starting from spatial resolution of 10 mm to 4 mm and then 1.2 mm in micro-PET. Positron is limiting the theoretical spatial resolution whereas collimator design is limiting the spatial resolution. Therefore a proper nuclide should be elected to develop a drug. The imaging technique requires the injection of a β^+ positron emitting radiotracer. it accumulates in the region of interest inside the body, that helps to highlight the cellular metabolism of an organ or tissue, cell proliferation, or binding to specific receptors, enzymes or antibody to provide physiopathological and kinetic data. Detectors arranged in a ring all around the patient allow the detection of the photons emitted in coincidence, thereby determining the location of the site of annihilation and hence accumulation of the radiotracer in the organs. PET is based on the principle of coincidence detection. Computer system utilizes a mathematical algorithm that allows the reconstruction of the radiotracer distribution imaging. Indeed, by dispensing with the use of the mechanical collimator, a lower dose of radioactive vector molecules is more than sufficient to obtain an image of equivalent quality as compared to SPECT. PET technique also allows accurate dosimetric calculations and has been used for quantitative measurements since decades. A PET instrument is presented in Figure 3 located at CHU-Angers, France.

1.1.4 Multimodal Imaging (SPECT/CT & PET/CT)

The combination of different imaging techniques or modalities is called multimodal imaging. This allows detection using different imaging modalities through one labeling agent or a combination of various labeling agents [1]. Complementary information is collected from a single experiment using multimodal imaging. Hence, it allows taking the advantages of

technique's precise strengths, avoiding specific disadvantages, and consequently improving single diagnostic techniques [1, 2]. As an example to compensate the lack of anatomical information compared to other conventional imaging techniques (radiology, scanner, etc.), PET and SPECT have been coupled with X-ray scanners (CT), called a hybrid technique SPECT/CT and PET/CT to take the advantage of SPECT or PET and CT in a single experiment. A computer reconstruction will result in the fusion of the two images thus allowing the improvement of the anatomical localization.

Figure 3 Positron Emission Tomography Camera Present In Nuclear Medicine Department Of CHU-De Angers

1.1.5 Radioisotope Production

For the production of radioisotopes, there are two basic types of installations: nuclear reactor and particle accelerators.

1.1.5.1 Nuclear Reactor Produced Radioisotopes

Neutron rich radioisotopes are produced through nuclear reactor either by the process of neutron irradiation or fission of heavier nuclides that decays by electron emission (β^-) and excluding few exceptions. It is associated with nuclear medicine requires as β^- emitters are utilized for gamma emitting radionuclides for SPECT (^{99}Mo/^{99m}Tc) and therapy (^{131}I). Fission is not a desirable fabrication method, because radiochemical separation of both long and short-lived isotopes is lengthy process and producing low purity. In comparison neutron irradiation is a superior method nevertheless high neutron is required for sufficient yield of radioisotope. This method involves two types of fabrications using thermal neutrons and higher energy neutrons. Alternatives are under research to fill the gap and new production reactors especially for ^{99}Mo are studied.

1.1.5.2 Cyclotron Produced Radioisotopes

The beam of charged particles is accelerated by a cyclotron via alternating high-frequency voltage transmitted among two "D" shaped hollow metal sheet electrodes labeled "Dees" inside the vacuum chamber. A cylindrical gap among the two face to face positioned Dees, to pass particles through them. Then particles are injected in the provided space. The particles path is bended in a circle under the influence of magnetic field due to the Lorentz force which is acting perpendicular to the direction of particles motion. It comprises of two Dees, called D1 and D2, encased in an evacuated chamber. The Dees are kept isolated, and in the middle of the distance between the Dees ion source is placed. They are located between the poles of a powerful

electromagnet. High frequency oscillator is connected to Dees and magnetic field acts opposite to their planes. The phenomenon includes the release of a positive ion of charge q, mass m; it is accelerated to Dees bearing negative potential. The polarity of the Dees is inverted as long as the ion enters the distance between the Dees. Thus the beam is propelled again and travels with a greater speed in a larger diameter ring into the other Dee. It implies that the particle travels in the stream of a growing diameter, which is withdrawn using a deflector plate (D. P.) when it gets close to the edge. The high-energy particle can now hit the target. Basic structure of a cyclotron is shown in Figure 4.

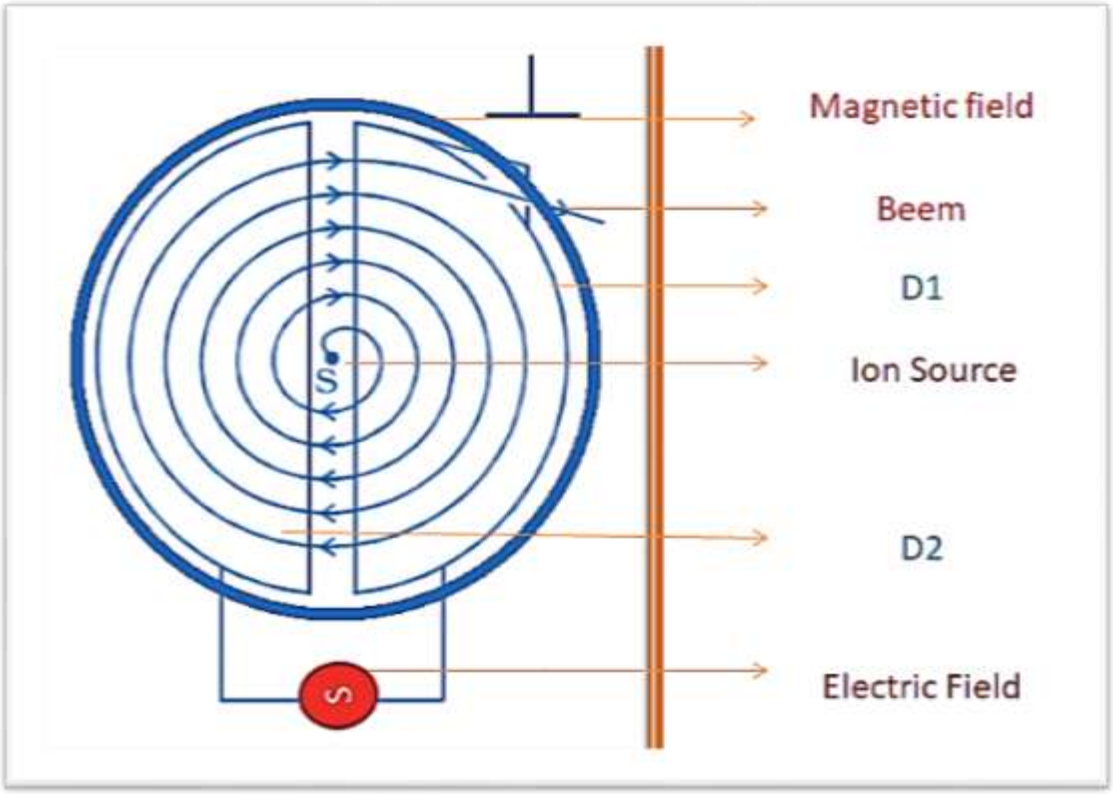

Figure 4 Basic structure of a cyclotron

After the advent of PET camera, positron emitters were required such as ^{11}C, ^{18}F, ^{13}N, ^{15}O. Conversely, unlike to β^-emitters' radioisotopes, these are neutron deficient isotopes. Hence

cannot be produced through neutron sources or nuclear reactors. As positron emitter radionuclide depends only upon the incident beam energy and initial target, and contrasted to nuclear reactor which could not be stopped and keep on generating the nuclear waste till finishing of fuel, but cyclotron can be stopped. A cyclotron Arronax to produce medical research isotopes is presented in Figure 5.

Figure 5 Cyclotron Arronax in Nantes dedicated to the production of radioisotopes for medical research

Example of fluorine-18 production through ^{18}F, ^{18}O (p, n) reaction as given in eq.1

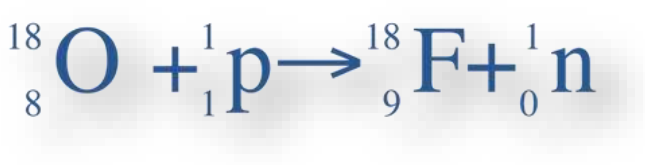

Equation 1

1.1.5.3 Radio Isotopic Generators

A generator of radionuclide fabrication is based on radiochemical separation scheme in which a parent and daughter nuclide is reached to equilibrium. It followed Rutherford and Soddy laws of exponential disintegration and accumulation. The quantity parent radionuclide should be as a minimum of 10 fold larger than daughter radionuclide half-life. As well the system must be effective for the high quality separation between daughter nuclide and parent nuclide along with high radionuclide and radiochemical purity.

1.1.5.3.1 Physics of Radioisotope Generators

Radioisotope generator life depends mainly on the parent nuclide half-life. Although, additional factors also affecting half-life of the system, such as radiochemical, chemical, and radionuclide purity of elution, as well as radiolytic damage to the material. Equilibrium of the decay of parent nuclide (^{99}Mo) is nearly stable as compared to daughter (^{99m}Tc) nuclide activity and apparently observed accumulation (Figure 6). An example of the ^{99}Mo/^{99m}Tc generator disintegration scheme is given eq. 2.

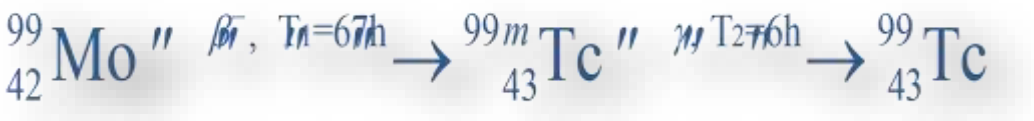

Equation 2

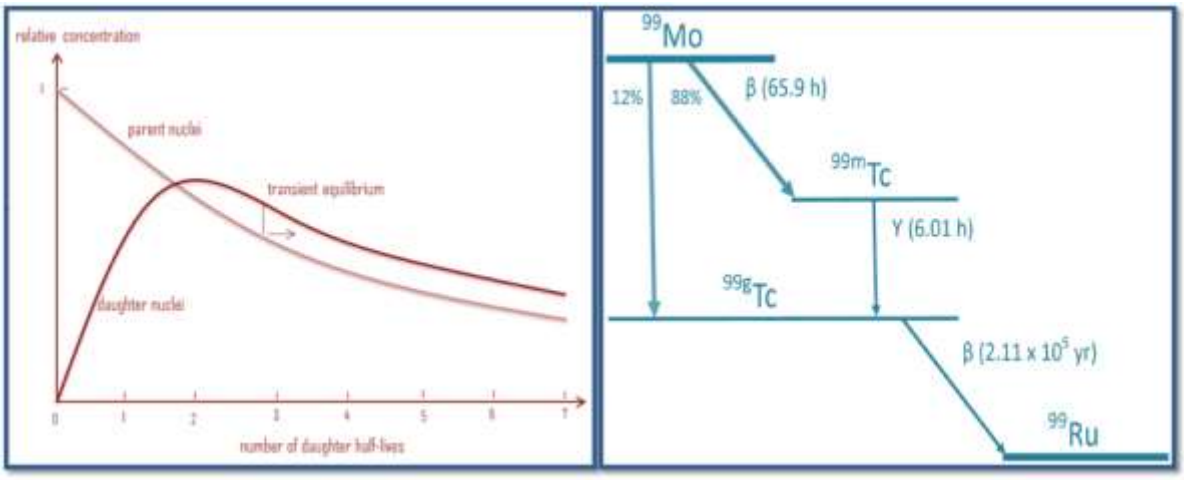

Figure 6 Production of daughter nuclide (^{99m}Tc) from parent nuclide (^{99}Mo) and equilibrium between them

An effective separation of the radionuclide is required as it allows the use of daughter nuclide and parent nuclide preservation to auxiliary production ofdaughter cells. Additionally, generator system should be reliable, simple and usage friendly. ^{99}Mo/^{99m}Tc generator is shown in shown Figure 7.

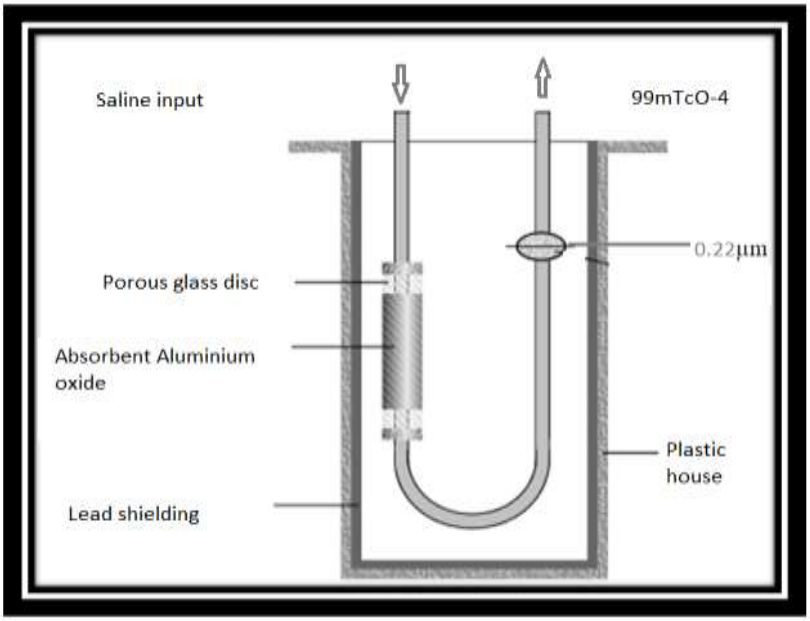

Figure 7 Schematics of the ^{99}Mo/^{99m}Tc generator's chromatographic column

Initial approach for separation was liquid-liquid extraction and still used such as $^{72}Se/^{72}As$. Long time of manipulation resulting high radiation exposure is not desirable. The column material should show high specificity for parent nuclide while very low attraction for daughter nuclide.

Column elution would yield the pure daughter solution ready for applications. To minimize a radiolytic effect, column material should be preferably inorganic origin. For $^{68}Ge/^{68}Ga$ generators, the inorganic matrices in use are TiO_2, SnO_2, α-Fe_2O_3, and Al_2O_3. Organic resins are also under observation as it has no metallic impurities. Different commercial generators are available in France for example Eckert and Ziegler's (TiO_2), and iThemba Labs's (SnO_2), former is FDA approved and showing best results. Later is cheap but possess high HCl content in eluate. $^{68}Ge/^{68}Ga$ generators Eckert & Ziegler IGG 100 is illustrated in Figure 8.

Figure 8 $^{68}Ge/^{68}Ga$ generator Eckert & Ziegler IGG 100

iThemba Labs generator may benefit from ^{68}Ga pre-labeling concentration and purification method to use eluted gallium. The detail of commercially available generators in France is presented in the Table 1.

Table 1 Different Gallium-68 generators available commercially in France and their characteristics

Laboratory	**ITG Garching ITG iQS®**	**Eckert & Ziegler**	**Eckert & Ziegler**	**iThemba LABS**	**Eckert & Ziegler**
Origin	Germany	Germany	UK	South Africa	Russia
Column Type	Organic	TiO_2	TiO_2	SnO_2	TiO_2
Solvent Volume for Elution	HCL 0.1N 4 mL	HCL 0.1N	HCL 0.1N 5 mL	HCL 0.1N 6 mL	HCL 0.1N 5 mL
Performance (initial)	80%	75%	70% (73%)	100 %	>75%
(long term)	NC	60%	NC	75% after 300 days	>75%
%^{68}Ga Release (initial)	<0.005%	<0.001%	0.001% (0.0001%)	<0.01	0.005% (0.011%)
(long term)	NC	<0.001%	0.0005% (200 elutions)	0.08% after 9 months	0.005% after 400 elutions (0.026%)

1.1.5.3.2 Radio isotopic Emissions

Both PET and SPECT diagnostic methods require the use of radioisotopes that can emit gamma photons. Principally, there are four types of decay leading to the emission of one or more gamma photons.

1.1.5.3.2.1 Pure Gamma Emissions

After radioactive transformation, a majority of nuclei generate daughter nuclei which are not at the lowest energy level (ground state); called metastable state (Figure 9). This excited state, is unstable and release its excess energy in the form of the electromagnetic radiation emission called gamma photons, it is nuclear isomerism or isomeric transition as shown in eq. 3.

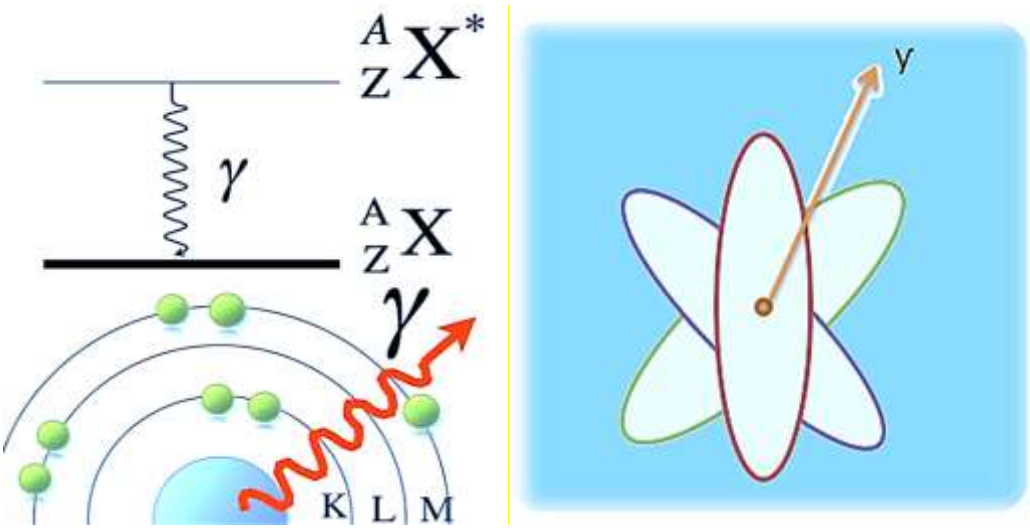

Figure 9 Procedure of radioactive gamma emission

$$ {}^{A}_{Z}X^{*} \rightarrow {}^{A}_{Z}X + \gamma $$ ---------- Equation 3

This gamma radiation therefore only appears following a decay (α, β-, β +, CE) of a nucleus which has the outcome of the radioactive transformation in the excited state. The energy of the gamma photon is equal to the de-excitation energy of the daughter nucleus, from which it comes. The energy range is between 60 KeV and 3 MeV for gamma photons and each radioisotope is characterized by its emission energies. As an example, metastable technetium-99m (^{99m}Tc), transform to technetium-99 (99Tc), after the emission of a gamma photon of energy of 140 KeV (Eq. 4).

$$ {}^{99m}Tc \rightarrow {}^{99}Tc + \gamma $$ ---------- Equation 4

1.1.5.3.2.2 Electronic Capture (EC)

The EC has the characteristic of emitting another radiation either of type X or an Auger electron following the rearrangement of the electronic process (step by step from the outermost layer to the innermost layer so as to fill the electronic gap). Nuclei with an excess of protons can undergo this mode of decay. The phenomenon is opposite to β^+ emission. It corresponds to the capture of an electron by a nucleus proton to form a neutron (Eq. 5).

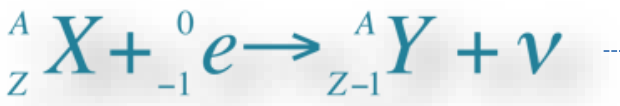

Equation 5

An example of EC is the transformation of iodine-123 to tellurium-123 (Eq. 6).

Equation 6

The resulting nucleus returns to the ground state from excited state after the release of gamma photon by isomeric transition as mentioned above.

1.1.5.3.2.3 B^+ Emissions

A B^+ emission is related to the nuclei which has excess protons. A proton in the unstable nucleus turns into a neutron and simultaneously emits an anti-electron called a positron or β^+ particle. The nucleus is therefore transformed as shown in Eq. 7.

$$ {}^{A}_{Z}X \rightarrow {}^{A}_{Z-1}Y + {}^{0}_{+1}\beta + \nu $$ ---------- Equation 7

For β^+ emission, depending on the energy of the β^+ particle, it covers an average free path 0.5 to 5 mm in the biological tissues that influence the resolution in imaging. After that annihilation leads to the emission of two gamma photons of 511 keV (corresponding to the energy equivalent of the mass of the electron and its antiparticle at rest) at 180° apart from each other (opposite direction) as seen in Figure 10.

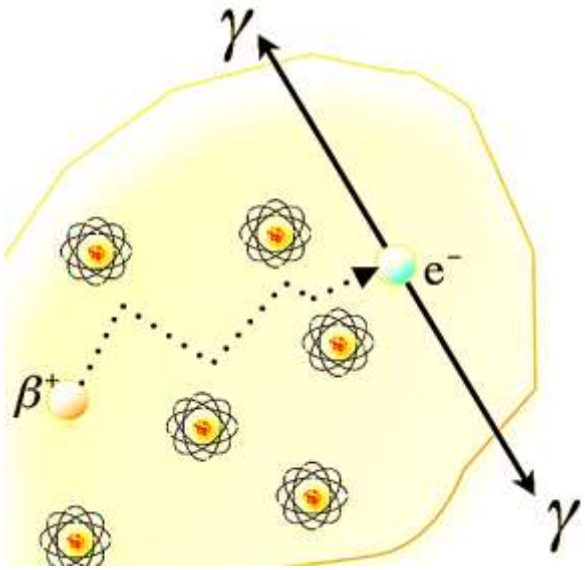

Figure 10 Radioactive disintegrations during annihilation of positron

Gallium-68 transformed to Zinc-68 with an average travel of 3.1 mm in water (Eq. 8).

$$ {}^{68}_{31}\mathrm{Ga} \rightarrow {}^{68}_{30}\mathrm{Zn} + {}^{0}_{+1}\beta^{+} + \nu $$ ---------- Equation 8

These bi-photonic emissions are the origin of applications in positron emission tomography (PET) imaging, also known as bi-photonic imaging.

1.1.5.3.2.4 B^- Emissions

Emissions of B^- are related to the nuclei which has excess neutrons (Figure 11). A neutron from an unstable nucleus is converted into a proton and spontaneously emits an electron in order to regain a stable nuclear state. This electron is called a β^- particle (Eq. 9).

$$ {}^{A}_{Z}X \rightarrow {}^{A}_{Z+1}Y + {}^{0}_{-1}\beta + \overline{\nu} $$ ---------- Equation 9

The energy deposited in the surrounding tissue is much greater than pure gamma emissions. As a result, this type of emitter is reserved for diagnostic and therapeutic aspects (theranostics).

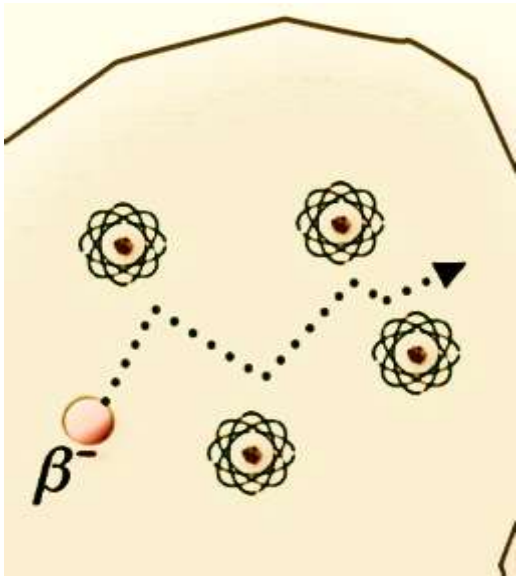

Figure 11 Average linear path of β^- particle

For example Lutetium 177 emits three β^- particles of different energies (498 KeV, 385 KeV and 176 KeV) used for the treatment of metastases (tissue penetration advantage of less than 2 mm) and two gamma particles of 113 keV and 208 KeV (detectable with a gamma camera) for imaging.

1.1.5.4 Radionuclides

The radionuclides are selected according to their physical properties (nature of the emission, half-life, and energy) and their chemical properties (ease of the chemistry used for radiolabelling the vector). For PET technology, the radionuclides used must be β^+ emitters. Thus after annihilation of the positron, two gamma rays with energy of 511 KeV is emitted in two opposite directions. These radionuclides must have transition energy greater than the annihilation energy, therefore greater than 1.022 MeV. Most of the atoms with these characteristics are light weight atoms such as fluorine, oxygen and carbon. Conversely, the gamma emitters used in SPECT are generally heavier elements, transition metals or halogens such as technetium-99m, indium-111 or iodine-123.

Furthermore, the biological relevance of the radioactive atoms used in PET is an undoubted advantage compared to the radionuclides used in SPECT. In fact, most of the molecules of biological interest such as, carbohydrates, nuclide acids, fatty acids, and proteins can easily incorporate positron-emitting radionuclides by a simple prosthetic approach. Some of the important radionuclides, their parent radionuclides and corresponding half-life are presented in the Table 2.

Table 2 Different Radionuclides, Production sources, and decay

Radionuclides	Production	T (1/2)	B Energy (KeV)	Decay (%, KeV)	Imaging Techniques
^{198}Au	^{197}Au (n,ϒ)^{198}Au	2.7 d	311.5-960.7	ϒ photons	Gamma Camera
^{76}Br	^{76}Se (p,n) ^{76}Br	16.2 h	1180-3941	β^+ (55)EC (45)	PET
^{14}C	^{14}N (n,p) ^{14}C	5730 y	49.5-156.0	β^+	PET
^{64}Cu	^{64}Ni (p,n) ^{64}Cu	12.7 h	278-653	β^- (17)EC (44)	PET
^{165}Dy	^{164}Dy (n,ϒ) ^{165}Dy	2.3 h	440.2-1286.7	β^-(1.286)	B^- Therapy
^{169}Er	^{168}Er (n,ϒ) ^{169}Er	9.4 d	99.6-350.9	β^-(350)	B^- Therapy
^{18}F	^{18}O (p, n) ^{18}F	109.7 min	245-634	β^+(96.7) EC (0.1)	PET
^{68}Ga	^{68}Ge (n,p) ^{68}Ga	67.7 min	829-1899	β^+ (89) EC (11)	PET
^{3}H	^{6}Li (n, α) ^{3}H	12.3 y	5.7-18.0	β^+	PET
^{166}Ho	^{165}Ho (n,ϒ)^{166}Ho	26.8 h	665.1-1853.9	β^- (83)	B^- Therapy
^{124}I	^{124}Te (p,n) ^{124}I	4.18 d	820-2138	β^+	PET
^{131}I	^{131}Te (β^-) ^{131}I	8.0 d	181.7-806.9	β^+	PET
^{123}I	^{123}I (n, ϒ) ^{123}Te	13,3 h	159	CE (100 %)γ (84 %)	SPECT
^{111}In	^{111}I (n, ϒ)	67,3 h	171	CE (100 %) γ (90.2)	SPECT
^{99m}Tc	^{99m}Tc (n, ϒ)^{99}Tc	6 h	140,5	CI γ (89.6 %)	SPECT
^{177}Lu	^{176}Lu (n,ϒ) ^{177}Lu	6.7 d	133.3-497.8	β^-(498)	B^- Therapy
^{186}Re	^{185}Re (n,ϒ)^{186}Re	89.2 h	346.71069.5	ϒ photons	Gamma Camera
^{188}Re	^{188}W (n,ϒ)^{188}Re	17.0 h	764.3-2120.4	ϒ photons	Gamma Camera
^{153}Sm	^{152}Sm(n,ϒ) ^{153}Sm	46.5 h	224.2-808.2	β^-(808)	B^- Therapy
^{86}Y	^{86}Sr (p,n) ^{86}Y	14.7 h	664-3141	β^+ (33)EC (66)	PET
^{90}Y	^{90}Sr (p,n) ^{90}Y	64.1 h	933.6-2280	β^- (2.282)	B^- Therapy
^{89}Zr	^{89}Y (p,n) ^{89}Zr	3.3 d	397-901	β + 23EC (77)	PET

It contrasts somewhat SPECT radionuclides i.e. technetium-99m, which are of very little biological relevance. The latter does not exist in endogenous biomolecules and due to its

chemical properties requires administration in the form of a complex with a cold vector kit (radiopharmaceutical drug).

From a physical point of view, the majority of radionuclides used in PET have a short half-life that has an advantage from a dosimetric point of view for the patient during a medical examination and a disadvantage given that most of them have to be produced using a cyclotron, which makes logistics management very complex. On the other hand, the radionuclides used in SPECT because of their long half-lives make it possible to observe biological processes in vivo for several hours or even several days post injection. Now days there are positron-emitting radionuclides that can be produced by a generator i.e. Gallium 68, that can offer great flexibility at the organizational level, hence proved a revolution in the positron emission tomography imaging. A gallium-68 generator for daily production of ^{68}Ga and dose calibrator for dose measurements located at CHU-De-Angers is presented in the Figure 12.

1.1.5.4.1 Temporal Resolution

The possibility of performing dynamic imaging in nuclear medicine is one of the new challenges in this discipline. Indeed, the study of the biodistribution of radiopharmaceuticals offers a better understanding of the underlying physiopathological processes. To do this, it is essential to accurately collect a large number of events (high decay frequency) over a given period of time with acceptable image quality. This makes it possible to quantify the events and to follow kinetically the distribution and elimination of the radiopharmaceutical. PET imaging (electron collimation) offers an intrinsic advantage of assessing all disintegrations over time hence feasible for dynamic studies while this event is not possible in SPECT due to presence of mechanical collimator.

Figure 12 Class A high-energy armored enclosure used for the elution of the $^{68}Ge/^{68}Ga$ generator and to produce on site gallium-68 radio-labeled radiopharmaceuticals present at CHU-De-Angers

1.2 Pulmonary Embolism

Pulmonary embolism (PE) or deep vein thrombosis (DVT), are the clinical presentation of venous thromboembolism (VTE), (Figure 13), considered as the third most frequent cardiovascular syndrome next to myocardial infarction and stroke [3]. PE and DVT incidence rates lie between 39-115 & 53–162 per 100,000 population annually, respectively [4]. VTE incidence is about eight times greater in the aged individuals (≥80 years), consequently, longitudinal studies are presenting an increasing trend of PE incidence rates annually [5-7] over time. World Health Organization (WHO) recent analysis in 2000–2015 showed Mortality Database showed a usual trend of 38,929 deaths per year related to PE in the 41 states of European Region [8]. It does not occur only in the patients with history of surgery or obesity but also found in healthy people after pregnancy or long air travel [9, 10].

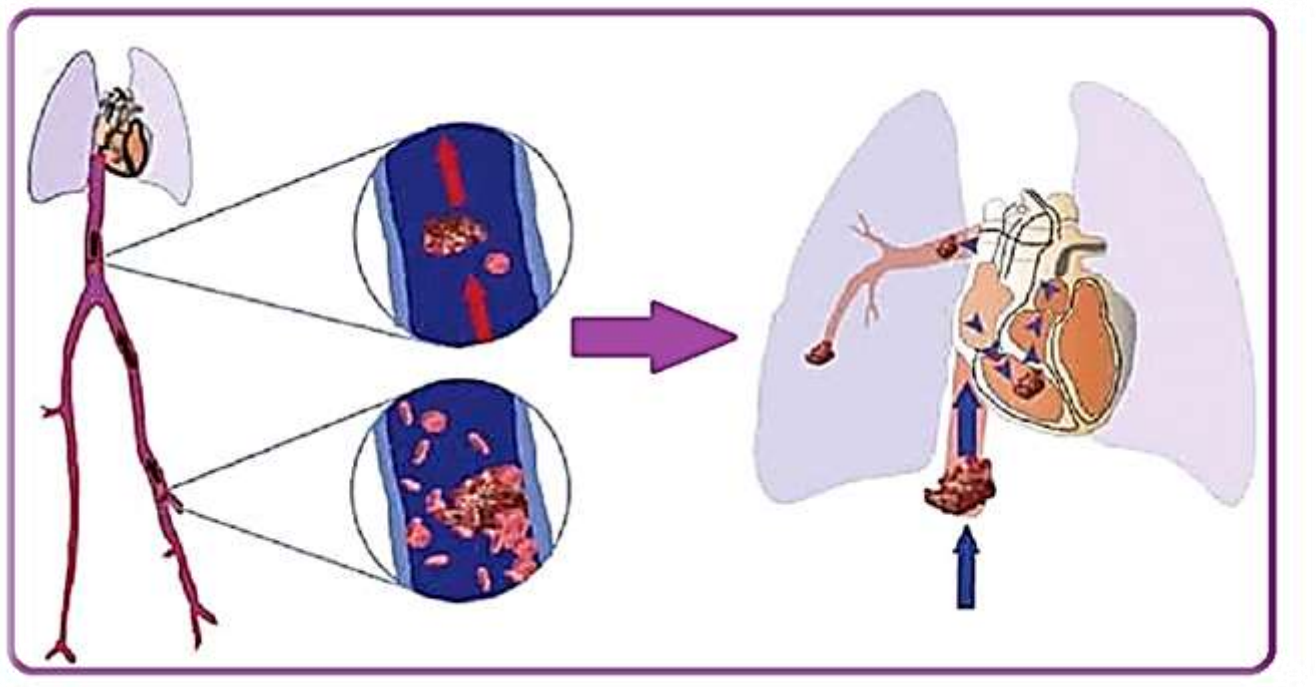

Figure 13 Physiopathology of pulmonary embolism (PE). A thrombus originate in the deep veins of the legs dislodge and move through the venous system to reach pulmonary arterial circulation leading to PE, modified from ref. [11]

PE has 30% mortality rate that can be improved to 8% if timely detected. About 35% of patients with suspicion of PE are ruled out but contrarily many are diagnosed in post-mortem [12], so immaculate diagnosis of PE is essential.

Rudolph Virchow (1821-1902), a well-known German pathologist, described the pulmonary embolism for the first time after the autopsies of patients with sudden deaths. Today the term triad of Virchow (Figure 14) refers to the combination of three factors that contribute to the initiation of a venous thrombus, i.e., vein wall alteration, haemostasis change (hypercoagulability) and venous stasis [13].

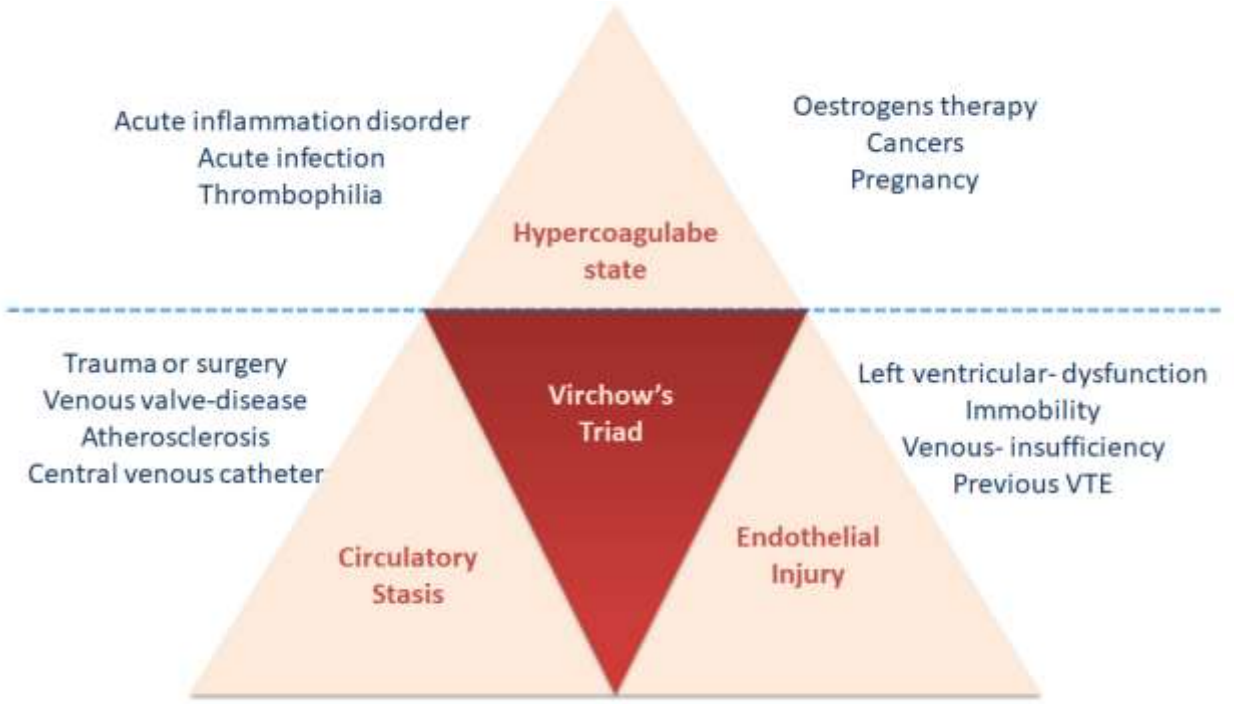

Figure 14 Virchow's Triad

To understand well the Virchow's triad, knowledge of thrombus formation/pathophysiology is essential. As Virchow's triad described the pathogenesis of VTE [49] include stasis, changes in endothelial of vessel wall after injury are well described here in thrombosis.

1.2.1 Thrombus Pathophysiology

Thrombosis is a complex physiological process that can cause oxygen deficiency and consequently tissues infarction due to formation of thrombus. Arterial thrombosis is triggered primarily after the vessel wall injury, which is often due to mechanical injury or atherosclerotic plaque rupture [14-16]. Extracellular sub-endothelial matrix (ECM) is exposed in vessel wall injury that begins the activation and fast recruitment of platelets. Receptors of Glycoprotein platelet (GP) and the von Willebrand Factor (vWF) i.e. Ib-IX-V perform a vital role in binding the platelets at the injury site and von Willebrand Factor serves as a linker between platelets and the collagen fibrils (type I, III and VI). During normal circulation, soluble vWF is not sensitive towards platelets while the immobilized vWF is highly sensitive for platelets [14, 17, 18]. Coagulation factors (VII, XI) expression and recruitment of fibrinogen to convert into fibrin by the action of thrombin culminates in a clot network [14]. Venous thrombosis is caused by hypoxia or inflammatory stimulation on the endothelium surface, contributing to a surface manifestation of adhesion receptors [19, 20]. Such receptors make it easier to attach circulating leukocytes and micro-vesicles. Leukocytes produce micro-vesicles, rich in tissue factor (TF) that can bind to the surface of platelets (PSGL-1) to sustain the process of coagulation triggered from endothelial injury by vascular TF (Figure 15).

Extensive cross-communication takes place among inflammation and coagulation networks. Fibrin, a clot mortar, recruits and activates platelets further through platelet receptor $\alpha_{IIb}\beta_3$ [21] as well as attracts leukocytes by interacting with the $\alpha_M\beta_2$ (mac-1) receptor. Fibrin binding of leukocytes increases phagocytosis [22].

In the pro-coagulation process, there is an inter-relationship between the coagulation and inflammation for activating anti-coagulation pathways focused around Protein C/S, antithrombin, and inhibitors of Tissue Factor Pathway (TFPI).

Virchow's triad described many years ago VTE pathogenesis [23], i.e. endothelial changes, stasis, and increase in thrombogenicity of blood contribute to VTE. Additional factors include abnormalities in the fibrinolytic mechanisms and inflammation [20]. Most of the patients validate the criteria of Virchow's triad [24-26].

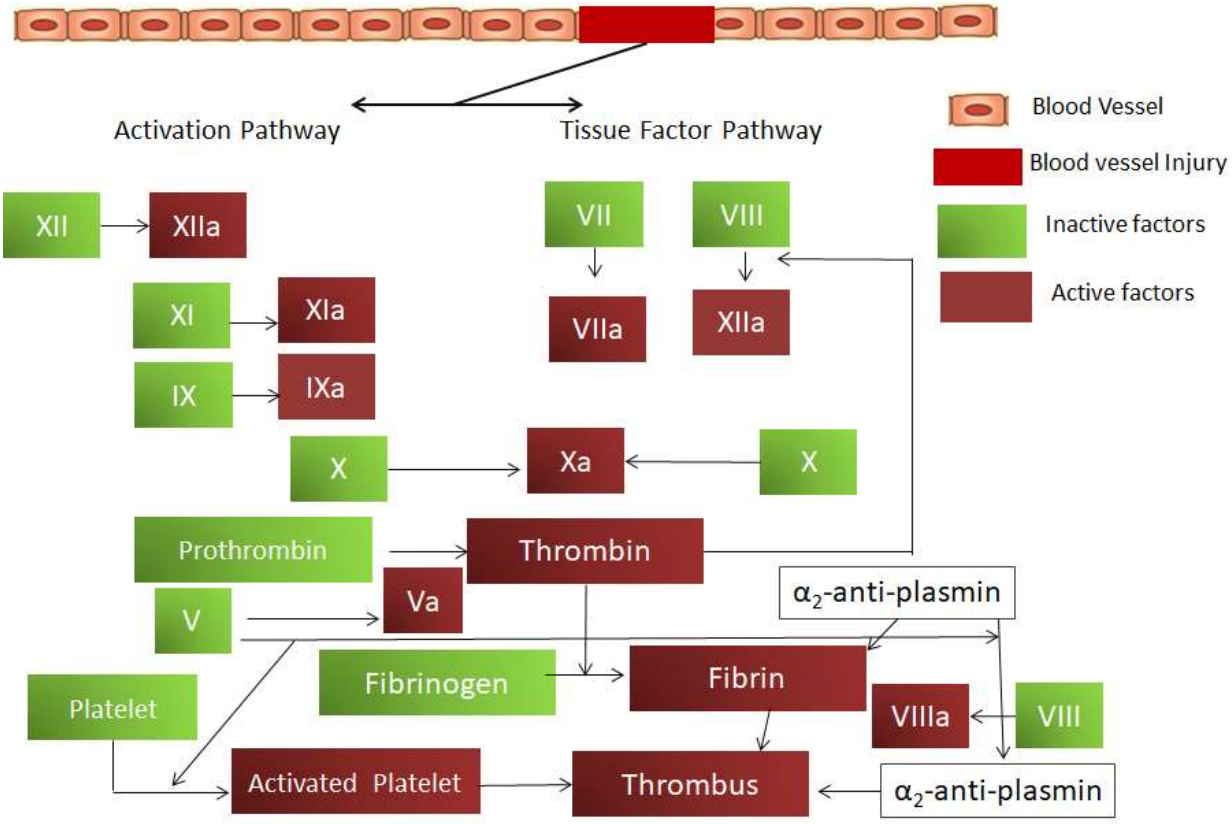

Figure 15 Mechanism of thrombus formation following blood vessel injury

Additionally, pulmonary embolism, not unusually, can be non-thrombotic owing to the movement and embolization of different cell forms in pulmonary arterial circulation (fat cell,

trophoblastic cell tumor cells), bacteria or fungi, foreign material, (sudden and dramatic complication of childbirth representing the third cause of maternal mortality in France) amniotic fluid or air [27, 28]. The medical effects of non-thrombotic embolism are not purely mechanical compared to conventional pulmonary embolism thrombosis but are also based on its existence.

1.2.2 Epidemiology

Venous thromboembolism is a lethal condition with average incidences of 108 per 100 000 persons annually among Whites, VTE incidence strongly correlates with age; extremely rare in the childhood (5 per hundred thousand), and increases with aging exponentially to 500–600 per 100,000 in people age more than 75 years) [29, 30]. Generally, both women and men are equally affected but young women are slightly more at risk because of an association among pregnancy and VTE, and an increased risk due to oral contraceptives usage. This case is reverse in old age, as the frequency of PE in men is higher than in the women [30, 31].

Mortality rate associated to PE can be 25% if not treated [32], but rate could be decreased to 2–8% with suitable anticoagulant treatment in 3 months after diagnosis [33]. In the first month following diagnosis, mortality is caused due to hemodynamic instability [34, 35], but after 1 year or more of follow up of diagnosis, other complications, for instance congestive heart failure, chronic lung disease, and malignancy, are major causes for mortality [35, 36]. Statistics showed PE mortality may reach to 35–45% due to malignancy, 24–27% due to all-causes, although recurrent PE cases contribute to 2.5–7.0% [36, 37]. The risk of early death associated with patients of pulmonary embolism symptoms is 18-fold higher than deep vein thrombosis patients alone [38, 39]. Pulmonary Embolism alone after onset reduced survival up to 3 months. For

nearly one quarter of patients of pulmonary embolism, the clinical demonstration is a sudden death [29]

According to Kroger *et al.* the occurrence of venous thromboembolism and pulmonary embolism is probably underestimated in a number of different epidemiological studies due to clinical difficulties: Patients who died of undiagnosed pulmonary embolism; undiagnosed symptomatic patients; patients correctly diagnosed but not included in the study; asymptomatic and therefore undiagnosed patients. The first bias will vary by country and practice frequency of autopsies, for example, the frequency of autopsies is low in France [40], leading to a sub-estimated number of deaths from pulmonary embolism and therefore, ultimately, to an underestimation of the incidence of pulmonary embolism. The second approach is explained by the non-specificity of the symptoms of venous thromboembolism, which sometimes makes it difficult to diagnose. The third prejudice may be constrained by the most detailed assertion possible, backed by computerized monitoring of patient records. Finally, the existence of asymptomatic patients cannot be excluded and is the fourth bias in these studies. Given these prejudices it is estimated that between 60,000-100,000 patients die every year from pulmonary embolism in the US according to data of NCHS, USA, which constitutes more deaths than those caused by myocardial infarction or stroke.

1.2.3 Key Risk Factors

For VTE several risk factors are identified that could be divided as: i) acquired, ii) genetic susceptibility, iii) hormonal influence, iv) mixed-origin risk factors [41]. Strongest risk factors are divided in two types. In first category, mutations that cause loss-of-function in genes that encode naturally occurring anticoagulants for example SERPINC1 (that encode protein C, S and

antithrombin), PROS1, and PROC. Secondary pulmonary embolism occurs in patients with one or more risk factors and acquired clinically recognizable, hypercoagulable due to deficiency or abnormality of inherited coagulation proteins. Different risk factors to thromboembolic disease are mentioned below (Table 3).

Table 3 Risk factors favor the occurrence of venous thromboembolism

Hereditary risk factors	Environmental risk factors
Protein C deficiency	Age
Protein S deficiency	Surgery
Anti-thrombin deficiency	Immobility(transport, bed-rest, paralysis)
Factor V Leiden mutation	Cancer
Elevation of factor VIII	Oral contraception, hormones
Mutation of the prothrombin gene	Obesity
Elevation of factor IX	Pregnancy, Postpartum
Elevation of factor XI	Anti-phospholipids syndrome
Dysfibrinogenemia	myeloproliferative syndrome
Hyperhomocysteinemia	Central venous catheter, Nephrotic syndrome
Plasminogen deficiency	Chemotherapy

1.2.3.1 Environmental Factors:

1.2.3.1.1 Transportation:

The World Health Organization (WHO) results of the WRIGHT (WHO research Into Global Hazard of Travel) project concluded that the risk of developing VTE is doubled in transportation conditions favoring venous stasis, in particular the immobility of passengers [42]. Thus, not only the long hour's flights, but also in car or train trips, if passengers remain motionless for more than 4 hours promote the occurrence of VTE. This risk is particularly increased in patients who already bearing risk factors such as age over 50 years, thrombophilia or a history of VTE [43].

1.2.3.1.2 Obesity

Several studies have shown that pulmonary embolism is related to the people's body mass index (BMI) [44]. Thus obesity is associated with increased VTE cases. Kucher and colleagues inferred that patients of PE or DVT BMI was found higher (median 29.0 kg/m^2) as compared to MBI of patients with DVT (median 26.8Kg/m^2) [45]. Pomp and colleagues in two different large cohort studies, concluded that BMI 25–30 kg/m^2 which increases 1.7-fold risk of VTE, whereas BMI >30 kg/m^2 increases 2.4-fold risk of VTE [46, 47] Similar studies also proposed a link of VTE with overweight and obesity [48].

1.2.3.1.3 Hormones

The increased risk of pulmonary embolism includes oral contraception, childbirth, and menopause replacement therapy. The High Authority of Health (HAS), in its recommendations on the strategies of choice of contraceptive methods in women, said that every generation taking oral contraceptive pills are associated with an increased risk of accident thromboembolism. Pregnancy is a risk situation of VTE and although its incidence is rare in pregnant women (1 pregnancy per 1000); it is still 5 times more common than in the general population. Pulmonary

embolism in France is responsible from 5 to 10 deaths per year in pregnancy, making it a leading cause of maternal mortality [49]. During pregnancy the occurrence of VTE is promoted, first by mechanical factors (compression by the gravid uterus of the inferior vena cava resulting in decreased venous return, immobility etc.) and, biological factors, on the other hand (especially in the first quarter). In pregnant women, the risk of VTE and pulmonary embolism (secondary to caesarean) is greatly increased and prophylaxis should be taken into consideration [50].

1.2.3.1.4 Cancers

Cancer diseases are often the cause of thromboembolic events when producing procoagulant substances (tissue factor, cysteine protease) or rare vascular cuts. Marc Carrier and colleagues has mentioned in a systemic a review first time mentioned a correlation between venous thromboembolism (VTE) and the cancer [51, 52]. Before idiopathic thrombosis recurrence, there is an always suspected occult presence in the relationship between tumor and VTE [43]. In particular, after chemotherapy medication, the risk of VTE in the cancer population is multiplied by 3-5, making it the second cause of cancer death [49]. Recently Khorana and colleagues has presented the guidelines to manage the cancer patients with high risk of VTE [53].

1.2.3.1.5 Surgical Procedures

Operating and postoperative medical circumstances increase the thromboembolism risk. This risk will vary depending on the type of operation, with orthopedic operation being the most risky, followed by major urological, gynecological, vascular and neurosurgery procedures. For example, in 40% to 60% of cases after orthopedic surgery in the absence of a prophylaxis to thromboembolic complications [11, 54, 55], in 15% to 30% of cases after a high general operation [56, 57], 25% to 39% of cases per months after surgical glioma [58]. Additionally, after urologic treatment, pulmonary embolism is the primary reason of mortality and its

estimated 1 in 500 [59-61]. For the opposite, following laparoscope type of surgery the low incidence of thromboembolism enables the establishment of prophylaxis.

1.2.3.2 Hereditary Factors

Most recently, slightly more common causes of thrombophilia are studied in 107 patients between 2015 and 2017 of patients mean age 39.6 years. The ratio of female/male was 1.7. The study concluded that genetic defects of B-Fibrinogen-455 and Factor V G1691A were higher in patient groups. As well as other factors include methylene tetrahydrofolate reductase (MTHFR), genetic variant C677T and glycoprotein IIb/IIIa in platelet polymorphism A2 (PlA2) [62].

The well-studied and most common VTE genetic cause is prothrombin G20210A and Factor V Leiden gene mutation [63]. Subsequently, other autosomal factors such as protein S and protein C defects are identified but essentially their unusual features rendered them uncommon causes. Some other factors include resistance to active protein C (secondary to gene V mutation). Increased risk of venous thrombosis by five to ten times than general population was the result of (R506Q), which is a source of resistance to activated protein C [64]. Some key genetic factors present in the general population are shown in Table 3.

1.2.4 Pathogenesis

The above-described risk factors interfere alone or in conjunction with one or more of the three components of Virchow's triad in order to develop thromboembolic disease. Several acquired or non-acquired factors and hereditary factors are also responsible. Venous stasis is one important components of pathogenesis of thromboembolism: the studies in paralyzed patients showed that venous thrombus is formed in areas where blood flow is slower (calf or thigh vein opposite the valve) [65]. This phenomenon is found in the situations of physical inactivity (transport, bed rest) where muscles no longer play their role of pump and drive venous blood flow. It follows a local

accumulation of blood that can lead, firstly, activation of coagulation and, second, a parietal altered, the latter may in turn be the cause of bleeding disorders. This is due to an imbalance between anti-coagulant and pro-coagulant substance. If this disorder is caused by a genetic variable, there is a lifetime risk that VTE will be present and biologic tests showed about 50 percent positive results. In addition, prophylaxis may be implemented until the risk is reduced, in case if this hyper-coagulation is triggered by an environmental factor (hormone therapy, pregnancy, cancer).

Virchow's third element, especially important in the pathogenesis of VTE is the alteration of the vascular wall as it can occur after trauma or surgery (Figure 15). The risk of VTE was increased after operation of full hip or knee, an increased VTE risk was reported immediately after the procedure, so 3 months follow up after surgery was planned and therefore the patient was released from the hospital system after long time. This threat requires extensive prophylaxis [66, 67] for consideration.

1.2.5 Pathophysiology

1.2.5.1 Etiology of Acute Pulmonary Embolism

Pulmonary embolism is caused by dislodging thrombus origininated mostly in the leg deep veins, seldom the upper extreme veins renal and pelvic, and hardly in right atrium of heart. After dislodging, it starts travelling in the form of embolus from right heart side towards the lungs arteries (Figure 1). Inside the pulmonary arteries, thrombus would break down or further lodged in the pulmonary arterial bed and if it is big, remains in the central pulmonary artery, and produces a ‘saddle embolism’, which in return may results into a severe dyspnea and collapse. If this thrombus travels to smaller arteries, results into pulmonary infarction, that causes a severe pain during respiration.

1.2.5.2 Hemodynamic Consequences

The most important of these alterations is the increase in vascular resistance of the pulmonary arterial bed. Literature revealed that the pulmonary hemodynamic changes resulted from pulmonary embolism are primarily due to vasoconstriction of smaller pulmonary arteries or arterioles, apparently through a reflex action. This mechanical blockage of lung vasculature is considered to be the cause of hemodynamic alterations. Vasomotor response of pulmonary embolism transiently increases pulmonary arteriolar resistance, whereas mechanical blockage causes a constant pulmonary hypertension. The occlusion of a lung artery by a thrombus will cause a sudden increase in afterload. In response, the right heart will elevate his heart rate, preload and contractility in an attempt to maintain a constant pulmonary flow. The increased pressure changes the compliance and pulmonary arterial resistance. These consequences are secondary to a sudden and abrupt occlusion of the pulmonary artery and/or its dividing branches. The pulmonary vascular network is a high-speed, low-pressure tissue. Indeed, the lung is infused by the entire cardiac output and the pressure at the pulmonary artery is 6 times less than that of the aorta (Figure 16). The onset of pulmonary arterial precapillary hypertension (PAH), depends on the extent of the obstruction. In patients without a history of cardiopulmonary pathology, for less obstruction than 30%, pulmonary artery pressure (PAP) will increase moderately (10 mmHg), cardiac output and the mean pressure being maintained by several compensatory mechanisms such as tightness in healthy vasculature and usage of vessels that are usually nonfunctional or closed). Precapillary PAH has an average pressure of 40-50 percent which rise exponentially during pulmonary arterial resilience to a rate of 40 mmHg [67]. In addition to the afterload, the volume of distribution (VD) potential is raised, and a diminishing of left ventricular preload is observed, which is exacerbated by dilation of right ventricle (RV).

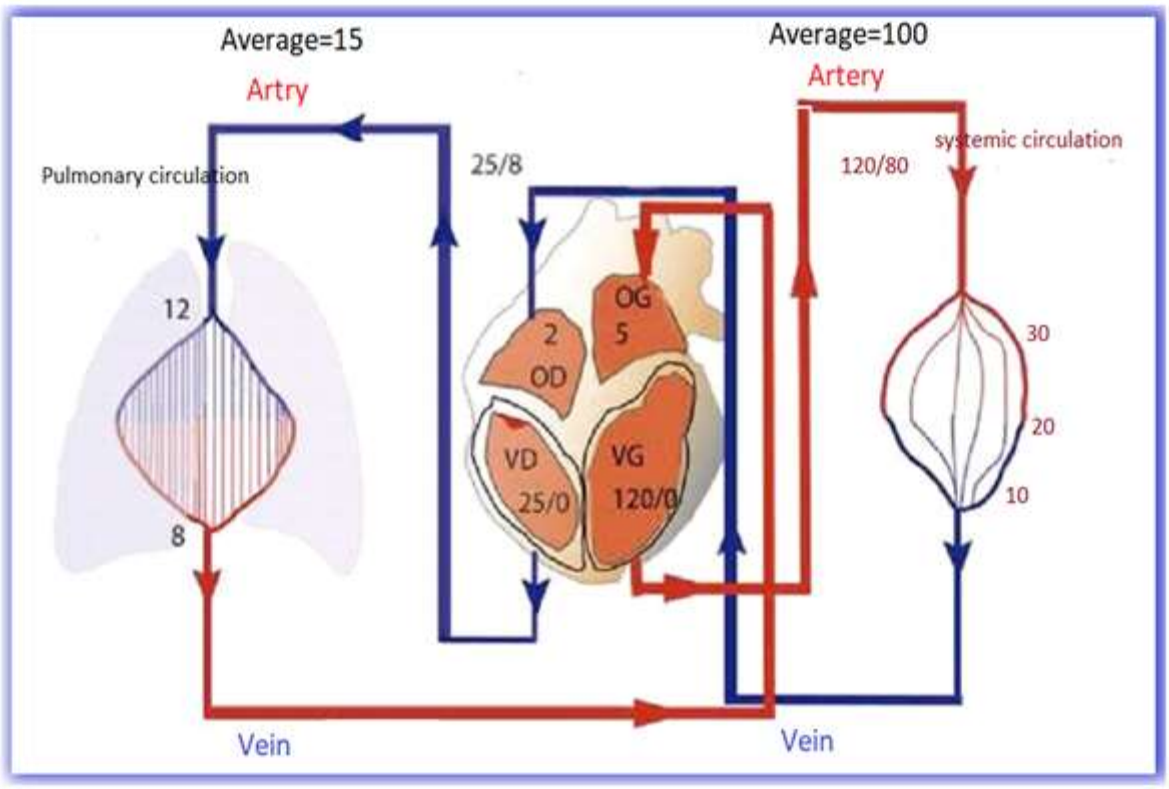

Figure 16 Systemic and Pulmonary Pressure (mmHg) modified from ref. [11]

Increased right intraventricular pressure helps to diminish the right coronary perfusion, making it even worse after blood pressure drops [68, 69].

1.2.5.2.1 Right Ventricle (RV) Failure

In PE, right ventricle (RV) dysfunction is the leading cause of mortality (Figure 17). Pulmonary vasculature possesses little resistance normally, suggesting that right ventricle has thin walls and low contractility as compared to left ventricle. Additionally, contractility of RV is reserved to volume or small pressure overload due to RV low mass of, consequently, in the RV afterload a sudden increase make right ventricle vulnerable, such as in the case of acute PE.

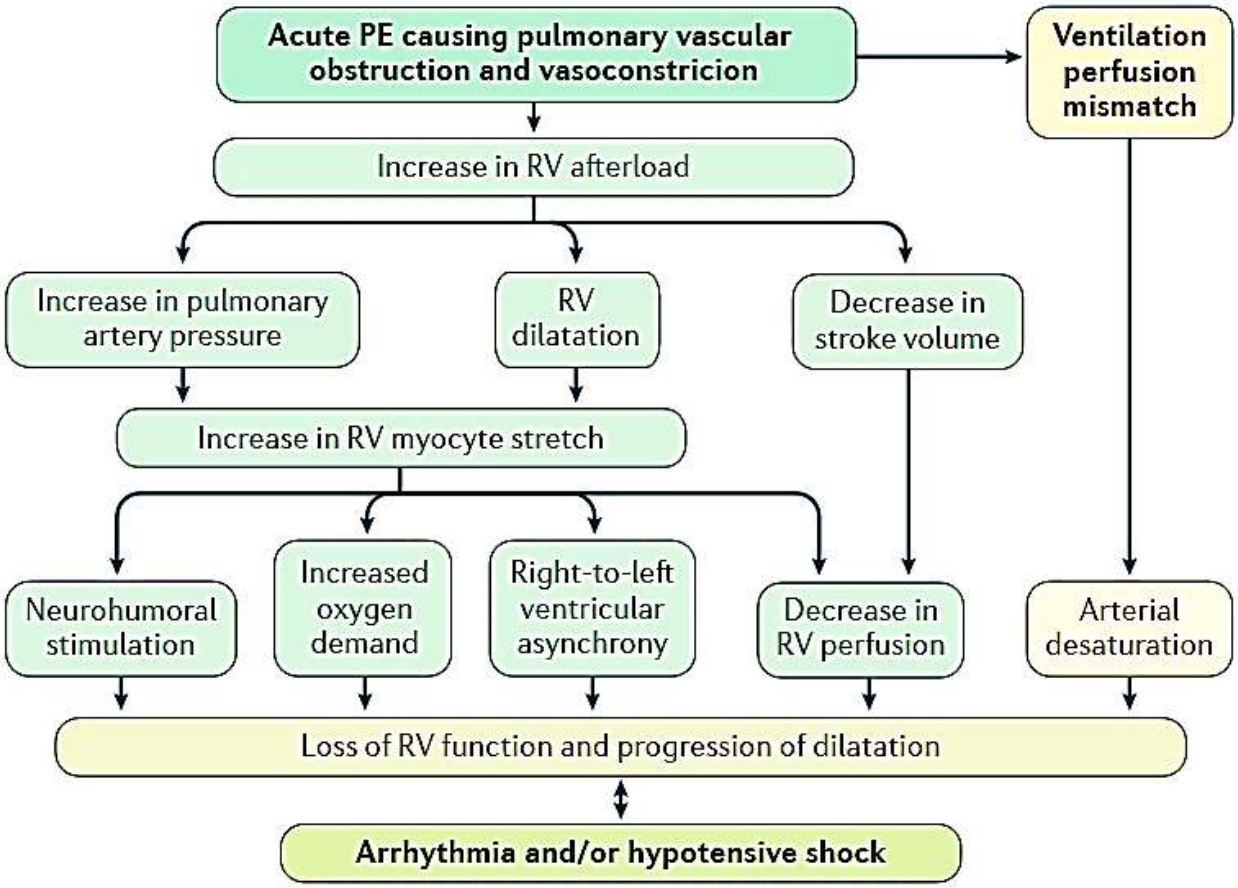

Figure 17 The sequence of RV failure in acute PE. Acute pulmonary embolism (PE) will induce pulmonary vascular obstruction and increased right ventricle (RV) afterload. published from ref [70] with permission

In acute PE, RV afterload increament is caused by mechanical obstruction of emboli present in the pulmonary vascular system, or a slight magnitude is due to the obstruction-related vasoconstriction activated by the vaso-active mediators (i.e. thromboxane A_2, serotonin) [70].

Rise in the pressure of pulmonary arteries results into RV dilatation increment, causative to increase in the stretch of RV myocyte and this reflects myocardial stretch or damage biomarkers increment. After too much increase in the afterload, RV dilatation turns out to be maladaptive, leading towards RV failure [70].

1.2.5.3 Abnormal Gas Exchange

A decline in pulmonary surfactant production, hemorrhagic alveolite development, and inflamma -tory release by mediators and hypoxemia are induced by pulmonary embolism. In the absence of cardiovascular disease, however (pulmonary infarction), necrosis of the lung tissue may persist [53, 71]. The type and volume of the bolus, the degree of occlusion, the coronary activity and the period since the thromboembolic occurrence appear is ambiguous in the process of triggering the gaseous transfer anomalies [72]. The key cause of hypoxemia is the mismatch of ventilation and perfusion and a right-left shunt or a rise of the alveolar dead zone. A redistribution of the blood results in the unbalancing between ventilation and perfusion [73]. The effects of lung and bronchial blood microcirculation (pulmonary events) evolving cardiomyopathy and, ultimately, pulmonary oxygen and carbon dioxide exchange are comprehensively complex.

1.2.6 Prevention and Treatment

1.2.6.1 Pharmaceutical Prophylaxis

Although, due to the heterogeneity of the population, it is difficult to obtain precise figures on the incidence of VTE in the population of hospitalized medical patients, some studies found an incidence of 10 to 30% in the absence of anticoagulant therapy [74]. French Agency for Health Safety of Products published guidelines on good practice for thromboembolic disease prevention and treatment [74]. These are based on a systematic literature review and supplement North American and European published recommendations [75].

In 2019 latest guidelines are available on the prevention of VTE in cancer patients [76, 77]. Consensusably, the use of VTE prophylaxis is recommended in all hospitalized patients (medical or surgical) for whom the presence of cancer is known or suspected in all patients undergoing

lumpectomy and in patients already undergoing VTE to minimize the recurrence of thromboembolic events [78].

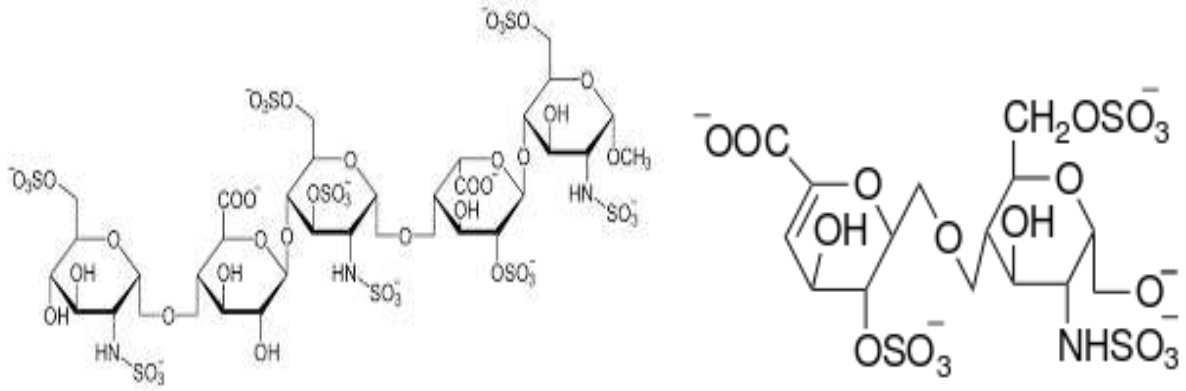

a) b)

Figure 18 Structure of commercial anticoagulant drugs a) Fondaparinux structure b) Low Molecular weight heparin (LMWH) structure

In general, with the exception of counter-indication, any patient with cancer must be hospitalized for management of Thromboprophylaxis where low molecular weight heparin (LMWH) is preferred to other anticoagulant therapies (Figure 18 b). The perioperative implementation of the terminology of Thromboprophylaxis and diagnosis is the topic of French guidelines [79]. Depending on the type of surgery performed, these are based on risk stratification VTE. Operations with medium to high risk of VTE e.g. severe orthopedic or abdominal surgery, high-risk hysterectomy, open prostate and bladder surgery, aortic surgery, intracranial neurosurgery are usually the focus of prophylactic recommendations based on postoperative treatment rather than perioperative anticoagulation. Low molecular weight heparin (LMWHs) are often recommended as compared to alternative prescription drugs and the length varies depending on the type of procedure and the severity.

1.2.6.2 Mechanical Thromboprophylaxis

As we have seen, thromboembolism is multifactorial comprising of the combined action of several factors as mentioned in Virchow's triad's three components (Figure 14).

Mechanical prophylaxis means low or band anti-thrombotic restraint (Figure 19), intermittent pneumatic compression, plantar compression will oppose venous stasis, attempting to compensate for the function of the pump and accelerate the venous blood flow of the lower limbs [79]. In all cases, clinical patients under VTE prophylaxis are advised to use low or band restraining anti-thrombotic as a substitute of drug where it is contradicted [74]. The review of studies comparing fibrinolytic activator (streptokinase, urokinase or tissue plasminogen activator), unfractionated heparin (UFH), Fondaparinux (Figure 18 a), suggests the use of fibrinolytic therapy in the acute phase of pulmonary embolism only when combined with a shock [74]. The relay of heparin therapy is suggested after fibrinolysis to reduce the risk of recurrence. In patients who does not face shock, the establishment of a fibrinolytic treatment has not shown superior efficacy compared to heparin role in an intermediate severity embolism (dysfunction or right ventricular dilatation). With respect to the diagnosis of the initial phase of pulmonary embolism, treatment with warfarin, UFH, LMWH or fondaparinux is recommended [74] to reduce the risk of recurrence of thromboembolic events Figure 21.

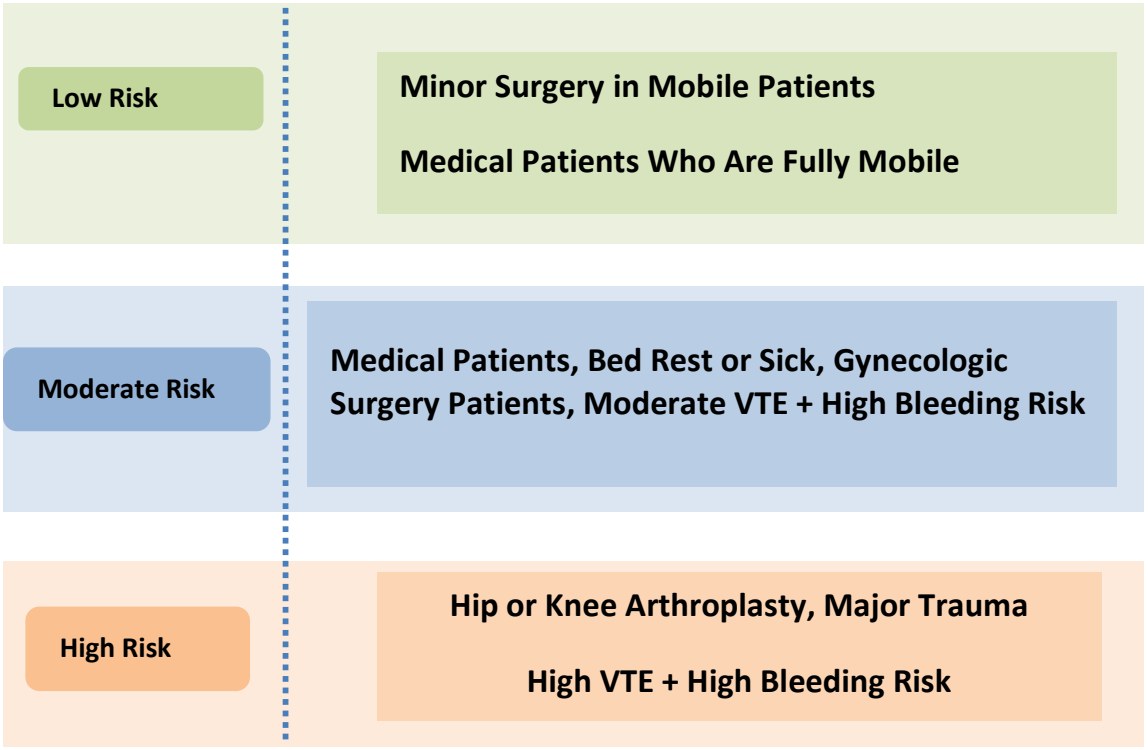

Figure 19 Patients symptoms: with low, middle and high risk of Pulmonary Embolism

1.2.7 Pulmonary Embolism (PE) Diagnosis

However, there is no evidence of a decrease in the absolute number of cases detected in PE but in those who suspected of a condition from 30–35% two decades ago reduces to 15–25%. The lower incidence of confirmation of PE, however, reflects an escalation in clinician's knowledge. Increased awareness of probable PE and modern, non-invasive tests that streamlined a diagnostic procedure may contribute to a lower threshold in clinical practice screening. In most cases, PE related signs or symptoms have no problem-solving accuracy and are not sufficiently sensitive or specific to include or exclude PE. It could be more accurate to incorporate risk factors, signs and symptoms. For example, a rule of eight parameters i.e. age: 50 years; heart rate: more than 100 bpm, saturation of oxygen: 95%, preliminary VTEs, recent procedure or accident, a haemoptysis and unilateral use of oestrogens and leg swelling are known as the Pulmonary Embolism Rule-out Parameters (PERC). Despite major public health problems [80] and the alarm bells of some institutions and learned societies [81-84], pulmonary embolism remains a threat, due to deficiencies in care and premature mortality avoidance for prophylaxis inducing diagnosis. Almost 94 per cent of the patients who died had not received any treatment because there was no diagnosis of pulmonary embolism [85]. In multicenter studies patients with low implicit clinical probability (PERC) pulmonary embolism could be excluded showing low false-negative results percentage [86, 87] although it is still continues to be decided whether PERC and other judgment guidelines could be used successfully or not. All other medically suspicious PE patients must receive comprehensive biomarking procedures for severe thrombosis and/or MRI (e.g. D-Dimer). Modern algorithms for PE diagnosis includes probability pretest testing, D-Dimer analysis, if necessary, imaging of chest [69]. In contrast, myocardial infarction was steadily

improved in its implementation, with major advances in the detection and diagnosis procedure, contributing to an almost 60% decrease in the death rate [88-90].

1.2.7.1 Pulmonary Embolism Clinical Management

The PE related symptoms vary according to the degree of vascular blockage in lungs and extent of physiological reserve of the patient. Dyspnea, hypoxemia, can be seen as a V/Q disturbance. Blood extravasion can cause pleuritis, hemoptysis or cough. The increase in the resistance of pulmonary vasculature may cause Electrocardiographic (ECG) strains, dilatation of right ventricle, pleural effusions, hypokinesis, serious right cardiovascular blockage that can manifest as high voltage, cardiac arrest or pulseless electrical activity or syncope.

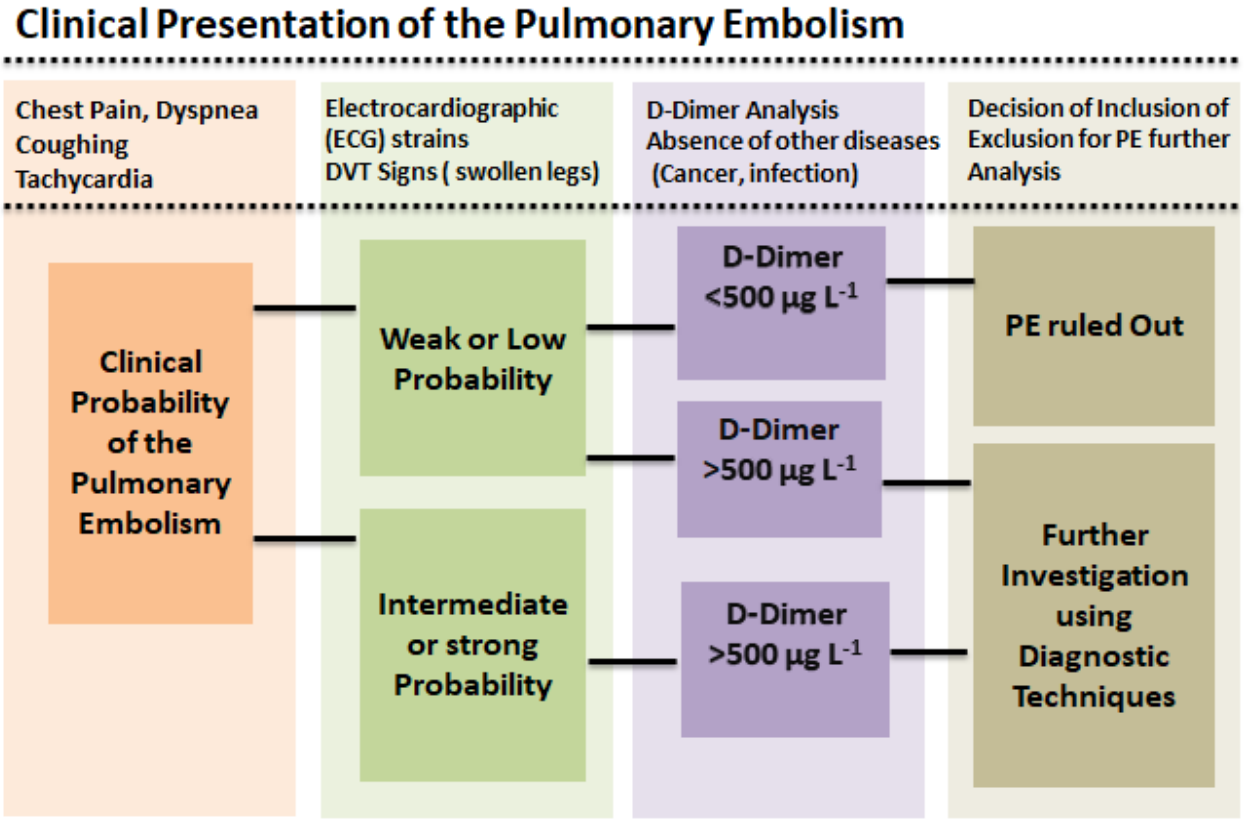

Figure 20 Clinical presentation of pulmonary embolism

In case of atrial seventh defect, it may be hypoxia that were previously closed open and cause important cardiac shunting [91].

Dyspnea (80%), Tachycardia (68%), and chest pain (58-66%) are the most prominent medical symptoms observed in pulmonary embolism (Table 4). These signs are however not specific and can be compared in suspected PE patients who have been removed from their diagnosis. For example, hypoxaemia is frequent, but ≤ 40% patients have normal values of arterial oxygen saturation (SaO_2) and 20% patients have normal levels of alveolar arterial oxygen gradient.

Table 4 Signs and symptoms of patients suspected of PE [92-94]

Symptoms and Characteristics	PE patients incidence
Chest pain	58–66
Coughing	43
Dyspnea	80
DVT signs (red and swollen lower limb, pain on palpation)	35-47
Heart strain signs on right-side electrocardiogram	35–47
Hemi-diaphragmatic elevation on chest radiograph	21
Hemoptysis 6–13 Neck vein distension	30
Hypoxia (PaO2 <80 mmHg)	21
Lung auscultation crackles	68
Loud P2 (pulmonary valve closure sound) 2 Abbreviations	21
Pleural effusion on chest radiography (circulatory collapse)	20
Sounds of breathing decreased	21
S1Q3T3 on electrocardiogram	2-15
Tachycardia (>100 beats per minute)	68
Tachypnea (>20 breaths per min)	26-37

Certain other medical signs including temperature over 38.5°C, tachycardia, tachypnea, hemoptysis and shock can direct the diagnosis without being able to express so much [95].

Nevertheless, all medical signs are included in assessing a clinical likelihood for PE [92]. On this basis, some medical prevision score was developed now regarded as pre-test, the wells and Geneva score being the most confirmed and recognized [96]. These results are comparable [97] and the same as an estimate of a clinician with a reproductive advantage [98]. They cannot confirm PE but they established almost two classes, with low probability and the other with high likelihood of PE [99]. These findings include history and physical examination information but also for the Geneva score, more analysis of evidence (arterial blood gases, chest X-Ray) and the alternate treatment less likely to be PE in the Wells score (Table 5). These elements seem similar to the weaknesses of both scores because the above-mentioned two additional tests are not always available in practice for any given patient and the last item in the Wells score strongly depends on the clinician's degree of knowledge [99].

A prospective diagnostic study called PECAN (Diagnosing Pulmonary Embolism in the context of Common Alternative diagnoses in primary care) is carried out at Dutch Institute of primary care. Patients involved in this study were having suspected acute PE and managed according to YEARS diagnostic algorithm. Patients carefully excluded for PE on the basis of their history, physical examination, and negative D-dimer test. Nevertheless, mostly D-dimer test results are false positive, causing several ‘unnecessary’ referrals in the secondary care. So novel YEARS algorithm is introducing the flexible validated thresholds of D-dimer depends on the results of pretest risk, is capable to safely rule out PE. Notably, by fixing threshold of D-dimer it was

accompanied 14% less CTPA than the standard. This algorithm even though promising yet not validated [100].

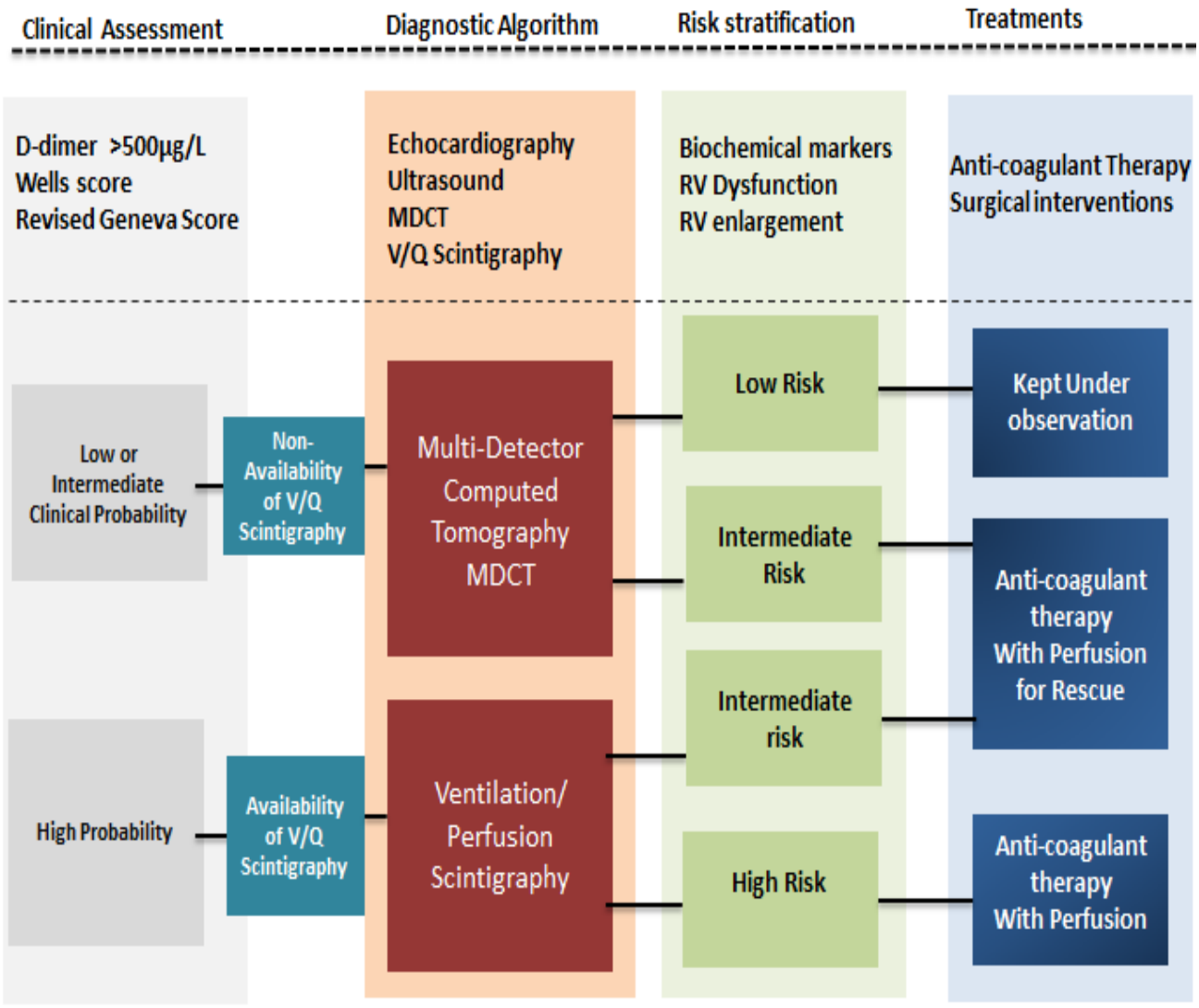

Figure 21 Pulmonary embolism suspected patients with >500 µg/L presented for further analysis

Biologically, D-dimer, which are specific products of fibrin degradation, their amount may rise in cases of acute VTE up to levels equal to eight times the normal [101]. The existence of quantitative tests of high sensitivity may permit, thanks to the excellent negative predictive value

of the test, remove the PE (Figure 20) when the rate of D-dimer is less than 500 μg.L^{-1} [102, 103].

However, D-dimer rise in many other diseases (cancer, inflammation, infection, surgery, myocardial infarction) or situations (elderly, hospitalization, pregnancy), is limiting greatly the diagnostic utility of the test in these populations.

For the patients with intermediate and strong probability of PE or patients with weak probability yet higher D-dimer >500 μg/L, according to wells score [104] are presented to further diagnosis using diagnostic techniques as described in Figure 21.

Recently a meta-analysis and systematic review compared revised Geneva score and the Wells score. Study indicated that sensitivity range of Wells score is 63.8% - 79.3% and of revised Geneva score is 55.3% - 73.6%. Conclusivly, Wells score seems more predictive as compared to revised Geneva score of suspicious patients to estimate PE [105].

The suspected PE patients directed for further screening are presented for different tests according to their symptoms as for elevated heart rate echocardiography (ECG) and for DVT signs of red or swollen legs, ultrasound of the calf and legs. After these tests, if the Ventilation/perfusion (V/Q) scintigraphy is available the patients are screened through it and if it is not available then multi-detector computed tomography (MDCT) has been employed for screening of PE suspected patients. Mostly the undetected patients of MDCT are presented for V/Q studies for further confirmation. Low or intermediate or high probability PE patients are given anti-coagulant therapy for different time periods and final perfusion study is performed before stopping the treatment as shown in Figure 21.

Table 5 Main pretest score for pulmonary embolism diagnosis (Modified Geneva & Wells Score) [104]

Modified Geneva score		Wells Score	
Factors	**Scores**	**Factors**	**Scores**
Pre-disposing factors		**Pre-disposing factors**	
Age > 65	+1	History of DVT or PE	+ 1.5
History of DVT or PE	+ 3	Recent surgery / immobilization	+ 1.5
Recent surgery <1 month	+ 2	Cancer	+1
Progressive neoplasia	+ 2		
Symptoms		**Symptoms**	+1
Unilateral calf pain	+ 3	Hemoptysis	
Hemoptysis	+ 2		
Clinical signs		**Clinical signs**	+ 1.5
Cardiac frequency		Cardiac frequency	+ 3
> 95 / minute	+ 5	> 100 / minute	+ 3
75 - 94 / minute	+ 3	Signs of DVT	
Pain palpation and uni-lateral edema	+ 4	**Lack of differential diagnosis**	
Clinical probability	**Total**	**Clinical probability**	**Total**
Low	0 - 3	Low	0 - 1
Average	4 - 10	Average	2 - 6
Strong	≥ 11	Strong	≥ 7

1.3 Imaging Modalities Used For PE Detection

Molecular imaging tools are playing a good role for PE diagnosis especially CT-angiography and ventilation/perfusion (V/Q) imaging [106, 107], showing high sensitivity and specificity [9, 108]. Many scientific studies claimed that V/Q SPECT/CT offered superior diagnostic performance and can be considered as first-line imaging modality in clinical settings especially in patients of chronic kidney disease (CKD) and pregnant women [109, 110]. Other major imaging techniques include MRI and ultrasound, that are not efficient in lungs diagnostics [111, 112]. In ultrasound, due to near total reflection interference of first air tissue, transmitted waves could not penetrate the lung. In MRI, T_2*of the lung tissue is short because of ±5ppm disturbance of magnetic field from outside of the alveoli. Ultra-short-TE and Gadolinium are used to improve MRI imaging but some patients showed CKD contraindications or accumulation in healthy brain tissues [113, 114]. Hence, MRI in lung scintigraphy remains uncommon in clinicians. Magnetic particle imaging (MPI) is an emerging technique using magnetic field of low frequency for imaging super paramagnetic iron oxide (SPIO) particles of high accuracy. MPI possesses ideal imaging contrast due to zero interference from background tissue [115, 116] and can be considered superior to SPECT/CT and CT as free from ionizing radiations [117]. One MPI scanner system has been built and used for imaging but it is not sufficient for clinical translation of the technique so MPI is still an experimental method. In recent years ^{68}Ge/^{68}Ga generator availability has opened up new era of molecular imaging. PET/CT is considered superior to SPECT camera [118] due to rapid imaging (10-20 min) and high spatial resolution with improved image quality and sensitivity. PET/CT has been utilized by some groups for PE V/Q imaging utilizing ^{68}Ga-MAA microparticles intravenous injections [119].

1.3.1 Pulmonary Angiography Computed Tomography (CTPA)

Pulmonary angiography computed tomography (CTPA) is a diagnostic technique to image pulmonary arteries in order to diagnose pulmonary embolism. Pulmonary angiography was clinically introduced in the early 90 [120], and still most popular technique [121]. The first CT having 1 line of detectors, had a limited sensitivity of approximately 70% (30% false negatives) when compared to a combined diagnostic strategy (pretest probability), lower extremity ultrasound, scintigraphy ventilation/perfusion and angiography [122]. This first generation of CT angiography was replaced by multi-detector CTs (MDCT) scanners having 4, 8, 16, 32 or more rows of detectors for the simultaneous acquisition of 4, 8, 16 lines for thinner slices of thickness 1.25 mm. On these devices, i.e. with at least 8 channels, acquisition is rapid (approximately 10 seconds) thereby enabling acquisition in one same apnea in dyspneic patients [123]. MDCT now a days possess ever growing multiple rows of parallel X-Rays detectors, some are exceeding 250 detectors and can rebuild more than 500 slices at a time. In MDCT, every line of detectors is automatically recording data when the gantry rotates. Hence, the patient volume (up to 16 cm) along the longitudinal axis, Z-axis is imaged with 256 detectors at each gantry revolution. Scanning volume can be done without table motion with large area detector scanners and it is very useful for cardiac imaging. The rotating time for the gantry is 0.5 seconds or less [124]. The acquisition can be performed during a single breath to reduce artifacts due to respiratory motion and follow the arrival of the contrast agent in the pulmonary arterial system level after single

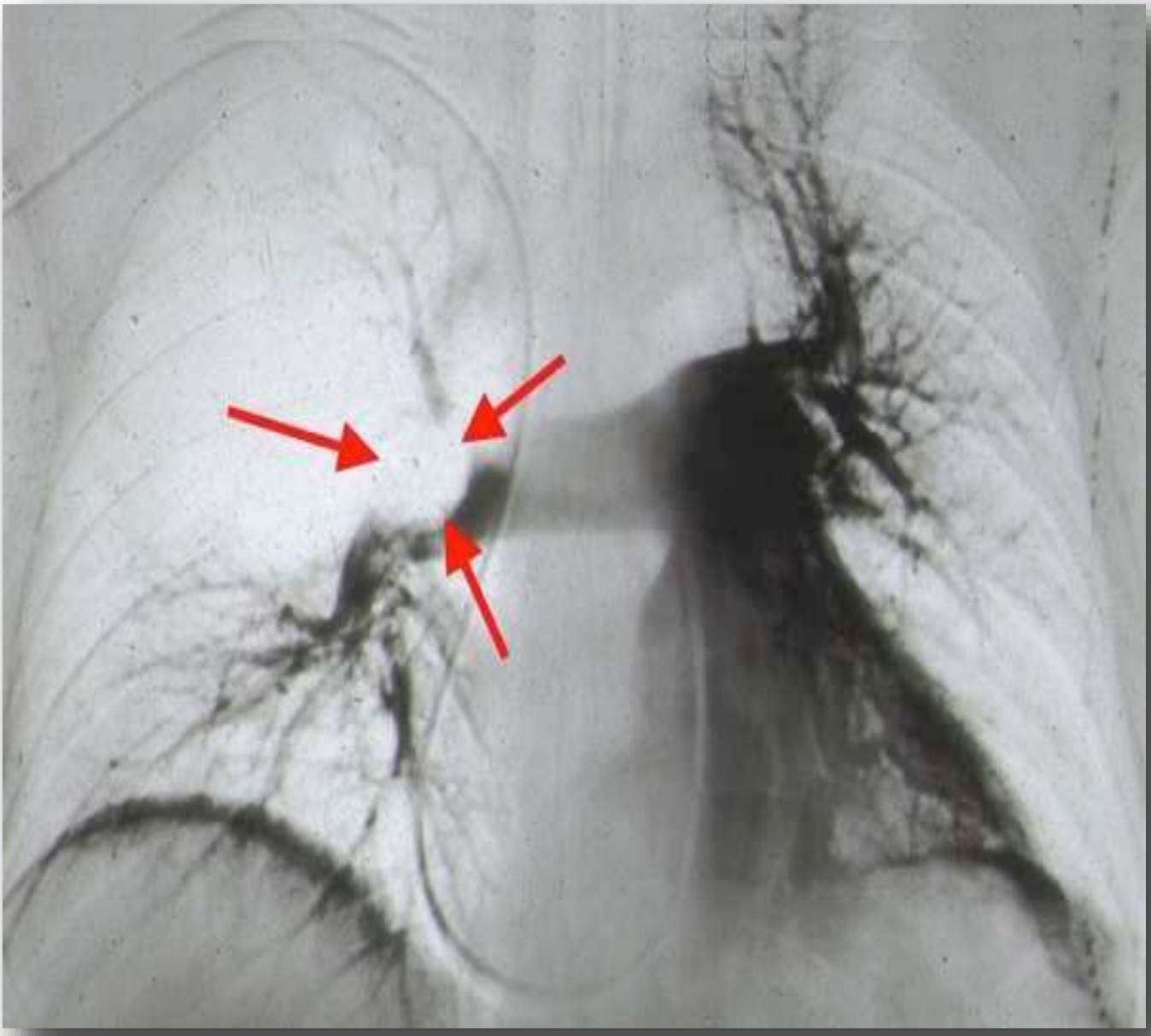

Figure 22 Example of pulmonary angiogram after iodinated contrast agent injection. A pulmonary embolism is in the territory of the artery right upper lobe (red arrows), published from ref. [11].

intravenous injection. Since the scan is fast, contrast agents can be quickly injected to achieve excellent vascular opacity and to reduce contrast agent volumes [125].

Contrast agent is administered through a bolus injection intravenously 5 mL/sec and scanning is started when the scanner shows left atrium or pulmonary arteries to be opacified. Delay between injection start time and scanning is averagely 10-15 seconds for pulmonary artery opacification but longer for left atrium. CTPA scan shows pulmonary vessels as contrast filling, appearing as dark and any defect with mass filling (blood clot/embolism) appearing as white in place of contrast. Scan noise may interfere in large number of patients but slices reconstruction at reduced thickness results in decrease of noise and increase in accuracy. For pulmonary embolism diagnosis slices of thickness 1.25mm at an interval of 1.25 mm are sufficient. Although scanning is executed using thinnest detectors (0.625 mm) because acquiring thin sections offers better visualization of segmental and sub-segmental arteries and thus results in an improved sensitivity of the imaging. Direct diagnosis is made on the intraluminal detection gaps >2 mm [125]. Most studies suggest that pulmonary acquisition of CTA images should be performed during breath-holding [126]. Contrarily some studies demonstrated the acquisitions possibility during free-breathing through high-pitch CTPA [127].

Pulmonary Embolism Diagnosis-II (PIOPED II) investigations had evaluated the use of scanners 4, 8 and 16 channels in 824 PE suspected patients, without D-dimer assay, and found a sensitivity of 83% and a specificity of 96%, that corresponds to a positive predictive value (PPV) of 86% and a negative predictive value (NPV) of 95% [125]. Positive predictive value of the presented study is highly variable depending on the type of PE i.e. 97% for an embolism in the main street or lobar, 68% for segmental embolism and only 25% sub-segmental embolism. This study also highlighted that the changes in PPV and NPV was dependent on clinical probability of the PE (Wells score). Among the people with high clinical probability (Wells score above 6), PPV and NPV was 96 and 60% respectively, and corresponded to 40% of false negatives. For

patients with intermediate clinical probability PPV and NPV were 92 and 89% respectively. Finally, for patients with low clinical probability (Wells score <2), PPV and NPV of 58 and 96%, respectively and almost 42% of false positives [125]. Moreover, it is often criticized for pulmonary angiography for its low inter-observer concordance, returning to the PIOPED study the sub-segmental arteries reproducibility between two observers is 66% only [125].

A prospective study was conducted first time on the simultaneous comparison of diagnostic performance of V/Q SPECT, pulmonary CT angiography and SPECT/MDCT scanner in suspected PE patients. A study performed in Frederiksberg Hospital, Copenhagen, Denmark. The data based on 81 patients of suspected PE, showed that accuracy, sensitivity, and specificity was 91%, 97%, 88% for V/Q SPECT analysis, respectively, and for MDCT 88%, 68%, 100%, respectively and for V/Q SPECT/CT 99%, 97%, 100%, respectively. Consequently V/Q SPECT/CT showed superb diagnostic capability without using contrast enhancement [128].

After reviewing various studies, the diagnostic ability of CT-angiography varies depending on the patients studied. A meta-analysis including three studies involving over 2,000 patients with clinical probability of intermediate or high PE (Wells score >6), showed higher NPV (98.8%) [129]. New approaches in pulmonary CTA data acquisition, post-processing and evaluation, boost quality of image, and enhanced accuracy, as well as improved assessment in the management of patients and their prognosis [127]. Dual-source CT (DSCT) and high-pitch pulmonary CT Angiography scanners permit high-quality image acquisition. DSCT possess two X-Ray tubes arranged at 90° to each other that allow double energy acquisitions and offer new and exciting opportunities for lung scanning [130]. DSCT acquires two data sets at different levels of X-Ray energy [120, 131], (140 & 80 kVp) for a differentiation of the material according

to the densities of the same acquisition and can exploit the distribution of iodinated contrast material in pulmonary perfusion [120, 132]. DSCT offers improved temporal resolution and quality of image at reduced radiation dose and consequently decrease in artifacts motion in patients who could not hold breath.

Dual energy maps of perfusion due to material differentiation may offer advance prognostic and functional information than basic assessment of luminesce in pulmonary arteries. These mono-energetic images either provide a rescue from a sub-optimally scheduled contrast agent or reduction in the dose of contrast agent [127, 132, 133]. Furthermore, dual energy mapping of perfusion seems like wedge shaped defects corresponds to acute setting finding of scintigraphy [134] and in the follow-up of acute PE patients, perform SPECT scanning to detect pulmonary embolism [134, 135].

The continumous improvement and development in the hardware of CT system would offer reduced radiations and contrast agent as well as with improved quality of images [127, 136]. Strategies for dose reduction include modulation of tube current, high-pitch imaging modes, selection of tube voltage, adjustment of scanning range, Iterative Reconstruction (IR) and applications of reduced or optimized CTPA contrast agent injection protocols [137-139]. Lowering the voltage of tube for CT [140-143] is accompanied with increment of image noise. If we correlate it with virtual mono-energetic images, lowering the tube voltage results in higher iodine attenuation, due to decrease tissue penetration and high photoelectric effect associated with low energy X-Rays, results into high contrast that causes subsequent decrease in the volume of contrast material [144, 145]. Iterative Reconstruction (IR) is used to reduce image noise and artifacts, hence it could allow to maintain the image quality at reduced dose [146]. For examples

CTPA of high pitch (80-kV) having IR would decrease 50% dose of radiation, maintaining the image quality [147]. Numerous studies has validated that acquisitions with a system using low-tube-voltage, and high-pitch with IR, showed results of considerable decrease in the radiation dose with no compromise on image quality [147-149]. Utilizing this combination pulmonary examinations could be performed <1 second, using 20– 40 mL of the contrast agent [147, 150, 151] as well as could provide diagnostic imaging with <0.1 mSv for selected patients [148]. Due to limited output current of X-Ray tube it is unable to generate sufficient photons for obese patients thus DSCT second-generation has been utilized for them. Improvements in prognostication and in stratification of risk will offer additional upgrade CTPA assessments in the clinics [152].

1.3.1.1 Limitations of CTPA Modality

As computed tomography pulmonary embolism (CTPA) diagnosis utilize iodinated contrast media that is linked with contraindications some of them are described here.

1.3.1.1.1 Thyroid Dysfunction (Hyperthyroidism or Hypothyroidism)

Iodinated contrast media may induce hyperthyroidism or hypothyroidism (rarely). In geographical region where people are iodine-deficient, patients (2%) might develop hyperthyroidism [153, 154]. 0.25% of unselected patients show hyperthyroidism cases in 12 weeks [155]. Thyrotoxicosis induced by iodine in the elder people [156], may cause thyroid storm and cardiac arrest, if the case become worst [156]. Risks associated with Graves' disease/thyroid autonomy are potentially undiagnosed [157]. Thyroid storm patients should not be given iodinated contrast media and premedication of thiamazole might be helpful. Thyroid function should be monitored regularly through serum base line TSH measurement.

1.3.1.1.2 Iodine Hypersensitivity (Rare Cases)

Very rare pseudo allergic reactions of severe nature may occur, approximately 0.04%, which are seldom fatal. Premedication is advisable when CT is not used in an emergency scenario.

1.3.1.1.3 Renal Dysfunction: Complication Associated with CTPA

A CTPA severe complication is the contrast-induced acute kidney injury (CI-AKI) or contrast media-induced nephropathy (CIN). CI-AKI is a condition in which serum creatinine is increased after 48 to 72 h of iodine contrast agnet IV injection and it can cause renal chronic inadequacy and death [158, 159]. The hypothesis of connection between acute kidney injury (AKI) and IV iodinated contrast agent is challenged in some publications, but the data presented is controversial. A retrospective cohort study carried out at a single-center, showed that ratio of AKI development in three groups: 10.6% in contrast-enhanced, 10.2% in unenhanced and 10.9% in non-CT group [160]. Meta-analyses studies showed that contrast-enhanced and non-contrast-enhanced CT scans were not associated significantly with AKI [161, 162]. The third common cause CI-AKI observed is the hospital acquired AKI [160], it is multifactorial entity with >1 risk factor such as nephrotoxic drugs, contrast media, hypertension, diabetes mellitus, cardiac out-put reduction etc. [163].

1.3.2 Single Photon Emission (CT) Scintigraphy

Since its introduction (1960), ventilation perfusion (V/Q) is widely utilized to evaluate the patients of suspected/ known PE [164]. V/Q scanning was the selected method until 1990s in suspected PE patients. Conversely, large number of Prospective Investigation of Pulmonary Diagnosis (PIOPED I) studies showed confused probabilistic criteria for clinicians and thus high ratio of non-diagnostic assessments (65%) [165]. Later on Palmer *et al.* developed an algorithm for the calculation of quotient of ventilation and perfusion i.e. V/Q quotient images and it led to the quantitative V/Q SPECT. Bajc *et al.* verified that this methodology is superior to planar imaging showing superb inter observer agreement for sub-segmental defects in porcine PE model [166]. A number of articles have explained that SPECT and SPECT/CT demonstrated high sensitivity and specificity along with decreased radiation exposure [117, 167-170]. Therefore V/Q scintigraphy is the selected diagnostic test for many patients, including young and pregnant women, to avoid high radiation dose to breast and to enhance imaging accuracy in pregnancy [171-175]. V/Q SPECT imaging played a well-defined role both clinically and for research purposes. Voxel level V/Q information allowed V:Q matching ar regional lungs level (Figure 23). With co-registration, 3D V/Q dataset can be employed to obtain V:Q ration, fusion of CT and functional imaging, degree of deficit of perfusion relative to ventilation in pulmonary embolism patients.

Many research groups demonstrate the high values of specificity and sensitivity of V/Q SPECT/CT [117, 168, 170, 176] and can be considered as the first-line diagnostic modality to diagnose pulmonary embolism [177].

Lungs vascular system begins in right ventricle of heart, starting from the pulmonary artery that divides in two parts; right and left pulmonary arteries, which carry blood to lungs. Pulmonary arteries give to rise to branches to follow the bronchial distribution until the alveolar plexus. At the alveolar level after exchanging the respiratory gases, alveolar capillaries carry back the oxygenated blood in the left atrium of heart through pulmonary veins.

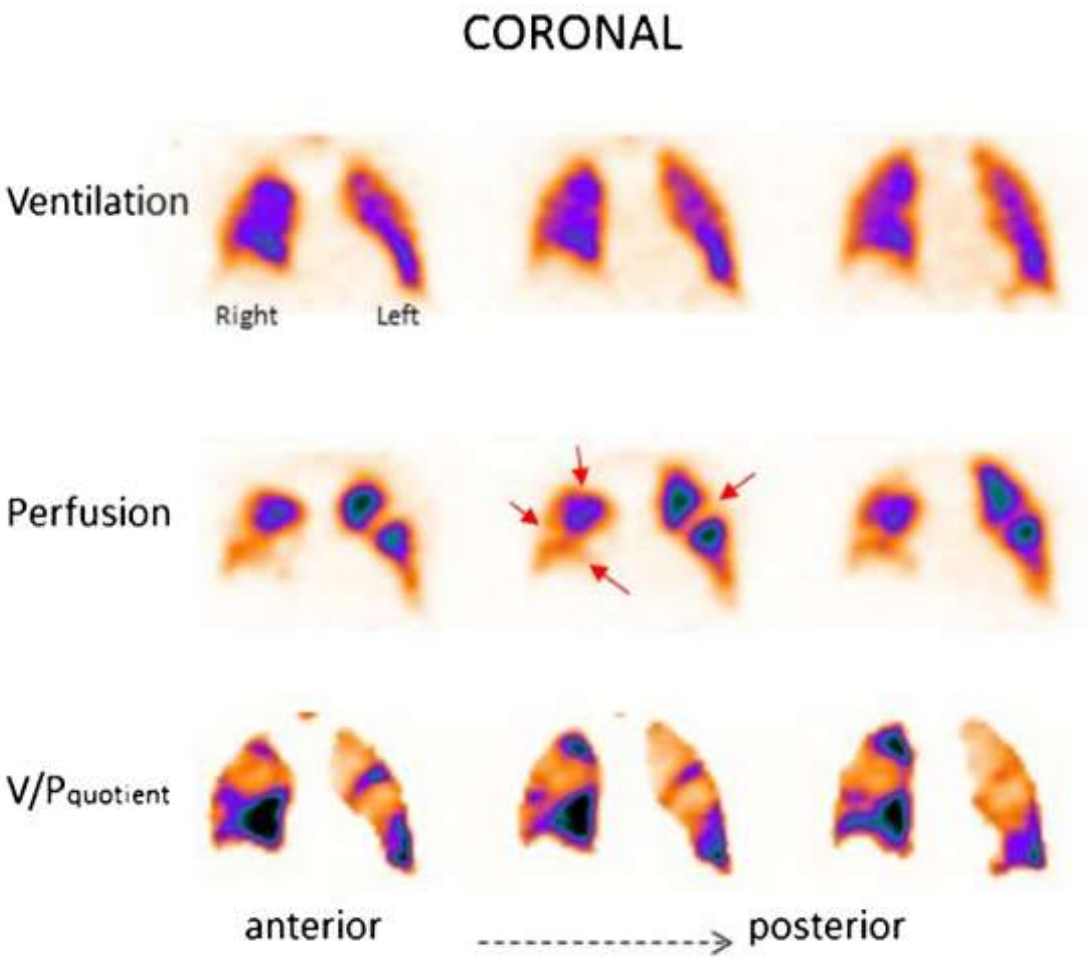

Figure 23 Coronal slices in a patient with PE. Multiple bilateral segmental perfusion defects (red arrows), are seen in areas with normal ventilation. These are delineated on V/Q quotient images which facilitate interpretation. Published from ref. [178]

Perfusion defects are the result of emboli which confirm anatomical distribution in lungs vasculature. Perfusion defects are lobar, segmental and sub-segmental in character. Perfusion

scans exploits the distinctive segmental anatomy of pulmonary arterial bed. Each segment (broncho-pulmonary) obtain blood supply from a single artery (Figure 24). The apex of each conical bronchopulmonary segments is towards the hilum and the base projection towards the pleural surface. Thrombous occlusion is disturbing the specific pulmonary artery consequently producing a characteristic subsegmental, segmental or lobar minor defect of wedge-shape mismatch between ventilation and perfusion and base projecting to the periphery of lungs (Figure 23, Figure 25). The materials used in routine for lung ventilation and perfusion (V/Q SPECT/CT) analysis include inert gases/aerosols and macroaggregates of albumin respectively as described here.

1.3.2.1 Lung Ventilation Scintigraphy

For regional ventilation mapping, following inert gases are used:

1.3.2.1.1 ^{133}Xe Ventilation Imaging

^{133}Xe is known historically as ventilation agent [32, 33]. Its half-life is 5-days that allow regional ventilation studies. Simple technique of single-breath is used mostly as explained in PIOPED-I study [34]. In the first 20s of inhalation of ^{131}Xe, one posterior view image is acquired. Inadequate information is received from the anterior parts of lung because ^{131}Xe (81 keV) has low energy. Often perfusion defects due to obstruction are considered as the mismatch, sometie leading towards false-positive results of PE [35]. ^{133}Xe availability is limited in Europe therefore seldome utilized to detect PE.

1.3.2.1.2 ^{81m}Kr Ventilation Imaging

^{81m}Kr is a gas produced from generator of rubidium (^{81}Ru) [36], with an ideal half-life (13s) and 193 keV gamma energy. Due to short half-life the ^{81m}Kr disappearance via decay is quicker from

the alveolar space than the exhalation process. The inhalation of the ^{81m}Kr during normal breathing rate is approximately proportional to the lungs regional ventilation. In lung compartments, deviance is from proportionality to very low or high regional ventilation relative to the local volume in alveoli [37]. It happened mostly in children (38). Through ^{81m}Kr ventilation steady-state, SPECT acquisitions or multiple planar imaging is feasible and recently,

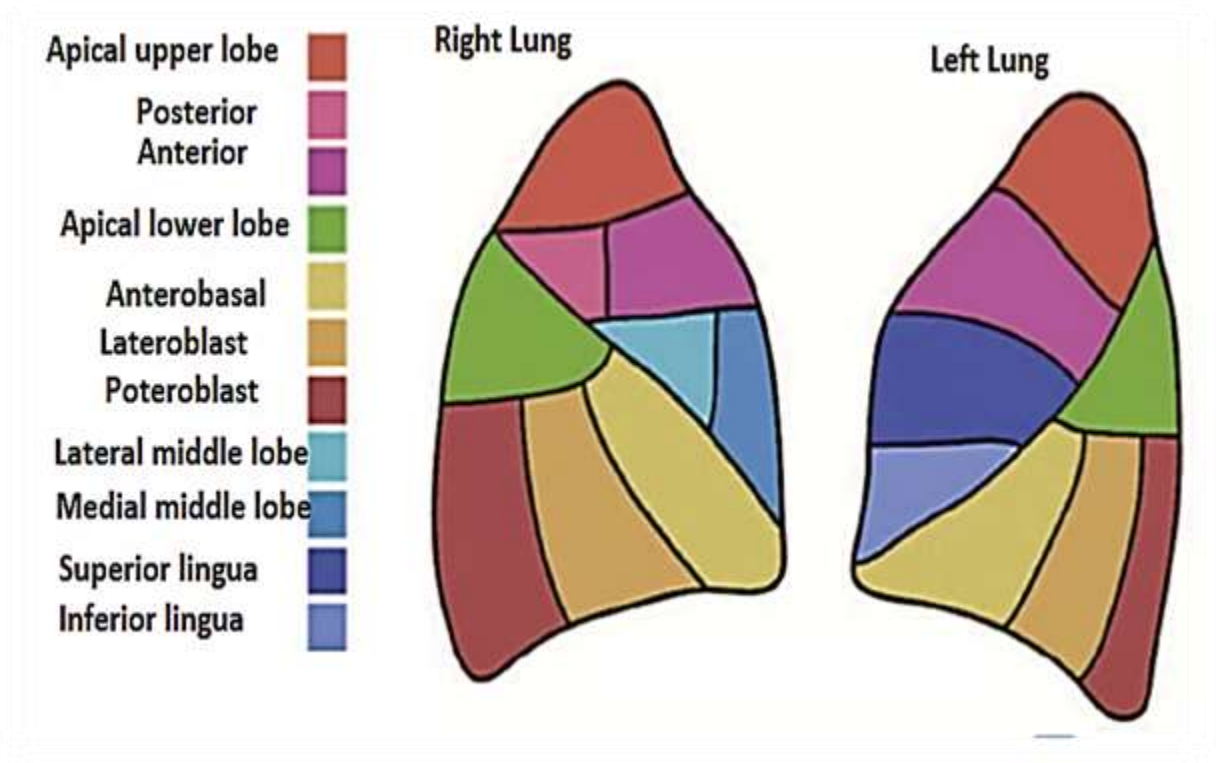

Figure 24 Regions of lungs shown in different colors, each receive blood from different artery

V/Q SPECT/low-dose CT is also possible [39]. ^{81m}Kr gas due to its deposition of airway does not cause any effect thus allowing ventilation and perfusion imaging simultaneously because ^{81m}Kr possesses higher gamma energy as compared to ^{99m}Tc (140 keV) a perfusion marker [40–42]. Half-life of ^{81}Ru is 4.6 h while generator life is only 1 day. Therefore high cost, need of daily new generator and limited access elucidates, why ^{81m}Kr is not commonly used. Though, ^{81m}Kr

still is an important substitute of aerosols mostly appropriate in children because of associated low radiation dose to the patients [38].

1.3.2.1.3 Radio Aerosols for Ventilation Imaging

Radio-aerosols are frequently used for the ventilation scintigraphy as it is two-phase system, comparatively time-stable that comprises suspended particles in the gas. These radio-labeled aerosols could be either a liquid or solid or mixture of both phases. After inhalation, deposition fraction, particles percentage in lungs depends mainly on their aerodynamic properties. With ultrafine nanoparticles (diameter 0.02µm), deposition fraction is almost 50%. These are deposited by diffusion mechanism mainly in alveolar region [43]. Deposition fraction reduces to 25% when the size of nanoparticles increases to 0.1 µm [44]. When particles size is 0.45 µm, it showed lowest deposition fraction [43] as this size is predominantly stable due to diffusion and sedimentation. The fine particles are capable of penetration in the alveolar region [45]. Impaction is the second deposition mechanism i.e. particles larger tha 1µm occurs in lower part respiratory region, particles larger than 5 µm in the upper part respiratory region, and smaller particles at stenosis with a turbulent flow. It results into hot spots, investigative of disease of obstructive airway. The pattern of breathing is important to deposit aerosol [46] i.e. with slow tidal breathing pattern larger particles can reach to the lungs periphery [47]. Various nebulizers are available in the market which can produce liquid aerosols. Mass median aerodynamic diameter (MMAD) of droplets should be of lowest possible size i.e. inhaled droplets would not surpass 2 µm. ^{99m}Tc-labeled diethylene amine pentaacetic acid (^{99m}Tc-DTPA), commonly used as liquid aerosol which is cleared by trans-epithelial diffusion from alveolar region [52]. It has a vriable biological half-life such as in healthy non-smokers 80±20 min, healthy passive smokers 45±8 min and in healthy smokers 24±9 min [53].

^{99m}Tc-DTPA is eliminated through kidneys glomerular filtration process. ^{99m}Tc-DTPA pulmonary clearance rate reflects the integrity of epithelial membrane of alveolar region [53, 54]. If clearance is at increased rate it results into shorter half-life which happens to alveoli inflammatory activity for example alveolitis (toxic or allergic nature). ^{99m}Tc-DTPA can be used for diagnostic purpose using scintigraphy (planar or tomography) to evaluate its clearance [55, 56]. During disease a continuous 20–45 min recording permits a comprehensive analysis to evaluate biphasic clearance [57–59].

An aerosol called Technegas is containing very small size ^{99m}Tc-labeled graphite particles that are produced at a high temperature [60, 61]. They are hydrophobic with diameter between 0.005–0.2 μm [62], conversely grown through aggregation process, and must be utilized within 10 min. It has been used in the field of nuclear medicine imaging past 30 years. Technegas is considered ideal agent for lung ventilation imaging with desirable small particle size. After inhaling, they penetrates further in the conducting airways then "sticks" to the airway lining [179] therefore static distribution of particles is greatly attractive and suitable in planar or SPECT scanning. From the alveolar region, graphite particles are slowly passed through the process of resorption. It has 135 h biological half-life [63] and produced analogous information during ventilation studies to ^{81m}Kr [64–68]. Technegas particles bear exceptionally small burden inside the lungs and equivalent to 50 μg of carbon soot and it is 100 times below compared to daily allowable particle pollution limit of vehicle exhaust. Conversely, during airway obstruction ^{99m}Tc-Technegas ventilation produce very rare hot spots. Inferring, ^{99m}Tc-Technegas proved clinically as the finest liquid aerosols [66, 69].

1.3.2.1.4 Lung Perfusion Scintigraphy

The theory of pulmonary perfusion imaging is the use of radioactive microparticles that are carried by the bloodstream after intravenous injection and distributed to the body depending on several factors, including their weight, patient posture during injection (sitting or supine) and loco-regional blood flow [180]. The microparticles will travel through the right heart during their journey and meet the arterial pulmonary circulation before being first encountered by the capillary arteriolar surface [45]. A temporary micro-embolization is created in the lungs at capillary level to accomplish perfusion scintigraphy study. The theory of pulmonary embolism scintigraphy diagnosis is based on the visualization of the absence of perfusion in the some section of certain lung segments opposite to normal ventilation (i.e. mismatch or inconsistency). Intrapulmonary reflex mechanisms of the lungs determine the complex tuning for ventilation/perfusion. Along with other factors, gravity also plays a vital role for blood distributed within lungs; therefore, during healthy situations, in upright position, a physiologic gradient is observed in perfusion of lungs from the base towards apex and during supine position from back towards front (Figure 24). In certain conditions, such as during pulmonary hypertension, physiologic gradient is altered thus representing a significant diagnostic criterion for lung perfusion scintigraphy. That's why patient's body position is important to record during the injection of radiotracer. Imaging is preferable to perform in patients, in upright position to minimize diaphragmatic motion and to increase chest cavity size. Images could be acquired in patient with decubitus or supine position. Macroaggregates of albumin (MAA) radiolabeled with ^{99m}Tc are the gold standard for lung perfusion scintigraphy. For this purpose commercially available MAA kits of particle size (15-100 µm), radiolabeled with ^{99m}Tc are injected into the peripheral vein. Distribution of particles defined the regional lung perfusion keeping in mind that

the number of particles should be at least 60,000 to attain their uniform distribution for the clear reflection of area under investigation [181].

In general, almost 400,000 particles are administered bearing in the mind more than 300 million, and 280 billion of pre-capillary arterioles and pulmonary capillaries in human lung, respectively. Thus this quantity i.e. 400,000 particles could cause obstruction of an insignificant portion of the lungs vessels. In patients of pulmonary hypertension or transplantation of single lung or heart shunt, a more reduced quantity of MAA particles (100,000-200,000) is recommended. In infants and children, particles number is further reduced according to their weight [182]. Imaging starts with ventilation scan using aerosols, then instantly followed by perfusion scan. After extensive analysis; the principles are developed to optimize doses of radioactivity, relationship of scanning time and activities for V/Q, collimator, number of rotations, size of matrix and reconstruction algorithm of images [183]. Generally, for V/Q imaging, 25–30 MBq and 140–160 MBq radioactivity; a general-purpose collimator; 60–64 rotations; matrix size 64 × 64 and dual head gamma-camera 120–128 projections are employed [183, 184]. Projection time should be 10 seconds and 5 seconds for ventilation and perfusion respectively. Low-energy high-resolution (LEHR) collimators require higher activities or longer acquisition times. During the entire image acquisition period patient position remain similar in order to compare ventilation and perfusion. Images are presented in the standard software which allows projections in coronal, sagittal and transverse and 3D images. Primary images are exploited to derive quotient V/Q images [183, 184]. For identification of V/Q matches and mismatches and to calculate quotient V/Q images, V/Q images should carefully aligned to each other (Figure 23).

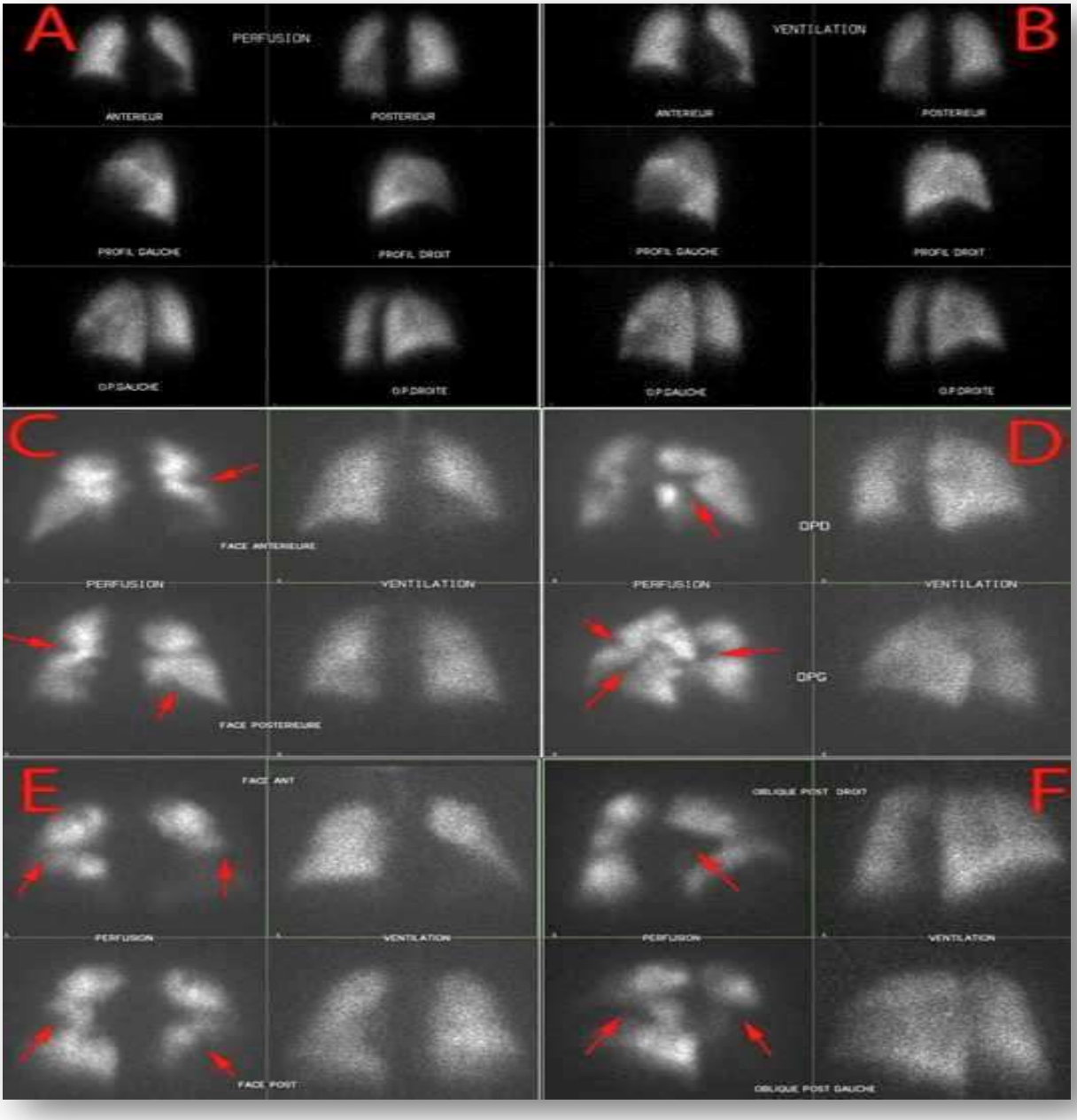

Figure 25 Examples of scans of ventilation perfusion planar mode. In a normal patient (Acquisition A and B) and two patients with pulmonary embolism (Acquisition C, D and acquisition E, F), published from ref. [11]

1.3.3 PE Management in Pregnant Patients

To diagnose pulmonary embolism (PE) in pregnancy poses unique circumstances and it is about five fold high than non-pregnant females of same age. The PE incidence during pregnancy is leading to non-obstetric reason of females deaths in the developed states. In pregnant women, PE and DVT incidence is approximately 1 and 3 %, respectively [185] and analogous in all 3 trimesters [186]. The accuracy of diagnostic tests are comprised of low PE prevalence [187, 188]. D-dimer is not helpful as it is raised during the period of pregnancy [189]. CTPA produced non-diagnostic results because of hemodynamics changes [109, 175, 190-192] as well as it bears hazards of high radiation. In order to avoid irradiation, Ultrasonography venous compression could be performed, though with low diagnostic yields [193]. V/Q SPECT can be a method of choice and to minimize radiation, 2-day protocol with Perfusion-only SPECT (^{99m}Tc-MAA, 50MBq) is performed on day 1; and due to low incidence ratio, PE is excluded usually in pregnant women (normal perfusion pattern) [186]. Anticoagulation therapy is initiated if perfusion pattern are found abnormal so on day 2, ventilation study would be performed, utilizing the lung-deposited activity (20–30 MBq). Using this strategy high specificity is obtained and sensitivity [145, 147] and after first trimester, V/Q SPECT one-day protocol woul be employed again.

Probabilistic reporting studies indicated a larger number of non-diagnostic reports in planar imaging (PIOPED-I) but on the contrary, V/Q SPECT is related to very few number of non-diagnostic reports.

According to EANM guidelines (2009), diagnostic cut-off for V/Q SPECT for positive PE, would be 1 or 2, segmental or subsegmental mismatch defects respectively, and this fact is further supported by other studies [194-196]. European Society of Cardiology (ESC),

recommendations of individualized approach is helpful to manage patients conservatively, and if deep vein thrombosis presence is excluded [197]. Patient with Wells score more than 4, possess 4-fold greater risk of having one or multiple emboli in the sub-segmental arteries [181].

The study of >5000 V/Q SPECT case reports interpretations, for pulmonary embolism diagnosis has shown 97–99% negative predictive value (NPV), 96–98% specificities, and 96–99%sensitivities. While non-diagnostic findings rates were 1–4% [168, 194, 195, 198-205].

V/Q SPECT also carries a low radiation burden to patient therefore suggested for pregnant women especially to avoid the exposure of breast (most exposed portion). With recommended activities, the total the effective dose for ventilation and perfusion is 2 mSv. This is quite low as compared to CT whose approximated effective doses is more than >5 mSv [206-208].

A meta-analysis and systematic literature review showed radiation for ventilation Perfusion SPECT exposure of 2.12 mSv compared to 4.96 mSv for CT pulmonary angiography [209]. Radiation doses in routine clinical scans found between 3.5-13.2 mSv for CTPA [206]. CT dose index from average doses to effective doses depends on many factors and varies among different facilities, such as patient weights, diameter of chest, and institutional protocol choices [206]. Generally effective doses are >5 mSv [206-208], In CTPA, female breast is the critical organ with radiation doses between 8.6-44 mSv [201, 210, 211]. Current CTPA variation decreased breast doses to 8.6-51.5mSv [211]. While V/Q SPECT radiation dose is < 1 mSv to the breast of female [201] . Fetal doses are very low and similar in both techniques [201, 210, 212].

1.3.4 Positron Emission Tomography (CT) Scintigraphy

In this modern era molecular imaging and particularly Nuclear Medicine have experienced an enormous revolution, along with the development of newer isotopes, and techniques such as positron emission tomography CT (PET/CT). It offers an opportunity to improve V/Q imaging in patients suspected of PE with reduced time of acquisition as well as retaining advantages of V/Q scanning over CTPA such as reduction in radiation, and no contraindication of iodinated contrast agent. [213, 214], and regional lung function assessment [214], evaluation of patients for the pre-surgical process for bronchoscopic lung volume reduction [215] and evaluation for pulmonary resection [216].

Thus PET is superior to traditional SPECT; carrying advantages, such as small acquisition time, greater sensitivity, high temporal and spatial resolution, as well as quantitative measurement capability [193, 217, 218]. ^{68}Ga an equivalent generator prepared carrier molecule of ^{99m}Tc has already substituting it in many nuclear medical application [219, 220] and now V/Q imaging on PET can be performed using Gallium-68 radionuclide for perfusion and ^{68}Ga-labelled equivalent of Technegas (Galligas) for ventilation.

The technique could be readily implemented for SPECT V/Q imaging with Technegas familiar people in clinical settings. Radiotracers preparation and acquisition of data are not very complicated. PET advantages also include its ability to obtain dynamic imaging, 3D data acquisition and measurement of regional changes in the alveolar permeability. Hence, PET V/Q imaging allows exceptional quality functional images.

A group has reported PET ventilation imaging for potential examination to produce pseudo ventilation images of respiratory-gated 4-D X-Ray CT [221, 222].

Additionally, functional parameters, like lobar function or regional V:Q matching, better signal-to-noise ratio, superior quality of V/Q PET images would be a crucial advantage over V/Q SPECT. Moreover, PET's ability to carry out 2 separate scans of ventilation on the same day is quite interesting feature for the researchers, subjects, and respiratory physiologists. PET/CT can play a preferable role for clinical and research applications if new chelating agents are designed which can bind with ^{68}Ga through fast and facile methods.

1.3.4.1 Lung Ventilation Scintigraphy

^{68}Ga-labeled equivalent of Technegas known as "Galligas" is produced for ventilation PET/CT lungs imaging [219, 223-226]. However, the optimization for the number of particles is compulsory in conditions of lungs vascular reserve such as pulmonary hypertension.

Technegas is described in detail in the previous section number: 1.4.2.1.3. Galligas could be prepared in a standard, unmodified Technegas generator. A small amount (~200 MBq), of the gallium chloride obtained from germanium-gallium generator, is added in the carbon crucible of Technegas machine along under standard heating protocol as used for technetium. Additional radiation precautions are required as the lead shielding of Technegas generator is appropriate for ^{99m}Tc (140 keV) and therefore PET radionuclide (511 keV) photons need more precautions for the staff such as increase in distance and decrease in time, due to greater radiation exposure in the preparation of Galligas. Along with excellent image quality of ventilation, conspicuous "rind" effect was observed due to enhanced concentration of radioactivity at the lungs posterior, which may be caused by microatelectasis i.e. lung is compressed under gravity at supine position, resulting an increase in count density [227, 228], [229].

1.3.4.2 Lung Perfusion Scintigraphy

^{68}Ga-labeled microspheres were used for perfusion imaging in the same way as ^{99m}Tc. With only difference is the short half-life of the radionuclide, so ventilation contribution (shine through) was not present in the subsequent perfusion as seen in ^{99m}Tc. Some authors reported to use reduced amount of radioactivity with ^{68}Ga-MAA [229]. ^{68}Ga-macroaggregated of albumin (^{68}Ga-MAA) has been used to perform perfusion imaging

About 40 years ago, the first report was published on lungs scanning using ^{68}Ga PET from Massachusetts General Hospital by Hnatowich and Chesler. They injected ^{68}Ga-albumin microspheres intravenously in dogs and obtained pulmonary perfusion images. This study suggested the possibility to perform lung perfusion scanning in humans using small amount of radioactivity ~20 MBq. Afterward groups performed radiolabeling albumin with ^{68}Ga using different chelators in order to enhance radiochemical purity and yields [230]. Mintun and Schuster, injected intravenously^{68}Ga-transferrin; and studied labeled proteins flux through lungs endothelium [231, 232]. Pulmonary blood flow derived through PET and volume measurements are used to calculate pulmonary edema and injury of lungs.

1.3.4.3 Clinical Studies

Hoffman performed first clinical study in 2011 by PET/CT using ^{68}Ga-labeled Macroaggregates of albumin and compared its results with the gold standard ^{99m}Tc-labeled macroaggregates of albumin by SPECT/CT. They labeled macroaggregates of albumin with $GaCl_3$ (50 MBq) at pH 6.5 according to a previously reported method [233], and incubated the formulation for 5 min at 70˚C. The study included ten patients suspected of PE. Both techniques produced comparable results while PET produced superior images [229]. Later on different groups labeled macroaggregates with gallium-68 and performed clinical studies [119], [234], [220-222]. The

studies indicated that purification and centrifugation improves the radiochemical purity (RCP) of MAA with gallium-68 and increase in lungs uptake (89% to 97%) and decrease in liver uptake [234]. The studies concluded that ^{68}Ga-labeled MAA utilized small radiopharmaceutical injected dose, mean 2 mSv dose of radioactivity to each patient with enhanced image quality (Figure 26), in small time [235-237]. Siva *et al.* used ^{68}Ga-labeled MAA for 4D-PET/CT lung perfusion studies, and visualized the lung function clearly during radiotherapy [238].

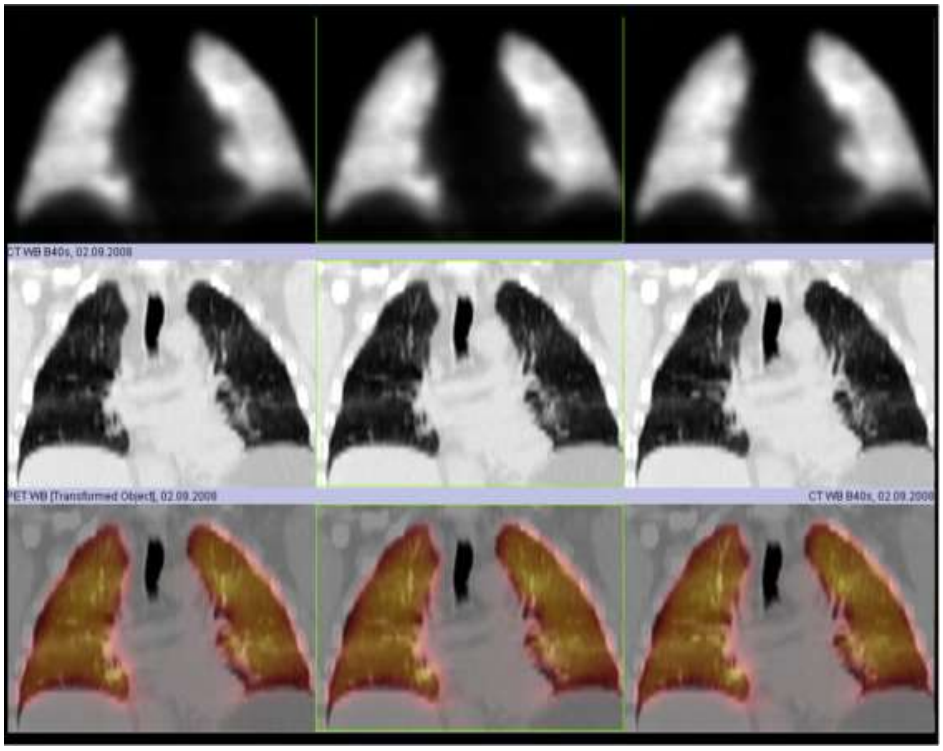

Figure 26 Normal lung perfusion PET/CT in a 54-year-old healthy volunteer obtained after injection of 50 MBq, ^{68}Ga-DOTA-MAA. Coronal view: upper row, PET perfusion image, middle row, CT image, and lower row, PET/CT fusion image, published with permission from ref. [119]

Recently Roux *et al.* performed a study to compare positron emission tomography CT (PET/CT) and computed tomography pulmonary angiography (CTPA) among 24 patients having suspection of PE. Patients were screened for ventilation/perfusion scintigraphy using PET/CT and compared to CTPA screening. Results showed that in 24 patients, 18 showed concordant

results for PET and CTPA tests while 6 patients showed disconcordant results. The joint analysis in 6 patients showed agreement in two cases (Figure 27 B & C). Among four patients, three showed a thrombus of subsegmental nature on CTPA (Figure 27 A). During long term follow-up, two of them had no venous thromboembolic activity and third patient with negative result on PET analysis but positive result on CTPA analysis posed serious complications. So efficacy and possible effectiveness of V/Q PET/CT has equivocal results to CTPA with some discordance [239].

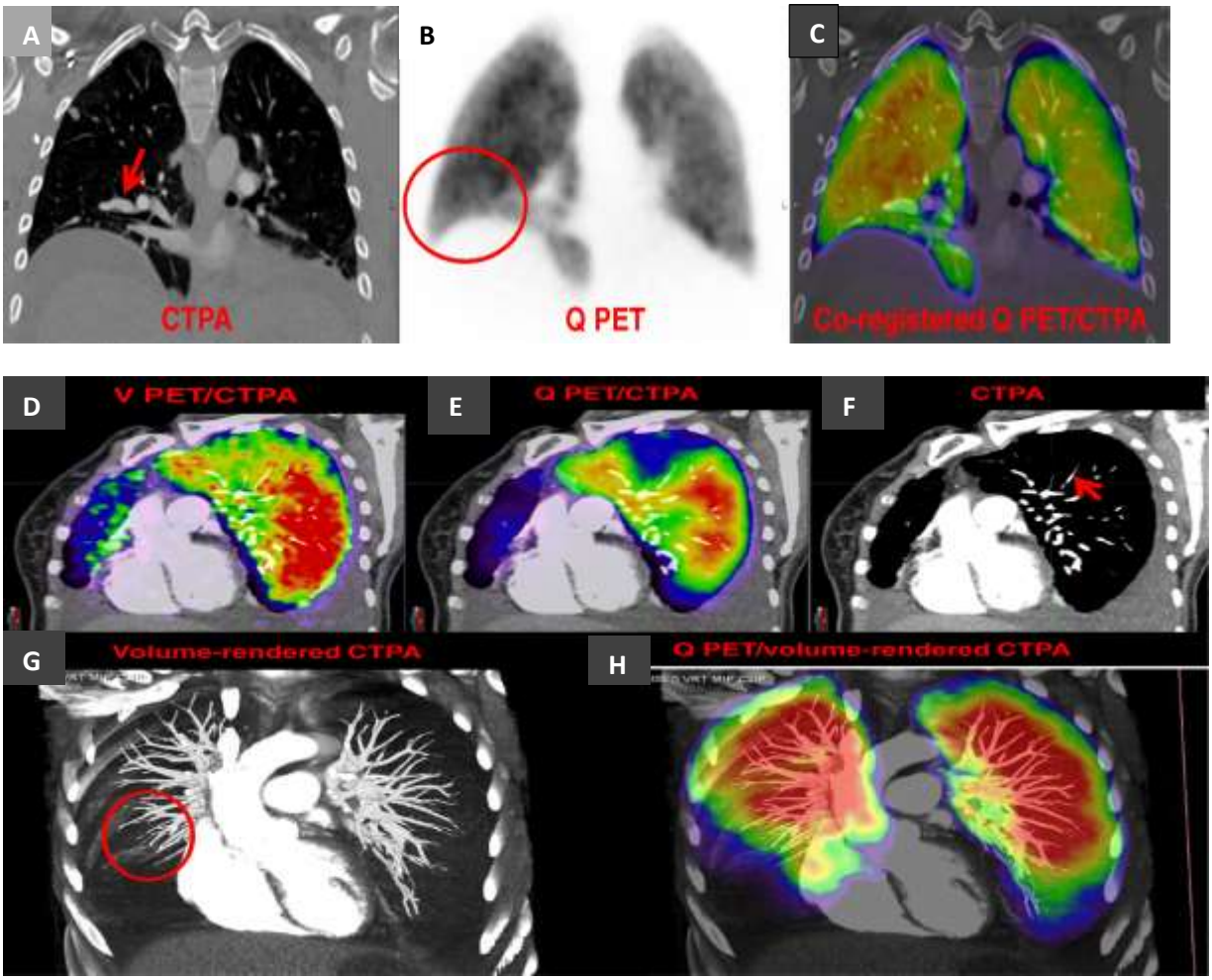

Figure 27 Patient imaging on CTPA and V/Q PET/CT, CTPA images A, F, G and PET images B, while PET/CT images C, D, E, H, published from ref. [239] with permission

1.3.5 Comparison of CTPA, SPECT/CT and PET/CT

Diagnosis of PE faces difficulties due to the lack of satisfactory gold standard to assess accuracy, sensitivity and specificity of diagnostic methods. False negative results would be followed-up for recurrence of PE to over-come this limitation. On 3 months follow-up basis of suspected PE cases (equivalent sensitivity) was assessed in 14,545 patients of CTPA excluding PE [87, 240-246] and in 1865 patients where V/Q SPECT excluded PE [128, 203, 204, 247]. The mean equivalent sensitivity was more than 95% in both studies. As the true sensitivity of results is not reflected and imaging test are mostly single events, and does not have records of follow-up. Sensitivities obtained from the relapse rates show that 16-64 rows CTPA and V/Q SPECT are capable of recognizing larger population of PE patients with a minor error of approximately five percent. Besides their efficiency these techniques has some limitations, as discussed here briefly and shown in Table 6. Risks associated with thyrotoxicosis (iodine-induced) is avoidable through pre-medication [159], but sometime risks remains serious. Elevation in serum creatinine levels and suppression in TSH levels are the relative contraindications to CTPA [125, 128].

I. A precondition of CTPA is high flow rates of contrast medium which cannot be attained in all the patients. Motion related artifacts are a cause of spatial resolution reduction, thus in trial PIOPED II, results of CTPA remained uncertain in 6.2% patients, and 10.6% in a subgroup, due to poor quality of images [125].
II. Resolution of CTPA is improved by the increasing the number of rows of detector in CT, but inconclusive results still remained 10%, which generally considered due to suboptimal contrast opacification or movement artifacts [248-250].
III. In patients with pregnancy and very low PE prevalence (3.3%), 5.9% results were inconclusive [251]. The radiation dose associated with V/Q scan is quite low; therefore it

could be a selected diagnostic test in young and pregnant women because of CT pulmonary angiography (CTPA) high breast dose and reduced accuracy in pregnancy.

IV. CTPA is available almost around the clock in all community hospitals and medical centers. While Nuclear Medicine department is not present in all hospitals and also not open during vacations so V/Q SPECT is seldom available on a 24-h basis. Consequently patients of suspected PE with signs of hypotension or shock are advocated for CTPA [250].

V. With radio-aerosol V/Q SPECT studies may also be non-diagnostic in patients of severe chronic obstruction pulmonary disease (COPD), but by using Technegas, this restriction could be eliminated [163, 194, 252, 253]. If the risks associated to contrast media are accounted the CTPA feasibility is limited in more patients than V/Q SPECT. CTPA is mostly recommended in the patients having haemodynamic instability [254, 255]. On the other hand, if the facility of gamma camera is accessible, even a single planar image is sufficient through perfusion scintigraphy to rule out massive PE [256].

VI. In a meta-analysis and systematic review CTPA and V/Q SPECT has equivalent performance [257]. V/Q SPECT was found superior to CTPA via ROC analysis in head-to-head comparison studies [257]. This was applied in specific cases of lung disease patients where PE could be diagnosed by CTPA [194, 258-260]. V/Q SPECT superior sensitivity is observed clearly in chronic pulmonary embolism patients where it has reference value but right catheterization and CTPA is also essential for patient care [261].

VII. A systematic review of literature indicated low radiation exposure of ventilation Perfusion SPECT (2.12 mSv, table.7) than CT pulmonary angiography (4.96 mSv). [262].

V/Q SPECT and CTPA, both techniques are displaying specific pros and cons. In some cases V/Q SPECT seems superior to CTPA (underlying lung diseases; undetermined PE with CTPA) [194, 258, 259, 262, 263] but in other cases both have same sensitivity [117].

Although SPECT offers significant improvement as compared to planar V/Q imaging for diagnostic accuracy, still it faced some limitations. SPECT images provide a poor spatial resolution. Additionally, due to lead collimator, gamma camera is not efficient enough to detect all the radiations and hence experiences poor sensitivity, as compared to total available photon flux.

Moreover, gamma camera need to be rotated around the patient in order to acquire SPECT data required for 3D images reconstruction. This process consumes a lot of time therefore difficult to acquire respiratory gating for motion correction or for dynamic imaging to reconstruct images. Typically Ventilation perfusion imaging by single photon emission tomography is performed during the tidal breathing which leads to distortion.

The above mentioned limitations are not faced by positron emission tomography (PET). PET imaging possess high sensitivity due to the presence of detectors in the form of a 360° ring that surround the subject. PET technology collimator is not used to define photon projections therefore more than double gain in the magnitude of the detection efficiency is observed when compared to SPECT.

Table 6 Comparison of Imaging Modalities used for PE detection

Imaging Modalities	Key Features	Limitations	Radiation Issues
Pulmonary angiography	• Historic gold standard	• Not freely available in all • centers Invasive procedure	• Highest radiation, effective dose 10-20 mSv
Planar V/Q Scintigraphy	• Strong validation in the outcomes of prospective management studies • Relatively cheap • Almost no contraindications	• Not available around the clock • Interobserver interpretation variability • Inconclusive in 50% cases • Cannot provide alternative diagnosis if PE is excluded • Results reported as ratios of likelihood	• Lower radiation exposure as compared to CTPA • Effective dose ~2mSv
V/Q SPECT	• Almost no contraindications are shown • According to data available high accuracy • Binary interpretation (PE vs. no PE) • Lowest rate of non-diagnostic tests	• Variability of diagnostic criteria Variability of techniques • Could not provide an alternative diagnosis if PE is excluded • No validation in outcome studies of prospective management	• Lower radiation as compared to CTPA • effective dose 2 mSv
CTPA	• Available around the clock in almost all centers • Strong validation of outcomes in prospective management • Could be an alternative diagnosis if PE excluded • Small acquisition time • Low rate of inclusive results	• Tendency to overuse due to easy accessibility • Radiation exposure • Exposure to iodinated contrast agent • Limited use in iodine allergy • Risk in pregnant and breast-feeding females • CTPA diagnosis relevant to subsegmental PE is unknown	• Significant exposure to breast tissues of females • Radiation effective dose 3-10 mSv

Thus physiological gating of respiratory cycle and dynamic imaging are possible. Increased sensitivity renders PET to use lower amount of radiation dose to the patients. A comparison of the radiation doses between SPECT and PET is given in Table 7.

Table 7 Radiopharmaceutical dose calculation for V/Q Scintigraphy by SPECT and PET

Radiopharmaceuticals	Target organs (Lungs) (mGy/MBq)	Effective dose (mSv/MBq)	Injected Activity MBq	References
^{81m}**kr**	0.0068	0.0007	40-400	[117]
^{99m}**Tc-Technegas**	0.110	0.0150	20-30	[218]
^{99m}**Tc-MAA**	0.067	0.0170	40-120	[128]
^{133}**Xe**	0.90	1.1	800	[108]
^{99m}**Tc-DTPA**	0.06	0.2	30	[108]
^{68}**Ga-Galligas**	8.5	1.1	10	[225]
^{68}**Ga-MAA**	28.4	3.6	40	[225]

PET has been used traditionally for accurate quantitative measurements but SPECT is restricted with qualitative applications but now it is possible with modern SPECT cameras and reconstruction algorithms. In the field of oncology, in order to manage related dieases and conditions, (^{18}F-FDG) PET/CT is present in most of the comprehensive hospitals.

But there are some limitations of PET/CT technique as mentioned below:

I. Contrary to SPECT, logistically PET requires some forward planning that's not compatible towards acute requests.
II. Though Galligas is produced in the same generator of Technegas, however the ^{68}Ga-radiolabeling is labor intensive and not compatible with it, typically to on call V/Q services.
III. The capital cost of PET/CT camera is quite high as compared to the camera of SPECT/CT.

IV. The radiation dose from ^{68}Ga, a positron emitter, is higher than pure gamma emitter i.e. ^{99m}Tc, so less activity is used due to enormous sensitivity gain of PET however maintaining the comparable radiation dose to subject.

V. Another limitation though not very recurrent, i.e. positron range post nuclear decay and prior annihilation by electron. Travelling range of a positron is determined by two main factors 1) energy of positron 2) and media surrounding density; while ^{68}Ga produces degradation in spatial resolution because ^{68}Ga has high energy (E_{max}=1.898 MeV) contrast to ^{18}F (E_{max}=0.633 MeV); while lungs density when air filled is low (*p*=0.2-0.3 g/cc) as compared to the solid mass (*p*=1 g/cc). Theoretical factors might have less effect than motion due to breathing or cardiac cycle.

VI. Additionally V/Q PET might offer only a better-quality of resolution, keeping same functional information. Although the fact that higher resolution is desired

In conclusion keeping in mind V/Q PET/CT pros and cons, this technique can present a better alternative of V/Q SPECT with superior imaging qualities, resolution, small time for acquisition, small radioactivity usage while keeping all the above mentioned benefits of ventilation/perfusion scintigraphy over computed tomography pulmonary angiography (CTPA) although it would be more useful if it made cost effective and available clinically in all nuclear medicine departments.

1.4 Radiotracers Based Imaging of PE

Imaging of thrombus has rich history date back in the early 19thcentury and still continued. This continuous effort is drove by an unfixed clinical issue, conceivably, highest for pulmonary embolism, eroded or ruptured carotid coronary atherosclerotic plaques and ischemia-reperfusion injury. While molecular imaging of thrombus with contrast agents and single photon emission computed tomography used in almost medical imaging, each offering unique features with their own strength and weakness as described in the previous chapter in detail.

Regardless of years of research, for direct imaging probes, fibrin and platelets remained the principal thrombus targets and for in-direct imaging of pulmonary embolism, macroaggregates have demonstrated their hold over the clinic.

Primarily molecular imaging can be categorized on the basis of target (thrombus) visualization methods as shown in Figure 28.

I. Direct Imaging of Thrombus/Pulmonary Embolism

II. Indirect Imaging of Thrombus/Pulmonary Embolism

Both imaging techniques show some common issues noted 40 years ago and still persists making DVT and PE imaging a great challenge, for example in direct imaging technique, acute thrombus is imaged with sensitivity, while aged thrombus has remained a challenge. Secondly anti-coagulants interfering in imaging results, but clinically heparin is the requirement of patients suspected of PE, DVT or coronary ruptured plaque prior to the confirmation. For indirect imaging, synthesis of microparticles originated from non-human/animal sources has proven to be a great challenge. Unfortunately, blood derived products which carry a potential risk of viral disease transfer remained prevalent such as macroaggregates of albumin/human serum albumin;

commercially used as gold standard particle kits for lung thrombus or pulmonary embolism detection.

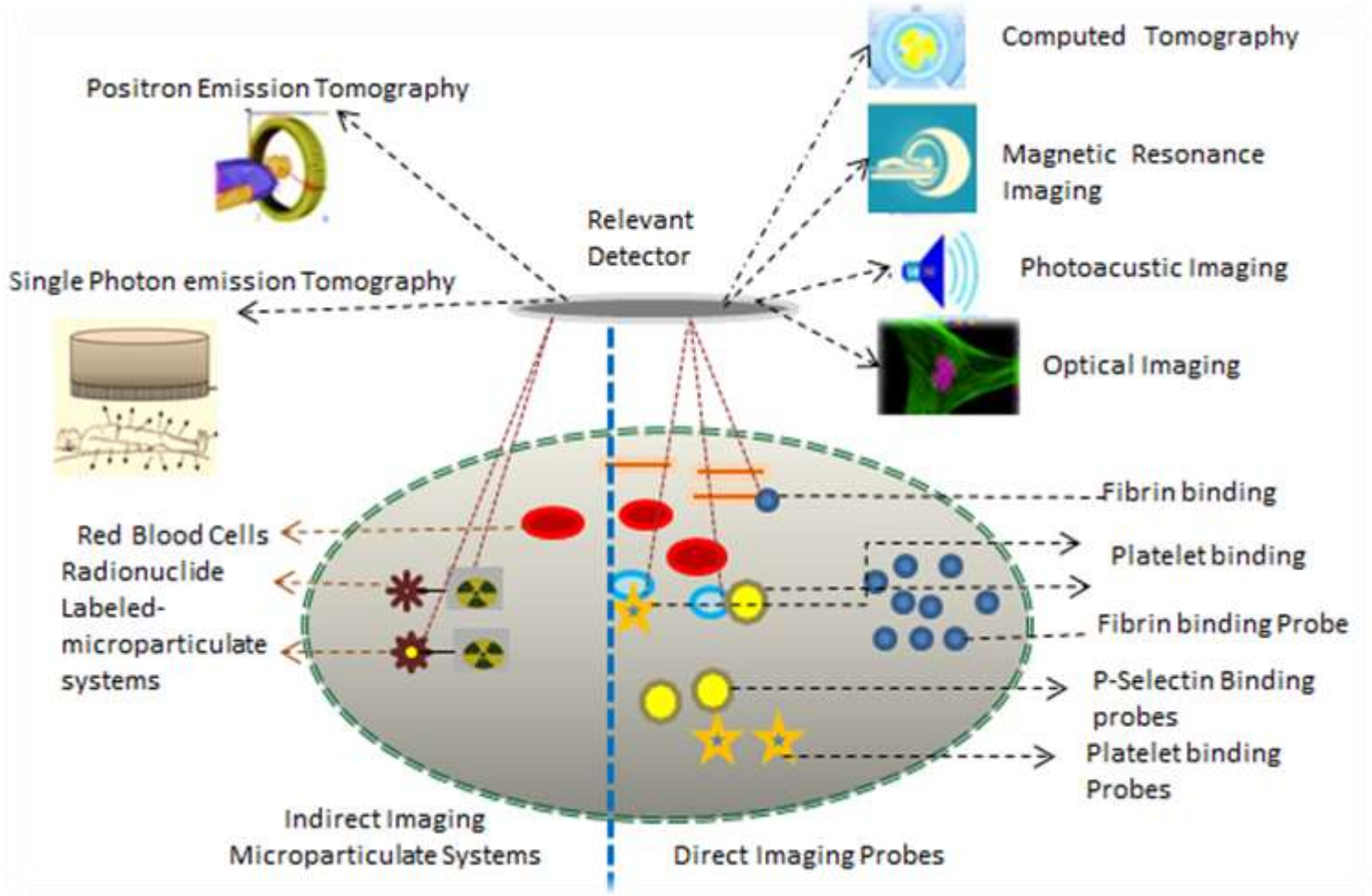

Figure 28 Direct and Indirect Imaging of Thrombus

These basic issues could be overcome, but advanced measurements are mandatory and an escape from previous approaches is a must. Here we discuss about various probes and microparticulate systems designed and developed for this perspective.

1.4.1 Direct Imaging of Pulmonary Embolism

Non-invasive imaging targeting particular moieties involved in thrombus formation is called direct imaging and has demonstrated capacity to detect thrombus in diverse disease models and in the patients.

1.4.1.1 Targets for Thrombus Imaging Probes

Probes of direct imaging are designed to bind with the components active during thrombosis and offers a highly specific non-invasive approach that can help to improve and develop the current diagnostic mechanism of imaging modalities. Up till now, numerous targets have been explored to understand their binding capacity for thrombus imaging. Most popular targets include activated platelets, fibrin, and enzymes, synchronized in the cascade of coagulation, i.e. factor XIII and thrombin. Both fibrin and activated platelets are present only in the thrombus and the healing wounds therefore represent highly specific potential targets to image thrombus (Figure 15). In acute PE, fibrinogen and activated platelets are susceptible and cross-linked to propagate thrombus formation.

1.4.1.2 Platelet Targeting Probes

Other epitopes that target platelet surface includes vWF, GPVI and P-selectin. They have varying affinity towards activated platelets. P-selectin targeting is unique and delineated between the non-activated and activated platelets.

1.4.1.2.1 P-Selectin Targeting Probes

Fucoidan, a sulfated polysaccharide based on brown seaweed, is a natural mimic of SLeX. This probe showed 2 orders of interaction with P-selectin than low-molecular-weight (LMW) sulfated polysaccharides. Furthermore, in-vivo it was assessed in ischemia–reperfusion models.

Letourneur *et al.* [264] showed that ^{99m}Tc labeled fucoidan has detected arterial thrombi in rat models using SPECT imaging (Figure 29). ^{99m}Tc-fucoidan sensitivity and retention in arterial thrombus detection and myocardial ischemic reperfusion was excellent. Recently, this group also performed MRI analysis using ultra-small super-paramagnetic iron oxide nanoparticles (USPIO) with coating of fucoidan.

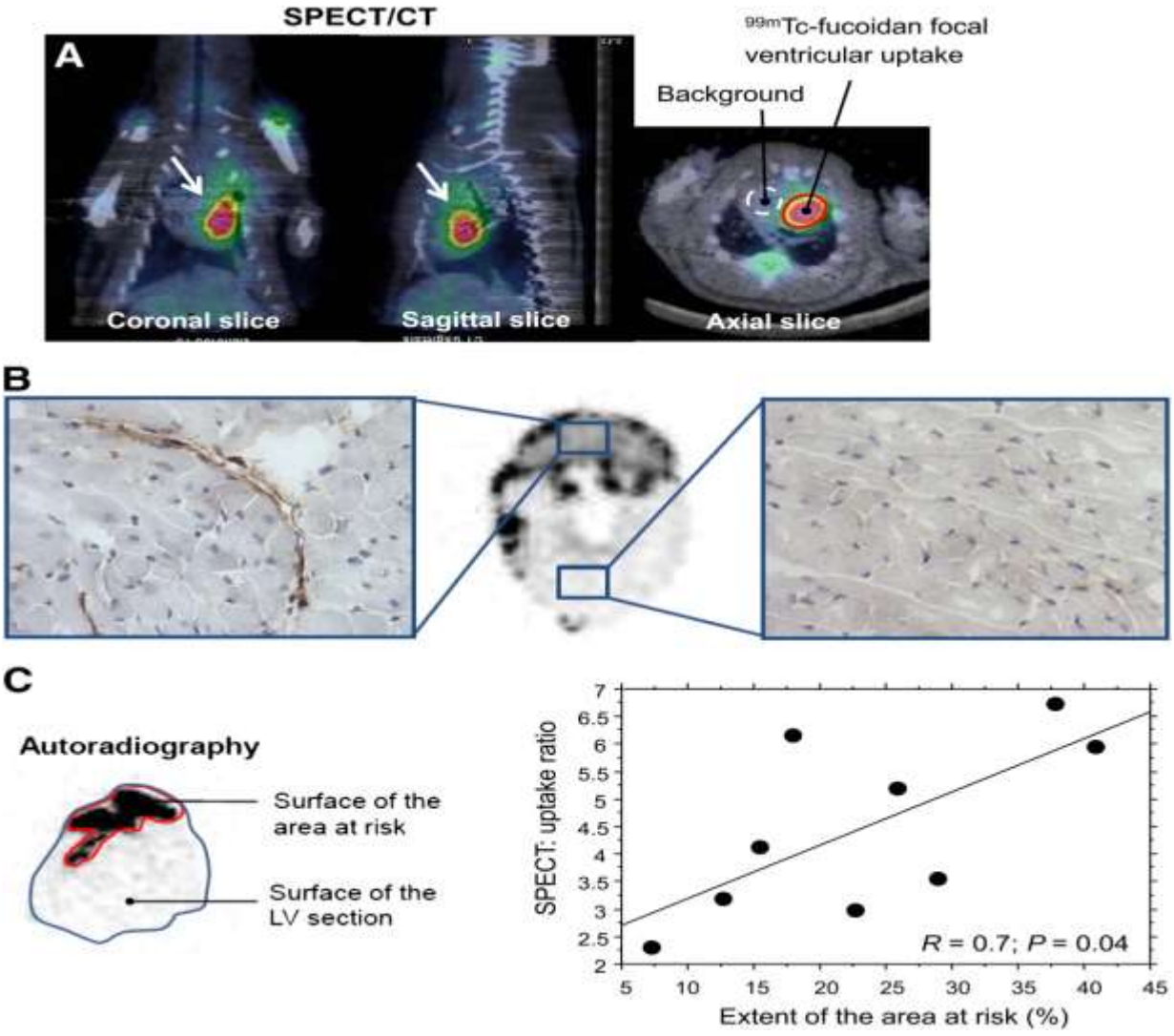

Figure 29 ^{99m}Tc-fucoidan (P-Selectin) Thrombus Visualization reprinted from research originally published in JNM by Rouzet *et al.* 2011 [264]

Some probes for direct imaging of thrombus are presented in Figure 30. While general mechanism of diagnosis of thrombus in direct imaging is presented in Figure 33

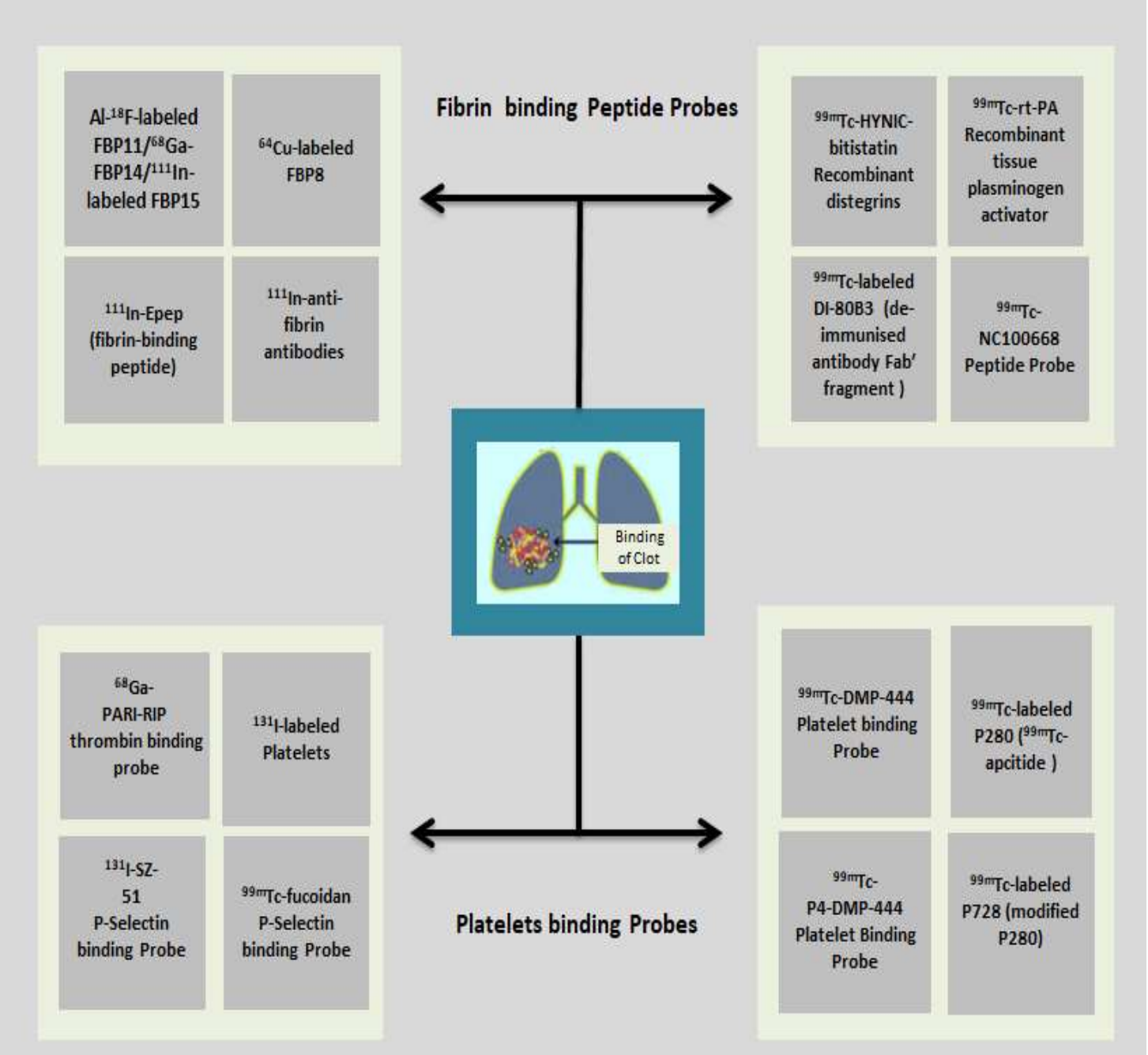

Figure 30 Radiopharmaceuticals for Direct imaging of Thrombus in DVT and Pulmonary Embolism

1.4.1.2.2 Radiolabeled Platelet as Probes

^{111}In labeled platelets since late 1970s, provided platelet physiologic data to decide about therapeutic assessment of angioplasty, atherosclerosis, venous thrombosis and vascular grafts and it was FDA approved method for functional imaging of thrombus [265].

Nevertheless the method is time-consuming i.e. 24 h imaging delay, low Signal-to-noise ratio, and lack of underlying pathological condition documentation. Therefore, more robust methods are required.

1.4.1.2.3 Glycoproteins IIb/IIIa Targeting Probes

1.4.1.2.3.1 Cyclic Arg-Gly-Asp (RGD)

Platelets expressed glycoproteins IIb/IIIa (GPIIb/IIIa), to make platelet bridges that are predominately present in the thrombi. Receptors antibody that can target platelet GPIIB/IIIA receptors could detect thrombi. Activated platelets present >80,000 receptors (GP IIb/IIIa) [266, 267] on their membrane. Short peptide analogues of Arg-Gly-Asp prepared synthetically are active in thrombus and tumor targets [268-272]. Their long circulation problem was alleviated using small chain peptides [273-279]. Therefore they showed higher affinity with fibrin than the fibrinogen and also bear potential benefits of faster clearance from bloodstream and their capability to penetrate in fibrin mesh [264, 278, 280]. Zhou and colleagues [268] reviewed extensively cyclic RGD applications.

Apcitide is a polypeptide of synthetic origin that can bind to activated platelet receptors (GIIb/IIIa). In 1998, Food and Drug Administration, United States approved Apcitide for the clinical use. It has been extensively explored for acute DVT and PE detection [268, 281, 282], as

shown in Figure 31. ^{99m}Tc-labeled apcitide was investigated in 19 patients by Dunzinger *et al.* for the detection of acute DVT and PE using SPECT and results were compared to phlebography and/or ultrasonography [283]. Out of 6 patients, one PE patient was detected using ^{99m}Tc-labeled apcitide. This radiotracer showed 87% sensitivity and 100% specificity for acute DVT and conversely low sensitivity for PE.

In multicenter trial of Phase III, Thaillefer *et al.* studied thromboembolism with ^{99m}Tc-apcitide scintigraphy [284] and compared to contrast venography. 280 patients included in the study showing within 10 days of signs of DVT or surgery of high risk DVT. ^{99m}Tcapcitide scintigraphy and contrast venography blind results showed 73.4% sensitivity, 67.5% specificity and 69.1% agreement. This study comprised of patients with previous DVT and might be confounded with venography. In patients sub-set without history of DVT, there was 90.6% sensitivity, 83.9% specificity and 87.3% agreement; hence this radiotracer has the potential to image acute DVT. Further ^{99m}Tc-apcitide (P280) [277, 285] comparative investigation with contrast venography at multiple time points showed 85.4% sensitivity, 88.3% specificity, along with ratios of positive likelihood, and negative likelihood are 7.38 & 0.154, respectively. Bates and colleagues studied ^{99m}Tc-apcitide [273] in 38 newly diagnosed DVT and 40 previous DVT patients with ultrasonography abnormalities and found sensitivity (92%) and specificity (82% & 90%) for two expert readers. Though, they reported for new physicians a low accuracy and inter-reader agreement. Another GP IIb/IIIa receptor antagonist is ^{99m}Tc-DMP444 [286] to target activated platelets. It showed an active incorporation in the DVT and PE thrombi in arterial [276, 287] and venous system. Kelm and coworkers detected in 10 patients of DVT (confirmed by US and D-Dimer) using ^{99m}Tc labeled DMP 444 planar imaging and showed high activity correlated with US findings. Another monoclonal antibody Anti GPIIIa, SZ21, and chSZ21 [267],

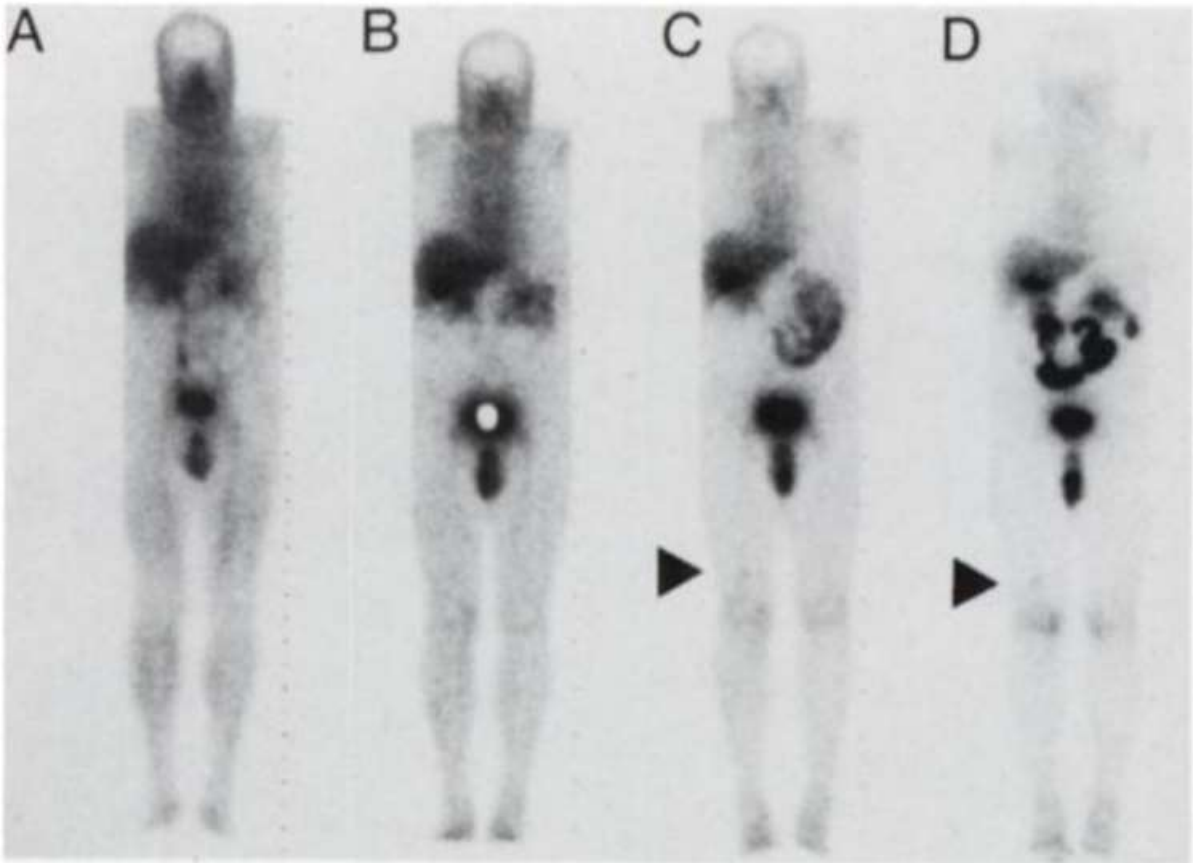

Figure 31 Anterior whole-body images (1000kcts) Collected at (A) 15 min, (B) 60 min, (C) I20 min and (D) 240 min post IV administration of ^{99m}Tc-P280. Arrowheads indicated thrombus in the right leg, diagnosed between 120-240 min after injection of the radiotracer. Published from the research originally published in *JNM,* Muto et al. 1995 [281]

investigated in mouse/human chimeric versions and human in canine PE and DVT models on planar images and showed an uptake after 30 min and 3 h. Target-to-background ratios were for DVT/ muscle=117, PE/ lung=12.8 and for DVT/blood= 7.2.

Both probes (^{99m}Tc-P280, ^{99m}Tc-DMP444), has illustrated reduced sensitivity/specificity towards pulmonary embolism detection because of their low uptake in thrombus and radioactivity

accumulation for prolonged time in blood and the chest region. Intrinsically, these probes have been discontinued.

Peptides present in the viper venoms are called disintegrins which have the ability to bind via GIlb-IIIa receptor of active platelets. Knight *et al.* labelled eight disintegrins i.e. *albolabrin, barbourin, bitistatin, achistatin, eristostatin, halysin,* and *mambin* with ^{123}I, and compared for PE diagnosis in canine models.^{123}l-labeled bitistatin showed higher embolus-to-blood ratios than fibrinogen, echistatin, platelets, halysin or mambin with low background and visualized pulmonary emboli [288] as shown in Figure 32.

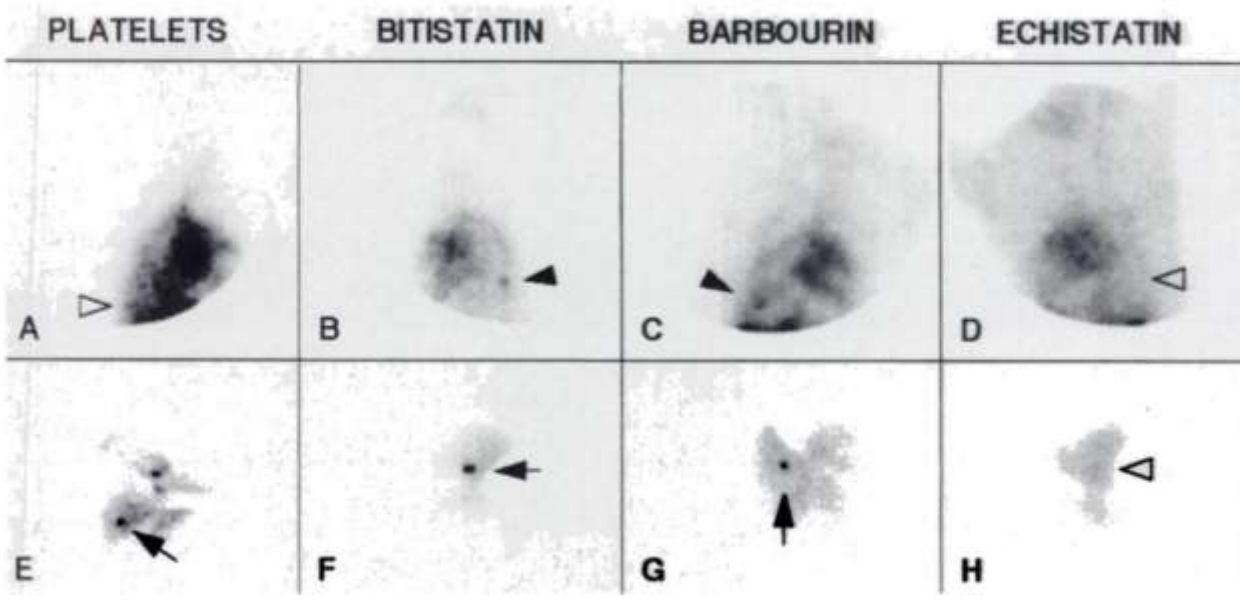

Figure 32 Planar images of dogs chests **(A-D)** after 3.5 h of radiotracer injection (^{99m}Tc-HMPAO-labeled autologous platelets or ^{123}l-disintegrins). Pulmonary emboli are shown by solid arrows, and outlined arrows showed those emboli not visualized through scintigraphy. Ex-vivo images of the lungs from **E-H** of same animals placed on face of collimator to acquire counts for 20 min. Embolus was not visualized in right lateral view of **A** using ^{99m}Tc-HMPAO-labeled autologous platelets, however clearly seen by ex-vivo lung image of **E**; In case of ^{123}l-bitistatin, embolus was shown in noth views of B and F; In case of ^{123}l-barbourin, embolus was seen both in C and G; In case of ^{123}l-echistatin, embolus was not seen in both views of D and H. Reproduced from research originally published in *JNM,* knight *et al.* 1996 [288].

Knight prepared ^{99m}Tc-Hydrazinonicotinic acid-bitistatin (^{99m}Tc-HYNIC-bitistatin) called recombinant bitistatin (rbitistatin) using a bifunctional chelating agent to radiolabeled bitistatin with technetium-99m with high RCP >97%. Pre-clinical study in dogs (n = 6) using SPECT planar imaging of DVT and PE showed high uptake after 30 min of the injection and uptake persists for 4 h [289]. Bitistatin recombinant version phase-I clinical trial confirmed its ability to bind to platelets. Future work is required to interpret bitistatin role in clinic [290]. Potential hazard of using venoms (poison) of snake as well as animal derive proteins carry a potential risk of disease transfer. Recombinant version solved this problem but the process of synthesis is very long including multistep reactions and requires purifications.

1.4.1.3 Enzyme Targeting Probes

Two enzymes categories present in fibrinolytic system related to hemostasis include:

i. Plasmin
ii. Plasminogen activator

Plasminogen activator are further divided as: i) urokinase-type plasminogen activator ii) tissue-type plasminogen activator (TPA) which are synthesized in the vessels endothelial cells and subsequently released into the bloodstream.

TPA and plasminogen bind to fibrin during clots formation. Fibrin-bound plasminogen is converted by TPA to plasmin, which sequentially degrades in the fibrin [291]. They seem attractive target for thrombus imaging due to close connectivity between plasmin and TPA and thrombus formation.

1.4.1.3.1 Plasmin Targeting Probe

^{99m}Tc-labeled Plasmin is used in numerous studies to evaluate DVT through gamma camera [292-297] and results were compared to phlebography. The results illustrated promising sensitivity and specificity but accuracy for DVT diagnosis was not satisfactory, especially in patients of hip surgery [294].

1.4.1.4 Plasminogen Targeting Probes

Harwig and colleagues [298] have investigated radio-iodinated plasminogen to detect thrombi. The radiotracer detected clots on 2 day (Thrombus/blood ratio: 7.8 ± 2.4) until 6 days (in 80% cases) of thrombus formation but there was variations in thrombus-blood ratios which may be due to plasminogen release.

Butler *et al.* developed [299]^{99m}Tc-recombinant tissue plasminogen activator (^{99m}Tc-rt-PA) to diagnose venous thrombosis by scintigraphy imaging. TPA is a protease enzyme that is formed naturally in endothelium of vessel. TPA converts plasminogen to plasmin with the help of two sites: catalytic and fibrin binding sites. rt-PA binds directly to fibrin instigating conformational changes which significantly increase catalytic activity of plasminogen. They labeled rt-PA with ^{99m}Tc to allow the scintigraphic imaging of thrombi and demonstrated sensitivity and specificity of 86% and 93% respectively of variable age's thrombus of calf vein in humans.

Brighton *et al.* [300] investigated ^{99m}Tc-rt-PA uptake in acute DVT, 30 days after the diagnosis. rt-PA activation site becomes inactive but fibrin binding still persisted. With thrombus aging some fibrin sites become available for radiotracer binding. 74 patients of acute DVT symptoms were assessed for US and ^{99m}Tcrt-PA imaging and results showed high uptake (72%) on 7th day

and no uptake (0%) on 30th day. They inferred that ^{99m}Tc-rt-PA can differentiate between new and old ones. The general mechanism of direct imaging of thrombus is shown in Figure 33.

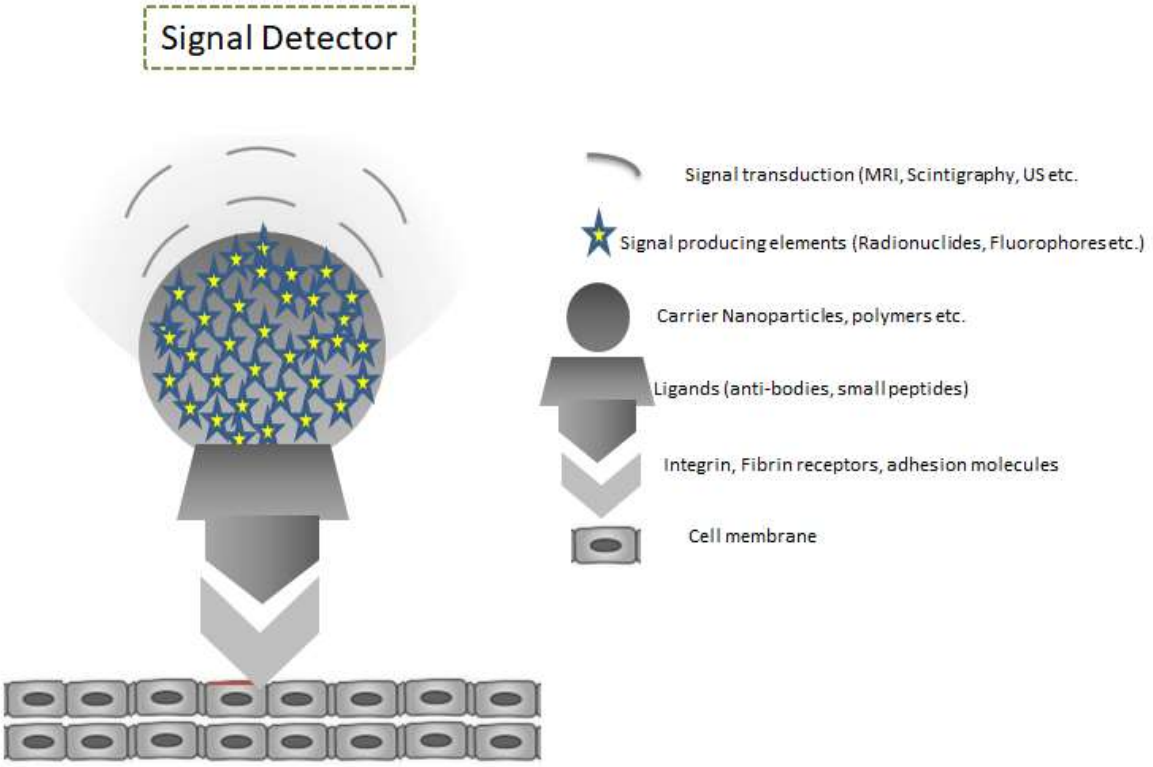

Figure 33 General Mechanism of Direct Imaging of Thrombus in DVT and PE

1.4.1.5 Fibrin Targeting Probes

Fibrin is the major constituent of arterial or venous thrombi. Fibrinogen is a soluble, complex and large glycoprotein (340 kDa) and converted to fibrin by thrombin during thrombus formation process [301]. Fibrinogen after synthesis in the liver circulates at the level of 200/400 mg/dL in plasma. During the phenomenon of blood coagulation, prothrombin transformed into thrombin; that subsequently transforms the soluble fibrinogen into the insoluble fibrils of fibrin [302].

Two sets of 3 polypeptide chains are present in fibrinogen namely: α, ß and γ. fibrinopeptides cleavage A and B from the alpha and beta chains is facilitated by thrombin, generating monomers of fibrin that after polymerization converted into fibrin fibrils and consequently insoluble fibrin network producing scaffold of thrombus [303, 304].

These fibrin fibrils developed auxiliary cross-linked elements to make a stabilized clot by the circulation of clotting factor XIIIa (FXIIIa). Further than cross-linking, to stabilize the fibrin clots, FXIIIa entrapped alpha-2-antiplasmin [305] and TAF, inhibitors of fibrinolysis and thrombin activatable (procarboxypeptidase B) [306] respectively, and interact with cell adhesion receptors. Factors such as factor Xa used for activated coagulation thrombin and are also entrapped by fibrin network and become temporarily inactive. Fibrin also triggers pro-coagulant and anticoagulation pathway by the activation of factor XIII and plasminogen activators [307] respectively.

Fibrin and related proteins remains a major target of VTE investigations in the literature as discussed here in following paragraphs. Initially ^{125}I-labeled fibrinogen was the popular probe for targeting fibrin but abandoned due to low specificity, sensitivity and long delay time of imaging [308-311]. ^{131}I, ^{111}I labeled polyclonal antibodies also developed for imaging venous thrombi, but their long half-life long delay time for imaging restricted their use [312]. Then ^{99m}Tc labeled monoclonal antibodies has solved the problems of specificity, half-life and facile clearance from body.

1.4.1.5.1 Fibrin Alpha Chain Probes

A tri-peptide showing binding with alpha chain of fibrin has been introduced by Laudano and Doolittle [313]. Additionally Kawasaki and colleague [314] prepared some probes on the same

basis with potent activity for thrombin clots. Thakur and coworkers [315] have investigated pentapeptide fibrin alpha chain that can bind to C terminal of gamma chain to detect acute DVT or PE in animal models. ^{99m}Tc-labeled TP 850 binds to thrombin with modest affinity in animal models of DVT and PE while rapid clearance from blood.

Aruva *et al.*, [316] prepared a swine models of DVT and PE, and imaged thromboembolism using probe TP 850. ^{99m}Tc-TP 850 showed a modest affinity with a fast blood clearance while high probe uptake in DVT and PE thrombi.

1.4.1.5.2 D-dimer Targeting Probes

Another very specific monoclonal antibodies family was raised to D-dimer, site made by cross-linking of neighboring fibrin D-domains [317-320]. This neo-epitope is not present in fibrinogen or monomeric fibrin fibrils, and rats' biodistribution and immune-scintigraphy studies showed its high specificity to thrombus and normal background noise.

Fibrin connects D-domains covalently to antigenic sites for which antibodies are designed. Monoclonal antibodies (DI-DD3B6/22) are the primary class of antibodies prepared for this purpose [317, 321]. The next generation "DI-DD3B6/22-80B3 Fab" fragments [322, 323] has optimized efficacy and modified structure after replacing the sequences which are not involved in antigen detection of human equivalent. ^{99m}Tc-DI-80B3 has detected acute thrombi of PE and DVT in animals. Clinical trials (Phase-I, II) of the antibodies have shown encouraging results. This probe showed unique characteristics i.e. clot anatomical localization, in patients it distinguished new or old lesions. Furthermore, it can identify proximal or distal DVT and obese patients, where ultrasound seems difficult to interpret.

Morris *et al.* used ^{99m}Tc labeled antifibrin Fab' fragments [322] to visualized PE and DVT through SPECT. The antibody could not detect subsegmental emboli in animal models (dogs).

^{111}In-labeled-antibodies against fibrin ß-chain, D- Dimer for DVT imaging are compared by Morris *et al.* [324] during anticoagulation therapy in dogs using gamma camera. Anti-beta chain was 60% sensitive but D-dimer was 100% sensitive. The ratio of clot/ blood was 7.8 ± 2.0 in anti-beta and 24.5 ± 2.8 in anti-D-dimer group. Macfarlane *et al.* [317] in phase-I trial image 26 patients of acute DVT using ^{99m}Tc-DI-80B3 for safety. In phase-II multicenter cohort trial in 82 patients of DVT, Douketis *et al.* [325] investigated ^{99m}Tclabeled-DI-80B3 for diagnostic accuracy and safety. They found in proximal DVT, sensitivity and specificity values 84% and 97%, respectively with no adverse effects but low accuracy values in distal DVT and unable to comment on DVT recurring due to limited number of studied population.

The fibronectin is among the abundant plasma proteins and is involved in fibrin dimers cross-linking due to its adhesive properties [326]. The fibronectin part of ^{99m}Tc-FBD contains is responsible to direct it to the blood clots. ^{111}In-FBD in its initial pilot study showed encouraging results obtained after 18-24 h of radiotracer injection. Afterward, Thaillefer reported that ^{99m}Tc-FBD illustrated 80% overall sensitivity, while 87%-97% in the proximal DVT and 56%-78% in distal DVT [326, 327].

1.4.1.5.3 Factor XIII Targeting Probes

Factor XIII, an endogenous protein used for clotting, i.e. involving in the crosslinking of polymerized fibrin molecules and providing stability in the thrombus formation. As factor XIII is a good target to detect active thrombosis. Factor XIII primary studies showed comparative ability

to bind to thrombus [328]. Due to its high molecular weight and low clearance from blood, further studies were halted.

A novel, diagnostic probe based on thrombosis-specific (FXIII) was prepared in 2003 and identified the target[329]. Then McCarthy *et al.* [330, 331] synthesized an efficient multimodal, factor XIII based nanoparticles.

Another radiotracer ^{99m}Tc-labeled NC100668 developed to diagnose thromboembolism and its structure resembles to human α2-antiplasmin, a substrate of factor XIIIa (FXIIIa) factor. NC100668 consists of 13-amino acid peptide, and possess chelating properties to bind with radiometals. Plasma clot assay showed its higher uptake than (^{14}C) dansyl cadaverine, a well-known FXIIIa substrate in plasma clot assay. *In-vivo* biodistribution in Wistar rats showed higher uptake in blood clots and radioactivity was excreted rapidly through urine with little background retention [332]. ^{99m}Tc-NC100668 showed retention only with active blood clots might be through a specific mechanism (FXIIIa mediation), as FXIIIa is responsible to stabilize and crosslink fibrin blood clots. This facilitated PE imaging with greater specificity than indirect imaging methods which rely on anatomical changes of perfusion deficit [326, 333, 334]. Clinical studies for ^{99m}Tc-NC100668 metabolism and pharmacokinetics in healthy human volunteers showed that radioactivity clearance with same ratio in both genders, and >half of 82% was passed through urine after 2h with half-life of 12 min and followed by gradual decrease to final elimination half-life of 10.5 h [335]. Edwards D. *et al* investigated the rapid removal from body and did not show any negative impact on the test substance ability for scanning blood clots [336]. Despite good preclinical and clinical studies for metabolism and stability, no

representation of this technique clinically and no probe is available for lung perfusion studies in humans.

1.4.1.6 Fibrin Beta Chain Targeting Probes

Target of numerous studies focusing on thrombus imaging has been the fibrin and various types of anti-bodies are reported in the literature [278,316, 337-339]. T2G1 [340, 341], 59D8 [318] are the antifibrin antibodies that bind on beta-chain of fibrin to 7-amino acid specific for cross-linking of thrombus activation [328]. Preliminary human studies of ^{111}In labeled 59D8, indicated 87% sensitivity and specificity for both till 4 hours post injection as compared to 159 patients [312, 342-346] of venography. The problem of half-life and blood clearance still persists. ^{99m}Tc labeled T2G1 indicated an overall sensitivity 80 and 94% in DVT in patients [312, 343]. As heparin might interfere in antibody binding to fibrin, thus a monoclonal antibody GC4, has been introduced which bind fragment D of fibrin showed affinity with old thrombi and showed a higher uptake along with heparinization compared with T2G1 [347]. Another illustration is fragment E that is a plasmin product of fibrin.

^{111}In labeled ^{64}C5, a monoclonal antibody, a beta-chain specific was prepared and utilized for pulmonary emboli diagnosis in canine (n=6) [348]. Fibrin specific antibodies imaging based human trials showed encouraging sensitivity and specificity.

^{111}In labeled antifibrin antibody [15, 342] in 33 VTE patients showed sensitivity 97% vs. venography. Jung *et al.* used above mentioned probe and reported 84% and 81% of sensitivity and specificity, respectively in high probability patient of DVT [345]. Another study including 10 patients found 85% and 100% of sensitivity and specificity, respectively [344]. Another antifibrin antibody called DD3B6/22 was studied by Bautovich *et al.* [349] showed 100%

sensitivity in 20 patients. Conversely, these probes failed to show optimal binding with thrombi during the course of anti-coagulation therapy [323].

1.4.1.6.1 Cyclic Fibrin-Binding Probes

Cyclic fibrin binding probe is comprised of motif (EP-2104R) for fibrin-binding and moieties of Gd-1,4,7,10-tetraazacyclododecane-1,4,7,10 tetraacetic acid (DOTA), to study PE using MRI [339, 350-352]. Phase II clinical trials of EP-2104R (Figure 34) produced encouraging outcomes in 53 patients with previously confirmed thrombi [339, 350-352]. Standard scanner 1.5 T present in the clinical set up had visualized thrombi producing high signal and contrast to background noise ratio.

Sirol *et al.* [353] induced thrombus in guinea pigs as model and assessed the fibrin targeted probe EP-1242 injection using T1-weighted high-resolution MRI. The probes showed an improved detection of small fibrin-rich thrombi.

Starmans *et al.* introduced ^{111}In labeled fibrin-binding peptide (FibPep) which showed high fibrin binding in-vitro; clearly visualize thrombi in-vivo using SPECT and fast blood clearance [337].

Starmans *et al.* in another study [354], has introduced EPep, ^{111}In-labeled-peptide (^{111}In-EPep) for fibrin binding that incorporate EP-2104R's (Figure 34) to compare it with above mentioned probe (FibPep). These two peptide probes showed almost similar affinity and metabolic profile.

Ciesienski and colleagues [338] designed three new probes based on EP-2104R for PET and the two sequences that showed high fibrin affinity are conjugated to ^{64}Cu-DOTA [350-352, 355]. Two probes showed fourfold thrombus to background ratio in vivo and accurate arterial

thrombus detection by hybrid MR-PET imaging. On the other hand, probes showed long blood residual activity even after 2h hence these probes are needed to modify in future. ^{64}Cu-labeled FBP8, a short chain comprising of 6-aminoacid cyclic peptides, has detected PE and DVT, in SPECT imaging and ex vivo counting confirmed the lung emboli location [356]. PET quantification revealed that uptake of probe was higher in new clots than in old ones and biodistribution showed rapid body clearance, primarily through renal pathway [357]. An Epix Pharmaceutical IP estate designed probe a highly efficient fibrin-binding probe namely, ^{64}Cu-labeled FBP8. The limitation of this probe is its higher activity uptake in acute thrombi and reduced uptake in aged clots.

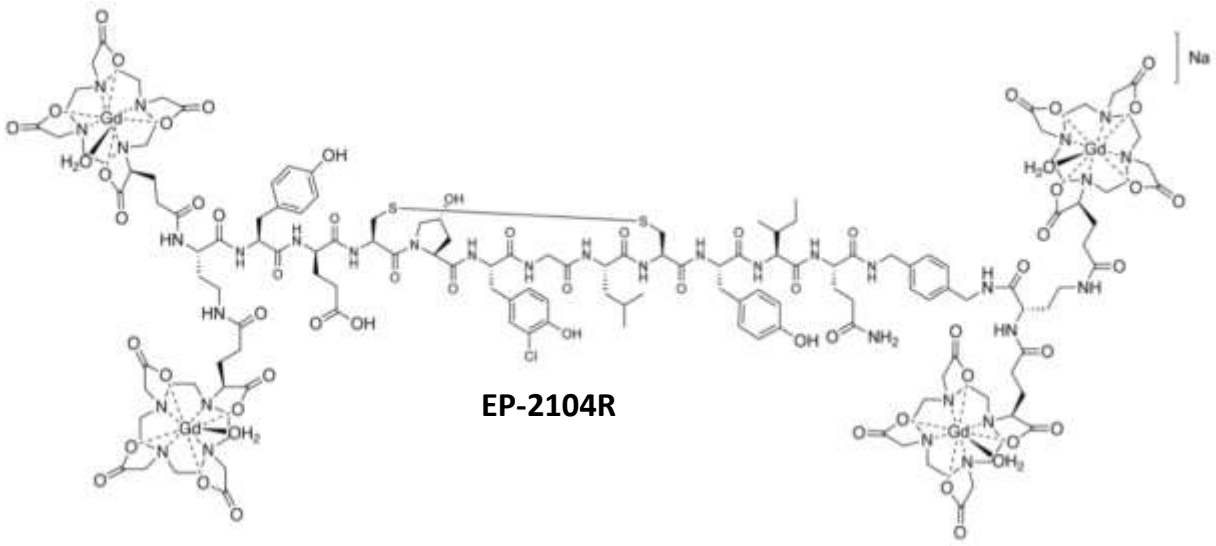

Figure 34 Structure of EP-2104R Gd-based fibrin-binding probe

Ay and coworkers [358] introduced FBP7 probe and detected arterial thrombosis with promising results in animal models. Yet the animal models have occlusive/non-occlusive carotid arterial thrombi, so these probes might be similarly useful in the venous thrombosis. Then based on EP-2104R, a newly fabricated near infra-red fluorescence (NIRF) probes was investigated called

FTP11-Cy7 [321] in thrombi of in-vivo DVT. The Hara and colleagues [321] found that probe binds with acute and sub-acute thrombi with high target to noise ratio.

Uppal and colleagues [355] imaged arterial thrombus using probe based on EP-2104R in rat model through PET/MR modality. Thrombus signal enhancement was observed in animals on MR and PET imaging after administration of the probe.

1.4.1.7 Inflammatory Cells Targeting Probe (^{18}F-FDG)

^{18}F-FDG, glucose analog, major energy source and hence various cells take it, including coagulation and inflammation for instance macrophages, lymphocytes, and endothelial cells. Since the VTE process is closely related to inflammation as well adhesion molecule expression and subsequent FDG uptake in thrombus [280, 359].

Previously FDG-PET/CT ability for differentiating new and recurrent VTE, discrimination between tumor thrombosis and VTE is studied [360]. FDG-PET/CT applicability in one imaging method as an all and to categorize new patient and non-proximal areas such as PE, sagittal sinus thrombosis, upper extremity, pelvic area, and calf, is still uncertain and further studies are required.

Rondina *et al.* [359] used FDG-PET/CT to diagnose thrombi with 87.5-100% sensitivity and specificity in 12 patients which were previously confirmed for lower limb thrombosis. A negative correlation was observed between maximum activity in thrombus and symptom onset time of DVT, signifying a decrease with time, a requirement to differentiation between new and old thrombi. Some Radiopharmaceuticals designed for direct imaging of thrombus the ultimate cause of DVT and PE are shown in Table 8.

Table 8 Radiopharmaceuticals designed for direct diagnosis of thrombi of DVT and PE

Radiopharmaceuticals	Source of origin	Targeted site	Study population	Authors & References	Technique
(EWVDV–Ink-PFH)	Short peptide	P-Selectin	--	Xu *et al.* 2020 [361]	Multimodality
^{99m}Tc-fucoidan	Polysaccharide brown seaweed	P-selectin, Platelets	Animals	Rouzet *et al.*, 2011 [264]	SPECT
TAP-SiO2@AuNPs	Gold Nanoparticles	Plasminogen sensitive	Animals (n=3)	Kwon *et al.* 2018 [362]	mCT/NIRF
Fumagillin prodrug	Cu-based nanoparticles	αvβ3-integrin	Animals	Zhang *et al.* 2015 [363]	PA/NIR/PET
Fib-GC-Au-NPs	Gold and chitosan	Fibrin sensitive	Animal	Kim et al [364]	mCT
PARI-RIP-Cy7	Peptide based	Thrombin	Animals (n=5)	Page *et al.* 2015 [365]	NIR/PET
^{131}I-SZ-5	Monoclonal antibody	P-selectin (GMP-140)	Animals/ mouse-human chimeric model	Gu J, Liu *et al.*,1997, Wu G *et al.* 1991, Gu JM *et al.*, 1996	SPECT
Anti D-dimer ^{99m}Tc-DI-80B3 Fab' fragment	De-immunized antibody	D-Domain	Human Phase-II trial (n=82)	Douketis *et al.*,2012 [325]	Planar Scintigraphy
^{111}In-anti D-dimer	D-Dimer	D-Domain	Animal	Morris *et al.*, 2004 [323]	Planar Scintigraphy
^{99m}Tc-rt-PA	Serine protease enzyme	Tissue plasminogen activator	Human (n=79)	Butler *et al.*, 1996 [299]	Planar Scintigraphy
^{99m}Tc-rt-PA	Serine protease enzyme	Tissue plasminogen activator	Human (n=74)	Brighton *et al.*, 2007 [300]	Planar Scintigraphy
^{123}I-t-PA	Serine protease enzyme	Tissue plasminogen activator	Animal	De Bruyn *et al.*, 1995	Planar Scintigraphy
^{111}In-FBD	Peptide based	Fibronectin	Human (n=62)	Rosenthall *et al.*, 1995	Planar Scintigraphy
^{131}I-Plasminogen, ^{123}I-Plasminogen	Enzyme	Plasmin	Animal	Harwig *et al.*, 1976	Planar Scintigraphy
^{99m}Tc-Plasmin	Enzyme	Plasmin	Animal	Dahlborn *et al.*, 198	Planar Scintigraphy
^{111}In labeled platelet	Platelets	Platelet	Animal/Human (multiple studies)	Thakur *et al.*, 1976; Knight *et al.*, 1978	Planar Scintigraphy
Cyclic RGD Peptide (^{99m}Tc-Apcitide, P280)	Small peptide	Platelet, GP IIb/IIIa receptor	Human (n=19); Human (n=280, Phase III)	Dunzinger *et al.*, 2008; Taillefer *et al.*, 2000	Planar Scintigraphy
Cyclic RGD Peptide (^{99m}Tc-DMP 444, ^{99m}Tc-P4 DMP 444)	Small peptide	Platelet, GP IIb/IIIa receptor	Animal; Human (n=11)	Fang *et al.*, 2011; Klem *et al.*, 2000	Planar Scintigraphy
Cyclic RGD Peptide (^{99m}Tc-Bitistatin)	Small peptide	Platelet, GP IIb/IIIa receptor	Animal; Human (n=4, Phase I)	Knight *et al.*, 2000; Knight *et al.*, 2007	Planar Scintigraphy
^{99m}Tc-TP 1201 ^{99m}Tc-TP 1301	Enzyme	Platelets receptor	Animals	Pallela *et al.*, 1999	Planar Scintigraphy
^{99m}Tc-TP850	Enzyme	Fibrin, Alpha chain	Animals	Aruva *et al.*, 2006; Thakur *et al.*, 2000	Planar Scintigraphy
^{111}In-59D8, ^{111}In-T2G1, ^{111}In-GC4, ^{111}In-64C	Antibody Antibody Antibody	Fibrin, Beta Chain	Animal/Human (multiple studies)	Morris *et al.*, 1997; Alavi *et al.*, 1990; Jung *et al.*, 1989; Lusiani *et al.*, 1989; DeFaucal *et al.*, 1991; Stratton *et al.*, 1994, …	Planar Scintigraphy
Cyclic fibrin binding peptide (EP-2104R)	Peptide	Fibrin	Human (n=14, n=10)	Vymazal *et al.*, 2009; Spuentrup *et al.*, 2008	MRI
^{111}In-EP-2104R (FibPep)	Peptide	Fibrin	Animal	Starmans *et al.*, 2013	SPECT
^{111}InFBP15	Peptide	Fibronectin	Animal	Oliveira *et al.*, 2015	SPECT
^{64}Cu-DOTA-FBP EP-2104R	Peptide	Fibrin	Animal	Cieskienski *et al.*, 2013	PET/CT
EP-2104R based probe	Peptide	Fibrin	Animal	Uppal *et al.*, 2011 [355]	PET/MR
EP-1242	Peptide	fibrin	Animal (n=12)	Sirol *et al.*,	
Al^{18}F-FBP11	Peptide	Fibronectin	Animal	McBride et at. 2013	PET/CT
^{68}Ga-FBP14	Peptide	Fibronectin	Animal	Oliveira *et al.* 2015	PET/CT
^{89}Zr-102-10 (anti-Bβ and anti-γmAb)	Antibody	Region 102-10	Animal	Hisada *et al.*, 2013	PET/CT
CLIO-FXIII	Nanoparticles	Factor XIII	Animal	McCarthy *et al.*, 2009, Tung *et al.*, 2003	NIRF/MRI
^{18}F-FDG	Glucose based	Active inflammatory cells	Human (n=36)	Rondina *et al.*, 2012 [359]	PET/CT
^{18}F-FDG	Glucose based	Active inflammatory cells	Human (n=15)	Hess *et al.*, 2014 [366]	PET/CT

Hess *et al.* [366] investigated in 15 patients suspected PE and/ or DVT using FDG-PET/CT >24 h after diagnosis was ruled out or confirmed according to local guidelines. Linear increase of FDG uptake in pulmonary vasculature show the presence of DVT/PE, and if no FDG uptake DVT/PE is absent. Authors indicated that FDG-PET/CT correctly rule out or diagnose acute DVT in all the patients however less favorable for PE cases i.e. out of 6 PE patients only 2 were found positive. From these studies, it is concluded that FDG-PET/CT is capable to detect deep vein thrombosis. However, confounding factors may contribute to produce false positive results i.e. co-existing infection and inflammation would be considered when FDG-PET/CT is interpreted to diagnose DVT.

One of the benefits of this technique is its capability to visualize venous system thrombi of anatomical regions i.e. pelvis. These clots could not be imaged using other imaging modalities. Pelvis is a place of clot formation and subsequently pulmonary embolism molecular imaging using FDG-PET might be helpful to detect clots in this region. Imaging modalities used for direct imaging are listed in the Table 9.

Table 9 Current Imaging Modalities used for the diagnosis of thrombus

Modality	Key features and Limitations of Imaging Modalities	Radiation Type	Availability
SPECT	Nuclear imaging technique that uses the direct gamma radiations emitted by radioisotopes such as iodine-123 (13 h) or technetium-99m (6 h) Well established, widely available and cheaper than PET Good sensitivity (10^{-10}–10^{-11} mol/L) Limited spatial resolution (7–15 mm) Simultaneously image several radionuclides (differentiated by their energy) Used to provide the anatomical perspective	Y-rays	Yes
PET	Nuclear imaging technique that uses positron emitting radionuclides such as Ga-68 (68 min) or fluorine-18 (110 min) High sensitivity (10^{-11}–10^{-12} mol/L) Limited spatial resolution (5–7 mm) Production of radiolabeled isotopes is expensive and requires the proximity of a cyclotron Molecular imaging of targets such as enzymes or protein sites Biodistribution of tracers, protein binding and metabolism and quantification of dose Poor anatomical resolution, ionizing radiation	ß$^{+}$emissions, Y-rays	Yes
MRI	Versatile modality with wide variety of soft tissue contrasts available Non-ionizing radiations, based on the magnetic properties of hydrogen nuclei placed in a high magnetic field High spatial resolution (0.2–1 mm) very low sensitivity (10^{-3} to10^{-5} mol/L) but better than CT Provide anatomical, functional and metabolic information Poor temporal resolution, high costs	Radio waves	Yes
Ultrasound	Sound waves, non-invasive intravascular, 0.3-0.4 mm, 0.1-0.2 mm, Good temporal resolution, low cost, real time, requires access to transducer, operator dependent, limited field of view	Sound waves	yes
CT	Spatial resolution 0.5-1 mm, High resolution technique based on X-ray attenuation in tissues, functional-anatomical imaging, Rapid, and effective 3D images	X-rays	Yes

Functional ↑ Anatomical

1.4.2 Indirect Imaging of Pulmonary Embolism

In indirect imaging microparticulate system (>10 µm) following their IV administration become trapped in first encountered capillary bed, which are present in lungs [367], hence they occluded pulmonary capillaries and distribute equally in the pulmonary vasculature to elucidate the lung fields clearly [367]. On similar grounds it should be considered that microparticles entrapment function in the form of microembolus would interfere in normal flow of blood and constrained tissue function. Thus toxicodynamic outcomes are directly correlated with number of microparticles administered that ranging from undetected to morbidity or eventual mortality. Size of the microparticles is also critical in order to determine not only the targeted tissue specificity but also site of trap within the tissue. A number of studies have shown the effect of size and number of the biodegradable rigid microparticles in rats i.e. IV injection of 2.1E7 of microparticles (15 ± 5 µm MPs) caused death in < 15 h, but decreasing the number particles to 1.6E7 (15 ± 5 µm MPs) did not cause mortality [368]. Another study stated that particles of size 24 ± 1 µm (~8E6) has resulted 16 h survival rate in 60% rats while this dose found non-lethal in dogs [369].

Therefore to develop an optimal microparticulate system based on the strategy of microembolization requires a precise knowledge of organs response to both number and size of administered microparticles. Particles can be divided into two types depending on their degradation behavior:

i. Non-biodegradable microparticles (Historical Particles)

ii. Biodegradable microparticles

1.4.2.1 Historical Particles (Non-Biodegradable Particles)

Non-biodegradable microparticles are historic microparticles designed in the early 1900s to image lungs fields. In 1946, occlusion of pulmonary artery was performed first time using ^{63}Zn-sulfide suspension in a pectin solution. 100 mCi of ^{63}Zn was injected intravenously to rabbits and patient. Due to short half-life (38.3min) of ^{63}Zn and difficult manipulations, it could not gain clinical popularity. Then Muller & Rossier in 1950 used gold particles (30-50 µm). ^{198}Au particles produced good results for pulmonary occlusion and considered a better system due to its long half-life (65h), and high specific weight. Haynie *et al.* in 1963 used ^{203}Hg labeled ceramic microspheres (50±10µm) and visualized the pulmonary occlusion through scintillation scanning technique in mongrel dogs and obtained clear images in 15-30 min and no activity was found outside lungs [370]. These particles produced favorable results but as they are unable to degrade and remain stuck in the living body thus considered hazardous for the living system hence never used again.

1.4.2.2 Biodegradable Microparticles

Particles that do not accumulate inside the body permanently and cleared from living systems over time after degradation in their size are called biodegradable microparticles. These microparticles are prepared from various sources: blood derived particles (human serum albumin microspheres (HSA) microspheres and macroaggregates of albumin (MAA)), polymeric microspheres (PLGA, PEG-PLGA, PLA), metal derived microparticles (tin fluoride colloid and calcium phytate particles), acid halide derivatives (RC=OX), chitosan derived particles (CHSg), particles using recombinant version of HSA (rHSA, rMAA) and plant derived particles (starch based microparticles). A brief description of particles is given below.

1.4.2.2.1 Blood Derived Microparticulate Systems

Human serum albumin (HSA), is 69 kDa protein comprising of 585 amino acids synthesize by liver and is the single most abundant among all proteins of serum and mainly involve in the transportation of vitamins, medications, hormones, minerals, steroids throughout the body. It contains fifty nine lysine, thirty four cysteine, twenty four arginine, and sixteen histidine residues. It's a multi-domain macromolecule, responsible of maintaining oncotic pressure. Its normal concentration range in blood is 35–55 g/L [371]. The particles derived from the human blood serum albumin are the first class of microparticles used for the lung perfusion study by Taplin *et al.* who successfully visualized lung fields in dogs. The human serum albumin (HSA) particles since their discovery are considered as the gold standard for lung perfusion scintigraphy. HSA prepared in spherical form of size range 10-50 µm is called HSA microspheres and in the aggregated form of size range 10-100 µm is called macroaggregates of albumin (MAA) as shown in Figure 35. HSA microspheres and macroaggregates are metabolized quickly and cleared over time besides their physical and chemical stability, and amenable for large scale production [372].

1.4.2.2.1.1 Human Serum Albumin Microspheres (HSA)

HSA has a rich background in the history of lung perfusion studies. Lung scanning agents based on albumin have proven track record of safety with only contraindication of allergic hypersensitivity [373]. HSA prepared from albumin since early 1960s using various techniques comprising solvent coaccervation, water/oil emulsion, spray-drying or pH coaccervation and radiolabeled with a variety of radionuclides according to the relevant era.

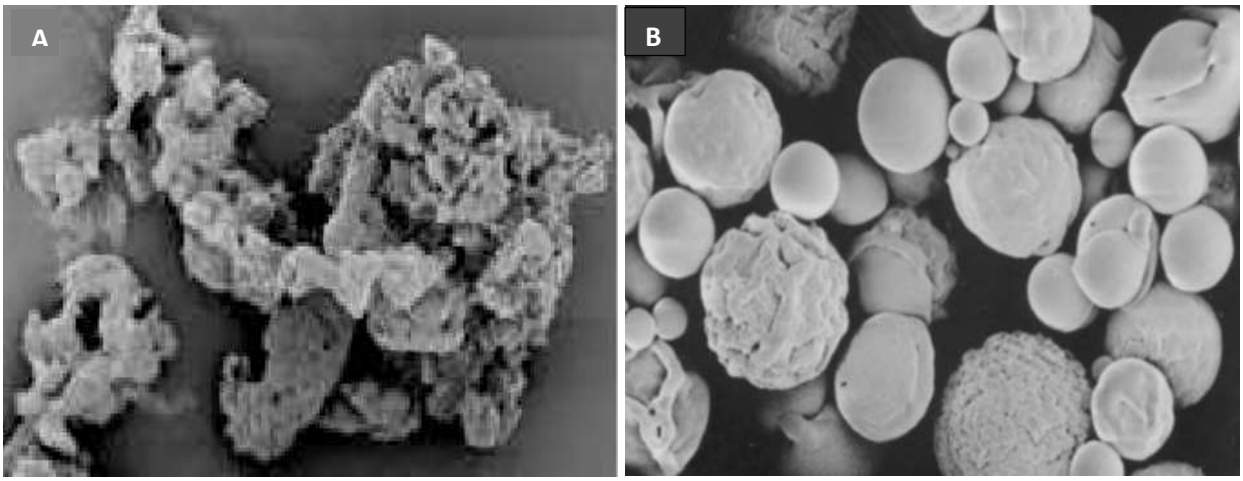

Figure 35 Observed with SEM micrography A) Macroaggregates of albumin (MAA) B) Human Albumin Microspheres (HSA)

1.4.2.2.1.1.1 $^{125}I/^{131}I$ labelled Human Serum Albumin: ($^{125}I/^{131}I$ -HSA)

HSA radiolabeling and imaging studies have been started since 1953 when in a pilot study non crystalized HSA (^{131}I-labeled albumin) was injected to a 31 years old female. At that time, radioactive iodine (^{131}I, ^{125}I) was considered as the most convenient radionuclide for labeling plasma proteins [374, 375]. Its complexes remained stable *in-vitro* and *in-vivo* against enzymatic action in lungs for 2 days, and showed no accumulation or interference due to other organs [376]. Taplin prepared ^{131}I-labeled human serum albumin microspheres (^{131}1-HSA) of mean size 15 µ to image lungs in dogs. The results demonstrated that lung fields were immediately visualized after I.V. injection with an approximate half-life of 1 h in lungs but there second study showed background noise [377]. Later on Dworkin *et al.* prepared ^{131}I-labeled HSA microsphere according to Taplin *et al.* by heating the mixture of HSA microspheres (commercial RISA) of size (50 microns), 1% albumin solution at 75˚C (pH 5.7) [378]. These particles visualize pulmonary artery bed but encountered the issues of in-vivo instability and large size i.e. first

would result into insufficient time to visualize the lungs fields and the second issue might lead into the embolization of arterioles.

Later on Zolle *et al.* prepared microspheres of albumin by dispersion of small volume of albumin solution in cotton oil with constant agitation. They produced radiolabeled microparticles of suitable size range 12-44µm that showed >90% accumulation in lungs capillaries. These smaller particles showed superior characteristics such as reduction in pulmonary toxicity, radiation exposure and cerebral embolic complications [379].

1.4.2.2.1.1.2 ^{68} Gallium-labeled human serum albumin microspheres: (^{68}Ga-HSA)

Contrarily to technetium-99, the labeling procedure of gallium-68 is simple as it can make complexes without the use of reducing agents. But there are certain necessary adaptations required prior to labeling with ^{68}Ga such as preparation of pure gallium and suitable chelates for it's labeling i.e. proteins could not make direct complexes with ^{68}Ga. These two issues were solved by the introduction of purifying columns and surface functionalization of proteins.

Introduction of functional groups on the surface of proteins is called surface functionalizing. This process can ease the radiolabeling process and reduce the time of the reaction (short half-life of ^{68}Ga) as proposed by Benisek & Richards and Sundberg *et al.* who utilized methyl picolinimidate and EDTA for this purpose [380, 381]. Later on Chesler *et al.* in 1974, produced ^{68}Ga-labeled HSA microspheres (10µ & 30µ) and obtained high quality PET images of artificially embolized dogs lungs [382]. Soon after, Krejcarek and Tucker used DTPA to create hexadentate chelating sites on the protein surface. Synthesis process was simple and achieved by DTPA attachment on protein surface through amide bond, a better alternative of Sundberg method without the involvement of intermediate [383]. Afterward Wagner and Welch utilized

Krejcarek and Tucker method to produce ^{68}Ga labeled DTPA-HSA microspheres (RCP 95%) and PET images of dogs lungs had clearly identified the areas of decreased perfusion [384].

Initially ^{68}Ga eluate has encountered a problem of associated impurities thus purifying columns were developed. As separation of ethylene diamine tetra acetic acid (EDTA) from ^{68}Ga eluate (gallium-EDTA) is required to obtain pure ^{68}Ga and due to the short half-life of radionuclide a quick purification method is essential. Therefore Carlton and Hayes introduced an ion exchange column (Bio-Rad AG l-X_2) and HCl was passed through the column to dissociate ^{68}Ga-EDTA complex [385]. Afterward Hnatowich *et al.* introduced a simple extension of Carlton column to obtain pure gallium, procedure included a glass syringe column plugged with glass wool, filled with Bio-Rad Ag 1-×2, 50-100 mesh chloride. According to this method ^{68}Ga-pharmaceutical preparation took 30-35 min with a radiochemical purity 60-70% [386]. Authors carried out first study of ^{68}Ga-labeled human serum microsphere with radiochemical purity (RCP) ~90%. The radiotracer (^{68}Ga-Sn-HSA) showed a good stability (2 h) in dogs lungs which is a sufficient time to perform lung perfusion studies in clinical settings [386]. Then Yvert *et al.* have introduced some changes in above mentioned column to obtain $GaCl_4^-$. They filled column with quartz wool and rinsed with HCl, distilled water and buffer mixture [NaOH, Na_2HPO_4 and phenol red]. The column eluate after sterilization was placed in water bath at 60-65˚C, centrifuged, liquor (supernatant) was decanted carefully, and final ^{68}Ga-labeled particles showed the radiochemical purity of (RCP) 88-91% [387]. Later on Maus *et al.* eluted ^{68}Ga from a commercial gallium-68 generator which contains a modified tin dioxide column.

Table 10 Different radiopharmaceuticals prepared from Human serum albumin microspheres

Publications	Radiotracers	Modality	Characteristics and important points	Population	References
Cohen *et al.* Bennhold *et al.* **1956**.	^{131}I-HAS	Y-Camera	Imaging of 31 year old lady	Humans	[374];[375]
Areil & Quinn *et al.* **1963** Quin & Whitley *et al.* **1964**	^{131}I-HAS,^{51}Cr-RBC, ^{203}Hg-CM	Y-Camera	^{203}Hg-CM found better, but HSA is more stable in-vivo	Animals	[388]
Taplin *et al.* **1964 (** 15 µ)	^{131}I-HSA	Y-Camera	Detected PE in dogs and later in patients	Animals/humans	[377]
Dworkin *et al.*1964 (50 µ)	^{131}I-HAS	^{131}I-HSA	Easy radiolabeling with ^{125}I, ^{113}In, ^{99m}Tc, short half-life;	Animals	[378]
Zolle *et al.* **1970** (12-44 µ)	^{125}I-HAS, ^{113}In-HAS, ^{99m}Tc-HAS	Y-Camera	Suitable particles, uptake decrease in lungs early RCP >90%, suitable for lung perfusion; Reduced toxicity & exposure	Animals	[379]
Rhodes et al. **1971**	^{99m}Tc-HSA	Y-Camera	Labeled HSA microspheres kits with $^{99m}TcO^{-}_{4}$.RCP~83%, 10-40 µm size, clear images of lungs, detect PE in patients suspected of PE	White mice/Human	[389]
Carlton and Hayes *et al.* **1971**	^{68}Ga-HAS	PET	Prepared Bio-Rad A G1-X_2 ion exchange column; pure ^{68}Ga-HSA	--	[385]
Hnatowich *et al.* **1975**	^{68}Ga-HAS	PET	Prepared a purify column, obtained RCP >90±5%; prepared ^{68}Ga-Sn-HSA, stable for 2h *in-vivo*, lung perfusion study	Animals	[386]
Yvert *et al.* **1975**	^{68}Ga-HAS	PET	Column glass syringe filled with quartz wool, pure ^{68}Ga, RCP 88-91%	--	[387]
Chesler *et al.* **1975** (10-30µ)	^{68}Ga-HAS	PET	labeled with ^{68}Ga (Lanthanum) good lungs images in dogs	Animals	[382]
Krejcarek &Tucker. **1977**	^{68}Ga-DTPA-HSA	PET	DTPA-HSA surface modification and labelled with ^{68}Ga,obtained 95% RCP, Detect PE in lungs lobes in animals	Animals	[383]
Wagner and Welch. **1979**	^{68}Ga-DTPA-HAS	PET	DTPA-HSA labeled by ^{68}Ga-Oxines and RCP=95%, good lungs images	Animals	[384]
Willmont, CHEN *et al.* **1989**	^{125}I-HAS	Y-Camera	Easy radiolabelling conditions, Stable for 2 days *in-vivo*	Animals	[376]
Maus et al. **2011 (**10-30 µm)	^{68}Ga-HSA	Micro PET	^{68}Ga was eluted by a modified tin dioxide column, process took <30 min for ^{68}Ga-HSA preparation, RCP 79±5%,	Animals	[236]

The radiolabeling method to obtain ^{68}Ga-labeled HSA was simple and took only 30 min producing an RCP of 79±5%. The resulting ^{68}Ga-labeled HSA microspheres (10-30 µm) produced fine tune images of lung and can be used for lung perfusion studies. Further detail of purification of ^{68}Ga is available in the section of ^{68}Ga-labeled MAA. Some HSA microspheres based radiopharmaceuticals' are presented in the Table 10.

1.4.2.2.1.2 Macroaggregates of albumin (MAA)

Macroaggregates of albumin (MAA) are prepared from human serum albumin (HSA) in the form of aggregates (10-100 µm) as shown in Figure 35. Human serum albumin (HSA) is the 60% of total protein present in blood serum and most widely used in many therapies [390, 391]. Its brief detail is given in the section of blood derived microparticles.

MAA are the biodegradable particles just like HSA microspheres and as small arterioles of lungs are filtering out smaller microspheres, thus, these soluble microparticles would occlude lungs for short time only. After this discovery many groups have put their efforts to fabricate MAA injectable formulations for lung perfusion study. Aggressive research was focused to prepare a radiopharmaceutical formulation which can produce high radiochemical purity in small time via simple and easy methods that should be compatible with the daily routine practices of clinical settings. Gradually MAA kits were introduced which were optimized over time and finally Lyster *et al.* succeeded to produce MAA kits with promising results, till then kits are available in the commercial market and used successfully for lung perfusion scanning in human clinics. A brief overview of the MAA based radiopharmaceutical is presented hereafter.

1.4.2.2.1.2.1 ^{131}I-labelled Macroaggregates of Albumin: (^{131}I-MAA)

Taplin *et al.* [377] prepared ^{131}I-macragregates of albumin in two sizes using modified Benacerraf [392] procedure.

I. Small size particles colloidal suspension (10-20 mµ)

II. Large size particles suspensions (1-5 µ)

^{131}I-macragregates of albumin in-vivo (1-5 µ) evaluation in dogs showed clear images of lung fields soon after IV injection of radiotracer but liver became visible after 1h which showed the

release of albumin macroaggregates from lungs towards liver. The albumen particles were accumulated in liver's Kupffer cells and then released from liver through a proteolytic enzymatic digestion process [164, 377, 378, 393-395]. Later on this group has conducted phase-I clinical trials in 100 patients. They injected 5–25 macroaggregates of albumin. The results illustrated that the radiotracer has diagnosed regional pulmonary emboli before the recognition of signs in chest X-ray assessment and also verified safety of the drug in humans [396].

1.4.2.2.1.2.2 ^{99m}Tc-labelled Macroaggregates of Albumin: (^{99m}Tc-MAA)

^{99m}Tc has advantage on other radionuclide such as ^{131}I, due to its suitable half-life (6 h) and generator synthesis (^{99}Mo/^{99m}Tc). Thus ^{99m}Tc-labeled macroaggregates of albumin (^{99m}Tc-MAA) Since its discovery has become a revolution in the history of medical imaging and considered as the gold standard for lung perfusion scintigraphy [397, 398]. However, the optimization of its radiolabeling procedures (^{99m}Tc-MAA) took a long way in order to acquire the standard desired radiopharmaceutical. In the start, the radiolabelling procedures involved the on spot aggregation of ^{99m}Tc-labelled albumin or ^{99m}Tc-labelled sulfur colloid and albumin [397, 398] before labeling. These methods faced major drawbacks of considerable daily practice requirement, substantial manipulation, and radiation exposure along with variations in the particles size and radiochemical purity [397, 398]. Thus as an alternative, many laboratories were forced to use ^{131}I-MAA although with less desirable characteristics than ^{99m}Tc [399-402]. Meanwhile, separate ready to use kits of MAA particles were prepared successfully. It turns into a breakthrough and commercial kits become available in the market. It has reduced the manipulation time and solved the problems of on spot aggregation. However, these kits also faced some short comings such as need certain manipulations and occasionally showed different radiochemical purity or sometime

instability (liver uptake) [403-406]. At that moment Lyster *et al.*, introduced a kit with superior qualities such as suitable particle size, simple radio-labeling procedure and stable for 2 months at 4˚C. For radiolabeling purpose MAA kits only require to incubate with radionuclide (^{99m}Tc) without difficult manipulations. Authors used human serum albumin, sodium acetate buffer and stannous chloride to prepare ^{99m}Tc-Sn-MAA, which ultimately showed an encouraging uptake of 97.30 %ID in lungs and 1.6% in liver [407]. Different MAA based radiopharmaceuticals investigated until now are illustrated in Table 11.

Table 11 Radiopharmaceuticals prepared from macroaggregates of albumin (MAA)

Radiotracers	Characteristics and important points	Publications	Modality	References	Study subjects
^{99m}Tc-MAA (5-25 µ)	Safer and identify PE in human	Taplin and Jhonson **1964**	Y-camera	[377, 396]	Animal/human
^{99m}Tc-S-MAA	radiation exposure; Variable particles size	Taplin & MacDonald **1971**	Y-camera	[398]	Animal/human
^{131}I-MAA	Long half-life, radiation exposure	Gwyther & Field **1966**	Y-camera	[399]	Animals/human
^{99m}Tc-MAA	Variations in size and RCP	Peterson & Bonte **1967**	Y-camera	[400]	Animals
^{99m}Tc-S-MAA	Better qualities but considerable work	Cragin & Webber **1969**	Y-camera	[402]	Animals
^{99m}Tc-MAA	Considerable work for daily practice	Suprenant & Wabber **1969**	Y-camera	[401]	Animals/human
^{99m}Tc-MAA	Breakthrough, MAA Lyophilized kits	Deutsch & Redmond **1972**	SPECT	[403]	Animals/human
^{99m}Tc-MAA	Kits become available commercially	Robbins & Fortman **1972**		[406]	
^{99m}Tc-MAA	Still require manipulations: variations in RCP some time	Lowes & Gydesen **1973**		[405]	
^{99m}Tc-MAA	liver uptake	Aljanabi & Yousif **1983**		[404]	
^{99m}Tc-Sn-MAA	Stable, Simple methods for labeling, suitable particles size, revolution in MAA kits	Lyster & Scott. **1974**	SPECT	[407]	Animals/human
^{99m}Tc-Sn-rMAA	Recombinant (rMAA, rHSA) RCP >99% comparable to MAA; Excellent lung images, never used afterward due to high cost and difficult reaction steps	Hunt & Frier *et al.* **2006**	SPECT	[408]	Animals/human
^{68}Ga-MAA	RCP ~97.0, but ^{68}Ga eluate showed impurities thus never used again	Green & Even. **1989**	PET	[408]	Animals/human
^{68}Ga-MAA	Purified ^{68}Ga eluate; high RCP seen	Zhernosekov *et al.* **2007**	PET	[233]	Animals
^{68}Ga-MAA	TiO_2-based generator of ^{68}Ga; RCP>99%	Mathias & Green. **2008**	PET	[409]	Animals
^{68}Ga-MAA	TiO_2- column, ^{68}Ga; RCP= 79±5%, lungs images, in-vivo stability 1 h	Maus *et al.* 2011	PET	[236]	Animals
^{68}Ga-MAA	Primary study in suspected PE patients and compared with ^{99m}Tc-MAA SPECT	Hoffman *et al.* **2011**	PET	[219]	Humans
^{68}Ga-MAA,	purify columns, pure ^{68}Ga to label MAA	Amor *et al.* **2013**	PET	[410]	Animal/human
^{68}Ga-MAA	label MAA with pure ^{68}Ga, lung perfusion	Ament *et al.,* **2013**		[225]	
^{68}Ga-MAA	MAA kits label to ^{68}Ga, RCP 90-100%, lung perfusion study	Shanehsazzadeh *et al.* **2015**	PET/CT	[234]	Animals/human
^{68}Ga-MAA		Jalilian, Lahooti *et al.* **2017**	PET/CT	[235]	Humans
^{68}Ga-DOTA-MAA	^{68}Ga with MAA via fast methods	Mueller *et al.* **2017**	PET/CT	[119]	Humans
^{68}Ga-MAA	lung perfusion studies on 4D PET/CT	Siva *et al.* **2017**	PET	[238]	Humans

1.4.2.2.1.2.3 ^{68}Ga-labeled Macroaggregates of Albumin: (^{68}Ga-MAA)

In the meantime a need arose to search an alternative of ^{99m}Tc due to the worldwide shortage of ^{99}Mo that decays to produce ^{99m}Tc which is used approximately in 600,000 medical procedures for imaging purposes per week [236]. Thus on parallel grounds surrogates of ^{99m}Tc is searched and ^{68}Ga being a generator produced radionuclide could serve the purpose. Thus some groups have analysed ^{68}Ga-labeled macroaggregates of albumin (^{68}Ga-MAA) as a substitute for conventional V/Q imaging by PET/CT.

^{68}Ga was successfully labeled with MAA for the first time by Green & Even in 1989. Process included the addition of ^{68}Ga eluate to MAA kits in the presence of acetate buffer at pH 4.7, and heated at 74˚C for 15 min. ^{68}Ga-MAA was vortex mixed with saline and centrifuged to isolate pure ^{68}Ga-MAA to produce a radiochemical purity of 97.0±0.5% [230]. As discussed earlier there was a problem of impurities with ^{68}Ga eluate. However this method was never used again, possibly due to the irregularity & impurities associated with ^{68}Ge/^{68}Ga generator. Later on Zhernosekov *et al.* has developed an efficient system for the purification of ^{68}Ga eluate. This process has become a breakthrough to obtain pure ^{68}Ga for direct radiolabelling of biomolecules. Purification and pre-concentration was achieved by attaching a miniaturized column having cationic exchange resin. Using this process 97% pure ^{68}Ga eluate was obtained in just 4 min and amount of impurities of ^{68}Ge (IV) were reduced by a factor of 10^4, while Fe (III), Ti (IV), and Zn (II) were reduced by a factor of 10, 10^2, and 10^5, respectively. This method is easy to automate and guarantees safe preparation and high yield of ^{68}Ga-labelled radiopharmaceuticals for routine clinical PET applications [233].

Then Mathias and Green radiolabeled macroaggregates of albumin efficiently with commercially available eluate of titanium based gallium-68 generator.^{68}Ga chloride was eluted from generator using HCl (0.1N), and buffer of pH range 5 to 6 (sodium acetate). Acquired ^{68}Ga-acetate suspension was added to MAA kit and resulting mixture was incubated for 15 minutes at 75˚C with gentle shaking (300rpm). ^{68}Ga-MAA formulation was centrifuged, suspended in saline solution and resulting RCP was about 99.8% [409].

Maus *et al.* [236] has prepared pure ^{68}Ga using ^{68}Ge/^{68}Ga generator with a modified tin dioxide column with HCl (0.6 N). MAA kits were washed with saline solution (n=3), centrifuged, reconstituted with water, mixed with ^{68}Ga eluate in the presence of pH 4, HEPES buffer following incubation for 20 min at 75˚C with gentle agitation. The process of preparation of ^{68}Ga-labeled MAA took less than 30 min, and radiochemical purity was (RCP) 79±5%. ^{68}Ga-labeled MAA biodistribution studies showed good activity uptake in rats' lungs with 1 h stability. This method is simple and can be optimized to increase RCP values.

In a parallel investigation first clinical study in human patients (2M, 3F) was performed by Hoffman *et al.* Authors showed that V/Q PET/CT clinical results were comparable to V/Q SPECT/CT [229].

Mueller *et al.* in 2017 reported a robust and simple method of labeling ^{68}Ga with MAA and resulting radiochemical purity was >99% without using $SnCl_2$. They developed two methods for labeling for labeling MAA with ^{68}Ga i.e. manual labeling and automatic labeling method [119].

I. Manual procedure to develop ^{68}Ga-MAA

Under aseptic conditions, MAA kits were equipped with vented spikes and buffer was added to them with gentle agitation. ^{68}Ga was added to the mixer, heated at 90˚C and neutralized with sodium phosphate buffer, and resulting radiochemical purity was >99%. The general scheme is given in Figure 36.

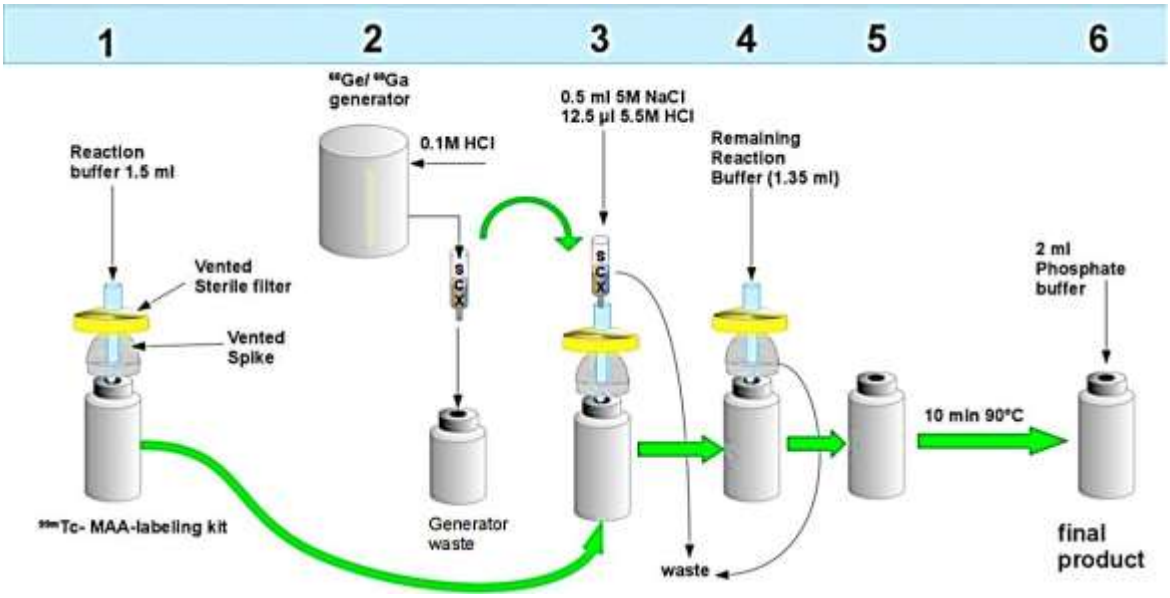

Figure 36 Schematic drawing of the manual labeling of the MAA-labeling kit with 68Ga, published with from ref [119]

II. Automatic procedure to develop^{68}Ga-MAA

In this method an automatic system, sterile cassette, and SCX vial were used containing a mixture of saline and hydrochloric acid. Sodium acetate buffer of 4.5 and sterile water was added to MAA kits and transferred to a preheated reaction vial at 95˚C of module cassette and then heated for 10 min at 115˚C. Product vial was connected directly to module cassette as shown in Figure 37. Automated synthesis took 14 min at pH 6–7. Ion exchange resins used were in a combination of anion/cation exchange resins, and designed in four steps: Elution, Cleaning Purification and Extraction**.** Radiochemical purity obtained was more than 99%. Authors found

that activity about 20 MBq was sufficient to produce high quality images of ^{68}Ga-labeled MAA using V/Q PET/CT with low radiation exposure (2 mSv) to each patient. Results showed ^{68}Ga-labeled MAA PET/CT produced superior images than ^{99m}Tc-MAA SPECT/CT in small time [119].

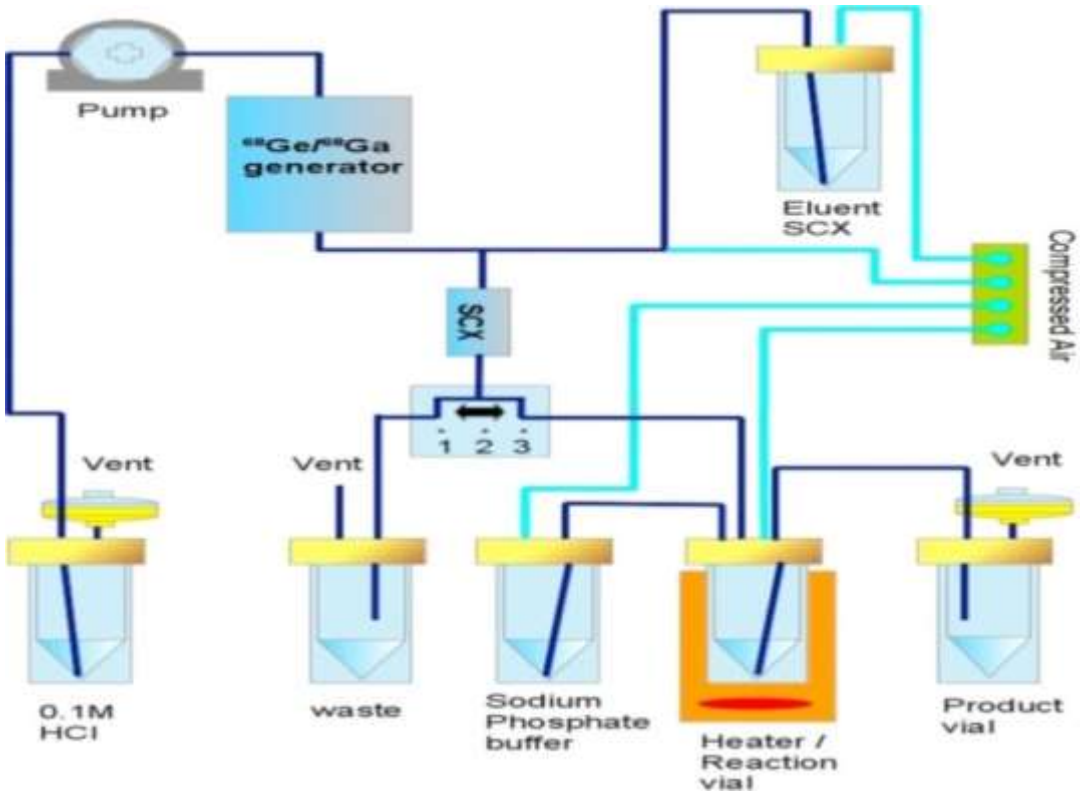

Figure 37 Diagram of the automated Modular Lab EAZY (Eckert & Ziegler) radio-synthesis system, published with permission from ref [119]

Limitations of Blood Derived Particles

I. MAA size distribution did not fulfill the requirements (Figure 35) of optimum specifications (20-40 µm) for the allocation of pre-capillary arterioles. Orientation of MAA in blood flow is important in order to determine "efficient size". It becomes difficult to predict MAA *in-vivo* behavior. The ideal perfusion microparticles should be

sphere-shaped, and a size distribution of 30 µm approximately in order to allow particles distribution in capillaries only. As about 10^4 microparticles are injected, that's why this size remains safe for lungs perfusion studies hence no adverse scene is observed with MAA clinically. Aggregate degeneration is an additional factor causing size distribution inconsistent and unreliable.

II. Human Serum Albumin (HSA/HAM) is spherical shape (10-50 µm) microspheres and acknowledged as ideal lung perfusion agents. Since HSA kits require harsh radiolabelling conditions and possess thiosulfate as a reducing agent and detergent as a part of excipients. Hence HSA microspheres in spite of their suitable size, shape and stability in liver-lung shunt (LLS) patients than ^{99m}Tc-MAA [412] still the prevalence of MAA over HSA as lung perfusion agent is due to its easy preparations.

III. MAA and HSA bear side effects ranging from nausea to cardiac arrest [413, 414] although adverse responses are exceptional and bear the potential risk associated with blood-derived products to transmit viral infection [390], specifically Hepatitis C and the HIV

IV. ^{68}Ga-MAA used for lung perfusion PET/CT study, was prepared from MAA kit originally designed for labeling with ^{99m}Tc. In order to get high labeling yield, multiple washing steps of the kit are mandatory which increase manipulation time [234] and hence may cause contamination of the product. MMA lyophilized kit to label with ^{68}Ga is still not available commercially.

Due to the potential hazard of the two established ^{99m}Tc labeled albumin microspheres (^{99m}Tc-HAM, 10±50 µm) and macroaggregates of albumin (^{99m}Tc-MAA, 10±90 µm)

radiopharmaceuticals, some microparticles were explored as a surrogate of MAA/HAM as discussed below.

1.4.2.3 Synthetic Polymeric Particles

Polymeric particles have been prepared as injectable drug with surface modifications to increase their blood circulation and target lungs. A few examples of polymeric particles with high lungs uptake are given below.

Sato et al. used taxol-loaded PLGA microspheres (30.1µm) for lung targeted delivery. These microspheres showed high uptake in lungs while liver showed no uptake [415].

Zhang et al. used cisplatin loaded-^{125}I-labeled bovine serum albumin microspheres (CDDP-^{125}I-BSA-MS) of size 7-25 µm to be investigated in mice through IV injection. The microspheres showed high uptake of >97% ID in lungs while blood and other organs showed no accumulation. Photomicrographs showed cisplatin BSA microspheres in the capillaries and precapillary arterioles of lung that cleared gradually over time [416].

Wang *et al.* developed gelatin microspheres for drug delivery to target lungs with >87% of gelatin microspheres have size between 5.1-25.0 µm. In-vivo distribution in mice showed that gelatin microspheres targeted the lung >3 to 35 times as compared to blood and rest of organs [417]. Meanwhile Gref *et al.* prepared biodegradable nanospheres from biocompatible copolymers i.e. poly (lactic- co-glycolic acid) (PLGA), poly-caprolactone (PCL) etc. These particles showed a high blood circulation time and no uptake in liver [418].

Emodin (1,3,8-trihydroxy-6-methylanthraquinone; Figure 38) has the potential to target lungs and to avoid toxicities of other organs such as liver, it was attached to polymeric particles called polylactic acid microspheres (PLA). The resulting polymeric microspheres loaded emodin (ED-

PLA-MS) with mean size (9.7±0.7µm), have primarily targeted mice lungs after IV injection [419]. Besides high lungs uptake of above mentioned synthetic polymeric particles, they were never explored for lung perfusion scintigraphy.

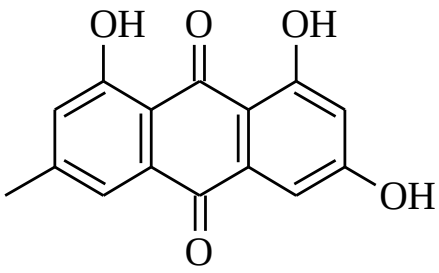

Figure 38 Structure of Emodin

Derived from the results of above studies, copolymers such as PEG±PLA [methoxy-poly (ethylene glycol)-poly (lactide)] and PEG±PLGA [poly (ethylene glycol)-poly (lactide-coglycolide)] and PLA (poly (co-lactic acid) identical to the size of HAM microspheres are prepared and explored for lung scintigraphy.

1.4.2.3.1 Poly (DL-Lactic-co-glycolic acid; PLGA) labeled with ^{99m}Tc: (^{99m}Tc-PLGA)

Biodegradable microspheres developed from polymers of synthetic origin like poly (DL-Lactic-co-glycolic acid): PLGA 41 KDa, methoxy polyethylene glycol-PLGA (PEG-PLGA) 47 KDa [420, 421], polyvinyl alcohol (PVA) and Poloxamer-188, polyethylene glycol (PEG) 10 kDa. These are copolymers prepared on the Gref *et al.* principle which showed that polymeric coating has reduced the liver uptake on nanoparticles. These polymeric particles were assessed for their lung perfusion efficiency and results were compared with human serum albumin microspheres (HAM).

The polymeric microspheres were synthesized using method of solvent evaporation. Labeling was performed with ^{99m}Tc (2.5-3 mCi) by mixing microspheres in the presence $SnCl_2$ and

poloxamer-188 under sterile atmosphere. The resulting radiochemical purity was more than 95% and *in-vivo* lungs uptake was for ^{99m}Tc-HAM was 99%, for ^{99m}Tc-PLGA (Poloxamer 8%)-20 was 67% and for ^{99m}Tc-PLGA (PVA) was 30%. The polymeric particles were found mostly in the liver except lungs. From these unexpected results authors inferred that morphological surface modifications and size distribution is not the only criteria for the particles to target lungs vasculature as these modified polymeric microspheres were of identical size and shape to HAM microspheres. Thus authors used bovine serum coating on polymeric particles but it did not change the results.

Consequently ^{99m}Tc-PLGA (Poloxamer-8%)-20 produced good initial images but liver overlaps were shown after sometimes and in PLGA (PVA) images liver was more visible than lungs [422]. These polymeric particles were unable to compete with HAM.

1.4.2.3.2 Poly-(L-Lactide, PLA) microspheres labeled with ^{99m}Tc: (^{99m}Tc-PLA)

Later on Hafeli et al. in 2010 prepared biodegradable monosized (9.0±0.4µm) non-toxic microspheres consisting of poly-(L-lactide, PLA) with bis-(picolylamine) at their end. These particles are fabricated via microfluidic glass chip technology and radiolabelling was performed by^{99m}Tc-tricarbonyle using an Isolink kit (Mallinkrodt). The formulation was heated at 75 ̊C and centrifuged for 30min at 1000rpm. Microspheres produced by microfluidic chip were of perfect spheres [423] and showed a lung uptake of 79.6±3.8% ID in mice lungs at 15 minutes post administration [423]. Mono-sized PLA particles showed attractive properties of well-defined size, shape, and high uptake in lungs that make it a suitable candidate for lung perfusion studies.

Limitations of Synthetic Polymeric Particles

I. Potential radiopharmaceuticals for lung perfusion prepared from polymers such as lactic-co-glycolic acid copolymers (PLGA) or grafted methoxy polyethylene glycol (PEG-PLGA), poly vinyl alcohol (PVA), polyethylene glycol (PEG) did not meet the requirements of lung perfusion agents. Although there size was favorable but they were unstable in-vivo so unable to produce high quality images of lungs fields.

II. In addition synthetic polymers preparation methods require toxic organic solvents during their radiolabelling process and laborious procedure. These manipulations are not feasible in clinical set ups.

III. Polymeric particles called PLA is offering suitable spherical shape and size (~10 µm) compatible with the size of human pulmonary capillaries. Preliminary animal studies showed the potential of the particles and further preclinical and clinical trials are essential to explore its performance.

Radiopharmaceuticals developed for in-direct imaging of PE are shown in Table 12.

Table 12 Radiopharmaceuticals Designed for In-direct Diagnosis of Pulmonary Embolism

Microparticles	Source of origin	Radionuclide	Population	Authors & year	Modality	References
Ceramic microspheres, 50 micron	ceramics	^{203}**Hg**	Animals	Haynie *et al.*,1963	Gamma camera	[370]
Macroaggregates of Albumin (MAA, 10-100µm), HSA microspheres	Blood derived	^{99m}**Tc/**^{131}**I**	Animals/humans	Taplin *et al.*,1963; Taplin *et al.*, 1971	Gamma camera	[396]
Albumin Sulphur microspheres (10-50 µm)	Blood derived	^{99m}**Tc**	Animals	Cragin *et al.*, 1969	Gamma camera	[402]
Tin colloid of MAA (10-100 µm)	Blood derived	^{99m}**Tc**	Gold standard	Lyster *et al.,* 1974	SPECT	[407]
MAA (10-100 µm)	Blood derived	^{68}**Ga**	Animals	Even & Green *et al.* 1989	PET	[230]
Tin fluoride colloid (SnF_2) (3-5 µm)	Synthetic chemical	^{99m}**Tc/**^{68}**Ga**	Humans	Tspoles *et al.*, 2006 Tspoles *et al.,* 201	SPECT/CT PET/CT	[424] [425]
Chitosan glycol microspheres (CHSg) (30.1±4.8 µm)	Chitosan (bio pesticide from shells of lobsters/crabs/ shrimp	^{99m}**Tc** ^{68}**Ga**	Animals	Amor *et al.* 2013 Amor *et al.,* 2014	SPECT/CT PET/CT	[237] [411]
Recombinant Human Serum Albumin	Yeast (Natural)	^{99m}**Tc**	Animals/humans	Fleer R *et al.*, 1991	SPECT	[426]
Pegylated Human serum Albumin (DPA-HAS) (PLGA) 41 KDA	Blood derived	^{99m}**Tc**	Animals	Park *et al.* 2019	SPECT	[427]
(PEG-PLGA) 47 KDa, PVA 10 KDa, PEG 10 KDa	synthetics Polymers	^{99m}**Tc**	Animals	Delgado *et al.,* 2000	SPECT/CT	[422]
Recombinant MAA (rMAA)	Yeast (Natural)	^{99m}**Tc**	Animals/humans	Hunt *et al.,* 2006	SPECT/CT	[408]
PLA, mono-sized (9.0±0.4 µm)	Synthetics polymer/microchip technology	^{99m}**Tc**	Animals	Hafeli *et al.,* 2010	SPECT/CT	[423]
Carbonyl halide $(CO)_5I$	chemical Halides	^{99m}**Tc**	Animals	Miroslavo *et al.* 2009	SPECT/CT	[428]
Starch Based microparticles (9-74µm)	Potato starch (Natural)	^{99m}**Tc**	Animals	Lacoeuille *et al.,* 2010	SPECT/CT	[429]
Calcium phytate	Calcium phytate	^{99m}**Tc**	Animals	Pimental *et al.*, 2005	SPECT/CT	[430]
Particles (15-3 µm)	(synthetic)	^{68}**Ga**	Humans	Hsieh *et al.*, 2016	PET/CT	[431]

1.4.2.4 Metal Based Microparticles

1.4.2.4.1 ^{99m}Tc & ^{68}Ga labeled Tin Fluoride Microspheres: (^{99m}Tc/^{68}Ga-SnF_2)

Stannous fluoride is previously famous for oral hygiene for about 65 years. SnF_2 is popular in the filed of nuclear medicine to prepare technetium-99m labeled tin fluoride colloid. This radiocolloid delivers technetium-99m to white blood cells. The tin fluoride colloid is prepared from two-part kit. The stannous fluoride part is either frozen formulation or freeze dried and it is the main component to prepare tin colloid.

Chris Tsopel for the first time explored tin fluoride (SnF_2) microspheres as lung perfusion agent. The colloid SnF_2 (tin fluoride) is deleloped from commercially available kits (A+B) kit (A= NaF, B=SnF_2)]. For radiolabeling ^{99m}Tc-pertechnetate (20-1000 MBq) and saline was added in thawed B vial having a breather needle. Different reaction conditions were tested and it was found that air helped to produce large size of particles at room temperature. Radiochemical purity was 99.4±0.4% and biodistribution studies showed a high uptake of ^{99m}Tc-SnF_2 colloid particles (89±1%) in lungs [424].

Later the same group in 2016 prepared ^{68}G-labeled SnF_2 microspheres. They prepared tin fluoride colloid microspheres following the same procedure as discussed above. The tin fluoride colloid was labeled with $^{67}GaCl_3$ after heating at 100˚C. Size distribution analysis showed that 74% of particles were 3–5 μm and 26% particles were >5 μm in diameter. ^{67}Ga-*h*-SnF_2 optimal formulations showed radiochemical purity ≥97%, and lungs uptake of 41±3%, and liver plus spleen showed 41% and in carcass 18% at 20 min post IV injection in rats [425].

1.4.2.4.2 ^{99m}Tc & ^{68}Ga labeled Calcium-Phytate Particles: (^{99m}Tc/ ^{68}Ga-Ca-phytate)

Phytic acid exists mainly in grains or seeds and the storage form of energy for plant kingdom. It occurs mostly as heterometal salt of magnesium or calcium in nature. It acts as metal scavenger in corrosion inhibitor and topical cosmetics. Its chelating properties for metals are exploited to prepare different chemicals and radiopharmaceuticals for diagnostic and radiotherapy. ^{99m}Tc-Ca-phytate radiocolloid (300-1000 nm) are generally used for hepatoscintigraphy.

Pimental has reported in 2005 a kit derived from phytic acid which is capable of forming complex with Ca^{+2} cation that can occlude pulmonary capillaries and serve as lung perfusion agent [430].

Later on this group in 2016 reported the radio-synthesis of ^{68}Ga-labeled-Ca-phytate particles from commercially available phytate kit. The kit was reconstituted with NaCl, and added to $^{68}GaCl_3$, filtered, and then $CaCl_2$ was added with gentle swirling, and heated for 30 min at 100˚C, cooled, and finally neutralized with $NaHCO_3$ to attain pH 6-7. ITLC was performed with citric acid as eluent and resulting RCP was 99%. The particles were of diameter 15-3 µm and showed 2 h *in-vitro* stability. ^{68}Ga-Ca-phytate *in-vivo* studies in Sprague Dawley female rats showed 93% uptake in lungs. The calcium phytate particles labeled with ^{68}Ga produced high quality PET images as compared to gold standard ^{99m}Tc-labeled MAA SPECT [431].

Limitations of Metal Based Microparticles

I. ^{67}Ga-*h*-SnF2 showed variations in particles size and radiotracer optimal formulations showed 41% activity uptake in lungs at 20 min of injection and hence liver interference was quite obvious. This radiopharmaceutical is not suitable for lung scanning; further optimization of the particle size can improve the lungs uptake values and consequently

would produce good lungs images. ^{99m}Tc-SnF_2 and ^{68}Ga-Ca-Phytate seems useful for lung perfusion scintigraphy and further studies are required to prove the potential of new radiopharmaceutical. There is a room for improvement in the procedure to perform radiolabeling at room temperature and to increase the size of particles i.e. 3 µm as it is very small compared to human pulmonary capillaries.

Radiopharmaceuticals designed and developed for indirect imaging of pulmonary embolism is shown in the Figure 39.

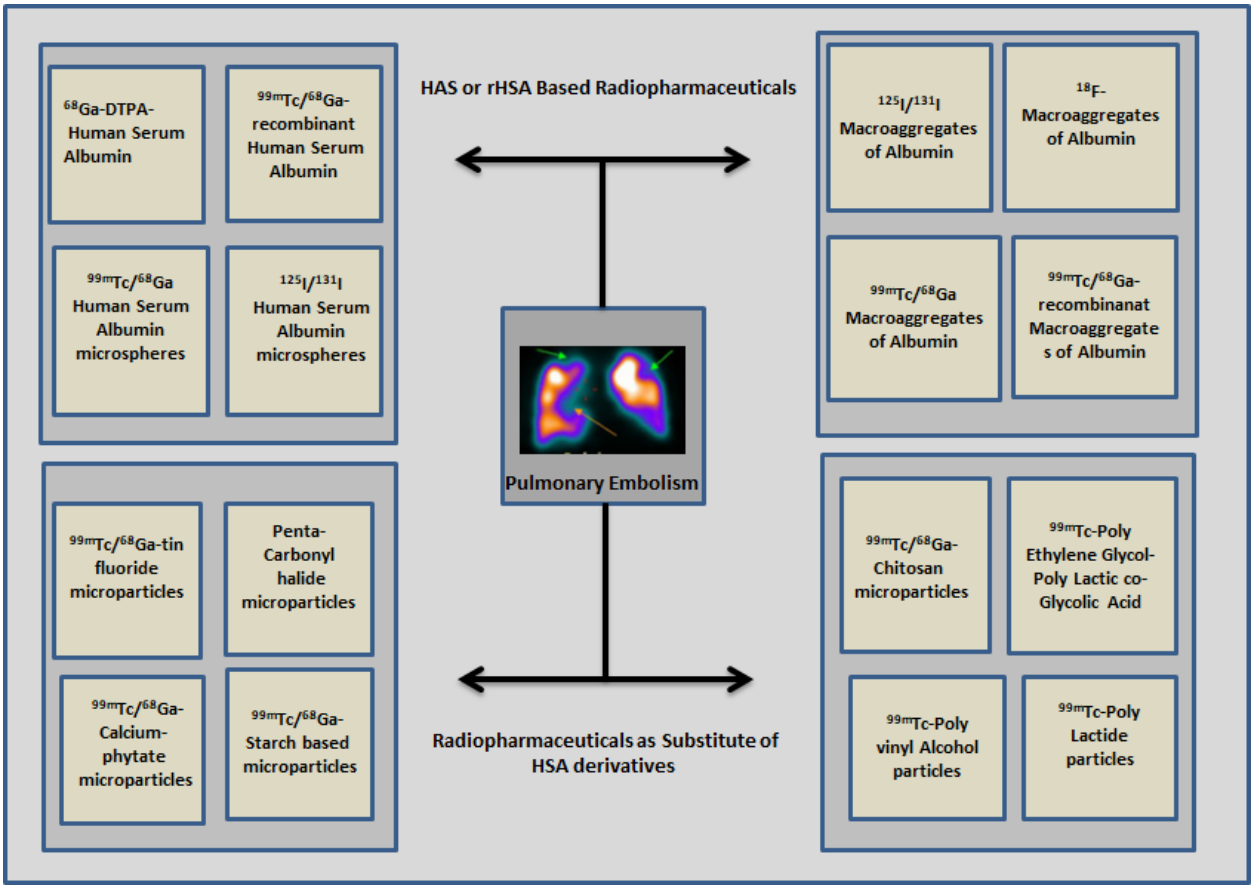

Figure 39 Radiopharmaceuticals designed for indirect imaging of Pulmonary Embolism

1.4.2.5 Acid Halide Based Radiopharmaceuticals

1.4.2.5.1 ^{99m}Tc labeled Carbonyl Halides $(CO)_5I$: [^{99m}Tc-$(CO)_5I$]

RC=OX are called the acid halides or acyl halides contains the carbonyl group. This CO group (ketone group) is highly reactive and makes complexes readily. It has been extensively explored as a potential radiopharmaceutical. Technetium labeled penta-carbonyl halide is a neutral, volatile, and lipophilic and showed specific affinity towards lungs.

Miroslavov *et al.* prepared technium-99m labeled carbonyle halide particles. The procedure adopted carbonylation of pertechnetate ($^{99m}TcO^{-4}$) at high pressure and temperature (160 atm, 170°C) with hydrogen halide (HI) for 40 min. Radiochemical purity of ^{99m}Tc-labeled penta carbobyle halide [$^{99m}Tc(CO)_5I$] was 98% and its *in-vivo* studies in Chinchila rabbits showed an uptake of 70% in lungs and stayed there for 20 minutes [428]. After that liver becomes clear and caused interference.

Limitations of Acid Halides based Radiopharmaceuticals

I. The system requires high temperature and pressure to synthesize desired radiotracer.
II. Lungs stay time is small so tracer is unstable *in-vivo* conditions, and could not offer a sufficient time to perform lung perfusion studies
III. Uptake of lungs is better than PLGA particles (70%) but could not attain the pharmacopeia of commercially used MAA (93%), therefore not recommended for lung perfusion studies.
IV. This radiopharmaceutical is based on acid halide which contains a C=O group which is very reactive and reacts quickly with water, amines or alcohols.

1.4.2.6 Recombinant Human Serum Albumin (rHSA)

As HSA is extremely prone towards proteolytic degradation [432], and is responsible to maintain plasma colloid osmotic pressure (25-33 mm Hg), isolation required the fractionation of human plasma and may involve the possibility of contamination of viruses or prions [432, 433]. Therefore to fill the gap recombinant HSA (rHSA) has been prepared as discussed below.

In past decades extensive research work is done for the improvement of rHSA expression level, containing yeast, bacteria, plant and animals cells. Recombinant protein high deposition might trigger some unexpected toxic effects on host, and aggregation or degradation can diminish the levels of recombinant protein. Furthermore, HSA is a single chain consisting of 585 amino acids as monomer units, comprising of 35 cysteines (34 disulphide bonds). In a large recombinant protein formation of complex disulphide-bonds might create a problem for the production of protein and its folding system, consequential into potentially incorrect folding or low expression of the rHSA whereas rHSA is highly expressing in host cells. Most popular host cells used for creating copies of HSA include prokaryotic, eukaryotic, animal and plant cells as discussed below.

E. coli has been tested as a host to produce rHSA through genetic coding. For this purpose HSA cDNA encoding gene was inserted in expression cassette that transformed the host (E. coli), yielding 2.5 g/L rHSA but its major part is insoluble that may be because of improper folding in cytoplasm or protein aggregation [434]. The expression in Bacillus subtilis has resulted into soluble HSA, with correct cleavage at the N-terminus. Salinas et al. showed some progress with E. coli and successfully engineered disulphide-bonds expression and a novel strategy for rHSA in prokaryotes [435] but the expression levels are very low. Recently, Sharma et al. has reported functional and enhanced soluble rHSA protein production in the host system of *E. coli*. Authors

claimed to achieve cheap and high expression of rHSA in *E. coli* and can be utilized on industrial scale [436].

Initially preparation of rHSA in eukaryotes cells is challenging and several grams of protein are required for starting a process. Various types of yeasts are tested to express protein such as Pichiapastoris, Kluyveromyces lactis, Hansenula polymorpha and Saccharomyces cerevisiae. Expression levels from mg to g/L are obtained using different strategies such as use of signal peptide, introns and promoters as well as optimization of culture medium, cyclic fed batch and cultures of fed-batch [437]. Subsequent to optimization methylotrophic strains containing S. cerevisiae and P. pastoris proved an attractive option for rHSA production. While the rHSA proteolytic degradation remains a problem for both yeasts species. This problem is solved by introduction of new system called PichiaPink™ to decrease the protease impact for both yeast species (P.pastoris and S.cerevisiae) without degradation has reached up to 334 mg/L on industrial scale [438].

To prepare rHSA using plants, first attempt was employed in the leaves of tobacco and potatoes tubers. From total soluble protein it showed a very low expression level (0.02%) only, possible due to degradation. In potato tubers rHSA accumulated about 0.2% of TSP. rHSA expression has increased up to 11.1% of TSP using tobacco-leaf un-translated regions but unfortunately, protein was degraded [439]. Alternative approaches has increased expression of rHSA using culture of plant-cell suspensions about 15 mg/L & 11.88 mg/L in rice and in tobacco Bright Yellow-2 cells [440]. Although these levels are very low as compared to yeast system, and signifying further optimization of system. An example of recombinant protein synthesis process using tobacco leaves is shown in Figure 40.

A group reported rHSA expression from rice endosperms with expression level of rHSA 10.58% of TSP. This expression was 20-fold greater as compared to rHSA minimum level required commercially [441]. This is a cereal crop and natural source of protein preparation, and ideal place for rHSA high yield synthesis at the field level for industrial scale [442].

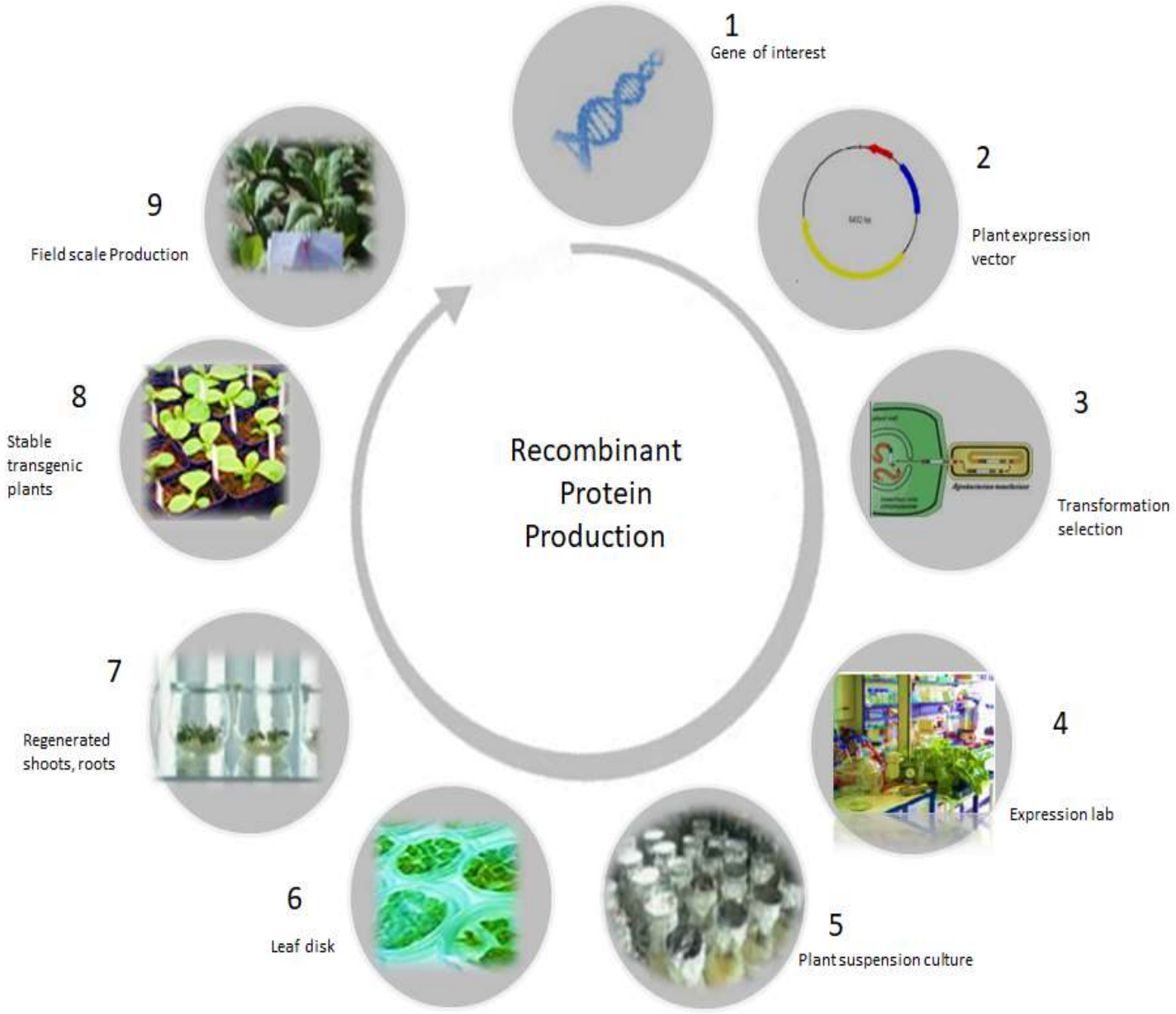

Figure 40 Schematic representation of production of recombinant protein (in tobacco)

The ideal hosts to produce rHSA are the animal cells because mammals can produce high quality of protein with similar glycosylation, solubility and biological activities.

Table 13 Production of rHSA using various host organisms

Host Organism	Expression Level	Publication and year
Escherichia coli	14-20% of TSP	Sharma et al. 2017 [436]
Escherichia coli	2.5 g/L	Lawn et al. 1981 [434]
Escherichia coli	7% of TSP	Latta, Philit et al. 1990 [446]
B. sublitis	Not specific	Saunders et al. 1987 [447]
Saccharomyces cerevisiae	20-150 mg/L	Kang et al. 1998[448]
Saccharomyces cerevisiae	30 mg/L	Quirk et al. 1989 [449]
Saccharomyces cerevisiae	73-334 mg/L	Li et al. 2011 [438]
Pichia Pastoris	8-12 g/L	Below et al. 2008 [450]
Pichia Pastoris	1.34 g/L	Bushell et al. 2003 [437]
Pichia Pastoris	40-80 mg/L	Kobayashi et al. 2000 [451]
Kluyveromyces lactis	3 g/L	Fleer et al. 1991 [426]
Kluyveromyces lactis	62 mg/L	Blondeau et al. 1994 [452]
Kluyveromyces lactis	>50 mg/mL	Lodhi et al. 2005 [453]
Kluyveromyces lactis	1 g/L	Salila et al. 1999 [454]
Mice	2.5 g/L	Shani et al. 1992 [444]
Mice	0.001-0.035 g/L	Shani et al. 1992 [444]
Mice	0.002-10 g/L	Hurwitz et al. 1994 [455]
Mice	N.D.	Shani et al. 1992 [444]
Mice	0.16 g/L	Barash et al. 1999 [456]
Mice	0.001-1.6 g/L	Barash et al. 1999 [456]
Mice	1-2 g/L	Barash et al. 1993 [445]
Mice	0.21-3.54 g/L	Huang et al. 2001 [457]
Mice	0.05-11.95 g/L	Wu et al. 2012 [443]
Cattle	1-2 g/L	Echelard et al 2009 [458]
Silkworm	3.0 µg/mL	Ogawa et al. 2007 [459]
Potato	0.02 % TSP	Sijmons et al. 1990 [460]
Tobacco suspension cells	11.88 µg/mL	Sun et al. 2011 [440]
Tobacco leaf	11.1 % TSP	Millan et al. 2003 [439]
Potato tuber	0.1-0.2 % TSP	Farran et al. 2002 [461]
Rice Suspension cells	11.5% TSP	Huang et al. 2005 [462]
Rice seeds	1.4-10.58% TSP	Lau et al. 2009 [441]
H. polymorpha	0.55 g/L	Heo et al. 2003 [463]
H. polymorpha	460 mg/L	Cox et al. 2000 [464]
H. polymorpha	1.3 g/L	Kang et al. 2001 [465]

In order to achieve enhanced levels of rHSA, the blood is the best platform but due to the difficult purifications, secretory tissue containing fluid are the mammary glands, which are alternative emerging promising bioreactor for proteins [443-445]. To enhance the rHSA expression various factors are applied such as introns, whey acidic protein (WAP) and β-lactoglobulin (β-LG).

A group successfully obtained high rHSA expression in mice using WAP promoter but still it's unable to satisfy the market demand due to low milk yield [443]. Thus bigger animals were tested such as sheep, cattle and the levels of expression varies between 1-2 g/L in cattle with 40 g/L lactation [458]. In 2006, Hunt *et al.* prepared recombinant macroaggregates of albumin (rMAA) from recombinant human serum albumin (rHSA) [408]. Authors performed a comparative study among rMAA, commercial MAA and in-house MAA. Results showed similar RCP values (99%) are produced for all the three types of MAA and excellent lungs images were obtained in New Zealand white rabbits [408]. Furthermore, rHSA has shown comparable results to HSA [466-474] and have the potential to act as a substitute of HSA [408].

Limitations of Recombinant HSA microspheres and MAA (rHSA and rMAA)

I. In order to avoid from the potential microbiological risk associated with human or animal's originated blood-derived medicinal products, recombinant version of these particles was introduced using yeast, animals or plants. But rHSA bear the problem of low expression or aggregation of it which might lead to improper protein folding i.e. large disulphide complex bonding is difficult to copy in the host cells. Consequently, if the level of expression is not very high it would be difficult to meet the requirements.

II. Recombinant MAA or HSA technology besides low expression also face the complexity of the preparation methods and related isolation/ purification of protein is costly.

III. rHSA derived from animals, yeast and bacterial might bear some potential hazards of disease transfer although plant based rHSA is free from this risk and seems attractive especially from rice.

1.4.2.7 Polysaccharides Based Microspheres (Fungi/Invertebrates)

1.4.2.7.1 ^{99m}Tc/ ^{68}Ga Labeled Chitosan Microspheres: (^{99m}Tc -CHSg/^{68}Ga-NOTA-CHSg)

Chitosan is an oligosaccharide (carbohydrate) derived from chitin (polysaccharide), which is found in the exoskeleton of arthropods (invertebrates) or in cell walls of fungi. Chitosan (Figure 41 A) is a biological origin polysaccharide. Chitosan is a copolymer consisting of 2-amino-2-deoxy-D-glucopyranosis (D-glucosamine) and 2-acetamido-2-deoxy-D-glucopyranosis (N acétyl-D-glucosamine) as monomeric units. These monomers units are connected by glycosidic bonds at positions 1 & 4 as shown in Figure 41 C. Although natural, it is usually prepared from chitin corresponding to a polymer only made up of units of N-acetyl-D-glucosamine (Figure 41 B).

Amor-Coarasa et al. in 2013 fabricated biodegradable microspheres of size range 30.1±4.8 µm from chitosan glycol (CHSg) through water in oil emulsion method. Technetium-99m is used directly to radiolabel CHSg microspheres (^{99m}Tc-labeled CHSg). While CHSg microspheres were surface functionalized using S-2-(4-Isothiocyanatobenzyl)-1,4,7-triazacyclononane-1,4,7-triacetic acid (p-SCN-Bn-NOTA) prior labeling with ^{68}Ga.

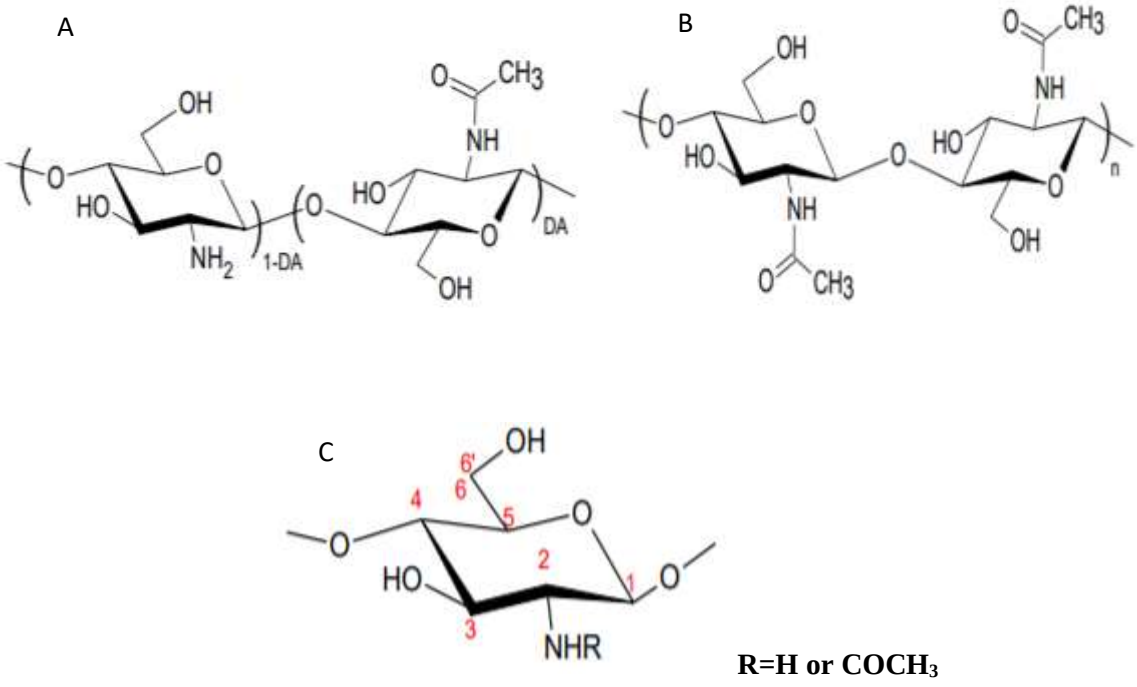

Figure 41 Chemical Structure of A) Chitosan B) Chitin C) Bonding (active) sites of chitin 1,4

Both radiopharmaceuticals ^{99m}Tc-CHSg and ^{68}Ga-NOTA-CHSg showed high lung uptake values 91.6±6.5%, 98.9±0.2% at 2h respectively [410]. These chitosan particles have practical size, spherical shape and surface functionalization (p-SCN-Bn) has increased the stability of the radio-complex. Chitosan particles possess an attractive half-life of 18–24 hours which is thought to be ideal for lung perfusion.

Limitations of Chitosan Based Microspheres

I. Chitosan is derived from lobsters, shrimps, insects, fungi etc. and widely used as biopesticide. Due to animal or fungal sources origin they may be potentially harmful and does not meet the requirement of non-animal based particles

II. Besides encouraging results in animals no clinical trials has been carried out

1.4.3 Concluding Remarks

The probes used for direct imaging are mostly originated from animal based materials such as peptides, antibodies etc., and bear a potential hazard of disease transfer. Furthermore some probes are derived from venoms, and may be poisonous and should not be administered intravenously, however, venom derived peptides may find utility in cancer lesions but could not be suggested for PE diagnosis. Later on recombinant versions of probes such as recombinant bitistatin (rbitistatin) and recombinant tissue-type plasminogen activator (rt-PA) were also developed. However ^{99m}Tc-labeled recombinant tissue plasminogen activator (^{99m}Tc-rt-PA) has produced promising results in clinics and seems interesting thrombus imaging agent while rbitistatin still needs to be explored. However probes synthesis processes are quite tedious and time consuming.

However for indirect imaging of pulmonary embolism, as HSA derived microparticles are the gold standard for lung perfusion scintigraphy and due to potential hazard associated with HSA, its recombinant version remained a source of attention since many years. But its production has faced certain problems of low expression or proteolytic degradation as well as high cost, large scale synthesis, complex processes and complicated purifications. Recently some groups claimed to achieve success to obtain high quality expression in E. coli, yeasts, rice seeds etc. But the most interesting host seems the rice transgenic seeds and amenable to prepare HSA on large field scale. But it still needs extensive work to obtain low cost industrial scale production of HSA.

The urge under the unmet clinical need in order to develop MAA/HAM alternatives a number of materials have been tested for their suitability as lung perfusion agent.

With the advent of polyethylene glycol, to increase the blood circulation time and increase the target efficiency, they were explored for lung targeting, but unfortunately pegylated

microparticulate system could not maintain its uptake in the lungs but after some modifications in size using microchip fabrications system, mono-sized poly lactide (PLA) has shown encouraging results, but this system lacks its translation in human clinics might be due to its synthetic nature.

The other interesting particles include metal derivatives such as ^{99m}Tc-labeled tin fluoride (^{99m}Tc-SnF_2) and ^{68}Ga-labeled calcium phytate particles (^{68}Ga-Ca-phytate), they showed favorable lung uptake and time for V/Q scanning, and further research is mandatory for their translation in clinics. As FDA took a lot time to approve some material for human clinics, thus a group tried an FDA approved material: chitosan derived microparticulate system, which showed an encouraging lung uptake but its long half-life does not seem compatible for lung perfusion study. Furthermore they are derived from animal sources (invertebrates or fungi) and might be harmful. In short despite comprehensive efforts, progressions to fabricate microparticles and to ensure their better trafficking through diagnostic techniques for lung perfusion and thrombus detection, no well-established gold standard for lung perfusion studies is available in human clinics.

Therefore novel biodegradable microparticles originated from natural, non-human/non-animal sources, with favorable features i.e. easy and robust radiolabelling methods, stable enough *in-vivo* to perform lung perfusion studies, and rapid clearance from living body, cheap, and amenable for industrial scale synthesis are awaited. To fill this gap our groups in France in collaboration with Cyclopharma Laboratories have introduced a microparticulate system derived from plant sources, called starch based microparticles (SBMP).

1.4.3.1 Plant Based Microparticulate System

1.4.3.1.1 ^{99m}Tc labeled Starch Based Microparticles: (^{99m}Tc-SBMP)

As mentioned above an optimal radiopharmaceutical specifications include: free from the risk of microbial transmission, can be developed as ready-to-use freeze dried kit format, can be radiolabeled with modern radionuclides easily and quickly, producing high radiochemical purity yields, compatible with the size of lung capillaries to perform lung perfusion studies in clinical set ups. To address this challenge, vegetal polysaccharides were selected as the basis for new potential radiopharmaceutical [11, 429, 475].

Starch microparticles were prepared according and also mentioned in following steps:

I. Sieved for desired sizes (20-50 µm) using an Air Jet sieving machine FTLBA
II. Then Starch particles were oxidized using sodium metaperiodate to obtain dialdehyde groups (Figure 42 A)
III. Then cadaverine: a biogenic polyamine was added to introduce amine groups on the aldehydes by nucleophilic addition followed by water eliminations to yield imines groups (Figure 42 B)
IV. These imines were reduced with sodium borohydride to produce starch based microparticles (Figure 42 C)
V. Then microparticles were fabricated into ready-to-use kits: each kit containing 20 mg of starch based microparticles and 1 mL of NaCl were freeze dried under vacuum to freeze dried kits in the bulk quantity [11, 429].

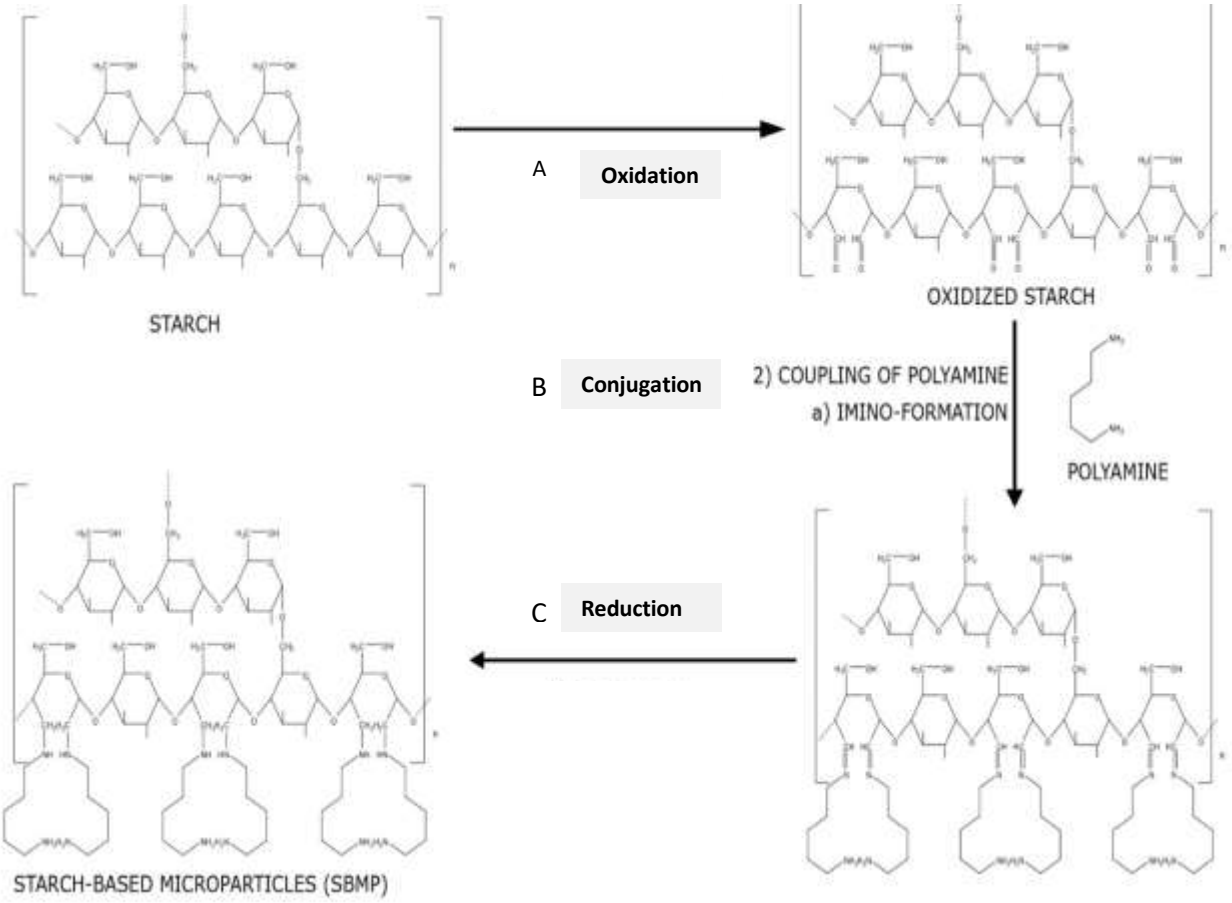

Figure 42 Chemical reactions involved in the synthesis of starch based microparticles: A) Oxidation, B) Conjugation and C) Reduction

1.4.3.1.1.1 Characterization & Radiolabeling Studies

Afterward the starch based microparticles were characterized for their size measurements, shape analysis. Size were measured using counting analyzer Multisizer 3 Coulter Counter and micrograph confirmed that size of particles range between 5-74 µm & 7-63 µm. SEM and confocal microscope analysis showed that these particles appeared as spherical or oval-shaped Figure 43 a. Confocal microscopy describes even distribution of fluorescence over the microparticles surface as clear in Figure 43 b and it confirmed the surface functionalization.

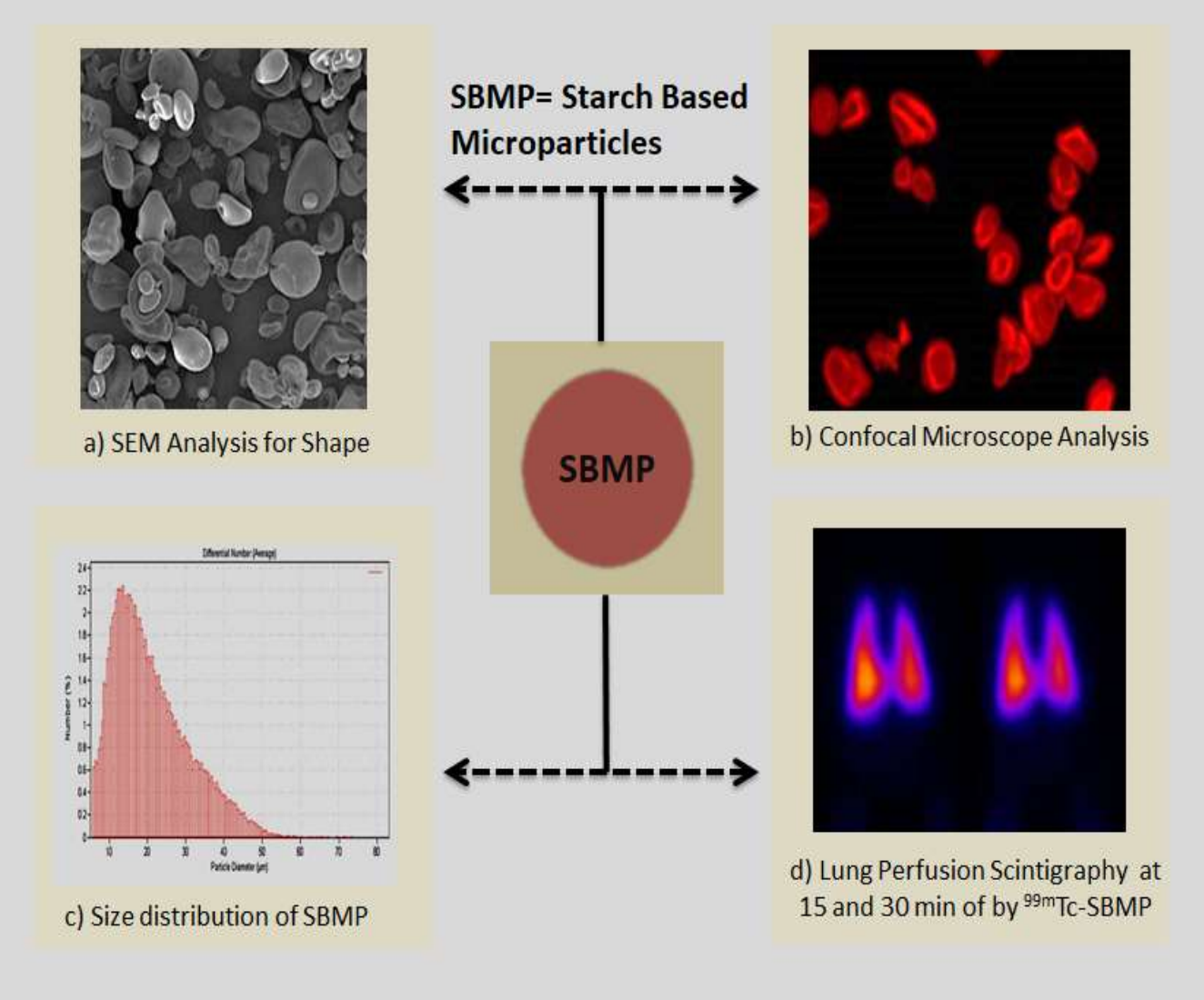

Figure 43 Starch-based microparticles observed with a) SEM view, b) Confocal microscopy images c) size distribution d) ^{99m}Tc-labeled SBMP lung perfusion study by SPECT at 15 and 30 min in rats

1.4.3.1.1.2 Radiolabeling and *in-vitro* Stability Studies

Starch based microparticles were radiolabeled with ^{99m}Tc (100MBq-10GBq) through a simple method at room temperature using acetate buffer and produced radiochemical purity was >95%.

Stability assessment of ^{99m}Tc-SBMP showed that radiopharmaceutical remained stable for 8h at room temperature (25 ̊C), and for 3h in the histidine challenge and 1h in the plasma at 37ºC.

1.4.3.1.1.3 Diagnosis of PE in Rats using ^{99m}Tc-SBMP

The planar scintigraphic static lung acquisitions revealed that tracer accumulated in lungs with a half-life of 3.2 ± 0.5 h, permitting V/Q scanning practicable Figure 43 d [475].

In vivo pulmonary embolism model was created in male Wistar rats and ^{99m}Tc-labeled starch-based microparticles successfully diagnosed pulmonary embolism in these artificially embolized lungs [11, 429, 476] as shown in Figure 44 B.

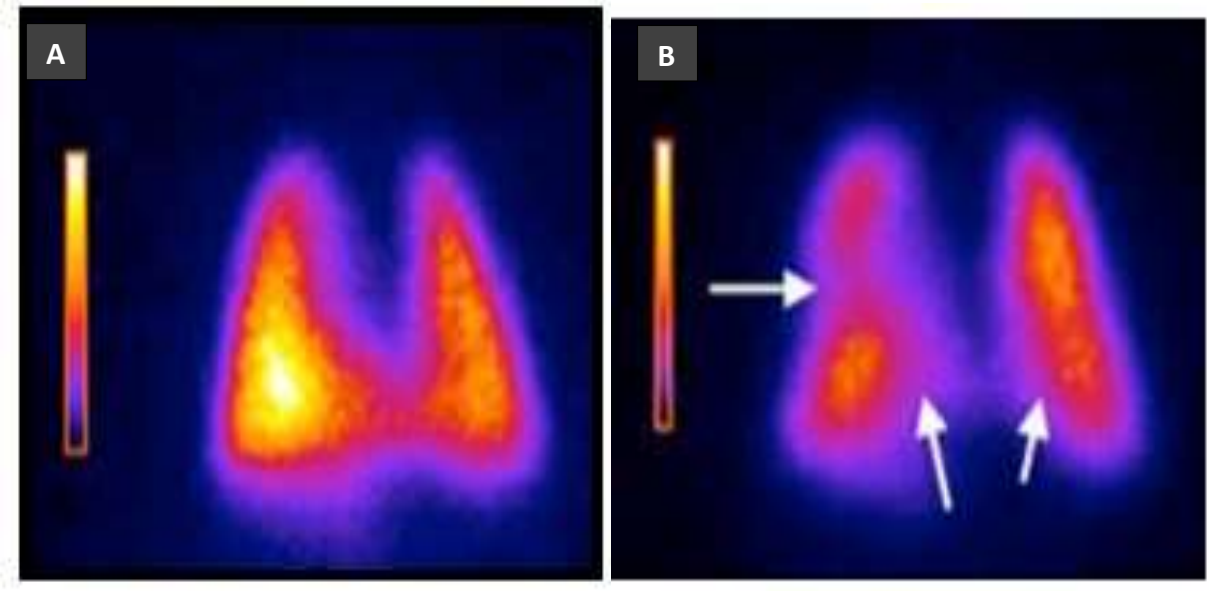

Figure 44 Scintigraphic images of Wistar rats lungs A) Healthy lungs B) Lungs with pulmonary embolism published from ref [11].

After obtaining encouraging results of ^{99m}Tc-labeled starch based microparticles, further preclinical and clinical trials are warranted to explore the benefits of this potential lung perfusion agent

1.4.4 Aims and Objectives

After the previous successful study of ^{99m}Tc-labeled starch based microparticulate system, our aim is to prepare a new radiopharmaceutical: ^{68}Ga-labeled starch based microparticles and evaluation of the new radiopharmaceutical for lung perfusion study and its behavior in living system through an emerging diagnostic technique PET/CT and dosimetry estimation for humans. Thus the objective of this study includes "radio-synthesis of ^{68}Ga labeled starch based microparticles (SBMP) with high radiochemical purity (RCP), characterization of new radiopharmaceutical (^{68}Ga-SBMP) for size measurement, *in-vitro* stability, lung perfusion studies by PET/CT, biodistribution and pharmacokinetics, and dosimetry estimation for human organs". Following hypotheses are derived from the research objective:

I. ^{68}Ga labeled starch based microparticles will be developed producing radiochemical purity more than 99%
II. The radiopharmaceutical will be stable *in-vitro* and *in-vivo*
III. Lungs uptake will be more than 80% while radioactivity uptake in liver plus spleen will be less than 5% at 15 min post IV injection of the radiotracer, consequently radiolabelled microparticles will accumulate in pulmonary vasculature right after the radiotracer injection to produce fine-tune PE/CT images of lungs without any background interference of liver plus spleen.
IV. Radiotracer will not stay in any major organs like liver, stomach, kidneys or bladder but rapidly cleared from the body over time through renal system
V. The estimated absorbed doses of ^{68}Ga-SBMP based on in-vivo PET/CT imaging will be less than standard of ^{99m}Tc-MAA SPECT (ICRP 80).

SECTION-II

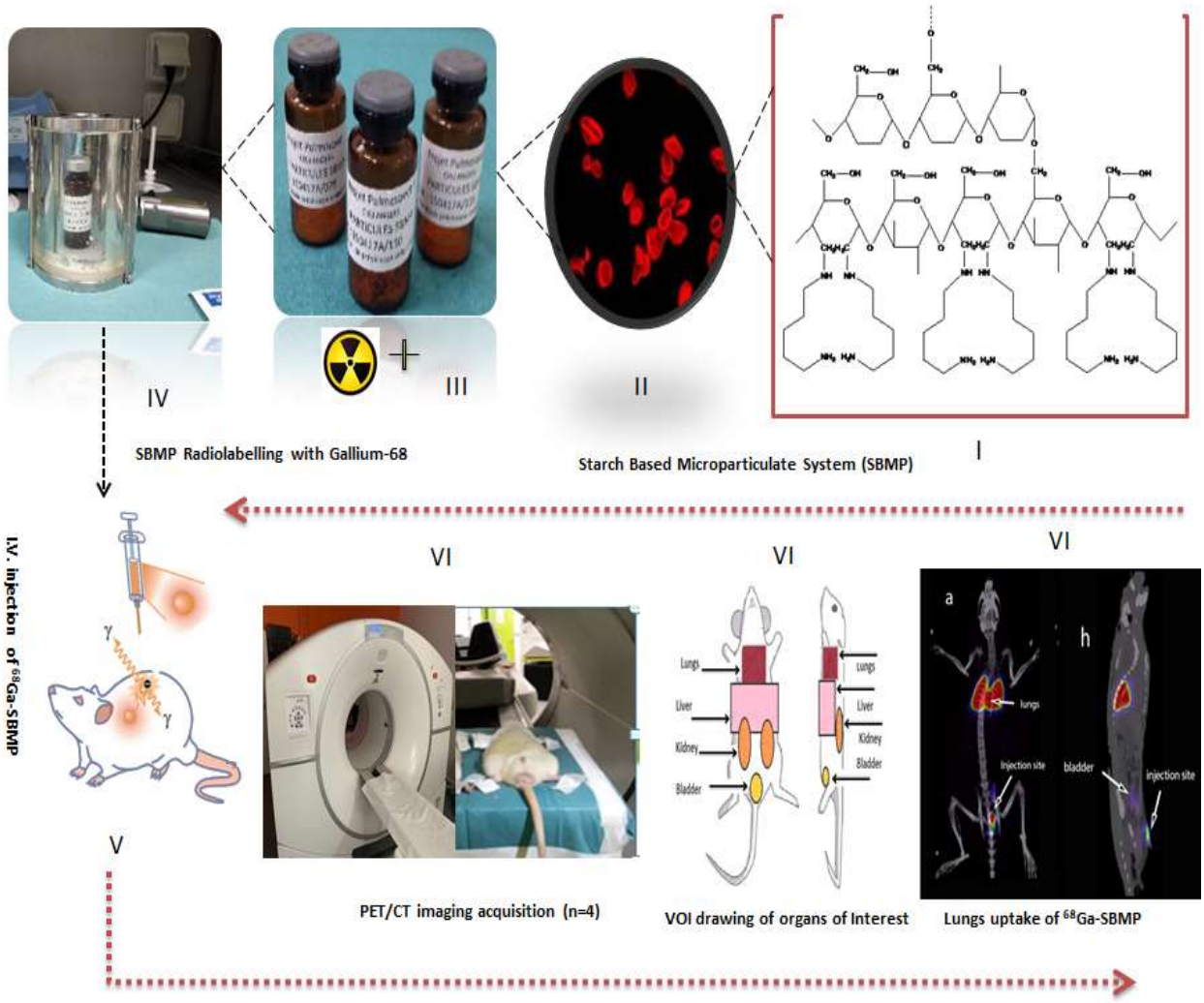

2. Experimental Work

The original work presented in this chapter is related to the development of a new injectable radiopharmaceutical based on the starch derived microparticulate system, ^{68}Ga-labeled SBMP for diagnostic applications in the field of nuclear medicine.

The presented study is conducted to evaluate the potential of new radiopharmaceutical as lung perfusion agent and assess the important characteristics of the ^{68}Ga labelled starch based microparticles in the living organism such as biodistribution, metabolic clearance, dosimetry that could influence overall efficacy of the radio-complex, and the particles a radionuclide delivery vectors. The healthy Wistar male rats were selected to study the pharmacokinetics and biodistribution modeling.

The experimental work started with the fabrication of raw material for the radiopharmaceutical which is the starch based microparticles (SBMP). Starch based microparticles kits were prepared in bulk quantities according to our patented method [477] which were used in the experiments generously. These kits were radiolabeled and subsequent to the development of radiopharmaceutical, characterization steps involved the size measurements of the starch based microparticles, *in-vitro* and *in-vivo* stability study, lung perfusion studies in rats through positron emission tomography (PET/CT).

The PET/CT imaging is exploited by Imalytics Work Station to calculate VOI statistics and to calculate Time Activity Curves. Besides, retention time in organs, the trend of activity in all organs with time, blood clearance kinetics, and excretion pathways along with stay time in kidneys and bladders was also assessed. The results obtained for dynamic imaging as percent of injected dose (%ID) for organs of interest were utilized to calculate TAC.

The experimental work also explain the key steps involved in the calculation such as model creation, characterization of phantom and its registration for the allocation of major organs. The next step of calculation of estimated dosimetry for rats' organs from Time Activity Curves (TAC) data using Excel software (version 14.7.3) and MIRD schema pamphlet N°11 and estimated absorbed doses for human organs. Further understandings of kinetic changes are essentially obtained after carrying out PET dynamic imaging. The schematically representation of experimental procedure is shown in section 4.1, Figure 54 and Figure 55.

Following publications are in process:

I. Abstract and poster published in The American Congress of the Society of Nuclear Medicine (SNM New Orleans 2020, SBMMI-A-1717-2020): on page 232

Authors: Shabnam Sarwar, PhD student[1,2,] Ouassim Medhioub, PharmD[3], Francis Bouchet, PhD[3], Pierre Jean Mention, MD[3], Francois Hindre[1,4], Pierre DRION, DVM, PhD[2], Roland Hustinx, MD[5], Nadia Withofs, MD, PhD[5], Franck Lacoeuille, PharmD, PhD[3,4] "***Development and preclinical Evaluation of^{68}Ga-radiolabelled Starch Based Microparticles for PET/CT Lung Perfusion Studies***" J Nucl Med. 2020; -- (Supplement --): ---P, Congress of the Society of Nuclear Medicine, New Orleans (July 2020).

Affiliations: [1]University of Angers, Angers, France, [2]University of Liege, Liege, Belgium, [3]Nuclear Medicine Department, University Hospital Angers, Angers, France, [4]GLIAD Team, INSERM UMR 1232, CRCINA, Angers, France, [5]Nuclear Medicine Department, University Hospital Liege, Liege, Belgium

II. "Development and Preclinical Evaluation of ^{68}Ga-radiolabeled Starch-Based Microparticulate System as PET/CT Lung Perfusion Agent" JNMMI & Research

Development and Preclinical Evaluation of ^{68}Ga-radiolabeled Starch-Based Microparticulate System: PET/CT Lung Perfusion Agent

2.1 Introduction

Pulmonary Embolism (PE) is a serious condition, which needs quick identification due to high mortality rate [33, 478]. PE diagnosis is challenging due to its non-specific symptoms and it has been reported among the most frequently missed diagnoses in the primary care [479, 480]. The lungs ventilation/perfusion (V/Q) scintigraphy, by the mean of Single Photon Emission Computed Tomography (SPECT/CT) and macroaggregates of albumin (MAA) labelled with ^{99m}Tc (^{99m}Tc-MAA) as lung perfusion agent, is still considered as an imaging modality of choice for the diagnosis of PE. However, SPECT/CT technique has some limitations such as lower spatial resolution or poor sensitivity compared to Positron Emission Tomography (PET/CT). With the recent availability of ^{68}Ge/^{68}Ga generator and the development of ^{68}Ga-labeled radiopharmaceuticals that can be produced on site and on demand, V/Q PET/CT appears now feasible. Thus, different groups have developed radiolabeling procedures of MAA with ^{68}Ga instead of ^{99m}Tc and successfully perform PET/CT lung perfusion studies [229, 234, 236]. However, MAA, as other blood-derivatives, carries a theoretical risk of disease transmission. For decades, many attempts were made to develop alternatives to MAA [289, 410, 422, 423, 428, 431, 481] but none was fully successful and the MAA successor is still awaited [482]. To address this challenge, few years ago, our team has developed a new microparticulate albumin-free carrier from vegetal origin, able to form complex with radiometals for nuclear medicine applications and especially for lung perfusion scintigraphy [429, 475, 476]. These starch-based microparticles (SBMP) exhibit favorable characteristics such as suitable particle size, availability

as freeze-dried kits and easy radiolabeling with various isotopes such as ^{99m}Tc, ^{68}Ga or ^{188}Re. Based on those promising results, the objective of the present work was to evaluate, for the first time, the performance of the ^{68}Ga-SBMP microparticles as radiotracer for lung perfusion PET studies. To meet this goal, radiolabeling, preclinical PET/CT studies imaging-based dosimetry estimation following intravenous injection of ^{68}Ga-SBMP were realized.

2.2 Materials and Methods

2.2.1 Reagents and Instruments

Potato starch was a kind gift from Roquette Freres (Lestrem, France). Sodium metaperiodate, sodium borohydride, cadaverine and sodium acetate trihydrate were purchased from Sigma Aldrich (USA). Deionized water was delivered by a Milli-Q plus system (Merck Millipore, Darmstadt, Germany). Solution of gallium trichloride ($^{68}GaCl_3$) was obtained from a 1.85GBq Galliapharm ^{68}Ge/^{68}Ga generator (batch number 10056GMGE25; Eckert&Ziegler, Germany) eluted with 5mL of 0.1N HCl Ultrapur solution (Eckert&Ziegler, Germany). Hydrophilic 5 µm syringe filters were purchased from Sartorius (Palaiseau, France). Perkin Elmer Automatic Gamma Counter was used for couting activity in the organs.

2.2.2 Preparation and Characterization of SBMP

SBMP were prepared according a previously described and patented method [475]. Briefly, starch microparticles of the desired size (20-50µm) were selected using an Air Jet sieving machine FTLBA (Filtra, Spain). Dialdehyde starch was then prepared by oxidation of starch microparticles with sodium metaperiodate. Biogenic polyamine (i.e. cadaverine) was then grafted onto aldehyde function of the periodate-oxidized starch microparticles through nucleophilic addition, leading to Starch-Based MicroParticles (SBMP). Ready-to-use kits of

SBMP were prepared by adding the desired amount of SBMP (20mg) and 1 mL of NaCl 0.9% to a sterile vial. The kits were then freeze-dried and kept under vacuum. As quality control, size distribution measurements of the SBMP were carried out through counting analyser Multisizer 3 Coulter Counter (Beckman Coulter. France). Five to ten mg of SBMP were suspended in a weak Isoton II electrolyte solution (Beckman Coulter, France) and drawn through a small aperture (200 µm), until at least 20,000 particles were counted.

2.2.3 Preparation of ^{68}Ga-SBMP

2.2.3.1 Radiolabeling Studies

Radiolabeling studies were realized at different pH conditions. After elution of the ^{68}Ge/^{68}Ga generator with a solution of HCl 0.1 M (5.5 mL), 1.5-2 mL of the $^{68}GaCl_3$ eluate was added to the kits (251±18 MBq) in the presence of acetate buffer solution (3.5 mL) of pH 3.5 (n=3), pH 4 (n=3) or pH 4.5 (n=3). After gentle swirling, the ^{68}Ga-SBMP were stored at room temperature and controlled for their radiochemical purity (RCP). Moreover, an *in vitro* radiolabeling stability study (up to 120 min) was conducted at the pH exhibiting the more favorable radiolabeling conditions. One way anova statistical analysis was performed among different conditions of same time points.

2.2.3.2 Radiochemical Purity Measurements

Radiochemical purity (RCP) was assessed according to a previously described method [429] consisting in the filtration of 0.5 mL to 1.0 mL of the radiolabeled suspension of ^{68}Ga-SBMP on a 5-µm syringe filter. Procedure includes pre-rinsing the 5 µm syringe filter with 1-2 mL saline at 1 drop per second rate, loading the ^{68}Ga-SBMP suspension (0.5-1 mL) following by rinsing

the filter using saline solution and air (Figure 46). The RCP was determined with the following equation at 10, 30, 60, 90 and 120 minutes after radiolabeling (n=3 per time points):

$$RCP\ (\%) = \frac{Filter\ activty\ \ (MBq)}{Filter\ activity\ (MBq) + Filtrate\ (\text{MBq})} \times 100$$

2.2.4 Preclinical Studies

2.2.4.1 Animals/Ethical Statements

All experimental procedures and protocols were reviewed and approved by the Institutional Animal Care and Use Ethics Committee of the University of Angers (France) with number (CEEA 2015-20). Animals were placed at University Hospital of Angers pet under standard conditions; 2 animals per cage. They were provided unlimited access to food and water. During the experiment period, temperature and humidity was controlled and animals were euthanized according to the prescribed procedure at the end of the experiment.

2.2.4.2 Lung Perfusion Studies of ^{68}Ga-SBMP

Lung perfusion studies were performed in healthy Wistar rats, weighing 345-460g (n=4). The rats were installed on a holder for PET imaging and provided isoflurane anesthesia (1.5%) for the whole duration of acquisitions (90 min). The suspension of ^{68}Ga-SBMP was administered (8-10 MBq) in a volume of 0.5 mL through penile vein.

2.2.4.3 PET/CT Imaging Acquisition Parameters

PET-CT acquisitions were realized on a TEP-CT Discovery IQ5 system (GE Healthcare). Dynamic PET images were acquired in list-mode for 90 minutes. re-framed separately for each rat starting at the time of injection (15 frames of 2s, 9 frames of 30s and 38-39 frames of 2 min) and reconstructed using a Bayesian penalised likelihood reconstruction algorithm (Q-Clear) (regularization parameter beta 350, FOV 150 mm, 256 x 256 matrix, slice thickness 3.26 mm, voxel size 0.00111923 mL). CT-based attenuation correction (CT lightspeed, 80 kVp, 275 mA, collimation 10 mm, slice thickness 1.25 mm, Pitch 0.9375, 1s/rot) was applied.

2.2.4.4 PET/CT: Registration and Image Analysis

Post-acquisition processing was realized using Imalytics Research Workstation (Philips, The Netherlands). Images were processed for manual registration in order to align target (PET) and reference (CT) images when necessary. The registered images were used for the following step of segmentation, VOIs contours were delineated on PET images (Lungs, bladder) or CT images (kidneys, liver, spleen and stomach) using semi-automatic delineation tools. VOIs statistics (Volume of the VOI, number of voxel in the VOI, activity of the VOI (max, mean, min) in Bq/mL) and time activity curve (Bq/mL as a function of time) in each VOI were obtained through Imalytics statistics module. % IA activity values of all rats (n=4) are compared using One Way ANOVA analysis (p=0.05).

Post mortem counting of organs for activity was also performed, in order to validate the results of PET/CT imaging, using Perkin Elmer Gamma Counter as injected dose per gram (%ID/g).

2.2.4.5 Imaging Based Dosimetry Estimation

2.2.4.5.1 Cumulated Activity Calculation

In each organ of interest *h*, the cumulated activity $\tilde{A}_h$ was calculated on the basis of time activity curves (TACs) of lungs, kidneys, bladder, stomach, spleen and liver obtained from PET images (decay corrected) of ^{68}Ga-SBMP in rats (n=4, mean ± SD). Non-decay-corrected TACs were expressed as the percentage-injected activity as a function of time and were fitted by a mono-exponential function or a polynomial function (to model uptake and clearance) with Excel® software (version 14.7.3) in order to obtain the activity function $A_h(t)$ in each organs of interest. The validity of the fitted activity function was estimated by calculating its Pearson's correlation coefficient (R^2). The cumulated activity was calculated by the area under curve (AUC) of the activity function $A_h(t)$ in each organ according equation 1 [483, 484].

$$\tilde{A}_h = \int_0^{\infty} A_h(t)\,dt \qquad (1)$$

2.2.4.5.2 Absorbed Dose Calculation

According to the MIRD methodology, the mean absorbed dose $\bar{D}(k \leftarrow h)$ in a target tissue k delivered by a radioactive material distributed uniformly within a source tissue h is given by the equation 2 [483, 484].

$$\bar{D}(k \leftarrow h) = \tilde{A}_h \times S(k \leftarrow h) \qquad (2)$$

S factor, $S(k \leftarrow h)$, is defined as the mean absorbed dose delivered in the target region k per unit cumulated activity in the source region h. In this study S factors have been extracted from dedicated table for ^{68}Ga radionuclide given in the MIRD pamphlet N°11 [485] and cumulated activity was obtained from PET images in rats (see above). Therefore the absorbed dose in target tissue k due to all sources organs h was given by the equation 3 [483, 484].

$$\overline{D}(k) = \sum_{h} \overline{D}(k \leftarrow h) \quad (3)$$

2.2.4.5.3 Equivalent and Effective Dose Calculation

The equivalent dose in a tissue T, H_T, is given by the equation 4, where W_R is defined as the radiation-weighting factor (W_R *=1 for X, gamma and electrons radiations)* ICRP publication 103 [486].

$$H_T = \sum_{R} W_R \times \overline{D}_{T,R} \quad (4)$$

The effective dose in the whole body is given by the equation 5 [483, 484], where W_T is the tissue weighing factor according to ICRP publication 103 [486].

$$E = \sum_{T} W_T \times H_T \quad (5)$$

2.2.5 Statistical Analysis

Graphs, mean, standard deviations and One Way ANOVA (p=0.05) were calculated by using Prism software 6.0 (v6.0g, Graph Pad software, La Jolla, USA).

2.3 Results & Discussion

2.3.1 Preparation of SBMP

The different steps undergone by the native starch microparticles (i.e. periodate oxidation followed by nucleophilic addition of biogenic amine) resulted in SBMP microparticles with a mean and median size of 23 and 21 µm respectively. The particle size analysis found a typical size distribution comprised between 10 and 60 µm (Figure 45) suitable with lung perfusion studies, with no particle above 100-µm and approximately 112,000 microparticles per mg of SBMP, leading to an extrapolate number of particles per kit around 2,240,000.

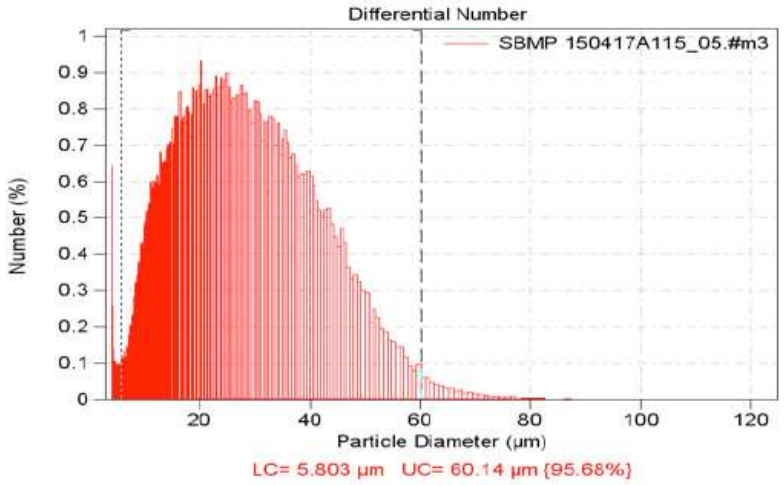

Figure 45 Particle size analysis of SBMP showing typical size distribution between 10 and 60 µm.

2.3.2 Radiolabeling of SBMP with ^{68}Ga

For radiochemical measurement, our selected membrane filtration method is efficient and reproducible and using filters of pore size >5µm is another validation of particles size. Furthermore pre-rinsing the filter with saline and air can minimize the hypothetical risk associated with filter absorption (Figure 46).

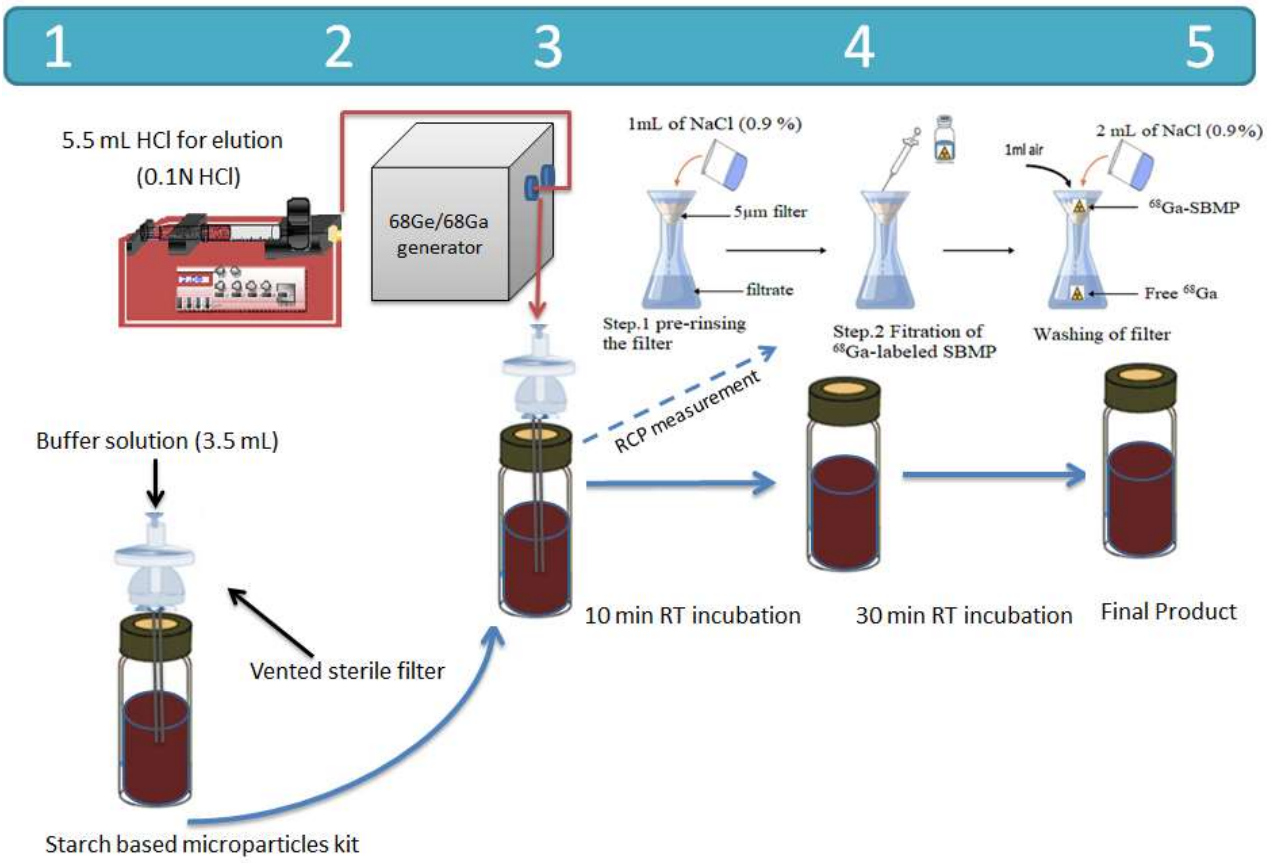

Figure 46 General scheme of radiolabeling procedure of starch based microparticles with gallium-68

As shown in the Figure 47 A, the RCP of ^{68}Ga-SBMP was, in our experiment, very dependent of the sodium acetate buffer pH used for the radiolabelling of the SBMP with the $^{68}GaCl_3$ eluate. Using a buffer solution of pH 3.5, the RCP of the ^{68}Ga-SBMP was always less than 80% (i.e.

44.95%±3.23, 69.03%±5.82, 79.1%±4.24 at 10, 30 and 60 min, respectively). In contrast, very high yields of radiolabeling were obtained for buffer pH 4 and pH 4.5, after only 10 min of incubation time (Figure 47 A). The optimal conditions were obtained with buffer at pH 4.5, leading to RCP of 99.52%±0.017, 99.70%±0.005 and 99.75%±0.01 after 10 min, 30 min and 60 min of incubation with the $^{68}GaCl_3$ eluate respectively. The *in-vitro* stability of the ^{68}Ga-SBMP labeling was investigated leading to very satisfying results with a RCP of 93.47%±0.14 after 2 hours (Figure 47 B). One away anova statistical analysis showed that there is no significant difference (p=0.05) among the same time point reading of different pH conditions and in-vitro stability readings.

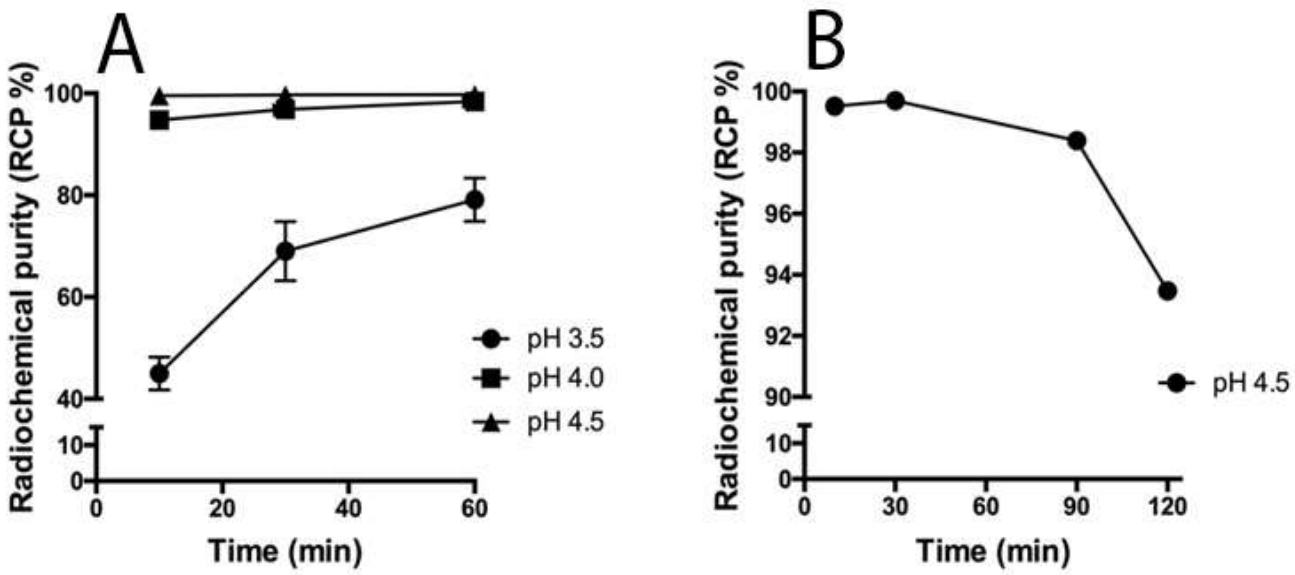

Figure 47 Radiochemical purity (%) according to various pH radiolabeling conditions (A) and in-vitro radiolabeling stability at pH 4.5 (B).

2.3.3 Lung Perfusion Studies of ^{68}Ga-SBMP PET/CT

The high yield and in-vitro stability of the radiolabelling of SBMP with ^{68}Ga (buffer pH 4.5) allowed us to consider in vivo PET lung perfusion studies with ^{68}Ga-SBMP. For that purpose,

0.5 mL of ^{68}Ga-SBMP, corresponding to approximately 224.000 microparticles, was injected into healthy Wistar rats (n=4) for dynamic PET acquisition. As expected, intravenous injection of the suspension of ^{68}Ga-SBMP was immediately followed by passive retention of the microparticles in the first arterial bed encountered (i.e. pulmonary artery bed). The PET images (Figure 48) and time activity curves (TACs) extracted from the dynamic acquisitions (Figure 49) showed that 5 min post-injection more than 95% of the radioactivity was found in the lungs (95.77%±2.80) and only very slight activities, less than 2%, were seen in the other organs (Table 14), such as liver (1.89%±1.10), kidneys (0.60%±0.19), bladder (0.45%±0.21), spleen (0.09%±0.07) or stomach (0.36%±0.30). Homogenous distribution of the ^{68}Ga-SBMP inside the lungs was observed on axial (Figure 48 e), sagittal (Figure 48 f and g) and coronal (Figure 48 h) planes PET images. A very high signal-to-noise ratio was observed on these PET images, as illustrated on Figure 48 (a to d), and only slight activities were detected for liver (Figure 48 f and g) or bladder (Figure 48 g and h). Due to technical failure during injection procedure, a residual activity was also detected at the site of injection, as shown on Figure 48 a or Figure 48 h.

Post mortem counting of organs for activity after 2 hour of the administration of radiopharmaceutical (^{68}Ga-SBMP) has validated the results of PET/CT in-vivo imaging data and showed that more than 60% of injected dose per gram was present in lungs while liver and spleen showed 0.041 and 0.039 % of injected dose per gram, respectively.

As illustrated, through decay corrected and non-decay-corrected time activity curves of the lungs (Figure 49) and through calculated kinetics parameters such as biological lung half-life (T_B= 422.13 min) or effective half-life (T_E= 58.35 min) (Table 14), the in-vivo stability of ^{68}Ga-SBMP was very good during the whole acquisition. Moreover, level of radioactivity in other organs

were quite stable during the whole acquisition time, showing only slight accumulation in the bladder due to renal clearance of the tracer, starting from 0.45%±0.21 at 5 min to 1.52±0.32 of injected activity at 60 min (Table 14).

Very small counts in the gut are suggesting the poor uptake and stay of radiotracer in the gut and clearance through the faeces is not recommended. Hence the entire radioactivity is cleared through urinary system including kidneys and bladder.

The percent injected activity values among similar organs of different rats (n=4) at same time points i.e. 5 min, 30 min, and 60 min, showed no significant difference at p=0.05 in One Way ANOVA analysis.

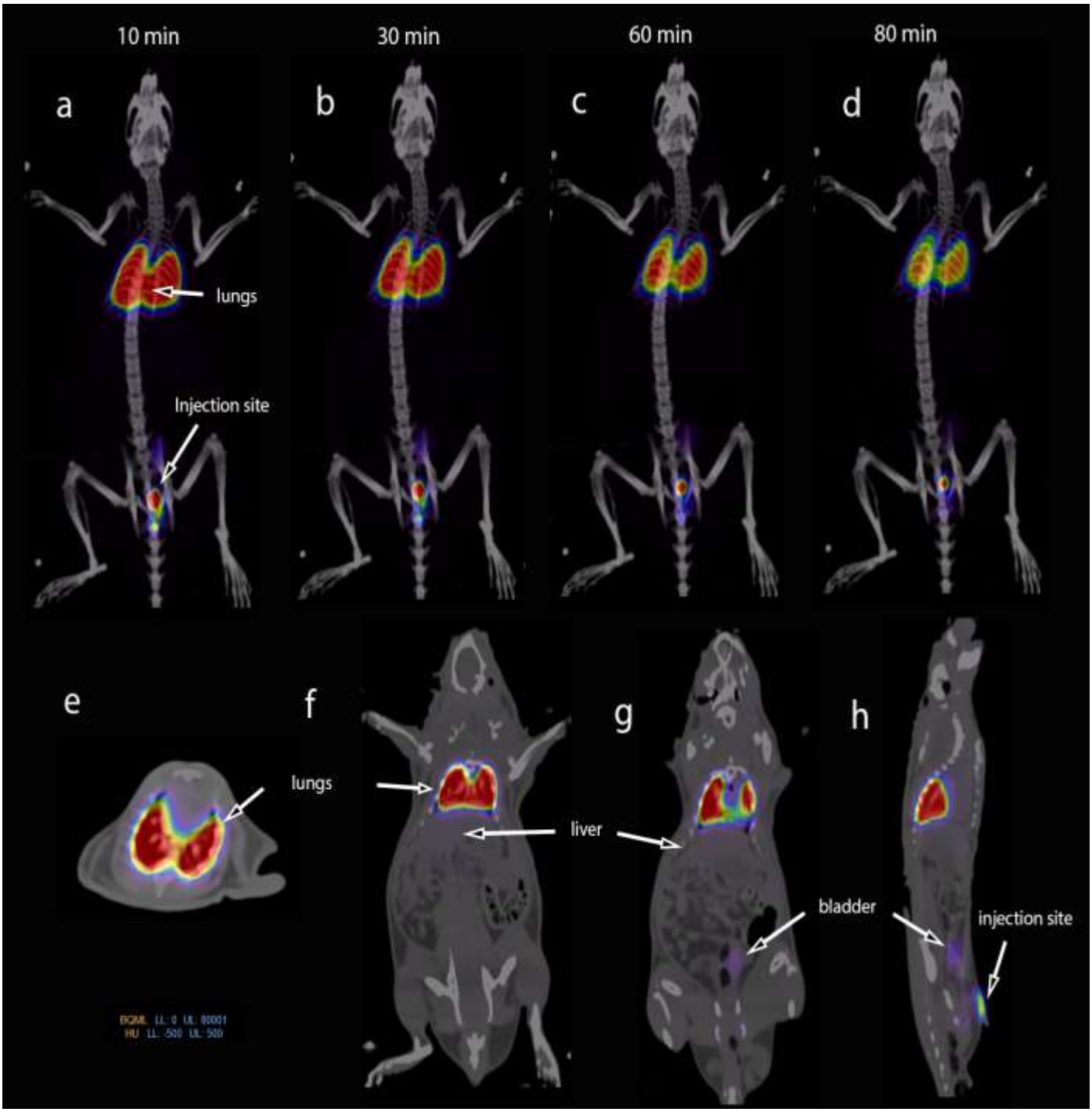

Figure 48: Typical Maximum intensity projection (MIP) image fused with CT of one rat at 10 min (a), 30 min (b), 60 min (c) and 80 min (d) after injection of ^{68}Ga-SBMP (8-10MBq). Axial (e) sagittal (f; g) and coronal (h) plane images of lung perfusion study after 60 min following by the intravenous administration of ^{68}Ga-SBMP (10 MBq) showing lung uptake and renal clearance (g and h) of the tracer.

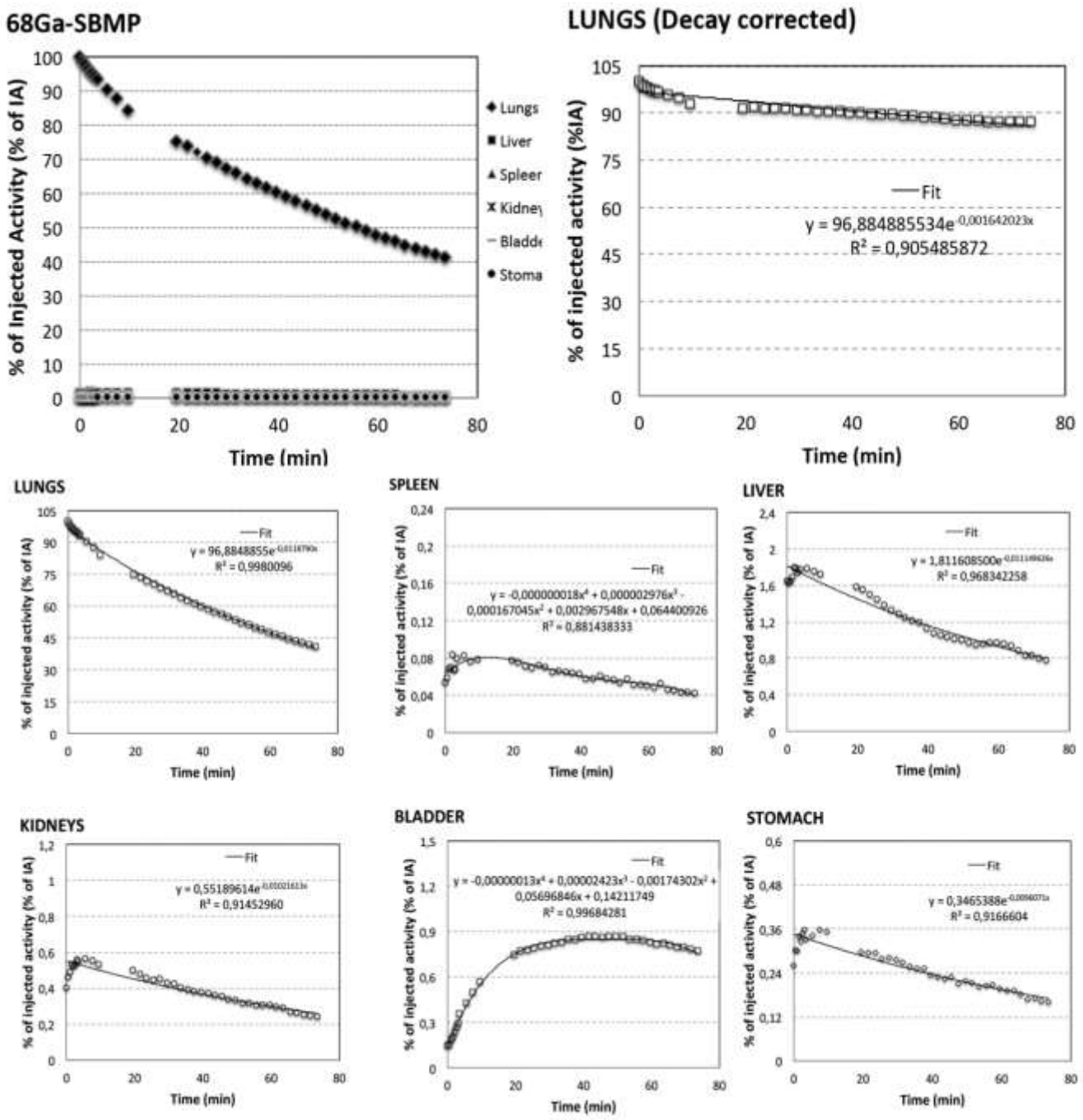

Figure 49 Time Activity Curves (TACs) extracted from PET lung perfusion studies following IV injection of ^{68}Ga-SBMP in rats (n=4). TACs were fitted using exponential (lungs, liver, kidneys and stomach) or polynomial function (spleen, bladder) in order to estimate the cumulated activity in each organ.

Table 14 Percentage of injected activity per organ according time, biological (T_B) and effective (T_E) lungs half-lives extracted from time activity curves and model fitting of the PET perfusion studies (n=4).

			Percentage of injected activity (decay corrected)		
Organs	**Biological Half-life (T_B)**	**Effective half-life (T_E)**	**5 min**	**30 min**	**60 min**
Lungs	422.13 min	58.35 min	95.77±2.80	91.15±6.76	87.90±7.85
Bladder	-	-	0.45±0.21	1.10±0.27	1.52±0.32
Kidneys	-	-	0.60±0.19	0.58±0.24	0.57±0.25
Liver	-	-	1.89±1.10	1.80±1.06	1.80±1.32
Spleen	-	-	0.09±0.07	0.09±0.08	0.09±0.08
Stomach	-	-	0.36±0.30	0.37±0.31	0.36±0.33

2.3.4 PET Imaging Based Dosimetry Estimation

For the determination of the cumulated activity $\tilde{A}_h$ in each target organ the time activity curves of lungs, kidneys, bladder, stomach, spleen and liver obtained from PET lung perfusion studies with ^{68}Ga-SBMP (Figure 49) were fitted (Table 15) on the basis of mono-exponential or polynomial functions. The validity of each of the fitted activity functions was very good, as shown by the Pearson's correlation coefficients values that were comprise between 0.881 and 0.998. Estimated cumulated activity in the lungs appeared to be 51 to 1770 times higher than for other organs (Table 15), leading to the highest absorbed dose of 1.07E-02 mGy/MBq (Table 16). As a co-comparison, much lower estimated absorbed doses were found to the kidneys, liver and bladder and 2.77E-04, 2.43E-04 and 2.22E-04 mGy/MBq, respectively. The resulting effective absorbed dose, extrapolated from PET perfusion studies with ^{68}Ga-SBMP in rats, for the whole body for an adult was estimated to be 1.360E-03 mSv/MBq for women and 1.359E-03 mSv/MBq for men (Table 16). On the basis of an injected activity of 150 MBq, the estimated effective absorbed should be 2.04E-01 mSv for women and 2.038E-01 mSv for men.

Table 15 Fitted activity function $A_h(t)$ obtained from TACs and the corresponding cumulated activity $\tilde{A}_h$ in each organ of interest.

Organs	$A_h(t)$	R^2	$\tilde{A}_h = \int_0^{\infty} A_h(t)\,dt$ [Bq.s]
Lungs	$y = 96.884885e^{-0.011879x}$	0.998	8412.22
Bladder	$y = -0.00000013x^4 + 0.00002423x^3 - 0.00174302x^2 + 0.05696846x + 0.14211749$	0.997	64.64
Kidneys	$y = 0.55189614e^{-0.01021613x}$	0.915	54.02
Liver	$y = 1.8116085e^{-0.011149626x}$	0.968	162.48
Spleen	$y = -0.000000018x^4 + 0.000002967x^3 - 0.000167045x^2 + 0.002967648x + 0.064400926$	0.881	4.75
Stomach	$y = 0.3465388e^{-0.0096071x}$	0.917	36.07

Ten years ago was developed in our team, as an alternative of Human Serum Albumin (HSA) or other blood derivatives, the concept of a new microparticulate system from vegetal origin able to form complex with radiometals for nuclear medicine applications and especially for lung perfusion scintigraphy [429, 477]. Owing to its properties, potato starch was chosen as starting material, it was modified by oxidization and coupling of a polyamine ligand, enabling modified starch to chelate radionuclides. These initial developments were optimized in order to obtain an experimental radiopharmaceutical with the best characteristics in terms of high radiochemical purity and stability leading to high signal-to-noise ratio (*in vivo*) [475]. Following this promising work, the ability of SBMP to chelate other radionuclides than technetium-99m was investigated. First attempts to radiolabel SBMP with gallium-68 and rhenium-188 were successful and the *in vivo* stability of the radiolabelling was demonstrated in a preliminary study , in a model of DENA-induced hepatocellular carcinoma (HCC) [476]. On this basis, objective of the present work was to evaluate, for the first time, the performance of the ^{68}Ga-SBMP microparticles as radiotracer for lung PET perfusion studies. To this end, additional radiolabelling studies were

carried out, in particular by studying the performance of the radiolabeling of the SBMP with ^{68}Ga according to various pH conditions.

Table 16 Estimation of human absorbed doses extrapolate from rats (n=4) after IV administration of ^{68}Ga-SBMP

Target organs	Absorbed dose (mGy/MBq)	Equivalent Dose (H_T) in tissue T (mSv/MBq)	W_T	Effective absorbed dose (mSv/MBq)
Adrenals	1.16E-04	1.16E-04	0.0171	-
Bladder	2.22E-04	2.22E-04	0.04	-
Bone total	4.55E-05	4.55E-05	0.01	-
GI (Stomach)	1.80E-04	1.80E-04	0.12	-
GI (SI)	1.61E-05	1.61E-05	0.12	-
GI (ULI)	2.15E-05	2.15E-05	0.06	-
GI (LLI)	6.62E-06	6.62E-06	0.06	-
kidneys	2.77E-04	2.77E-04	0.0171	-
Liver	2.43E-04	2.43E-04	0.04	-
Lungs	1.07E-02	1.07E-02	0.12	-
Marrow (red)	5.79E-05	5.79E-05	0.12	-
Muscle	6.10E-05	6.10E-05	0.171	-
Ovaries	9.69E-06	9.69E-06	0.08	-
Pancreas	1.30E-04	1.30E-04	0.0171	-
Skin	3.07E-05	3.07E-05	0.01	-
Spleen	1.34E-04	1.34E-04	0.0171	-
Testes	2.99E-06	2.99E-06	0.08	-
Thyroid	5.33E-05	5.33E-05	0.04	-
Uterus	9.95E-06	9.95E-06	0.0171	-
Total Body	2.15E-04	2.15E-04	0.071	-
Women	-	-	1	1.360E-03
Men	-	-	1	1.359E-03

In fact, several factors determine the success of the ^{68}Ga-radiolabeling, such as the temperature and the reaction time, the buffer used or the reaction volume, but among them the pH of the reaction is definitely the most important and sensitive [487]. Therefore, as for other chelates such as DOTA or NOTA, the use of buffers is necessary for the radiolabeling of SBMP with ^{68}Ga to

maintain the labeling media within the appropriate range of pH and avoid gallium-68 hydrolysis and chelators protonation. Highest radiochemical purity was obtained with the use of acetate buffer pH 4.5 leading to very rapid chelation by SBMP (RCP over 99% after 10 min) at room temperature without the need of a heating process, contrarily to that is observe with other chelates such as DOTA [487]. In addition, the *in vitro* stability of the labeling was good and appropriate for *in vivo* use (RCP still over 98%, 90 min after preparation), indeed, due to its short physical half-life ($T_{1/2}$=67 min), ^{68}Ga-based radiopharmaceuticals must be prepared extemporaneously and injected as soon as possible thereafter. In the light of these *in vitro* results, the biodistribution of the ^{68}Ga-SBMP following their IV administration was investigated in preclinical PET studies and validated through postmortem gamma counting of organs. The applied methodology (dynamic PET acquisition) has the advantage of allowing the determination of the radioactivity present at a given time and to obtain its elimination profile in any of the organs (time activity curves). The choice was made to limit the images segmentations to organs for which an uptake of ^{68}Ga was expected or visually detectable (i.e. lungs, liver, bladder, kidneys, spleen, stomach). The spreading of activity on PET images (poorer spatial resolution) outside anatomical CT structures of the organs with the highest uptake (lungs and bladder) led us to delineate these two particular organs on PET images. In addition, a basic mathematical modeling of the extracted time activity curves was realized in order to determine the cumulative activities in organs, which was used as the starting point for the dosimetric estimation in humans. The result of the PET studies with ^{68}Ga-SBMP indicates clearly a homogenous distribution of the tracer within the lungs with no significant distribution in other organs. The uptake in the lungs was stable during the whole acquisition time, the process of elimination of the tracer was slow

and mainly due to renal clearance as shown by the profile of time activity curves of the kidneys and bladder (Figure 49). These results are highly compatible with the use of ^{68}Ga-SBMP as radiopharmaceutical for PET lung perfusion studies, notably meets the criteria of the European Pharmacopoeia, i.e. still more than 85% of the tracer in the lungs 15 min post injection [488]

Before the administration of a new radiotracer to humans, preclinical biodistribution and dosimetry studies in animal models are required. These results can be extrapolated to humans in order to estimate the absorbed internal radiation dose, allowing therefore the safety of a radiotracer from its radiation hazard. In this study, we have predicted the absorbed dose from ^{68}Ga-SBMP PET studies instead of using data obtained by counting activity in dissected organs in traditional *ex vivo* studies. This simple method using PET images and time activity curves provides accurate number of disintegrations in a voxel per unit of activity administered to rats without the need to harvest animal organs. In our study the organ uptake data in animals were extrapolated to the equivalent uptake in humans without applying the method proposed by Sparks *et al.* [489] for two main reasons. First one is that the method of Sparks et al. implies the determination of a ratio between organs weight and total body weight in animal and human which implies the harvesting of the animal organs, which was not the philosophy of our *in vivo* PET imaging study. Second one is that the mechanism of biodistribution of our tracer, due to its diameter size, is mainly limited to the passive uptake and blocking of the ^{68}Ga-SBMP in the lung capillaries. The biodistribution profile of the ^{68}Ga-SBMP is not therefore species dependent or influenced by the weight ratio of the lungs in rats compared to that in humans but rather dependent of the inner diameter of the lung small arteries and capillaries. Another possible bias in our study was the use of a limited number of animals (n=4). Again, due to the physical

mechanism of tracer uptake in the lungs because of its size, the biodistribution is little subject to large variations in the healthy animal and led us to limit the number of animals. As indicated in our results the highest absorbed dose is located in the lungs and on a reasonable basis of an injected activity of 150 MBq, the estimated effective absorbed dose to human appears significantly lower (about 2.04E-01 mSv) compared to the 2 mSv observed after injection of a commercially available SPECT imaging tracer for pulmonary scintigraphy, i.e. ^{99m}Tc-MAA [490]. This difference can be explained mainly by the nature of the isotope present in the two tracers. Gallium-68 as a shorter physical half-live (T_P=67.7 min) than technetium-99m (T_P=6 hours) and higher radiation energy with consequently lower cross section to neighborhood [128]. The biological half-life of ^{99m}Tc-MAA is comprised between 6 to 12 hours and similar to the 422 min found for ^{68}Ga-SBMP in our study [411] and cannot explain the difference in dosimetry results.

2.4 Concluding Remarks

SBMP can be radiolabeled with ^{68}Ga rapidly, reproducibly, through a simple procedure at room temperature with excellent radiochemical purity and remained stable in-vitro for 2h at room temperature. Preclinical PET studies in healthy Wistar rat have shown a homogenous distribution of the ^{68}Ga-SBMP within the lungs with no significant distribution in other organ. Uptake in the lungs was stable during the whole acquisition time, the process of elimination of the tracer was slow and mainly due to renal clearance. These results are highly compatible with the use of ^{68}Ga-SBMP as lung perfusion radiopharmaceutical for PET/CT. Clinical trials are needed to confirm ^{68}Ga-SBMP as an alternative of ^{68}Ga-MAA.

SECTION-III

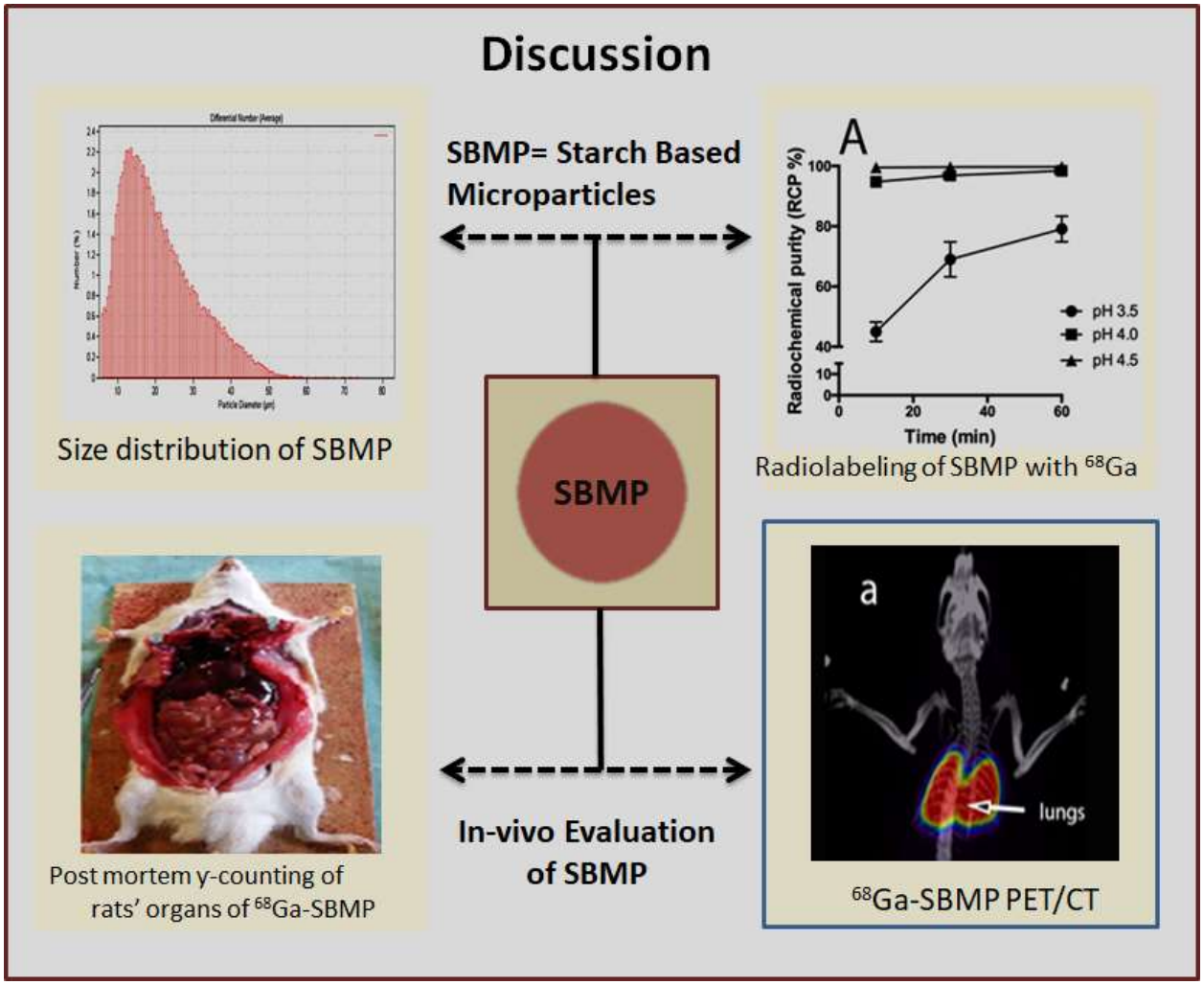
Discussion
SBMP= Starch Based Microparticles
SBMP
Size distribution of SBMP
A
Radiochemical purity (RCP %)
Time (min)
pH 3.5
pH 4.0
pH 4.5
Radiolabeling of SBMP with 68Ga
Post mortem γ-counting of rats' organs of 68Ga-SBMP
In-vivo Evaluation of SBMP
a
lungs
68Ga-SBMP PET/CT

3. General Discussion

This section mainly discusses the experimental results of newly designed and developed radiopharmaceutical for pulmonary perfusion scintigraphy. First of all this chapter describe the reasons to select materials and methods for our new radiopharmaceutical i.e. raw material comprising starch based microparticulate system, positron emission tomography (PET/CT) as an imaging modality for lung perfusion study and positron emitting radionuclide ^{68}Ga.

Subsequent discussion is mainly based on the unpublished experimental results of development of the new radiopharmaceutical, characterization for size, radiochemical purity of the radio-complex, in-vitro stability, and in particular the behavior of the drug inside the living organisms such as lung perfusion study, in-vivo biodistribution & pharmacokinetics, and finally dosimetry.

Discussion section also includes a comparison of the results of new radiopharmaceutical (^{68}Ga-labeled SBMP) to the previously designed one (^{99m}Tc-labeled SBMP). In the dosimetry section estimated absorbed doses in different human organs of ^{68}Ga-SBMP are compared to standard ^{99m}Tc-labeled MAA dosimetry available in ICRP 80.

3.1 Selection of Starch Microparticles

Starch based microparticles are selected as the raw material of our radiopharmaceutical due to following reasons. SBMP were designed from naturally occurring native starch, modified and functionalized, in such a way that mono-functional ligands become capable to form stable complex with radioactive transition metals. Starch has the advantage of being easily available, can be chemically modified [414], biodegradable even after intravascular injection [491], to exist in the microparticulate form and possess physicochemical properties of the size of the granules and

respective percentage of amylose and amylopectin contained in the granules [492, 493]. The ideal size of microparticles for a scintigraphic application of pulmonary perfusion should be equal to 15 ± 7 µm. However, some capillaries can have diameters up to 15µm while flexibility and deformability of microparticles can allow crossing a capillary of slightly smaller diameter [494]. Taking into account of these elements, SBMP, a microparticulate system with some particles ≥10 µm and an average size between 23 µm has met these requirements. In addition to its granulometric characteristics, it is insoluble in water, in consistent with a monograph in the European Pharmacopeia.

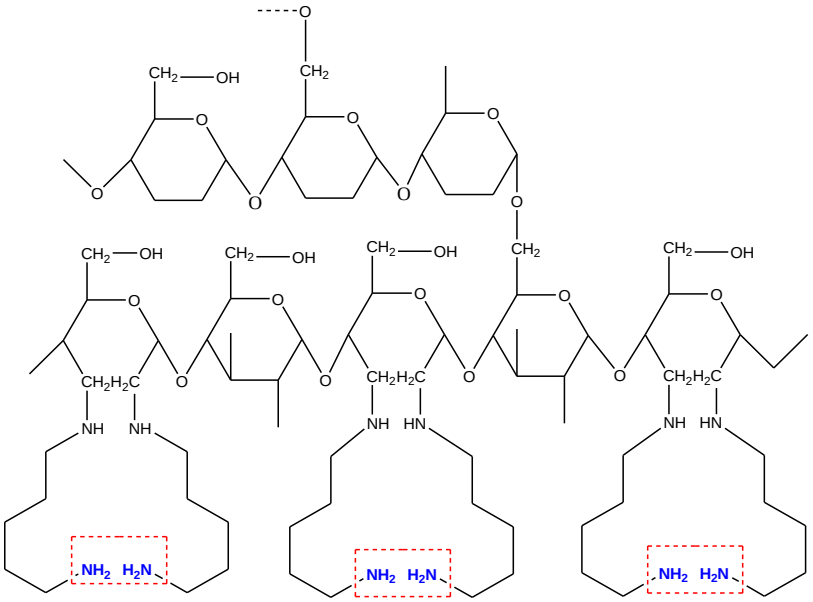

Figure 50 Structure of Starch Based Microparticulate System

The formation of a coordination complex between radionuclides and SBMP was possible due to the oxidation and reduction processes performed by aldehyde and polyamine grafting. Polyamine

(cadaverine) coupling on the surface of starch microparticles make them morphologically homogeneous (Figure 43 a), as compared to macroaggregates of albumin (Figure 35 A) [11, 475]. Having large number of functional groups on the surface of SBMP (Figure 50) make it feasible for radiolabelling with modern radionuclides. However, the percentage of nitrogen present in the microparticles cannot be a single criterion of choice for the radiopharmaceutical formulations for lung perfusion scintigraphy; it is the consideration of several characteristics, included size, and the ability to establish stable complexes with the radiometals, *in-vivo* behavior, and drug resident time in the body, metabolism and elimination procedure.

3.2 Selection of Imaging Modality and Radionuclide

Our selected imaging modality (PET) advantages include higher sensitivity, spatial resolution, and accurate signal quantification especially in small size of the target. Moreover dynamic imaging allows modeling and assessment of mechanism of interaction between target and imaging agent.

Thus PET biodistribution analysis, by the virtue of its safety, ease of use, less radiation hazard, time saving, could be an ideal for routine V/Q scintigraphy study in suspected PE patients. Furthermore a combination of PET with CT imaging, has provided anatomical co-registration, and further advanced the robustness of biodistribution imaging as well as agreed well with biodistribution studies.

Positron emitters for PET include ^{64}Cu, ^{89}Zr and ^{124}I, and ^{68}Ga, ^{18}F etc. Normally PET radionuclides have longer half-lives and take 2–4 days to clear from blood circulation; conversely ^{68}Ga and ^{18}F have relatively shorter half-life. The short half-life of ^{68}Ga (68-min) presents advantageous if the

repetitive examinations are required on the same day. ^{68}Ga other advantage is its high fraction of positron emission 89% than other isotopes such as ^{124}I (23%) and ^{64}Cu (19%).

Physical half-life of Gallium-68 (^{68}Ga) is 68 minutes which is attractively short but its long-lived germanium-68 generator making gallium a convenient radionuclide for many clinical applications i.e. single generator system based on germanium-68 could be utilized for 6-9 months (270.1 days) to produce gallium-68 efficiently on demand for the PET facility. Some scientists provoked ^{68}Ga as a "new technetium" because of its versatile features. Recently, with the advent of versatile chelators for ^{68}Ga, has generated an enormous interest to open new PET imaging applications. ^{68}Ga-DOTA-octretate "DOTATATE" was used to image malignancies like neuro-endocrine tumors and ^{68}Ga-PSMA prostate cancer since long times. Clinical imaging has illustrated comparatively lower radiation exposure in patients using ^{68}Ga-based agents than ^{99m}Tc or ^{18}F or ^{111}In based agents [6, 86, 87].

Keeping in view ^{68}Ga and PET benefits, in terms of high resolution and sensitivity, easy accessibility, dynamic imaging, rapid imaging protocol, repetitive examinations, low radiation burden and quantification have urged us to select this nuclide to label with our microparticulate system to perform lung perfusion scintigraphy through PET/CT (Q PET/CT).

3.3 Preparation and Characterization

The microparticles prepared in the form of lyophilized kits were characterized for size distribution measurement of the particles, afterward particles labeling with ^{68}Ga were underwent for *in-vitro* characterization of radiochemical purity measurements, stability assessment at room

temperature, and *in-vivo* characterization for the evaluation of biodistribution in live rats, and assessment for lung perfusion scintigraphy.

3.3.1 Size Measurement of SBMP

The analysis of the particle size distribution of the SBMP suspensions was performed by particle counter analysis (Multisizer ™ 3 Coulter Counter®). This technique that measures a potential difference between two electrodes dipped within the microparticles suspension to be measured. The meter analysis is perfectly suitable for the measurement of spherical microparticles, in the range from 4 to 200 µm, when the number of small particles we are dealing with, a certain number of oval particles, partially flattened or hollow [11]. However, the technique has the advantage of carrying out particle size analysis (at least 20,000 per measurement), that's statistically more representative than direct measurements in microscopy [11].

3.3.2 Development of ^{68}Ga-labeled SBMP and In-vitro Stability Study

Working on the labeling of microparticles with PET radionuclide (Gallium-68) is an important aspect of our research. Literature revealed that radiolabeling with gallium is a tedious job thus in spite of first preparation of ^{68}Ga-labeled macroaggregates of albumin by Green & Even in 1989,

Table 17 Some PET radionuclides and their frequently used chelators

Radionuclides	Imaging Modality	Representative Chelators
^{18}F	PET	N/A
^{68}Ga	PET	DOTA/NOTA
^{64}Cu	PET	DOTA/NOTA/sarcophagine
^{89}Zr	PET	DFO

this method was never used again. Afterward some groups have optimized the gallium-68 elution for purity and amount of activity which subsequently made ^{68}Ga available as a favorable PET

radionuclide for diagnostic imaging. However to bind with ^{68}Ga, protein requires certain chelating agents [328, 381] such as EDTA, DTPA, NOTA etc. (Table 17). However to obtain good reaction yield of gallium-68 complex, radiolabeling methods still required harsh conditions of temperature, pressure, or catalysts [425, 495-501]. Recent trending in the chelate designing for ^{68}Ga is to improve the radiolabeling procedure by reducing the temperature required for efficient complexing of ^{68}Ga [495-500]. Chelates radiolabeling at temperature and pH close to physiological conditions without the use of acid would reduce preparations required after the development of radiotracer, and simplifying the procedure of tracer production. A range of chelating agents have already been tested to enhance ^{68}Ga complexing abilities [495, 496, 502] such as ^{68}Ga-complexation of small molecule macrocycle 1,4,7 triazylcyclononae-1,4,7 triacetic acid (NOTA) is carried out at room temperature very efficiently, though addition of acid is still a requirement [500, 502-504]. Consequently, chelating agent fabrication for gallium to produce radio-complexes at room temperature without using acid or catalyst would be considered an ideal.

In the preview of above discussion contrary to previous studies, our radiolabeling procedure is simple, robust and carried out at room temperature just by incubating the particles with ^{68}Ga eluate for 10 min while producing more than 99% radiochemical purity, which is also compatible to the short half-life for our chosen radioisotope (68 min). The presence of terminal electron donor amine groups (-NH_2) as seen in structure of SBMP (Figure 50) are imparting basic characteristics and enabled them to react with acidic radiometals i.e. Gallium-68 (+3 oxidation state) [505-507] along with other factors as mentioned in the section 3.2.

We tested and validated radiochemical purity by membrane filtration method. This type of methodology has the advantage of considering the retention of microparticles smaller than the threshold of filter and proved a control of size of microparticles too. Because the small microparticles can be counted for activity with the filtrate, which is effective with the *in-vivo* application since the size of microparticles less than the diameter of the capillaries will not be retained at the pulmonary level and will participate in the noise of the image. For the sake of demand we opted for the use of filters of size larger >5µm contrary to those recommended (3µm) in the monograph of MAA of the European Pharmacopeia [508]. The method used is very easily implemented, requiring a filter (Sartorius Minisart® type) and a radioactivity counter (dose calibrator) and gives excellent reproducible results, with a little risk of overestimation of RPC because less than 2% of the filtered pertechnetate remains adsorbed on the filter. The methodology we adopted of pre-rinsing the filter with saline may increase the yield as described in the experimental section (Figure 46). The radiochemical purities observed for the most interesting formulations included the buffer solution of pH 4.5 at room temperature, which is quite higher (90%) than the limitations of European Pharmacopoeia [509] and also higher than reported studies [408, 422, 423] of other radiopharmaceuticals developed in recent years to substitute MAA. The stability of the radiolabelled SBMP with gallium-68 is more than 2 h at room temperature, and this is quite good time keeping in view the half-life of ^{68}Ga and sufficient to allow the use of microparticles after radiolabeling for lung perfusion studies. The radiochemical purity of ^{68}Ga radiolabeling with starch based microparticles in unfavorable conditions is also good even better than previous studies [236]. In our previous study In-Vitro stability was analysed after incubation of the radiopharmaceutical under vortex agitation for 30

min in Histidine Challenge (a metallic ion chelators) and Fetal bovine serum complex media (transferrin proteins, a natural iron chelator, can also chelate the ion Ga^{3+}) showed radiochemical purity of 99.8%±0.1 and 99.2%±0.1 after 30 min of incubation. In conclusion, starch based microparticles has the potential to radiolabel with gallium-68 through simple and robust method and resulting radiopharmaceutical remained stable for a sufficient time at room temperature in buffer as well as Histidine and FBS, making it possible to carry out labeling in identical conditions on commercial scale in human clinics as daily routine. Therefore after observing constant and reproducible results, In-vivo lung perfusion studies are started.

3.3.3 In-vivo Evaluation of Starch Based Microparticles

For animal study we selected male Wistar rats weighing between (350-460 g). These animals were placed at PET facility of CHU-De-Angers, under controlled conditions of food, water and environment. Rats were set on a board in supine position after proper gas anesthesia supply and injection site was decided to be the penile vein as it would be executed under the camera.

Injecting a radiopharmaceutical and especially containing microparticles is quite tricky. But more precisely the injection through the penile vein is a technical challenge in one of the dimensions of the vein on one hand, and the constrained conditions of injection on the other hand. The technical problems encountered during these injections (microparticles of ^{68}Ga-SBMP injected subcutaneously instead of intravenous) failed to obtain images of the pulmonary perfusion. After a comprehensive practice this problem was controlled. Another problem occurred during this study is related to the sedimentation of ^{68}Ga-labeled SBMP microparticles in different syringes during the time between the preparation of the syringes and the actual injection. The activity (MBq) measurement in each syringe before and after the

radiopharmaceutical injection showed a residual activity of the order of 30% relative to the activity prepared and despite a homogenization step correctly made before each injection. This order of magnitude is also found with the various microparticulate radiopharmaceuticals used for pulmonary perfusion scans. This problem can be solved during clinical studies by rinsing the catheter after radiopharmaceutical injection.

3.3.4 Lung Perfusion and Biodistribution Studies of ^{68}Ga-SBMP PET/CT

It is imperative that an ideal lung perfusion agent should possess sufficient amount of activity and residence time in lungs, minimum amount of activity in background organs, and rapid clearance from all body parts.

Literature illustrated that the particles of smaller size would pass through the pulmonary capillaries and shows an accumulation in liver, consequently a high background signal that would contribute noise/interference. Thus the size of the microparticles is crucial factor to design an imaging agent for targeting pulmonary vascular bed i.e. the particles larger than 10 μm are located mostly in lung, while ~100 nm are preferentially found in the liver and particles ≥0.2±3 μm are tend to accumulated in spleen, whereas particles <30 nm are accumulated in bone-marrow [510]. Consequently, liver, spleen and bone marrow are considered as the organs of particularly interest for managing the administration of microparticulate system for lung perfusion studies for indirect imaging of the pulmonary embolism. Despite the size of the particles, radiotracer distribution in the tissues of different organs is also mediated by capillary types and charge of the particles.

Subsequently dynamic PET imaging at several time points t=0 to t=80 min showed vigilant, quantifiable interpretation of the temporal imaging data, in view of the signal contribution by the

imaging agent that generated valuable information concerning the quantity over time of the imaging agent localization in the specific organs and ex-vivo counting of organs also confirmed that highest radioactivity was found in the lungs and <0.08% activity in the liver plus spleen.

PET studies also elaborated that an immediately uptake of the radiotracer in the lungs capillary bed (i.e. >90 percent of injected activity after 5 min of IV administration), fine tune images, short pulmonary half-life resulting a small radiation dose to patients and could produce superior images than gold standard (^{99m}Tc-labeled MAA).

SBMP remained *in-vivo* stable during whole acquisition period e.g. showing more than 80 percent injected dose per gram even after 80 min of intravenous administration of the radiotracer. This minor decrease was considered due to the degradation of microparticles in size and consistent with our previous studies of SBMP degradation i.e. gel filtration chromatography analysis of urine samples until 12 h post injection of ^{99m}Tc-starch-based microparticles, showed that the activity did not contain free technetium but it was heavy than free activity (^{99m}Tc only) suggesting that clearance of technetium-99m attached with particles [429].

The radiopharmaceutical based on starch based microparticulate system showed in PET clear differences in liver, kidney, and bladder, favoring lung/liver, lungs/stomach and bladder/kidney signals and patterns of the target to non-target distribution ratios of ^{68}Ga-labeled starch based microparticles compared to ^{99m}Tc-labeled starch based particles and ^{99m}Tc labeled macroaggregates of albumin are shown in Table 18. PET studies indicated that the imaging agent accumulation due to liver and spleen was below the requirement of European pharmacopeia (less than 5%). The low and steady counts in the liver over time elaborated that microparticulate system as contrasted with previous studies such as Tspoelas *et al.* 2016, Miroslavov *et al.* 2009

etc. [425, 428], after degradation and reduction in size did not migrated towards the liver. The signal is so weak that we could not assess any overlapping or interference due to liver plus spleen in PET/CT.

Table 18 In vivo characteristics of ^{68}-Ga-labelled starch based microparticles and Tc-99m-labelled starch-based microparticles (n=3) compared to Tc-99m MAA (n=3) after IV injection in Wistar rats

Microparticles	Lung half-life (hours)	Lung/liver t=15 min	Lung/stomach t=15 min	Lung/liver t=30 min	Lung/stomach t= 30 min
^{68}Ga-labeled starch based microparticles (^{68}Ga-SBMP)	7 ±0.2	50± 6.5	231±8	51±8	246.4±7.1
^{99m}Tc-labeled starch based microparticles (^{99m}Tc-SBMP)	3.2 ±0.5	88±20	184±52	87±25	154±45
^{99m}Tc-labeled macroaggregates of albumin (^{99m}Tc-MAA)	13.1±8.6	347±57	636±198	337±65	470±189

Furthermore, comparison of ^{68}Ga-labeled starch based microparticles using positron emission tomography (CT) results with previously conducted study of ^{99m}Tc-labeled starch based-

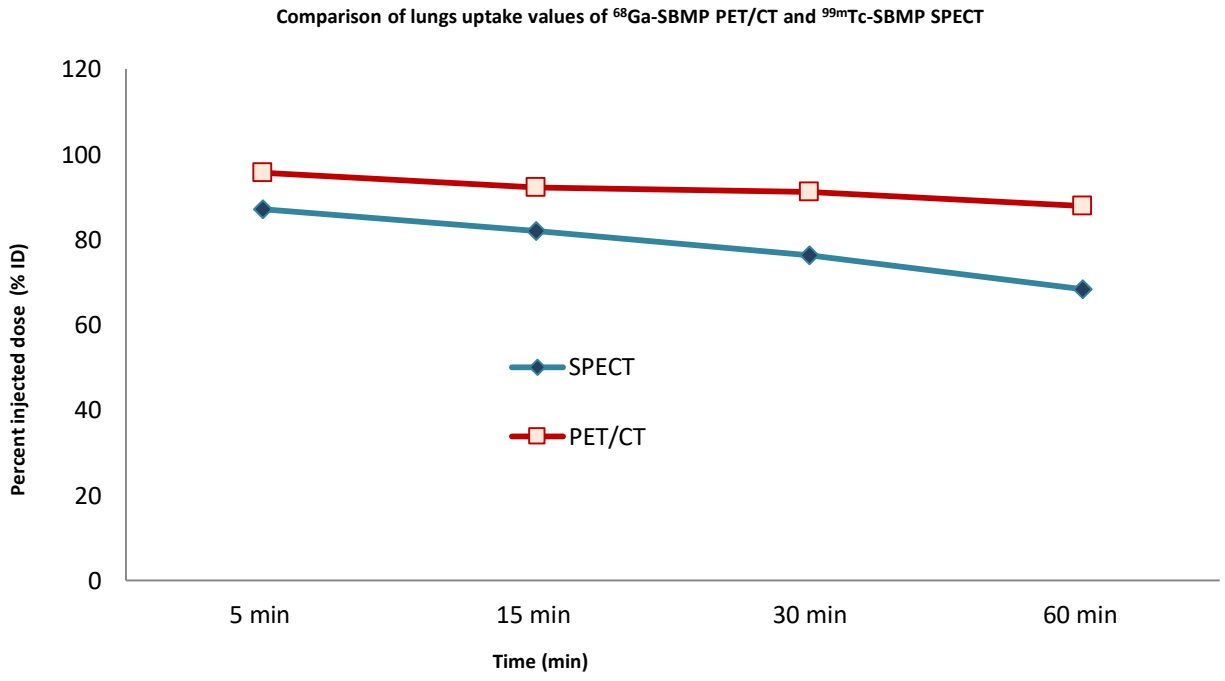

Figure 51 Comparison of lungs uptake values as percent injected dose per gram of ^{68}Ga-labeled SBMP PET/CT and ^{99m}Tc-SBMP SPECT

-microparticles though single photon emission computed tomography (SPECT) showed a good correlation with minor differences (Table 18 and Figure 51).

Kinetic model of clearance of ^{68}Ga-SBMP (Figure 52 A) from kidney to bladder showed a linear and steady trend for kidney while an increasing trend for bladder over time compared to ^{99m}Tc-SBMP as presented in (Figure 52 B).

However it does not astonish that consensus between multiple studies advocates that SPECT imaging underestimates the signals in denser tissues for instance heart, brain, and kidneys.

Starch based imaging agent due to its chemical composition, molecular weight, lipophilicity and size of particles, tissue clearance kinetics of activity would be expected to show a tissue distribution, pharmacokinetics, and metabolism routes compatible to planning lung perfusion studies. Starch microparticles produced Lungs/Liver, and Lung/Blood, the best signal-to-noise ratio as compared to different radiotracers fabricated during last 15 years to compete with MAAs [422, 428].

Dynamic PET acquisition is advantageous as it determines the radioactivity at a prescribed time point as well as provides the elimination profile i.e. time activity curves in organs of interest. Our selected organs for images segmentations include lungs, liver, bladder, kidneys, spleen, and stomach. The organs with highest activity uptake were delineated on PET images while the organs with less activity uptake were delineated on CT images using Imayltics Reseaerch workstation which was efficient to provide us VOIs statistics and the time activity curves.

The behavior of ^{68}Ga-labeled starch based microparticles appears as one of the most concordant drug to meet the requirements of lung perfusion tracer, the percentage of activity observed in

liver was the lowest hepatic activity compared to the previously designed MAA competitors [407, 422-424, 428] and stable until the total acquisition time [428].

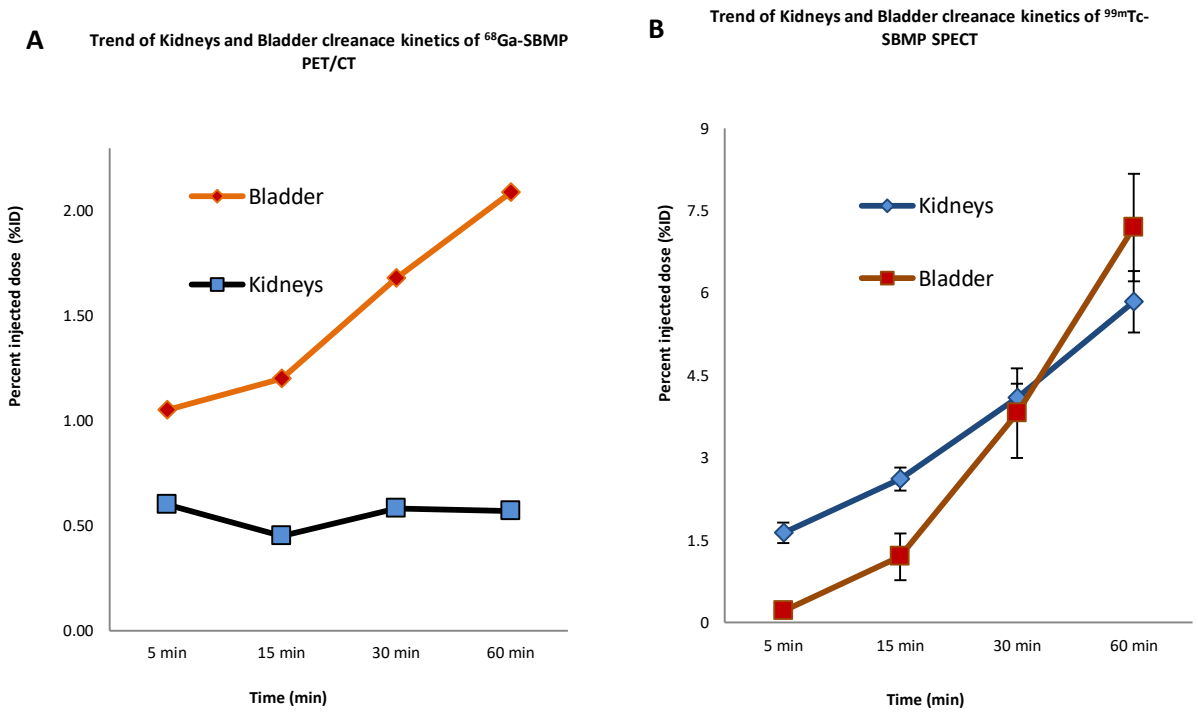

Figure 52 Trend of bladder versus kidney activity clearance kinetics of A) ^{68}Ga-labeled SBMP PET/CT B) ^{99m}Tc-labeled SBMP SPECT

3.4 Dosimetry Calculations

Applications of nuclear medicine imaging include radiopharmaceuticals that are emitting radiations such as ɣ-rays, positron emitters or ß-particles to patients for diagnostic purpose. This radiation exposure might be harmful for the patients, thus in most procedures radiation amounts (dose) are kept on certain low levels but it's contradictory with mechanistic biology observations i.e. keeping the radiations very low, and might be difficult for the physicians to assess efficiently the magnitude of potential risk or radiation exposure. Thus the challenge is to create a trade-off

between the quality of diagnosis and radiation dose and to determine a minimized or optimal effective dose to critical organs for risk stratification.

Mathematical modeling of the time activity curves was used to determine the cumulative activities in organs i.e. activity in organs of interest in rats as percentage-injected activity over time is derived from area under curve values (AUC). These cumulated activities were used as the basis of dosimetric estimation for humans.

Absorbed doses estimates in organ are the crucial basis of risk assessment for the diagnostic nuclear medicine procedures [511, 512], and usually required by the licensing authorities of radiopharmaceuticals. Over past decades, American Society of Nuclear Medicine assigned Medical Internal Radiation Dose Committee (MIRD) has developed estimation methods for absorbed dose in organs, called generally MIRD Schema [484, 513]. Comprehensive set of the effective dose equivalent values (EDE) published by International Commission on Radiological Protection (ICRP) is derived by MIRD schema method and organ absorbed doses data established radiopharmaceuticals is available in latest edition [514], which is utilized to calculate our dosimetry. Accordingly, using the cumulative activity [485] and multiplying it with factor "S" factor derived from anthropomorphic phantoms [91, 514], generated the absorbed dose value for an adult human. "S" factor is obtained from the table of ^{68}Ga radionuclide provided in MIRD pamphlet N°11 [485] and it is equal to mean absorbed dose in the target per unit cumulated activity. To obtain the equivalent doses for organs, radiation weighting factors are multiplied with absorbed doses.

Finally organ equivalent doses multiplied by ICRP tissue-weighting factor and then summing whole body results produces the value of an effective dose. Effective dose gives an estimate of

potential hazard from radiation and used most frequently in the evaluation of the appropriateness of the examination. Furthermore effective dose could not be measured rather it is a calculated amount. Various models and techniques are reported to calculate the optimize radiation dose. We have used MIRD schema and ICRP for the calculation of dosimetry in our study.

In the present study absorbed doses for human organs ^{68}Ga-labeled SBMP are estimated and compared to ^{99m}Tc-MAA: available standards dosimetry. According to the document ICRP 80 ^{99m}Tc-MAA dose in mGy/MBq for lungs 0.07 following by the organs liver 0.02, bladder wall 0.01, pancreas 0.01, adrenals 0.01, spleen 0.004 and for total body is 0.01 [490]. Estimates for human absorbed doses of ^{68}Ga-SBMP from PET/CT animal data in mGy/MBq for lungs 1.1E-02 followed by bladder 2.5 E-04, kidneys 2.4E-04, liver 1.9E-04, pancreas 1.3E-04, adrenals 1.14E-04, stomach 1.11E-04 and spleen 1.0E-04 as shown in Figure 53. For^{99m}Tc-MAA and ^{68}Ga-SBMP has ratios of lung to liver, Bladder, Pancreas, adrenals and spleen 4.2, 6.65, 11.5, 11.5, and 15.2 and for 54, 36.3, 84.79, 102 and 110, respectively. As obvious from the above comparison, gallium-68 labelled starch based particles demonstrated a very high target to non-target (T/NT) values of dosimetry as ^{99m}Tc-MAA.

However, PET/CT data could not be well compared with SPECT/CT data due to the energy difference. ^{68}Ga produces two gamma rays of 511 keV energy (and B^+) since high energy has lower cross section to neighborhood that's why lower dose delivers to them [128]. Thus ^{68}Ga-SBMP delivers lower doses as compared to ^{99m}Tc- MAA [234, 490].

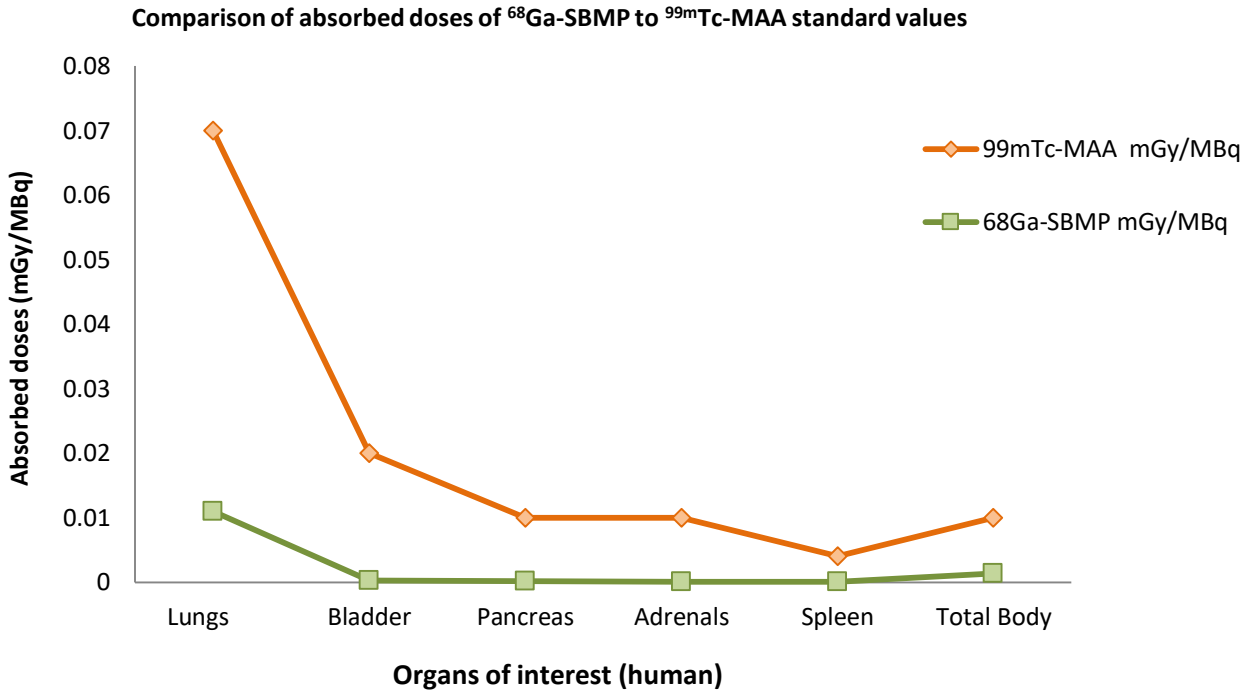

Figure 53 ^{68}Ga-SBMP estimated absorbed doses in human organs of interest (mGy/MBq) and comparison to absorbed doses of ^{99m}Tc-MAA (standard)

The resulting effective absorbed dose, extrapolated from PET perfusion studies with ^{68}Ga-SBMP in rats, for the whole body for an adult was estimated to be 1.360E-03 mSv/MBq for women and 1.359E-03 mSv/MBq for men.

On the basis of an injected activity of 150 MBq, the estimated absorbed for the lungs is 1.65 mGy, total body is 0.032 mGy and the estimated effective absorbed should be 2.04E-01 mSv for women and 2.038E-01 mSv for men as compared to the standards dosimetry for ^{99m}Tc-MAA (ICRP 80) after IV injection of ^{99m}Tc-MAA (185 MBq) the absorbed dose for lungs is 12.21 mGy, and for total body, absorbed and effective dose is 2.04 mGy, and 2.035 mSv (Table 19). These results showed comparatively quite low radiation exposure to human organs than the standard ^{99m}Tc-MAA as depicted in table 19.

Table 19 Estimation of human absorbed doses extrapolate from rats (n=4) after IV administration of ^{68}Ga-SBMP (150 MBq) compared to absorbed doses after IV administration of ^{99m}Tc-MAA (185 MBq)

Target organs	Absorbed dose (mGy) ^{68}Ga-SBMP	Equivalent Dose (H_T) in tissue T (mSv) ^{68}Ga-SBMP	Absorbed dose (mGy) ^{99m}Tc-MAA	Equivalent Dose (H_T) in tissue T (mSv) ^{99m}Tc-MAA	W_T	Effective absorbed dose (mSv) ^{68}Ga-SBMP	Effective absorbed dose (mSv) ^{99m}Tc-MAA
Adrenals	1.74E-02	1.74E-02	1.258	1.258	0.0171	-	-
Bladder	3.33E-02	3.33E-02	1.6095	1.6095	0.04	-	-
Bone total	6.83E-03	6.83E-03	9.44E-01	9.44E-01	0.01	-	-
GI (Stomach)	1.8E-04	1.8E-04	6.85E-01	6.85E-01	0.12	-	-
GI (SI)	2.42E-03	2.42E-03	3.70E-01	3.70E-01	0.12	-	-
GI (ULI)	3.23E-03	3.23E-03	4.10E-01	4.10E-01	0.06	-	-
GI (LLI)	9.93E-04	9.93E-04	2.96E-01	2.96E-01	0.06	-	-
kidneys	4.155E-02	4.155E-02	6.85E-01	6.85E-01	0.0171	-	-
Liver	3.65E-02	3.65E-02	2.96	2.96	0.04	-	-
Lungs	1.605	1.605	12.21	12.21	0.12	-	-
Marrow (red)	3.69E-03	3.69E-03	5.92E-01	5.92E-01	0.12	-	-
Muscle	9.15E-03	9.15E-03	5.18E-01	5.18E-01	0.171	-	-
Ovaries	1.45E-03	1.45E-03	3.33E-01	3.33E-01	0.08	-	-
Pancreas	1.95E-02	1.95E-02	1.04	1.04	0.0171	-	-
Skin	4.61E-03	4.61E-03	2.78E-01	2.78E-01	0.01	-	-
Spleen	2.01E-02	2.01E-02	7.59E-01	7.59E-01	0.0171	-	-
Testes	4.49E-04	4.49E-04	2.04E-01	2.04E-01	0.08	-	-
Thyroid	7.99E-03	7.99E-03	4.63E-01	4.63E-01	0.04	-	-
Uterus	1.49E-03	1.49E-03	2.20E-03	2.20E-03	0.0171	-	-
Total Body	3.20E-02	3.20E-02	2.04	2.04	0.0171	-	2.1487
Women	-	-	-	-	1	0.204	-
Men	-	-	-	-	1	0.20385	-

Tradionally the dissected organs radiation data is used for the calculation of dosimetry of the radiopharmaceuticals. This method can lead to some potential errors when applied to large species organs i.e. variations of inter-species metabolism which may introduce some errors when extrapolating the data from small animals to human organs [515, 516].

Whereas PET/CT data to estimate dosimetry for humans would be suitable for our radiopharmaceutical because ^{68}Ga-labeled SBMP is designed to block the lung capillaries on their first pass and stay there for long time. Furthermore, biodistribution of the ^{68}Ga-SBMP does not depend on the size of species or weight ratio of the lungs between different species but rather depends on the internal diameter of the lung capillaries. Additionally, the dynamic activity curve derived from the PET images provides accurate number of disintegrations per unit activity administered intravenously in rats.

However the calculations of absorbed dose for human organs by extrapolating radioactivity biodistribution from dissected tissues of the rats may provide different values [515, 516]. Nevertheless dosimetry calculations from PET/CT data are comparatively simple, fast, and cost-effective therefore used frequently to estimate dosimetry for humans from small animals data.

SECTION-IV

4. Conclusion and Perspectives

Preliminary studies of managing raw materials for our project was the preparation of the starch based microparticles by carrying out the oxidation and functionalization with a polyamine ligand, and convert them in ready-to-use-kits, under Argon atmosphere, containing the reducing agent ($SnCl_2$) under reproducible conditions to continue project. These freeze dried kits were used for the realization of radiolabeling experiments, to develop a radiopharmaceutical and after getting the control on percent radiochemical purity, the new radiotracer was characterized in terms of size of microparticles, radiochemical purity, *in-vitro* stability assessment that allowed the radiopharmaceutical drug for further *in-vivo* studies. The formulation comprising microparticles of average size between 20 and 30 µm and radiocomplex with ^{68}Ga produced more than 99% radiochemical purity (RPC%) just after 10 min of room temperature incubation which seems compatible keeping in view the short half-life of the radionuclide. In vitro stability studies showed that the radiotracer was stable for more than 2 hours at room temperature. Lung perfusion studies showed that radiotracer started accumulating in the lungs within few seconds of administration of radiotracer and remained there for the total acquisition time (80 min) with a desirable half-life (biological half-life (T_B= 422.13 min) and effective lung half-life (T_E= 58.35 min) showing good in-vivo stability of ^{68}Ga-SBMP. Postmortem counting validated the results of PET/CT i.e. highest radioactivity in lungs and less than 1% activity in liver plus spleen. The ^{68}Ga-labeled starch based microparticles produced crispy clear images of lungs with no background noise of liver or spleen. There was some activity observed at the site of injection due to the technical issues related to the delicacy of penile vein of rat. Biodistribution performed through dynamic PET study (n=4) imaging showed compatible behavior of the starch based

microparticles to lung perfusion scintigraphy. The radiotracer showed an average effective half-life of 60 min inside the body and without getting accumulation inside the organs started clearing from the body. After degradation and reduction in size the SBMP left the lungs capillary bed, decreasing its signal while no increment in the signal of liver or stomach was observed, suggesting that the drug as contrasted to MAA started clearing from the body without the interference of liver. Thus average organ residence time is not affected by the smaller particles of radiotracer. The excretion route of the drug is renal without being accumulating in kidneys and cleared rapidly through bladder. The trend of SBMP in living system for biodistribution is similar and concordant in both studies e.g. ^{68}Ga-SBMP PET/CT and ^{99m}Tc-SBMP SPECT. Finally the estimation of dosimetry by extrapolation of rats' data to adult human has provided us values of absorbed and effective doses which are very low as compared to gold standard, suggesting low radiation exposure to patients and safety for them.

Starch based microparticles evaluation for lung perfusion studies on PET/CT in rats models as well as favorable biodistribution and clearance profiles, safe dosimetry estimation, reassuring the diagnostic performances of starch based microparticles for humans Pulmonary Embolism diagnosis, knowing that the size of the emboli in human clinical is millimetric.

Furthermore PET biodistribution analysis, by the virtue of its safety, ease of use, less radiation hazard, time saving, could be an ideal for routine perfusion scintigraphy study in patients suspected of PE. A combination of PET with CT imaging, has provided anatomical co-registration, and further advanced the robustness of biodistribution imaging.

Due to their nature, the starch based microparticles are unlikely to transmit infectious agents and are capable to become commercially and clinically available, and can meet the challenge of the obligation to synthesize a surrogate of blood-derived particles. Moreover, their short half-life makes it possible to consider their use in an initial diagnostic procedure during a first pulmonary perfusion scintigraphy but also to have the possibility to follow, the same day fibrinolytic therapy through a second perfusion scintigraphy. This approach could lead to changes in current management of patients, provided that the properties (half-life of the lungs) obtained *in-vivo* in animals are identical in humans. The SBMP microparticles were developed with Cyclopharma Laboratories and amenable of large scale production from hundred mg to >10g for clinical studies in the form of sterile ready-to-use kits.

It is clear from the results that this compound deserves more investigation to delineate its activity scope and to elucidate its mechanism of action. In this respect our preliminary work has produced most promising findings for prompt start of the clinical trials. Hence clinical trials phase-1 is suggested to explore the potential of this new radiopharmaceutical originated from plant sources which is unique owing to its nature and characteristics among all the previously designed microparticulate systems for pulmonary perfusion studies as an alternative of macroaggregates of albumin.

4.1 Funding Source and Acknowledgement

The project was funded by Erasmus Mundus 2009-2013 (Decision N° 1298/2008/EC), NanoFar Program to Shabnam Sarwar under the title “European Doctorate in Nano-medicine and Pharmaceutical Sciences”. Author is thankful to the managing team of European Union Commission, Erasmus Mundus Joint Doctorate Program, and NanoFar for funding this project.

SECTION V

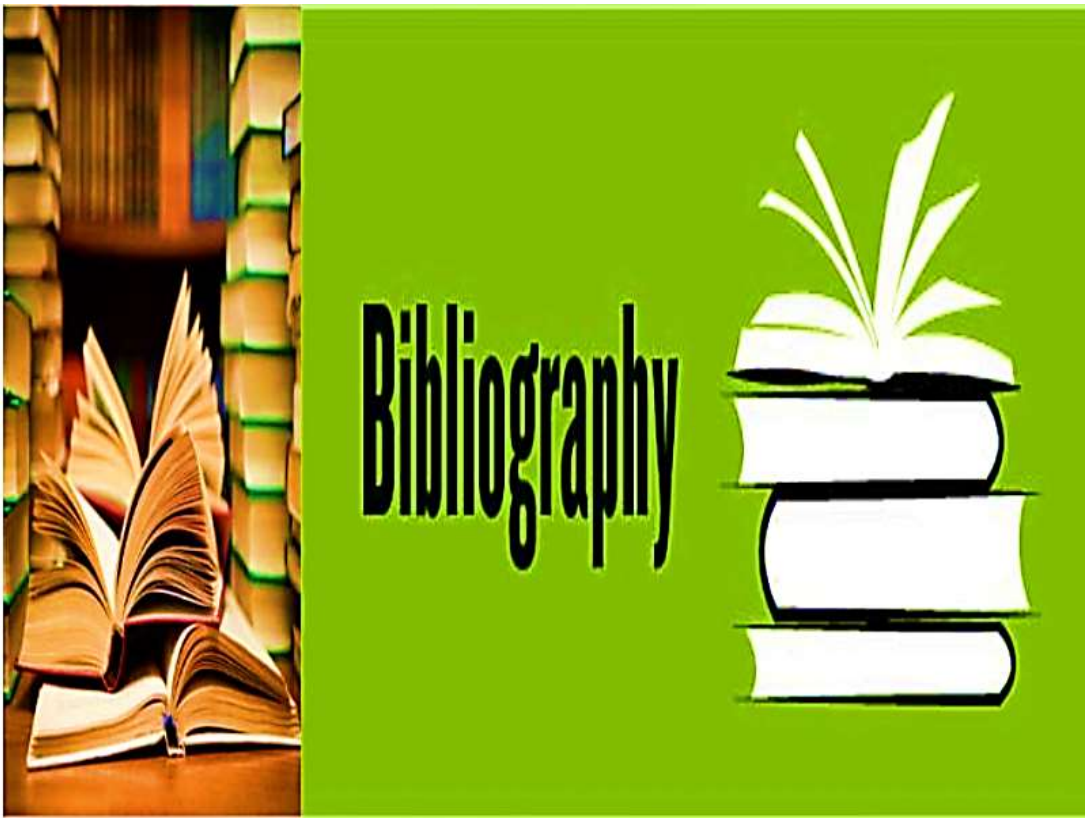

5. Bibliography

1. Srinivas, M., et al., *Cell tracking using multimodal imaging.* Contrast media & molecular imaging, 2013. **8**(6): p. 432-438.
2. Tang, Y., et al., *MRI/SPECT/fluorescent tri-modal probe for evaluating the homing and therapeutic efficacy of transplanted mesenchymal stem cells in a rat ischemic stroke model.* Advanced functional materials, 2015. **25**(7): p. 1024-1034.
3. Raskob, G.E., et al., *Thrombosis: a major contributor to global disease burden.* Arteriosclerosis, thrombosis, and vascular biology, 2014. **34**(11): p. 2363-2371.
4. Wendelboe, A.M. and G.E. Raskob, *Global burden of thrombosis: epidemiologic aspects.* Circulation research, 2016. **118**(9): p. 1340-1347.
5. de Miguel-Díez, J., et al., *Trends in hospital admissions for pulmonary embolism in Spain from 2002 to 2011.* European Respiratory Journal, 2014. **44**(4): p. 942-950.
6. Dentali, F., et al., *Time trends and case fatality rate of in-hospital treated pulmonary embolism during 11 years of observation in Northwestern Italy.* Thrombosis and haemostasis, 2016. **115**(02): p. 399-405.
7. Keller, K., et al., *Trends in thrombolytic treatment and outcomes of acute pulmonary embolism in Germany.* European Heart Journal, 2020. **41**(4): p. 522-529.
8. Barco, S., et al., *Trends in mortality related to pulmonary embolism in the European Region, 2000–15: analysis of vital registration data from the WHO Mortality Database.* The Lancet Respiratory Medicine, 2020. **8**(3): p. 277-287.
9. Rahimtoola, A. and J.D. Bergin, *Acute pulmonary embolism: an update on diagnosis and management.* Current problems in cardiology, 2005. **30**(2): p. 61-114.
10. Heit, J.A., et al., *Risk factors for deep vein thrombosis and pulmonary embolism: a population-based case-control study.* Archives of internal medicine, 2000. **160**(6): p. 809-815.
11. Lacoeuille, F., *Conception, developpement et évaluation d'un nouveau radiopharmaceutique pour la scintigraphie de la perfusion pulmonaire*, 2011, Université d'Angers.
12. Cohen, A.T., et al., *Venous thromboembolism (VTE) in Europe.* Thrombosis and haemostasis, 2007. **98**(04): p. 756-764.
13. Gregory, S.D., et al., *Chapter 18 - Cannula design*, in *Mechanical Circulatory and Respiratory Support*, S.D. Gregory, M.C. Stevens, and J.F. Fraser, Editors. 2018, Academic Press. p. 567-596.
14. Rivera, J., et al., *Platelet receptors and signaling in the dynamics of thrombus formation.* haematologica, 2009. **94**(5): p. 700-711.
15. Furie, B. and B.C. Furie, *Mechanisms of thrombus formation.* New England Journal of Medicine, 2008. **359**(9): p. 938-949.
16. Lippi, G., M. Franchini, and G. Targher, *Arterial thrombus formation in cardiovascular disease.* Nature Reviews Cardiology, 2011. **8**(9): p. 502-512.
17. Ruggeri, Z.M., *The role of von Willebrand factor in thrombus formation.* Thrombosis research, 2007. **120**: p. S5-S9.
18. Bryckaert, M., et al., *Of von Willebrand factor and platelets.* Cellular and Molecular Life Sciences, 2015. **72**(2): p. 307-326.
19. Wolberg, A.S., et al., *Venous thrombosis.* Nature Reviews Disease Primers, 2015. **1**(1): p. 1-17.
20. Wakefield, T.W., D.D. Myers, and P.K. Henke, *Mechanisms of venous thrombosis and resolution.* Arteriosclerosis, thrombosis, and vascular biology, 2008. **28**(3): p. 387-391.

21. Litvinov, R.I., et al., *The platelet integrin αIIbβ3 differentially interacts with fibrin versus fibrinogen.* Journal of Biological Chemistry, 2016. **291**(15): p. 7858-7867.
22. Haas, T.A., *Ligand Recognition Specificity of Leukocyte Integrin alpha (M) beta (2)(Mac-1, CD11b/CD18) and Its Functional Consequences.* 2015.
23. Bagot, C.N. and R. Arya, *Virchow and his triad: a question of attribution.* British journal of haematology, 2008. **143**(2): p. 180-190.
24. Chung, I. and G.Y. Lip, *Virchow's triad revisited: blood constituents.* Pathophysiology of haemostasis and thrombosis, 2003. **33**(5-6): p. 449-454.
25. Blann, A.D., *How a damaged blood vessel wall contibutes to thrombosis and hypertenasion.* Pathophysiology of haemostasis and thrombosis, 2003. **33**(5-6): p. 445-448.
26. Lowe, G.D., *Virchow's triad revisited: abnormal flow.* Pathophysiology of haemostasis and thrombosis, 2003. **33**(5-6): p. 455-457.
27. Peterson, L.-K.N., *Diagnosis and Management of Pulmonary Embolism in Pregnancy*, in *Adult Critical Care Medicine*2019, Springer. p. 315-350.
28. Srivastava, S., et al., *Venous Thrombosis could be Gender Specific, Women Beware!* Defence Science Journal, 2019. **69**(5).
29. Heit, J.A., et al., *Trends in the Incidence of Deep Vein Thrombosis and Pulmonary Embolism: A 35-Year Population-Based Study*, 2006, American Society of Hematology.
30. Silverstein, M.D., et al., *Trends in the incidence of deep vein thrombosis and pulmonary embolism: a 25-year population-based study.* Archives of internal medicine, 1998. **158**(6): p. 585-593.
31. Anderson, F.A., et al., *A population-based perspective of the hospital incidence and case-fatality rates of deep vein thrombosis and pulmonary embolism: the Worcester DVT Study.* Archives of internal medicine, 1991. **151**(5): p. 933-938.
32. Douma, R.A., P.W. Kamphuisen, and H.R. Buller, *Acute pulmonary embolism. Part 1: epidemiology and diagnosis.* Nat Rev Cardiol, 2010. **7**(10): p. 585-96.
33. Goldhaber, S.Z., L. Visani, and M. De Rosa, *Acute pulmonary embolism: clinical outcomes in the International Cooperative Pulmonary Embolism Registry (ICOPER).* The Lancet, 1999. **353**(9162): p. 1386-1389.
34. Sanchez, O., et al., *Prognostic factors for pulmonary embolism: the prep study, a prospective multicenter cohort study.* American journal of respiratory and critical care medicine, 2010. **181**(2): p. 168-173.
35. Nijkeuter, M., et al., *The natural course of hemodynamically stable pulmonary embolism: clinical outcome and risk factors in a large prospective cohort study.* Chest, 2007. **131**(2): p. 517-523.
36. Palla, A., et al., *The clinical course of pulmonary embolism patients anticoagulated for 1 year: results of a prospective, observational, cohort study.* Journal of thrombosis and haemostasis, 2010. **8**(1): p. 68-74.
37. Carson, J.L., et al., *The clinical course of pulmonary embolism.* New England Journal of Medicine, 1992. **326**(19): p. 1240-1245.
38. Janata, K., et al., *Mortality of patients with pulmonary embolism.* Wiener klinische Wochenschrift, 2002. **114**(17-18): p. 766.
39. Heit, J.A., et al., *Predictors of survival after deep vein thrombosis and pulmonary embolism: a population-based, cohort study.* Archives of internal medicine, 1999. **159**(5): p. 445-453.
40. Kröger, K., et al., *Incidence rate of pulmonary embolism in Germany: data from the federal statistical office.* Journal of thrombosis and thrombolysis, 2010. **29**(3): p. 349-353.

41. Lijfering, W.M., F.R. Rosendaal, and S.C. Cannegieter, *Risk factors for venous thrombosis–current understanding from an epidemiological point of view.* British journal of haematology, 2010. **149**(6): p. 824-833.
42. Organization, W.H., *WHO Research Into Global Hazards of Travel Wright Project: Final Report of Pahse I*2007: World Health Organization.
43. Baron, J.A., et al., *Venous thromboembolism and cancer.* The Lancet, 1998. **351**(9109): p. 1077-1080.
44. Ageno, W., et al., *Cardiovascular risk factors and venous thromboembolism.* Circulation, 2008. **117**(1): p. 93-102.
45. Collignon, M., *Radioisotopic studies and pulmonary thromboembolic diseases.* Revue des maladies respiratoires, 1999. **16**(5 Pt 2): p. 894-906.
46. Pomp, E.R., et al., *Risk of venous thrombosis: obesity and its joint effect with oral contraceptive use and prothrombotic mutations.* British journal of haematology, 2007. **139**(2): p. 289-296.
47. Kucher, N., et al., *Risk factors associated with symptomatic pulmonary embolism in a large cohort of deep vein thrombosis patients.* Thrombosis and haemostasis, 2005. **93**(03): p. 494-498.
48. Eichinger, S., et al., *Overweight, obesity, and the risk of recurrent venous thromboembolism.* Archives of internal medicine, 2008. **168**(15): p. 1678-1683.
49. Khorana, A., et al., *Thromboembolism is a leading cause of death in cancer patients receiving outpatient chemotherapy.* Journal of thrombosis and haemostasis, 2007. **5**(3): p. 632-634.
50. Khorana, A.A., et al., *Frequency, risk factors, and trends for venous thromboembolism among hospitalized cancer patients.* Cancer: Interdisciplinary International Journal of the American Cancer Society, 2007. **110**(10): p. 2339-2346.
51. Geerts, W.H., et al., *Prevention of venous thromboembolism: American College of Chest Physicians evidence-based clinical practice guidelines.* Chest, 2008. **133**(6): p. 381S-453S.
52. Carrier, M., et al., *Systematic review: the Trousseau syndrome revisited: should we screen extensively for cancer in patients with venous thromboembolism?* Annals of internal medicine, 2008. **149**(5): p. 323-333.
53. Khorana, A.A., et al., *Guidance for the prevention and treatment of cancer-associated venous thromboembolism.* Journal of thrombosis and thrombolysis, 2016. **41**(1): p. 81-91.
54. Rockson, H.B., et al., *Venous Thromboembolism Prophylaxis for Patients Having Elective Spine Surgery: When, Why, and How Much.* JBJS, 2019. **101**(13): p. 1220-1229.
55. Sweetland, S., et al., *Duration and magnitude of the postoperative risk of venous thromboembolism in middle aged women: prospective cohort study.* Bmj, 2009. **339**: p. b4583.
56. Emoto, S., et al., *Venous thromboembolism in colorectal surgery: Incidence, risk factors, and prophylaxis.* Asian journal of surgery, 2019.
57. Sakran, J.V., et al., *Prolonged operating room time in emergency general surgery is associated with venous thromboembolic complications.* The American Journal of Surgery, 2019.
58. Czap, A.L., A. Becker, and P.Y. Wen. *Thrombotic complications in gliomas*. in *Seminars in thrombosis and hemostasis*. 2019. Thieme Medical Publishers.
59. Kapoor, S., M.K. Jain, and L. Nayak, *Thrombosis*, in *Concise Guide to Hematology*2019, Springer. p. 149-161.
60. Seligsohn, U. and A. Lubetsky, *Genetic Susceptibility to Venous Thrombosis.* New England Journal of Medicine, 2001. **344**(16): p. 1222-1231.
61. Bergqvist, D. and G. Lowe, *Venous thromboembolism in patients undergoing laparoscopic and arthroscopic surgery and in leg casts.* Archives of internal medicine, 2002. **162**(19): p. 2173-2176.

62. Destek, S. and V.O. Gül, *Hereditary Thrombophilia Risk Factors In Patients With Venous Thromboembolism.* Eastern Journal of Medicine, 2020. **25**(1): p. 26-32.
63. Heit, J.A., F.A. Spencer, and R.H. White, *The epidemiology of venous thromboembolism.* Journal of thrombosis and thrombolysis, 2016. **41**(1): p. 3-14.
64. Dahlbäck, B., *Resistance to Activated Protein C Caused by the Factor V R506Q Mutation ls a Common Risk Factor for Venous Thrombosis.* Thrombosis and haemostasis, 1997. **78**(01): p. 483-488.
65. Dalen, J.E., et al., *Pulmonary embolism, pulmonary hemorrhage and pulmonary infarction.* New England Journal of Medicine, 1977. **296**(25): p. 1431-1435.
66. Wood, K.E., *Major pulmonary embolism: review of a pathophysiologic approach to the golden hour of hemodynamically significant pulmonary embolism.* Chest, 2002. **121**(3): p. 877-905.
67. Jorens, P., et al., *Nonthrombotic pulmonary embolism.* European Respiratory Journal, 2009. **34**(2): p. 452-474.
68. Benson, M.D., *Amniotic fluid embolism: the known and not known.* Obstetric medicine, 2014. **7**(1): p. 17-21.
69. Huisman, M.V. and F.A. Klok, *How I diagnose acute pulmonary embolism.* Blood, 2013. **121**(22): p. 4443-4448.
70. Huisman, M.V., et al., *Pulmonary embolism.* Nature Reviews Disease Primers, 2018. **4**(1): p. 18028.
71. Members, A.T.F., et al., *Guidelines on the diagnosis and management of acute pulmonary embolism: The Task Force for the Diagnosis and Management of Acute Pulmonary Embolism of the European Society of Cardiology (ESC).* European Heart Journal, 2008. **29**(18): p. 2276-2315.
72. Mer, M., et al., *Core Elements of General Supportive Care for Patients with Sepsis and Septic Shock in Resource-Limited Settings*, in *Sepsis Management in Resource-limited Settings*2019, Springer. p. 85-129.
73. Bajc, M., et al., *EANM guideline for ventilation/perfusion single-photon emission computed tomography (SPECT) for diagnosis of pulmonary embolism and beyond.* European Journal of Nuclear Medicine and Molecular Imaging, 2019: p. 1-23.
74. Khorana, A.A., *Cancer and thrombosis: implications of published guidelines for clinical practice.* Annals of Oncology, 2009. **20**(10): p. 1619-1630.
75. Streiff, M.B., *Prevention and Treatment of Venous Thromboembolism*, in *Consultative Hemostasis and Thrombosis*2019, Elsevier. p. 273-299.
76. Key, N.S., et al., *Venous thromboembolism prophylaxis and treatment in patients with cancer: ASCO Clinical Practice Guideline Update.* Journal of clinical oncology, 2019: p. JCO. 19.01461.
77. Gary, T., *Venous Thromboembolism*, in *Fundamentals of Vascular Biology*2019, Springer. p. 235-243.
78. Golightly, L.K., B.A. Simendinger, and T.H. Kiser, *Cancer-associated thromboembolism: antithrombotic management of hospitalized patients.* Journal of thrombosis and thrombolysis, 2019: p. 1-8.
79. MacDougall, D.A., et al., *Economic burden of deep-vein thrombosis, pulmonary embolism, and post-thrombotic syndrome.* American Journal of Health-System Pharmacy, 2006. **63**(20_Supplement_6): p. S5-S15.
80. Roth, G.A., et al., *Global and regional patterns in cardiovascular mortality from 1990 to 2013.* Circulation, 2015. **132**(17): p. 1667-1678.

81. Wells, P.S., et al., *Derivation of a simple clinical model to categorize patients probability of pulmonary embolism: increasing the models utility with the SimpliRED D-dimer.* Thrombosis and haemostasis, 2000. **83**(03): p. 416-420.
82. Stein, P.D., et al., *Clinical, laboratory, roentgenographic, and electrocardiographic findings in patients with acute pulmonary embolism and no pre-existing cardiac or pulmonary disease.* Chest, 1991. **100**(3): p. 598-603.
83. Chagnon, I., et al., *Comparison of two clinical prediction rules and implicit assessment among patients with suspected pulmonary embolism.* The American journal of medicine, 2002. **113**(4): p. 269-275.
84. Wicki, J., et al., *Assessing clinical probability of pulmonary embolism in the emergency ward: a simple score.* Archives of internal medicine, 2001. **161**(1): p. 92-97.
85. Goldberg, R.J., *To the Framingham data, turn, turn, turn*, 2009, Am Heart Assoc.
86. Penaloza, A., et al., *Pulmonary embolism rule-out criteria (PERC) rule in European patients with low implicit clinical probability (PERCEPIC): a multicentre, prospective, observational study.* The Lancet Haematology, 2017. **4**(12): p. e615-e621.
87. Freund, Y., et al., *Effect of the pulmonary embolism rule-out criteria on subsequent thromboembolic events among low-risk emergency department patients: the PROPER randomized clinical trial.* Jama, 2018. **319**(6): p. 559-566.
88. Iles, S., et al., *Clinical experience and pre-test probability scores in the diagnosis of pulmonary embolism.* Qjm, 2003. **96**(3): p. 211-215.
89. Le, G.G., M. Righini, and D. Mottier, *Clinical diagnosis of pulmonary embolism: a real challenge.* La Revue de medecine interne, 2007. **28**(6): p. 394-399.
90. Righini, M., et al., *D-Dimer for venous thromboembolism diagnosis: 20 years later.* Journal of thrombosis and haemostasis, 2008. **6**(7): p. 1059-1071.
91. Stein, P.D., et al., *Clinical characteristics of patients with acute pulmonary embolism: data from PIOPED II.* The American journal of medicine, 2007. **120**(10): p. 871-879.
92. Richman, P.B., et al., *Electrocardiographic findings in Emergency Department patients with pulmonary embolism.* Journal of Emergency Medicine, 2004. **27**(2): p. 121-126.
93. Le Gal, G., et al., *Disorders of pulmonary circulation.* Circulation, 2019. **3**: p. 08.
94. Stein, P.D., et al., *Clinical characteristics of patients with acute pulmonary embolism: data from PIOPED II.* The American journal of medicine, 2007. **120**(10): p. 871-879.
95. Ahmedy, F., A. Ahmad Fauzi, and J.P. Engkasan, *Asymptomatic tachycardia and acute pulmonary embolism in a case of tuberculosis spondylodiscitis.* Spinal Cord Series and Cases, 2018. **4**(1): p. 43.
96. Wallis, J.W., et al., *A comparative study of two rapid D-dimer tests for the exclusion of pulmonary embolism in symptomatic patients.* Thrombosis and haemostasis, 2000. **84**(11): p. 925-925.
97. Oger, E., et al., *Evaluation of a new, rapid, and quantitative D-Dimer test in patients with suspected pulmonary embolism.* American journal of respiratory and critical care medicine, 1998. **158**(1): p. 65-70.
98. Perrier, A., et al., *Non-invasive diagnosis of venous thromboembolism in outpatients.* The Lancet, 1999. **353**(9148): p. 190-195.
99. RIGHINI, M., et al., *D-Dimer for venous thromboembolism diagnosis: 20 years later.* Journal of thrombosis and haemostasis, 2008. **6**(7): p. 1059-1071.

100. van Maanen, R., et al., *Validation and impact of a simplified clinical decision rule for diagnosing pulmonary embolism in primary care: design of the PECAN prospective diagnostic cohort management study.* BMJ Open, 2019. **9**(10): p. e031639.
101. Sagel, S.S. and R.H. Greenspan, *Nonuniform pulmonary arterial perfusion: pulmonary embolism?* Radiology, 1971. **99**(3): p. 541-548.
102. Miller, G., et al., *Comparison of streptokinase and heparin in treatment of isolated acute massive pulmonary embolism.* Br Med J, 1971. **2**(5763): p. 681-684.
103. Remy-Jardin, M., et al., *Central pulmonary thromboembolism: diagnosis with spiral volumetric CT with the single-breath-hold technique--comparison with pulmonary angiography.* Radiology, 1992. **185**(2): p. 381-387.
104. Wells, P.S., et al., *Excluding pulmonary embolism at the bedside without diagnostic imaging: management of patients with suspected pulmonary embolism presenting to the emergency department by using a simple clinical model and d-dimer.* Annals of internal medicine, 2001. **135**(2): p. 98-107.
105. Shen, J.-H., et al., *Comparison of the Wells score with the revised Geneva score for assessing suspected pulmonary embolism: a systematic review and meta-analysis.* Journal of thrombosis and thrombolysis, 2016. **41**(3): p. 482-492.
106. Ghaye, B., et al., *Can CT pulmonary angiography allow assessment of severity and prognosis in patients presenting with pulmonary embolism? What the radiologist needs to know.* Radiographics, 2006. **26**(1): p. 23-39.
107. Miniati, M., et al. *Perfusion lung scintigraphy for the diagnosis of pulmonary embolism: a reappraisal and review of the Prospective Investigative Study of Acute Pulmonary Embolism Diagnosis methods*. in *Semin Nucl Med*. 2008. Elsevier.
108. Schembri, G.P., A.E. Miller, and R. Smart. *Radiation dosimetry and safety issues in the investigation of pulmonary embolism*. in *Semin Nucl Med*. 2010. Elsevier.
109. Cahill, A.G., et al., *Diagnosing pulmonary embolism in pregnancy using computed-tomographic angiography or ventilation–perfusion.* Obstetrics & Gynecology, 2009. **114**(1): p. 124-129.
110. Konstantinides , S., *Acute Pulmonary Embolism.* New England Journal of Medicine, 2008. **359**(26): p. 2804-2813.
111. Carroll, W., *Intensive Care, Accident & Poisoning: Prepare for the MRCPCH. Key Articles from the Paediatrics & Child Health journal*2016: Elsevier Health Sciences.
112. Phillips, T.L., *An ultrastructural study of the development of radiation injury in the lung.* Radiology, 1966. **87**(1): p. 49-54.
113. McDonald, R.J., et al., *Intracranial gadolinium deposition after contrast-enhanced MR imaging.* Radiology, 2015. **275**(3): p. 772-782.
114. Robson, M.D., et al., *Magnetic resonance: an introduction to ultrashort TE (UTE) imaging.* Journal of computer assisted tomography, 2003. **27**(6): p. 825-846.
115. Zheng, B., et al., *Quantitative magnetic particle imaging monitors the transplantation, biodistribution, and clearance of stem cells in vivo.* Theranostics, 2016. **6**(3): p. 291.
116. Rahmer, J., et al., *Nanoparticle encapsulation in red blood cells enables blood-pool magnetic particle imaging hours after injection.* Physics in Medicine & Biology, 2013. **58**(12): p. 3965.
117. Roach, P.J., G.P. Schembri, and D.L. Bailey, *V/q scanning using spect and spect/ct.* Journal of Nuclear Medicine, 2013. **54**(9): p. 1588-1596.
118. Hicks, R.J. and M.S. Hofman, *Is there still a role for SPECT–CT in oncology in the PET–CT era?* Nature reviews Clinical oncology, 2012. **9**(12): p. 712.

119. Mueller, D., et al., *Rapid Synthesis of 68 Ga-labeled macroaggregated human serum albumin (MAA) for routine application in perfusion imaging using PET/CT.* Applied radiation and isotopes, 2017. **122**: p. 72-77.
120. Pontana, F., et al., *Lung perfusion with dual-energy multidetector-row CT (MDCT): feasibility for the evaluation of acute pulmonary embolism in 117 consecutive patients.* Academic radiology, 2008. **15**(12): p. 1494-1504.
121. L. Gamerre, G.T., F. Lhuillier, C. Boisson, H.-J. Clement, J.-P. Viale, and *Embolie de liquide amniotique : évolution favorable d'une CIVD isolée et diagnostic biologique précoce,Annales Françaises d'Anesthésie et de Réanimation,.* ISSN 0750-7658,, 2006. **Volume 25,** (Issue 6,): p. Pages 633-637,
122. Perrier, A., et al., *Performance of helical computed tomography in unselected outpatients with suspected pulmonary embolism.* Annals of internal medicine, 2001. **135**(2): p. 88-97.
123. Kelly, A.M., et al., *Multidetector row CT pulmonary angiography and indirect venography for the diagnosis of venous thromboembolic disease in intensive care unit patients.* Academic radiology, 2006. **13**(4): p. 486-495.
124. Cronin, P., J.G. Weg, and E.A. Kazerooni. *The role of multidetector computed tomography angiography for the diagnosis of pulmonary embolism*. in *Semin Nucl Med*. 2008. Elsevier.
125. Stein, P.D., et al., *Multidetector computed tomography for acute pulmonary embolism.* New England Journal of Medicine, 2006. **354**(22): p. 2317-2327.
126. Bettmann, M.A., et al., *ACR Appropriateness Criteria® acute chest pain—suspected pulmonary embolism.* Journal of thoracic imaging, 2012. **27**(2): p. W28-W31.
127. Zhang, L.J., et al., *Computed tomography of acute pulmonary embolism: state-of-the-art.* European radiology, 2015. **25**(9): p. 2547-2557.
128. Gutte, H., et al., *Detection of pulmonary embolism with combined ventilation–perfusion SPECT and low-dose CT: head-to-head comparison with multidetector CT angiography.* Journal of Nuclear Medicine, 2009. **50**(12): p. 1987-1992.
129. Mos, I., et al., *Safety of ruling out acute pulmonary embolism by normal computed tomography pulmonary angiography in patients with an indication for computed tomography: systematic review and meta-analysis.* Journal of Thrombosis and Haemostasis, 2009. **7**(9): p. 1491-1498.
130. Thieme, S., et al., *Dual energy CT lung perfusion imaging—correlation with SPECT/CT.* European journal of radiology, 2012. **81**(2): p. 360-365.
131. Albrecht, M.H., et al., *Comprehensive comparison of virtual monoenergetic and linearly blended reconstruction techniques in third-generation dual-source dual-energy computed tomography angiography of the thorax and abdomen.* Investigative radiology, 2016. **51**(9): p. 582-590.
132. Lu, G.M., et al., *Dual-energy CT of the lung.* American Journal of Roentgenology, 2012. **199**(5_supplement): p. S40-S53.
133. Meyer, M., et al., *Where do we stand? Functional imaging in acute and chronic pulmonary embolism with state-of-the-art CT.* European journal of radiology, 2015. **84**(12): p. 2432-2437.
134. Meysman, M., et al., *Comparison of ventilation-perfusion single-photon emission computed tomography (V/Q SPECT) versus dual-energy CT perfusion and angiography (DECT) after 6 months of pulmonary embolism (PE) treatment.* European journal of radiology, 2015. **84**(9): p. 1816-1819.
135. Kang, M.-J., et al., *Dual-energy CT: clinical applications in various pulmonary diseases.* Radiographics, 2010. **30**(3): p. 685-698.

136. Henzler, T., et al., *CT imaging of acute pulmonary embolism.* Journal of cardiovascular computed tomography, 2011. **5**(1): p. 3-11.
137. Sarma, A., et al., *Radiation and chest CT scan examinations: what do we know?* Chest, 2012. **142**(3): p. 750-760.
138. Mayo, J. and Y. Thakur, *Pulmonary CT angiography as first-line imaging for PE: image quality and radiation dose considerations.* American Journal of Roentgenology, 2013. **200**(3): p. 522-528.
139. Park, C.H., et al., *The feasibility of sub-millisievert coronary CT angiography with low tube voltage, prospective ECG gating, and a knowledge-based iterative model reconstruction algorithm.* The international journal of cardiovascular imaging, 2015. **31**(2): p. 197-203.
140. Sodickson, A. and M. Weiss, *Effects of patient size on radiation dose reduction and image quality in low-kVp CT pulmonary angiography performed with reduced IV contrast dose.* Emergency radiology, 2012. **19**(5): p. 437-445.
141. Schueller-Weidekamm, C., et al., *CT angiography of pulmonary arteries to detect pulmonary embolism: improvement of vascular enhancement with low kilovoltage settings.* Radiology, 2006. **241**(3): p. 899-907.
142. Faggioni, L., et al., *80-kV pulmonary CT angiography with 40 mL of iodinated contrast material in lean patients: comparison of vascular enhancement with iodixanol (320 mg I/mL) and iomeprol (400 mg I/mL).* American Journal of Roentgenology, 2012. **199**(6): p. 1220-1225.
143. Szucs-Farkas, Z., et al., *Diagnostic accuracy of pulmonary CT angiography at low tube voltage: intraindividual comparison of a normal-dose protocol at 120 kVp and a low-dose protocol at 80 kVp using reduced amount of contrast medium in a simulation study.* American Journal of Roentgenology, 2011. **197**(5): p. W852-W859.
144. Pontana, F., et al., *Reduced-dose low-voltage chest CT angiography with Sinogram-affirmed iterative reconstruction versus standard-dose filtered back projection.* Radiology, 2013. **267**(2): p. 609-618.
145. Zhang, L.J., et al., *Feasibility of prospectively ECG-triggered high-pitch coronary CT angiography with 30 mL iodinated contrast agent at 70 kVp: initial experience.* European radiology, 2014. **24**(7): p. 1537-1546.
146. Geyer, L.L., et al., *State of the art: iterative CT reconstruction techniques.* Radiology, 2015. **276**(2): p. 339-357.
147. Lu, G.M., et al., *High-pitch computed tomography pulmonary angiography with iterative reconstruction at 80 kVp and 20 mL contrast agent volume.* European radiology, 2014. **24**(12): p. 3260-3268.
148. Schuhbaeck, A., et al., *Image quality of ultra-low radiation exposure coronary CT angiography with an effective dose< 0.1 mSv using high-pitch spiral acquisition and raw data-based iterative reconstruction.* European radiology, 2013. **23**(3): p. 597-606.
149. Hou, D.J., et al., *Clinical utility of ultra high pitch dual source thoracic CT imaging of acute pulmonary embolism in the emergency department: are we one step closer towards a non-gated triple rule out?* European journal of radiology, 2013. **82**(10): p. 1793-1798.
150. Boos, J., et al., *CT pulmonary angiography: simultaneous low-pitch dual-source acquisition mode with 70 kVp and 40 ml of contrast medium and comparison with high-pitch spiral dual-source acquisition with automated tube potential selection.* Br J Radiol, 2016. **89**(1062): p. 20151059.
151. Li, X., et al., *70-kVp high-pitch computed tomography pulmonary angiography with 40 mL contrast agent: initial experience.* Academic radiology, 2015. **22**(12): p. 1562-1570.
152. Albrecht, M.H., et al., *State-of-the-art pulmonary CT angiography for acute pulmonary embolism.* American Journal of Roentgenology, 2017. **208**(3): p. 495-504.

153. Rhee, C.M., et al., *Association Between Iodinated Contrast Media Exposure and Incident Hyperthyroidism and Hypothyroidism.* Archives of internal medicine, 2012. **172**(2): p. 153-159.
154. Jarvis, C., et al., *A low incidence of iodine-induced hyperthyroidism following administration of iodinated contrast in an iodine-deficient region.* Clinical Endocrinology, 2016. **84**(4): p. 558-563.
155. Hintze, G., et al., *Risk of iodine-induced thyrotoxicosis after coronary angiography: an investigation in 788 unselected subjects.* European journal of endocrinology, 1999. **140**(3): p. 264-267.
156. Alkhuja, S., R. Pyram, and O. Odeyemi, *In the eye of the storm: iodinated contrast medium induced thyroid storm presenting as cardiopulmonary arrest.* Heart & Lung: The Journal of Acute and Critical Care, 2013. **42**(4): p. 267-269.
157. Dave, A., J. Ludlow, and J. Malaty, *Thyrotoxicosis: an under-recognised aetiology.* Bmj Case Reports, 2015. **2015**.
158. Meinel, F.G., et al., *Predictive value of computed tomography in acute pulmonary embolism: systematic review and meta-analysis.* The American journal of medicine, 2015. **128**(7): p. 747-759. e2.
159. McDonald, R.J., et al., *Controversies in contrast material–induced acute kidney injury: closing in on the truth?* Radiology, 2015. **277**(3): p. 627-632.
160. Hinson, J.S., et al., *Using the Electronic Medical Record to Reduce Unnecessary Ordering of Coagulation Studies for Patients with Chest Pain.* Western Journal of Emergency Medicine, 2017. **18**(2): p. 267.
161. Aycock, R.D., et al., *Acute kidney injury after computed tomography: a meta-analysis.* Annals of emergency medicine, 2018. **71**(1): p. 44-53. e4.
162. McDonald, J.S., et al., *Risk of intravenous contrast material–mediated acute kidney injury: a propensity score–matched study stratified by baseline-estimated glomerular filtration rate.* Radiology, 2014. **271**(1): p. 65-73.
163. Radiology, A.C.o., *ACR Manual of Contrast Media, Version. 10.3; 2017*, 2018.
164. Wagner Jr, H.N., et al., *Diagnosis of massive pulmonary embolism in man by radioisotope scanning.* New England Journal of Medicine, 1964. **271**(8): p. 377-384.
165. Gray, H., J. McKillop, and R. Bessent, *Lung scan reports: interpretation by clinicians.* Nuclear medicine communications, 1993. **14**(11): p. 989-994.
166. Bajc, M., et al., *Lung ventilation/perfusion SPECT in the artificially embolized pig.* Journal of Nuclear Medicine, 2002. **43**(5): p. 640-647.
167. Bajc, M., et al., *Diagnostic evaluation of planar and tomographic ventilation/perfusion lung images in patients with suspected pulmonary emboli.* Clinical physiology and functional imaging, 2004. **24**(5): p. 249-256.
168. Reinartz, P., et al., *Tomographic imaging in the diagnosis of pulmonary embolism: a comparison between V/Q lung scintigraphy in SPECT technique and multislice spiral CT.* Journal of Nuclear Medicine, 2004. **45**(9): p. 1501-1508.
169. Roach, P.J., D.L. Bailey, and B.E. Harris. *Enhancing lung scintigraphy with single-photon emission computed tomography*. in *Semin Nucl Med*. 2008. Elsevier.
170. Roach, P.J., et al. *Spect/ct in v/q scanning*. in *Semin Nucl Med*. 2010. Elsevier.
171. Andreou, A.K., et al., *Does pregnancy affect vascular enhancement in patients undergoing CT pulmonary angiography?* European radiology, 2008. **18**(12): p. 2716-2722.
172. Jordan, E.J., et al., *CT pulmonary angiography in pregnant and postpartum women: low yield, high dose.* Clinical imaging, 2015. **39**(2): p. 251-253.

173. Litmanovich, D., et al., *Dose reduction in computed tomographic angiography of pregnant patients with suspected acute pulmonary embolism.* Journal of computer assisted tomography, 2009. **33**(6): p. 961-966.
174. Pahade, J.K., et al., *Imaging pregnant patients with suspected pulmonary embolism: what the radiologist needs to know.* Radiographics, 2009. **29**(3): p. 639-654.
175. U-King-Im, J.M., et al., *Quality of CT pulmonary angiography for suspected pulmonary embolus in pregnancy.* European radiology, 2008. **18**(12): p. 2709.
176. Bajc, M. and J. Jgi, *Quantitative Ventilation/Perfusion Tomography: the Foremost Technique for Pulmonary Embolism Diagnosis.* 2012.
177. Robinson, P.J., *Ventilation-perfusion lung scanning and spiral computed tomography of the lungs: competing or complementary modalities?* European Journal of Nuclear Medicine, 1996. **23**(11): p. 1547-1553.
178. Bajc, M., et al., *EANM guideline for ventilation/perfusion single-photon emission computed tomography (SPECT) for diagnosis of pulmonary embolism and beyond.* European Journal of Nuclear Medicine and Molecular Imaging, 2019. **46**(12): p. 2429-2451.
179. Isawa, T., et al., *Technegas for inhalation lung imaging.* Nuclear medicine communications, 1991. **12**(1): p. 47-55.
180. Jögi, J., et al., *Heart failure diagnostics based on ventilation/perfusion single photon emission computed tomography pattern and quantitative perfusion gradients.* Nuclear medicine communications, 2008. **29**(8): p. 666-673.
181. Angriman, F., et al., *Wells score and poor outcomes among adult patients with subsegmental pulmonary embolism: a cohort study.* Clinical and Applied Thrombosis/Hemostasis, 2015. **21**(6): p. 539-545.
182. Ciofetta, G., et al., *Guidelines for lung scintigraphy in children.* European Journal of Nuclear Medicine and Molecular Imaging, 2007. **34**(9): p. 1518-1526.
183. Palmer, J., et al., *Comprehensive ventilation/perfusion SPECT.* Journal of Nuclear Medicine, 2001. **42**(8): p. 1288-1294.
184. Bajc, M., et al., *Quantitative Ventilation/Perfusion SPECT (QV/PSPECT): A primary Method for Diagnosis of Pulmonary embolism.* 2004.
185. Gray, G. and C. Nelson-Piercy, *Thromboembolic disorders in obstetrics.* Best practice & research Clinical obstetrics & gynaecology, 2012. **26**(1): p. 53-64.
186. Bourjeily, G., et al., *Pulmonary embolism in pregnancy.* The Lancet, 2010. **375**(9713): p. 500-512.
187. Bajc, M., et al., *V/P SPECT as a diagnostic tool for pregnant women with suspected pulmonary embolism.* European Journal of Nuclear Medicine and Molecular Imaging, 2015. **42**(8): p. 1325-1330.
188. Kline, J.A., et al., *Systematic review and meta-analysis of pregnant patients investigated for suspected pulmonary embolism in the emergency department.* Academic Emergency Medicine, 2014. **21**(9): p. 949-959.
189. Sivandarajah, S., *Towards evidence-based emergency medicine: best BETs from the Manchester Royal Infirmary. BET 4: current evidence does not support the use of a negative D-dimer to rule out suspected pulmonary embolism in pregnancy.* Emergency medicine journal: EMJ, 2011. **28**(3): p. 245.
190. Bourjeily, G., et al., *Outcomes of negative multidetector computed tomography with pulmonary angiography in pregnant women suspected of pulmonary embolism.* Lung, 2012. **190**(1): p. 105-111.

191. Leung, A.N., et al., *An official American Thoracic Society/Society of Thoracic Radiology clinical practice guideline: evaluation of suspected pulmonary embolism in pregnancy.* American journal of respiratory and critical care medicine, 2011. **184**(10): p. 1200-1208.
192. Ridge, C.A., et al., *Pulmonary embolism in pregnancy: comparison of pulmonary CT angiography and lung scintigraphy.* American Journal of Roentgenology, 2009. **193**(5): p. 1223-1227.
193. Hurwitz, L.M., et al., *Radiation dose to the fetus from body MDCT during early gestation.* American Journal of Roentgenology, 2006. **186**(3): p. 871-876.
194. Bajc, M., et al., *Ventilation/perfusion SPECT for diagnostics of pulmonary embolism in clinical practice.* Journal of internal medicine, 2008. **264**(4): p. 379-387.
195. Grüning, T., et al., *Three-year clinical experience with VQ SPECT for diagnosing pulmonary embolism: diagnostic performance.* Clinical imaging, 2014. **38**(6): p. 831-835.
196. Le Roux, P.-Y., et al., *V/Q SPECT interpretation for pulmonary embolism diagnosis: which criteria to use?* Journal of Nuclear Medicine, 2013. **54**(7): p. 1077-1081.
197. Ikesaka, R. and M. Carrier, *Clinical significance and management of subsegmental pulmonary embolism.* Journal of thrombosis and thrombolysis, 2015. **39**(3): p. 311-314.
198. Bajc, M., et al., *Grading obstructive lung disease using tomographic pulmonary scintigraphy in patients with chronic obstructive pulmonary disease (COPD) and long-term smokers.* Annals of nuclear medicine, 2015. **29**(1): p. 91-99.
199. Begic, A., et al., *Ventilation/perfusion tomography–V/P-SPECT vs planar technique.*
200. Corbus, H., et al., *Diagnostic usefulness of lung SPET in pulmonary thromboembolism: an outcome study.* Nuclear medicine communications, 1997. **18**(10): p. 897-906.
201. Astani, S.A., et al., *Detection of pulmonary embolism during pregnancy: comparing radiation doses of CTPA and pulmonary scintigraphy.* Nuclear medicine communications, 2014. **35**(7): p. 704-711.
202. Quirce, R., et al., *Contribution of V/Q SPECT to planar scintigraphy in the diagnosis of pulmonary embolism.* Revista Española de Medicina Nuclear e Imagen Molecular (English Edition), 2014. **33**(3): p. 153-158.
203. Leblanc, M., F. Leveillée, and E. Turcotte, *Prospective evaluation of the negative predictive value of V/Q SPECT using 99mTc-Technegas.* Nuclear medicine communications, 2007. **28**(8): p. 667-672.
204. Le Roux, P.-Y., et al., *Safety of ventilation/perfusion single photon emission computed tomography for pulmonary embolism diagnosis.* European Journal of Nuclear Medicine and Molecular Imaging, 2014. **41**(10): p. 1957-1964.
205. Le Duc-Pennec, A., et al., *Diagnostic accuracy of single-photon emission tomography ventilation/perfusion lung scan in the diagnosis of pulmonary embolism.* Chest, 2012. **141**(2): p. 381-387.
206. Smith-Bindman, R., et al., *Predictors of CT radiation dose and their effect on patient care: a comprehensive analysis using automated data.* Radiology, 2017. **282**(1): p. 182-193.
207. Liang, C.R., et al., *Establishment of institutional diagnostic reference level for computed tomography with automated dose-tracking software.* Journal of medical radiation sciences, 2017. **64**(2): p. 82-89.
208. MacGregor, K., et al., *Identifying institutional diagnostic reference levels for CT with radiation dose index monitoring software.* Radiology, 2015. **276**(2): p. 507-517.
209. Phillips, J., J. Straiton, and R. Staff, *Planar and SPECT ventilation/perfusion imaging and computed tomography for the diagnosis of pulmonary embolism: a systematic review and meta-*

analysis of the literature, and cost and dose comparison. European journal of radiology, 2015. **84**(7): p. 1392-1400.
210. Isidoro, J., et al., *Radiation dose comparison between V/P-SPECT and CT-angiography in the diagnosis of pulmonary embolism.* Physica Medica, 2017. **41**: p. 93-96.
211. Sabarudin, A., et al., *Radiation dose reduction in thoracic and abdomen–pelvic CT using tube current modulation: a phantom study.* Journal of applied clinical medical physics, 2015. **16**(1): p. 319-328.
212. Grüning, T., et al., *Diagnosing venous thromboembolism in pregnancy.* The British Journal of Radiology, 2016. **89**(1062): p. 20160021.
213. Siva, S., et al., *High-resolution pulmonary ventilation and perfusion PET/CT allows for functionally adapted intensity modulated radiotherapy in lung cancer.* Radiotherapy and Oncology, 2015. **115**(2): p. 157-162.
214. Le Roux, P.-Y., et al., *Automatic delineation of functional lung volumes with 68 Ga-ventilation/perfusion PET/CT.* EJNMMI research, 2017. **7**(1): p. 82.
215. Leong, P., et al., *Reduced ventilation–perfusion (V/Q) mismatch following endobronchial valve insertion demonstrated by Gallium-68 V/Q photon emission tomography/computed tomography*. Respirology case reports, 2017. **5**(5): p. e00253.
216. Le Roux, P.-Y., et al., *Gallium-68 perfusion positron emission tomography/computed tomography to assess pulmonary function in lung cancer patients undergoing surgery.* Cancer Imaging, 2016. **16**(1): p. 24.
217. Oehme, L., et al., *Quantitative analysis of regional lung ventilation and perfusion PET with 68Ga-labelled tracers.* Nuclear medicine communications, 2014. **35**(5): p. 501-510.
218. Le Roux, P.-Y., P. Robin, and P.-Y. Salaun, *New developments and future challenges of nuclear medicine and molecular imaging for pulmonary embolism.* Thromb Res, 2018. **163**: p. 236-241.
219. Hofman, M.S., et al., *68Ga PET/CT ventilation–perfusion imaging for pulmonary embolism: a pilot study with comparison to conventional scintigraphy.* Journal of Nuclear Medicine, 2011. **52**(10): p. 1513-1519.
220. Le Roux, P.-Y., et al. *PET/CT lung ventilation and perfusion scanning using Galligas and gallium-68-MAA*. in *Semin Nucl Med*. 2018. Elsevier.
221. Kipritidis, J., et al., *Validating and improving CT ventilation imaging by correlating with ventilation 4D-PET/CT using 68Ga-labeled nanoparticles.* Medical physics, 2014. **41**(1): p. 011910.
222. Bailey, D.L., et al., *(68)Ga PET Ventilation and Perfusion Lung Imaging-Current Status and Future Challenges.* Semin Nucl Med, 2016. **46**(5): p. 428-35.
223. Borges, J.B., et al., *Ventilation distribution studies comparing Technegas and "Gallgas" using 68GaCl3 as the label.* Journal of Nuclear Medicine, 2011. **52**(2): p. 206-209.
224. Kotzerke, J., et al., *Ventilation-perfusion-lungscintigraphy using PET and 68Ga-labeled radiopharmaceuticals.* Nuklearmedizin, 2010. **49**(6): p. 203-208.
225. Ament, S., et al., *PET Lung Ventilation/Perfusion Imaging Using 68 Ga Aerosol (Galligas) and 68 Ga-Labeled Macroaggregated Albumin*, in *Theranostics, Gallium-68, and Other Radionuclides*2013, Springer. p. 395-423.
226. Callahan, J., et al., *High-resolution imaging of pulmonary ventilation and perfusion with 68Ga-VQ respiratory gated (4-D) PET/CT.* Eur J Nucl Med Mol Imaging, 2014. **41**(2): p. 343-9.
227. Hopkins, S.R., et al., *Vertical gradients in regional lung density and perfusion in the supine human lung: the Slinky effect.* Journal of Applied Physiology, 2007. **103**(1): p. 240-248.

228. Schembri, G.P., et al. *Artifacts and anatomical variants affecting ventilation and perfusion lung imaging*. in *Semin Nucl Med*. 2015. Elsevier.
229. Hofman, M.S., et al., *68Ga PET/CT ventilation-perfusion imaging for pulmonary embolism: a pilot study with comparison to conventional scintigraphy.* J Nucl Med, 2011. **52**(10): p. 1513-9.
230. Even, G.A. and M.A. Green, *Gallium-68-labeled macroaggregated human serum albumin, 68Ga-MAA.* International Journal of Radiation Applications and Instrumentation. Part B. Nuclear Medicine and Biology, 1989. **16**(3): p. 319-321.
231. Mintun, M.A., et al., *Measurements ofPulmonary Vascular Permeability with PET and Gallium-68 Transferrin.* J Nucl Med, 1987. **28**: p. 1704-16.
232. Schuster, D.P., J. Markham, and M.J. Welch, *Positron emission tomography measurements of pulmonary vascular permeability with Ga-68 transferrin or C-11 methylalbumin.* Critical care medicine, 1998. **26**(3): p. 518-525.
233. Zhernosekov, K.P., et al., *Processing of generator-produced 68Ga for medical application.* Journal of Nuclear Medicine, 2007. **48**(10): p. 1741-1748.
234. Shanehsazzadeh, S., et al., *Comparison of estimated human dose of 68Ga-MAA with 99mTc-MAA based on rat data.* Ann Nucl Med, 2015. **29**(8): p. 745-753.
235. Jalilian, A.R., et al., *Preclinical evaluation of 68Ga-MAA from commercial available 99mTc-MAA kit.* Iranian Journal of Pharmaceutical Research, 2017. **16**(4): p. 1415-1423.
236. Maus, S., et al., *Labelling of commercially available human serum albumin kits with 68Ga as surrogates for 99mTc-MAA microspheres.* Appl Radiat Isot, 2011. **69**(1): p. 171-5.
237. Amor-Coarasa, A., et al. *99mTc-MAA vs. 68Ga-MAA as Perfusion Agents*. in *Biomedical Engineering Conference (SBEC), 2013 29th Southern*. 2013. IEEE.
238. Siva, S., et al., *Ga-68 MAA Perfusion 4D-PET/CT Scanning Allows for Functional Lung Avoidance Using Conformal Radiation Therapy Planning.* Technol Cancer Res Treat, 2016. **15**(1): p. 114-21.
239. Le Roux, P.-Y., et al., *Independent and incremental value of ventilation/perfusion PET/CT and CT pulmonary angiography for pulmonary embolism diagnosis: results of the PECAN pilot study.* European journal of nuclear medicine and molecular imaging, 2019: p. 1-9.
240. Robert-Ebadi, H., et al., *Safety of multidetector computed tomography pulmonary angiography to exclude pulmonary embolism in patients with a likely pretest clinical probability.* Journal of thrombosis and haemostasis, 2017. **15**(8): p. 1584-1590.
241. Hammer, M.M. and H.I. Litt, *Risk of pulmonary embolism after a prior negative CT pulmonary angiogram.* The American journal of emergency medicine, 2016. **34**(10): p. 1968-1972.
242. Mos, I.C., et al., *Diagnostic outcome management study in patients with clinically suspected recurrent acute pulmonary embolism with a structured algorithm.* Thromb Res, 2014. **133**(6): p. 1039-1044.
243. Pesavento, R., et al., *The value of 64-detector row computed tomography for the exclusion of pulmonary embolism.* Thrombosis and haemostasis, 2011. **105**(05): p. 901-907.
244. van der Hulle, T., et al., *Simplified diagnostic management of suspected pulmonary embolism (the YEARS study): a prospective, multicentre, cohort study.* The Lancet, 2017. **390**(10091): p. 289-297.
245. van der Hulle, T., et al., *Is a normal computed tomography pulmonary angiography safe to rule out acute pulmonary embolism in patients with a likely clinical probability?* Thrombosis and haemostasis, 2017. **117**(08): p. 1622-1629.
246. van der Pol, L., et al., *Combination of pulmonary embolism rule-out criteria and YEARS algorithm in a European cohort of patients with suspected pulmonary embolism.* Thrombosis and haemostasis, 2018. **118**(03): p. 547-552.

247. Parekh, A., R. Graham, and S. Redman, *Ventilation/perfusion single-photon emission computed tomography: a service evaluation.* Nuclear medicine communications, 2017. **38**(8): p. 672-675.
248. Douma, R.A., et al., *Comparison of 4-and 64-slice CT scanning in the diagnosis of pulmonary embolism.* Thrombosis and haemostasis, 2010. **103**(01): p. 242-246.
249. Ciofetta, G., et al., *Guidelines for lung scintigraphy in children.* European Journal of Nuclear Medicine and Molecular Imaging, 2007. **34**(9): p. 1518-1526.
250. Members, A.T.F., et al., *2014 ESC Guidelines on the diagnosis and management of acute pulmonary embolism: The Task Force for the Diagnosis and Management of Acute Pulmonary Embolism of the European Society of Cardiology (ESC) Endorsed by the European Respiratory Society (ERS).* European Heart Journal, 2014. **35**(43): p. 3033-3080.
251. van Mens, T.E., et al., *Imaging for the exclusion of pulmonary embolism in pregnancy.* Cochrane Database of Systematic Reviews, 2017(1).
252. Bajc, M., et al., *Identifying the heterogeneity of COPD by V/P SPECT: a new tool for improving the diagnosis of parenchymal defects and grading the severity of small airways disease.* International journal of chronic obstructive pulmonary disease, 2017. **12**: p. 1579.
253. Nasr, A., A. Lindqvist, and M. Bajc, *Ventilation defect typical for COPD is frequent among patients suspected for pulmonary embolism but does not prevent the diagnosis of PE by V/P SPECT.* EC Pulmonology and Respiratory Medicine, 2017. **4**(3): p. 85-91.
254. Goldhaber, S.Z. and C.G. Elliott, *Acute pulmonary embolism: part I: epidemiology, pathophysiology, and diagnosis.* Circulation, 2003. **108**(22): p. 2726-2729.
255. Miniati, M., et al., *Accuracy of clinical assessment in the diagnosis of pulmonary embolism.* American journal of respiratory and critical care medicine, 1999. **159**(3): p. 864-871.
256. Waxman, A.D., et al., *Appropriate Use Criteria for Ventilation–Perfusion Imaging in Pulmonary Embolism: Summary and Excerpts.* Journal of Nuclear Medicine, 2017. **58**(5): p. 13N-15N.
257. Meng, J., et al., *A comparison of ventilation/perfusion single photon emission CT and CT pulmonary angiography for diagnosis of pulmonary embolism.* Zhonghua jie he he hu xi za zhi= Zhonghua jiehe he huxi zazhi= Chinese journal of tuberculosis and respiratory diseases, 2013. **36**(3): p. 177-181.
258. Moores, L., et al., *Multidetector computed tomographic pulmonary angiography in patients with a high clinical probability of pulmonary embolism.* Journal of thrombosis and haemostasis, 2016. **14**(1): p. 114-120.
259. Mahdavi, R., et al., *Agreement between SPECT V/Q scan and CT angiography in patients with high clinical suspicion of PE.* Annals of nuclear medicine, 2013. **27**(9): p. 834-838.
260. Leuschner, G., et al., *Suspected pulmonary embolism in patients with pulmonary fibrosis: Discordance between ventilation/perfusion SPECT and CT pulmonary angiography.* Respirology, 2016. **21**(6): p. 1081-1087.
261. Gopalan, D., M. Delcroix, and M. Held, *Diagnosis of chronic thromboembolic pulmonary hypertension.* European Respiratory Review, 2017. **26**(143): p. 160108.
262. Goldhaber, S.Z., *Risk factors for venous thromboembolism.* Journal of the American College of Cardiology, 2010. **56**(1): p. 1-7.
263. Ibanez-Bravo, S., et al., *Ventilation/Perfusion SPECT lung scintigraphy and computed tomography pulmonary angiography in patients with clinical suspicion of pulmonary embolism.* Revista Española de Medicina Nuclear e Imagen Molecular (English Edition), 2016. **35**(4): p. 215-220.

264. Rouzet, F., et al., *Radiolabeled fucoidan as a p-selectin targeting agent for in vivo imaging of platelet-rich thrombus and endothelial activation.* Journal of Nuclear Medicine, 2011. **52**(9): p. 1433-1440.
265. Thakur, M.L., et al., *Indium-111 labeled platelets: studies on preparation and evaluation of in vitro and in vivo functions.* Thrombosis research, 1976. **9**(4): p. 345-357.
266. Wagner, C.L., et al., *Analysis of GPIIb/IIIa receptor number by quantification of 7E3 binding to human platelets.* 1996.
267. Ji, S., et al., *Detection of Thromboembolism with 99mTc-labeled F (ab) 2 Fragment of Anti-glycoprotein IIIa Chimeric Monoclonal Antibody in Beagle Canines.* Thrombosis research, 2012. **130**(5): p. 703-708.
268. Zhou, Y., S. Chakraborty, and S. Liu, *Radiolabeled Cyclic RGD Peptides as Radiotracers for Imaging Tumors and Thrombosis by SPECT.* Theranostics, 2011. **1**: p. 58-82.
269. Shi, J., et al., *Evaluation of In-Labeled Cyclic RGD Peptides: Effects of Peptide and Linker Multiplicity on Their Tumor Uptake, Excretion Kinetics and Metabolic Stability.* Theranostics, 2011. **1**: p. 322-340.
270. Fani, M., H.R. Maecke, and S.M. Okarvi, *Radiolabeled peptides: valuable tools for the detection and treatment of cancer.* Theranostics, 2012. **2**(5): p. 481-501.
271. Zhang, Y., Y. Yang, and W. Cai, *Multimodality Imaging of Integrin α(v)β(3) Expression.* Theranostics, 2011. **1**: p. 135-148.
272. Zhou, Y., G. Shao, and S. Liu, *Monitoring Breast Tumor Lung Metastasis by U-SPECT-II/CT with an Integrin α(v)β(3)-Targeted Radiotracer(99m)Tc-3P-RGD(2).* Theranostics, 2012. **2**(6): p. 577-588.
273. Bates, S.M., et al., *Imaging characteristics of a novel technetium Tc 99m–labeled platelet glycoprotein IIb/IIIa receptor antagonist in patients with acute deep vein thrombosis or a history of deep vein thrombosis.* Archives of internal medicine, 2003. **163**(4): p. 452-456.
274. Brouwers, F.M., et al., *Evaluation of Tc-99m–Labeled Glycoprotein IIb/IIIa Receptor Antagonist DMP444 SPECT in Patients with Infective Endocarditis.* Clinical nuclear medicine, 2003. **28**(6): p. 480-484.
275. Lister-James, J., et al., *Thrombus imaging with a technetium-99m-labeled, activated platelet receptor-binding peptide.* Journal of Nuclear Medicine, 1996. **37**(5): p. 775-780.
276. Sakuma, T., et al., *Simultaneous integrin αvβ3 and glycoprotein IIb/IIIa inhibition causes reduction in infarct size in a model of acute coronary thrombosis and primary angioplasty.* Cardiovascular research, 2005. **66**(3): p. 552-561.
277. Taillefer, R., et al., *Comparison of early and delayed scintigraphy with (99m Tc)-apcitide and correlation with contrast-enhanced venography in detection of acute deep vein thrombosis.* The Journal of Nuclear Medicine, 1999. **40**(12): p. 2029.
278. Fang, W., et al., *Evaluation of 99mTc-labeled cyclic RGD peptide with a PEG4 linker for thrombosis imaging: comparison with DMP444.* Bioconjugate chemistry, 2011. **22**(8): p. 1715-1722.
279. Aruva, M.R., et al., *Imaging thromboembolism with fibrin-avid 99mTc-peptide: evaluation in swine.* Journal of nuclear medicine : official publication, Society of Nuclear Medicine, 2006. **47**(1): p. 155-162.
280. Saha, P., et al., *Leukocytes and the natural history of deep vein thrombosis: current concepts and future directions.* Arteriosclerosis, thrombosis, and vascular biology, 2011. **31**(3): p. 506-512.
281. Muto, P., et al., *Detecting deep venous thrombosis with technetium-99m-labeled synthetic peptide P280.* Journal of Nuclear Medicine, 1995. **36**(8): p. 1384-1391.

282. Bernarducci, M.P., *Radiolabeled peptides: overcoming the challenges of post-surgical patient management of venous thromboembolism.* Surgical technology international, 2004. **12**: p. 50-67.
283. Dunzinger, A., et al., *99m Tc-apcitide scintigraphy in patients with clinically suspected deep venous thrombosis and pulmonary embolism.* European journal of nuclear medicine and molecular imaging, 2008. **35**(11): p. 2082-2087.
284. Taillefer, R., et al., *Acute thromboscintigraphy with (99m) Tc-apcitide: results of the phase 3 multicenter clinical trial comparing 99mTc-apcitide scintigraphy with contrast venography for imaging acute DVT. Multicenter Trial Investigators.* Journal of nuclear medicine: official publication, Society of Nuclear Medicine, 2000. **41**(7): p. 1214-1223.
285. Davison, J.M., et al., *A novel diagnostic method for acute pulmonary embolism: technetium-99m apcitide scintigraphy.* Annals of internal medicine, 2004. **140**(11): p. 936-939.
286. Mousa, S.A., et al., *Novel technetium-99m-labeled platelet GPIIb/IIIa receptor antagonists as potential imaging agents for venous and arterial thrombosis.* Coronary artery disease, 1998. **9**(2): p. 131-141.
287. Scharn, D.M., et al., *Assessment of prosthetic vascular graft thrombogenicity using the technetium-99m labeled glycoprotein IIb/IIIa receptor antagonist DMP444 in a dog model.* Cardiovascular surgery, 2002. **10**(6): p. 566-569.
288. Knight, L.C., A.H. Maurer, and J.E. Romano, *Comparison of iodine-123-disintegrins for imaging thrombi and emboli in a canine model.* Journal of Nuclear Medicine, 1996. **37**(3): p. 476-481.
289. Knight, L.C., et al., *Imaging pulmonary emboli and deep venous thrombi with 99mTc-bitistatin, a platelet-binding polypeptide from viper venom.* The Journal of Nuclear Medicine, 2000. **41**(6): p. 1056.
290. Knight, L.C., et al., *Platelet binding and biodistribution of [99mTc]rBitistatin in animal species and humans.* Nuclear medicine and biology, 2007. **34**(7): p. 855-863.
291. Aoki, N., *Hemostasis associated with abnormalities of fibrinolysis.* Blood Reviews, 1989. **3**(1): p. 11-17.
292. Husted, S., et al., *Deep vein thrombosis detection by 99mTc-plasmin test and phlebography.* British journal of surgery, 1984. **71**(1): p. 65-66.
293. Lagerstedt, C., et al., *99m Tc plasmin in 394 consecutive patients with suspected deep venous thrombosis.* European Journal of Nuclear Medicine, 1989. **15**(12): p. 771-775.
294. Dahl, O.E., et al., *99mTc-plasmin uptake test is unreliable for diagnosing asymptomatic deep vein thrombosis after hip replacement surgery.* Thrombosis research, 1991. **62**(6): p. 781-784.
295. Christensen, S.W., et al., *Contact thermography, 99mTc-plasmin scintimetry and 99mTc-plasmin scintigraphy as screening methods for deep venous thrombosis following major hip surgery.* Thrombosis and haemostasis, 1987. **57**(03): p. 831-833.
296. Aronen, H., et al., *99m Tc-plasmin test in deep vein thrombosis of the leg.* European Journal of Nuclear Medicine, 1985. **10**(1-2): p. 10-12.
297. Dahlborn, M., et al., *Gamma camera detection of 99m TC-plasmin in the diagnosis of deep-vein thrombosis.* European Journal of Nuclear Medicine, 1984. **9**(11): p. 499-501.
298. Harwig, S., et al., *Radioiodinated plasminogen: an imaging agent for pre-existing thrombi.* Journal of nuclear medicine: official publication, Society of Nuclear Medicine, 1977. **18**(1): p. 42-45.
299. Butler, S.P., et al., *Technetium-99m-modified recombinant tissue plasminogen activator to detect deep venous thrombosis.* Journal of Nuclear Medicine, 1996. **37**(5): p. 744-748.
300. Brighton, T., J. Janssen, and S.P. Butler, *Aging of acute deep vein thrombosis measured by radiolabeled 99mTc-rt-PA.* Journal of Nuclear Medicine, 2007. **48**(6): p. 873-878.

301. Scheraga, H.A. and M. Laskowski Jr, *The fibrinogen-fibrin conversion*, in *Advances in protein chemistry*1957, Elsevier. p. 1-131.
302. Selmayr, E., I. Mahn, and G. Müller-Berghaus, *Crosslinking of soluble fibrin and fibrinogen.* Thrombosis research, 1985. **39**(4): p. 467-474.
303. Wolberg, A.S., *Determinants of fibrin formation, structure, and function.* Current opinion in hematology, 2012. **19**(5): p. 349-356.
304. Mosesson, M., *Fibrinogen and fibrin structure and functions.* Journal of thrombosis and haemostasis, 2005. **3**(8): p. 1894-1904.
305. Fraser, S.R., N.A. Booth, and N.J. Mutch, *The antifibrinolytic function of factor XIII is exclusively expressed through α2-antiplasmin cross-linking.* Blood, 2011. **117**(23): p. 6371-6374.
306. Walker, J.B. and L. Bajzar, *The intrinsic threshold of the fibrinolytic system is modulated by basic carboxypeptidases, but the magnitude of the antifibrinolytic effect of activated thrombin-activable fibrinolysis inhibitor is masked by its instability.* Journal of Biological Chemistry, 2004. **279**(27): p. 27896-27904.
307. Camiolo, S.M., S. Thorsen, and T. Astrup, *Fibrinogenolysis and fibrinolysis with tissue plasminogen activator, urokinase, streptokinase-activated human globulin, and plasmin.* Proceedings of the Society for Experimental Biology and Medicine, 1971. **138**(1): p. 277-280.
308. Lensing, A.W. and J. Hirsh, *125I-fibrinogen leg scanning: reassessment of its role for the diagnosis of venous thrombosis in post-operative patients.* Thrombosis and haemostasis, 1993. **69**(01): p. 002-007.
309. Kakkar, V., et al., *125I-labelled fibrinogen test adapted for routine screening for deep-vein thrombosis.* The Lancet, 1970. **295**(7646): p. 540-542.
310. Browse, N., *The 125 I fibrinogen uptake test.* Archives of surgery (Chicago, Ill.: 1960), 1972. **104**(2): p. 160.
311. Perrier, A., *Labeling the thrombus: the future of nuclear medicine for venous thromboembolism?*, 2004, American Thoracic Society.
312. Schaible, T.F. and A. Alavi. *Antifibrin scintigraphy in the diagnostic evaluation of acute deep venous thrombosis*. in *Semin Nucl Med*. 1991. Elsevier.
313. Laudano, A.P. and R.F. Doolittle, *Synthetic peptide derivatives that bind to fibrinogen and prevent the polymerization of fibrin monomers.* Proceedings of the National Academy of Sciences, 1978. **75**(7): p. 3085-3089.
314. KAWASAKI, K., et al., *Amino acids and peptides. XVIII. Synthetic peptides related to N-terminal portion of fibrin α-chain and their inhibitory effect on fibrinogen/thrombin clotting.* Chemical and pharmaceutical bulletin, 1993. **41**(5): p. 975-977.
315. Thakur, M.L., et al., *Imaging Vascular Thrombosis with 99mTc@ Labeled.* J Nucl Med, 2000. **41**: p. 161-168.
316. Aruva, M.R., et al., *Imaging thromboembolism with fibrin-avid 99mTc-peptide: evaluation in swine.* Journal of Nuclear Medicine, 2006. **47**(1): p. 155-162.
317. Macfarlane, D., et al., *Imaging of deep venous thrombosis in patients using a radiolabelled anti-D-dimer Fab' fragment (99m Tc-DI-DD3B6/22-80B3): Results of a phase I trial.* European journal of nuclear medicine and molecular imaging, 2009. **36**(2): p. 250-259.
318. Hui, K.Y., E. Haber, and G.R. Matsueda, *Monoclonal antibodies to a synthetic fibrin-like peptide bind to human fibrin but not fibrinogen.* Science, 1983. **222**(4628): p. 1129-1132.
319. Rylatt, D., et al., *An immunoassay for human D dimer using monoclonal antibodies.* Thrombosis research, 1983. **31**(6): p. 767-778.

320. Walker, K., et al., *Preclinical evaluation of 99mtechnetium-labeled DD-3B6/22 FAB'for thrombus detection.* Thrombosis research, 1991. **64**(6): p. 691-701.
321. Hara, T., et al., *Molecular imaging of fibrin deposition in deep vein thrombosis using fibrin-targeted near-infrared fluorescence.* JACC: Cardiovascular Imaging, 2012. **5**(6): p. 607-615.
322. Morris, T.A., et al., *Single photon emission computed tomography of pulmonary emboli and venous thrombi using anti–D-Dimer.* American journal of respiratory and critical care medicine, 2004. **169**(9): p. 987-993.
323. Morris, T.A., et al., *Improved imaging of deep venous thrombi during anticoagulation using radiolabelled anti-D-dimer antibodies.* Nuclear medicine communications, 2004. **25**(9): p. 917-922.
324. Morris, T.A., et al., *Antibodies against the fibrin β-chain amino-terminus detect active canine venous thrombi.* Circulation, 1997. **96**(9): p. 3173-3179.
325. Douketis, J.D., et al., *Accuracy and safety of 99mTc-labeled anti-D-dimer (DI-80B3) Fab'fragments (ThromboView®) in the diagnosis of deep vein thrombosis: A phase II study.* Thrombosis research, 2012. **130**(3): p. 381-389.
326. Taillefer, R. *Radiolabeled peptides in the detection of deep venous thrombosis*. in *Semin Nucl Med*. 2001. Elsevier.
327. Rosenthall, L. and J. Leclerc, *A new thrombus imaging agent. Human recombinant fibrin binding domain labeled with In-111.* Clinical nuclear medicine, 1995. **20**(5): p. 398-402.
328. Cerqueira, M.D. *Current status of radionuclide tracer imaging of thrombi and atheroma*. in *Semin Nucl Med*. 1999. Elsevier.
329. Tung, C.H., et al., *Novel factor XIII probes for blood coagulation imaging.* Chembiochem, 2003. **4**(9): p. 897-899.
330. McCarthy, J.R., *Nanomedicine and cardiovascular disease.* Current cardiovascular imaging reports, 2010. **3**(1): p. 42-49.
331. McCarthy, J.R., et al., *Multimodal nanoagents for the detection of intravascular thrombi.* Bioconjugate chemistry, 2009. **20**(6): p. 1251-1255.
332. Edwards, D., et al., *99mTc-NC100668, a new tracer for imaging venous thromboemboli: pre-clinical biodistribution and incorporation into plasma clots in vivo and in vitro.* Eur J Nucl Med Mol Imaging, 2006. **33**(11): p. 1258-1265.
333. Badimon, J.J. and V. Fuster, *Can we image the "active" thrombus?*, 2002, Am Heart Assoc.
334. Edwards, D., et al., *(99m)Tc-NC100668, a new tracer for imaging venous thromboemboli: pre-clinical biodistribution and incorporation into plasma clots in vivo and in vitro.* Eur J Nucl Med Mol Imaging, 2006. **33**(11): p. 1258-65.
335. Toft, K.G., et al., *NC100668, a new tracer tested for imaging of venous thromboembolism: pharmacokinetics and metabolism in humans.* Drug Metab Dispos, 2007. **35**(11): p. 1979-84.
336. Edwards, D., et al., *The in vivo and in vitro metabolic profile of 99mTc-NC100668, a new tracer for imaging venous thromboembolism: identification and biodistribution of the principal radiolabeled metabolite.* Drug Metab Dispos, 2006. **34**(7): p. 1128-35.
337. Starmans, L.W., et al., *Evaluation of 111In-labeled EPep and FibPep as tracers for fibrin SPECT imaging.* Molecular Pharmaceutics, 2013. **10**(11): p. 4309-4321.
338. Ciesienski, K.L., et al., *Fibrin-targeted PET probes for the detection of thrombi.* Molecular Pharmaceutics, 2013. **10**(3): p. 1100-1110.
339. Spuentrup, E., et al., *MR imaging of thrombi using EP-2104R, a fibrin-specific contrast agent: initial results in patients.* European radiology, 2008. **18**(9): p. 1995-2005.

340. Kudryk, B., et al., *Specificity of a monoclonal antibody for the NH2-terminal region of fibrin.* Molecular immunology, 1984. **21**(1): p. 89-94.
341. Rosebrough, S., et al., *Radioimmunoimaging of venous thrombi using iodine-131 monoclonal antibody.* Radiology, 1985. **156**(2): p. 515-517.
342. Alavi, A., et al., *Detection of thrombophlebitis with 111In-labeled anti-fibrin antibody: preliminary results.* Cancer research, 1990. **50**(3 Supplement): p. 958s-961s.
343. Alavi, A., et al., *Radiolabeled antifibrin antibody in the detection of venous thrombosis: preliminary results.* Radiology, 1990. **175**(1): p. 79-85.
344. De Faucal, P., et al., *Evaluation of indium-111-labeled antifibrin monoclonal antibody for the diagnosis of venous thrombotic disease.* Journal of Nuclear Medicine, 1991. **32**(5): p. 785-791.
345. Jung, M., et al., *Deep vein thrombosis: scintigraphic diagnosis with In-111-labeled monoclonal antifibrin antibodies.* Radiology, 1989. **173**(2): p. 469-475.
346. Lusiani, L., et al., *Immunoscintigraphic detection of venous thrombosis of the lower extremities by means of human antifibrin monoclonal antibodies labeled with 111In.* Angiology, 1989. **40**(7): p. 671-677.
347. Rosebrough, S.F., et al., *Thrombus imaging: a comparison of radiolabeled GC4 and T2G1s fibrin-specific monoclonal antibodies.* Journal of nuclear medicine: official publication, Society of Nuclear Medicine, 1990. **31**(6): p. 1048.
348. Kanke, M., et al., *Localization and visualization of pulmonary emboli with radiolabeled fibrin-specific monoclonal antibody.* Journal of Nuclear Medicine, 1991. **32**(6): p. 1254-1260.
349. Bautovich, G., et al., *Detection of deep venous thrombi and pulmonary embolus with technetium-99m-DD-3B6/22 anti-fibrin monoclonal antibody Fab' fragment.* Journal of Nuclear Medicine, 1994. **35**(2): p. 195-202.
350. Botnar, R.M., et al., *In vivo molecular imaging of acute and subacute thrombosis using a fibrin-binding magnetic resonance imaging contrast agent.* Circulation, 2004. **109**(16): p. 2023-2029.
351. Vymazal, J., et al., *Thrombus imaging with fibrin-specific gadolinium-based MR contrast agent EP-2104R: results of a phase II clinical study of feasibility.* Investigative radiology, 2009. **44**(11): p. 697-704.
352. Spuentrup, E., et al., *Molecular magnetic resonance imaging of coronary thrombosis and pulmonary emboli with a novel fibrin-targeted contrast agent.* Circulation, 2005. **111**(11): p. 1377-1382.
353. Sirol, M., et al., *Fibrin-targeted contrast agent for improvement of in vivo acute thrombus detection with magnetic resonance imaging.* Atherosclerosis, 2005. **182**(1): p. 79-85.
354. Starmans, L.W., et al., *SPECT imaging of fibrin using fibrin-binding peptides.* Contrast media & molecular imaging, 2013. **8**(3): p. 229-237.
355. Uppal, R., et al., *Bimodal thrombus imaging: simultaneous PET/MR imaging with a fibrin-targeted dual PET/MR probe—feasibility study in rat model.* Radiology, 2011. **258**(3): p. 812-820.
356. Blasi, F., et al., *Multisite thrombus imaging and fibrin content estimation with a single whole-body PET scan in rats.* Arteriosclerosis, thrombosis, and vascular biology, 2015. **35**(10): p. 2114-2121.
357. Blasi, F., et al., *Radiation dosimetry of the fibrin-binding probe 64Cu-FBP8 and its feasibility for PET imaging of deep vein thrombosis and pulmonary embolism in rats.* Journal of Nuclear Medicine, 2015. **56**(7): p. 1088-1093.
358. Ay, I., et al., *In vivo molecular imaging of thrombosis and thrombolysis using a fibrin-binding positron emission tomographic probe.* Circulation: Cardiovascular Imaging, 2014. **7**(4): p. 697-705.

359. Rondina, M.T., et al., *18F-FDG PET in the evaluation of acuity of deep vein thrombosis.* Clinical nuclear medicine, 2012. **37**(12): p. 1139.
360. Hess, S., et al., *Potential role of FDG PET/CT imaging for assessing venous thromboembolic disorders.* Clinical nuclear medicine, 2012. **37**(12): p. 1170-1172.
361. Xu, J., et al., *EWVDV-Mediated Platelet-Targeting Nanoparticles for the Multimodal Imaging of Thrombi at Different Blood Flow Velocities.* International Journal of Nanomedicine, 2020. **15**: p. 1759.
362. Kwon, S.-P., et al., *Thrombin-activatable fluorescent peptide incorporated gold nanoparticles for dual optical/computed tomography thrombus imaging.* Biomaterials, 2018. **150**: p. 125-136.
363. Zhang, R., et al., *alphaVbeta3-targeted copper nanoparticles incorporating an Sn 2 lipase-labile fumagillin prodrug for photoacoustic neovascular imaging and treatment.* Theranostics, 2015. **5**(2): p. 124-133.
364. Kim, J.-Y., et al., *Direct Imaging of Cerebral Thromboemboli Using Computed Tomography and Fibrin-targeted Gold Nanoparticles.* Theranostics, 2015. **5**(10): p. 1098-1114.
365. Page, M.J., et al., *Non-invasive imaging and cellular tracking of pulmonary emboli by near-infrared fluorescence and positron-emission tomography.* Nat Commun, 2015. **6**: p. 8448.
366. Hess, S., et al., *Efficacy of FDG PET/CT imaging for venous thromboembolic disorders: preliminary results from a prospective, observational pilot study.* Clinical nuclear medicine, 2015. **40**(1): p. e23-e26.
367. Kutscher, H.L., et al., *Threshold size for optimal passive pulmonary targeting and retention of rigid microparticles in rats.* Journal of Controlled Release, 2010. **143**(1): p. 31-37.
368. Cuénoud, H.F., I. Joris, and G. Majno, *Ultrastructure of the myocardium after pulmonary embolism. A study in the rat.* The American journal of pathology, 1978. **92**(2): p. 421-458.
369. Jones, A.E., et al., *Inhibition of prostaglandin synthesis during polystyrene microsphere-induced pulmonary embolism in the rat.* American Journal of Physiology-Lung Cellular and Molecular Physiology, 2003. **284**(6): p. L1072-L1081.
370. Haynie, T.P., et al., *Visualization of pulmonary artery occlusion by photoscanning.* JAMA, 1963. **185**(4): p. 306-308.
371. Fanali, G., et al., *Human serum albumin: from bench to bedside.* Molecular aspects of medicine, 2012. **33**(3): p. 209-290.
372. Swanson, D.P., H.M. Chilton, and J.H. Thrall, *Pharmaceuticals in medical imaging: radiopaque contrast media, radiopharmaceuticals, enhancement agents for magnetic resonance imaging and ultrasound*1990: McGraw-Hill.
373. Mather, S., *Adverse reaction to lung-scanning agent.* The Lancet, 1977. **309**(8017): p. 907-908.
374. Cohen, S., et al., *Distribution and elimination of 131I-and 14C-labelled plasma proteins in the rabbit.* Biochemical Journal, 1956. **62**(1): p. 143.
375. Bennhold, H. and E. Kallee, *Comparative studies on the half-life of I 131-labeled albumins and nonradioactive human serum albumin in a case of analbuminemia.* The Journal of clinical investigation, 1959. **38**(5): p. 863-872.
376. Willmott, N., et al., *Biodegradation rate of embolized protein microspheres in lung, liver and kidney of rats.* Journal of pharmacy and pharmacology, 1989. **41**(7): p. 433-438.
377. Taplin, G., et al., *Suspensions of radioalbumin aggregates for photoscanning the liver, spleen, lung and other organs.* Journal of Nuclear Medicine, 1964. **5**(4): p. 259-275.
378. Dworkin, H.J., et al., *Lung scanning with colloidal RISA.* Journal of Nuclear Medicine, 1964. **5**(1): p. 48-57.

379. Zolle, I., B. Rhodes, and H. Wagner Jr, *Preparation of metabolizable radioactive human serum albumin microspheres for studies of the circulation.* The International journal of applied radiation and isotopes, 1970. **21**(3): p. 155-156.
380. Benisek, W.F. and F.M. Richards, *Attachment of Metal-chelating Functional Groups to Hen Egg White Lysozyme AN APPROACH TO INTRODUCING HEAVY ATOMS INTO PROTEIN CRYSTALS.* Journal of Biological Chemistry, 1968. **243**(16): p. 4267-4271.
381. Sundberg, M.W., et al., *Selective binding of metal ions to macromolecules using bifunctional analogs of EDTA.* Journal of medicinal chemistry, 1974. **17**(12): p. 1304-1307.
382. Chesler, D., et al., *Three-dimensional reconstruction of lung perfusion image with positron detection.* Journal of Nuclear Medicine, 1975. **16**(1): p. 80-82.
383. Krejcarek, G.E. and K.L. Tucker, *Covalent attachment of chelating groups to macromolecules.* Biochemical and biophysical research communications, 1977. **77**(2): p. 581-585.
384. Wagner, S.J. and M.J. Welch, *Gallium-68 labeling of albumin and albumin microspheres.* Journal of nuclear medicine: official publication, Society of Nuclear Medicine, 1979. **20**(5): p. 428-433.
385. Carlton, J. and R. Hayes, *Rapid separation of generator-produced gallium-68 from EDTA eluate.* The International journal of applied radiation and isotopes, 1971. **22**(1): p. 44-45.
386. Hnatowich, D.J., *A method for the preparation and quality control of 68Ga radiopharmaceuticals.* Journal of nuclear medicine: official publication, Society of Nuclear Medicine, 1975. **16**(8): p. 764-768.
387. Yvert, J., et al., *Simple, fast preparation of gallium-68-labelled human serum albumin microspheres.* European Journal of Nuclear Medicine, 1979. **4**(2): p. 95-99.
388. Quinn, J.L., et al., *An approach to the scanning of pulmonary infarcts.* Journal of Nuclear Medicine, 1964. **5**(1): p. 1-8.
389. Rhodes, B.A., et al., *Lung scanning with 99mTc-microspheres.* Radiology, 1971. **99**(3): p. 613-621.
390. Gerken, G., et al., *Virus-associated receptors for polymerized human serum albumin (RpHSA) in patients with chronic active hepatitis B treated with recombinant leukocyte A interferon.* Digestion, 1987. **37**(2): p. 96-102.
391. Hawe, A. and W. Friess, *Stabilization of a hydrophobic recombinant cytokine by human serum albumin.* J Pharm Sci, 2007. **96**(11): p. 2987-2999.
392. Benacerraf, B., et al., *A study of phagocytic activity of the reticuloendothelial system toward heat denatured human serum albumin tagged with I131.* Res Bull, 1956. **2**: p. 19.
393. Quinn III, J.L., et al., *Early clinical applications of lung scintiscanning.* Radiology, 1964. **82**(2): p. 315-317.
394. Wagner, H.N., et al., *Regional pulmonary blood flow in man by radioisotope scanning.* JAMA, 1964. **187**(8): p. 601-603.
395. Takeda, Y., *Metabolism and distribution of autologous and homologous albumin-I 131 in the dog.* American Journal of Physiology--Legacy Content, 1964. **206**(6): p. 1223-1228.
396. Taplin, G., et al., *Lung photoscans with macroaggregates of human serum radioalbumin: Experimental basis and initial clinical trials.* Health physics, 1964. **10**(12): p. 1219-1227.
397. TAPLIN, G. and D. JOHNSON, *DORE EK, Ct al: Gastric photoscans with colloidal aggregates of radioalbumin. I*, 1963, NuclMed4.
398. Taplin, G.V. and N.S. MacDonald. *Radiochemistry of macroaggregated albumin and newer lung scanning agents*. in *Semin Nucl Med*. 1971. Elsevier.
399. Gwyther, M.M. and E. Field, *Aggregated Tc99m-labelled albumin for lung scintiscanning.* The International journal of applied radiation and isotopes, 1966. **17**(8): p. 485-486.

400. Peterson, C. and F. Bonte, *Technetium-99m macroaggregated albumin: A new lung scanning agent.* The International journal of applied radiation and isotopes, 1967. **18**(3): p. 201-202.
401. Surprenant, E., M. Webber, and L. Bennett, *Technetium lung scanning.* The International journal of applied radiation and isotopes, 1969. **20**(1): p. 77IN179-78IN8.
402. Cragin, M.D., et al., *Technique for the rapid preparation of lung scan particles using 99mTc-sulfur and human serum albumin.* Journal of Nuclear Medicine, 1969. **10**(10): p. 621-623.
403. Deutsch, M. and M. Redmond. *UNITARY FREEZE-DRIED KITS FOR PREPARATION OF TECHNETIUM-LABELED HUMAN SERUM-ALBUMIN*. in *Journal of Nuclear Medicine*. 1972. SOC NUCLEAR MEDICINE INC 1850 SAMUEL MORSE DR, RESTON, VA 20190-5316.
404. Al-Janabi, M.A.A., et al., *A new technique for the preparation of ready-to-use macroaggregated albumin (MAA) kits to be labelled with 99mTc for lung scanning.* The International journal of applied radiation and isotopes, 1983. **34**(10): p. 1473-1478.
405. Lowes, M. and F. Gydesen, *Clinical Evaluation of a New 99mTc-MAA Kit for Lung Scanning.* J Nucl Med Technol, 1973. **1**(2): p. 14-17.
406. Robbins, P., D. Fortman, and J. Lewis. *KIT FOR RAPID PREPARATION OF TC-99M MACROAGGREGATED ALBUMIN*. in *Journal of Nuclear Medicine*. 1972. SOC NUCLEAR MEDICINE INC 1850 SAMUEL MORSE DR, RESTON, VA 20190-5316.
407. Lyster, D., et al., *Preparation of a 99mTc-Sn-MAA kit for use in nuclear medicine.* Journal of Nuclear Medicine, 1974. **15**(3): p. 198-199.
408. Hunt, A., et al., *Preparation of Tc-99m-macroaggregated albumin from recombinant human albumin for lung perfusion imaging.* European journal of pharmaceutics and biopharmaceutics, 2006. **62**(1): p. 26-31.
409. Mathias, C.J. and M.A. Green, *A Convenient Route to [(68)Ga]Ga-MAA for Use as a Particulate PET Perfusion Tracer.* Appl Radiat Isot, 2008. **66**(12): p. 1910-1912.
410. Amor-Coarasa, A., et al., *-NOTA-CHSg and-CHSg Labeled Microspheres for Lung Perfusion and Liver Radiomicrospheres Therapy Planning.* Int J Mol Imaging, 2013. **2013**.
411. Amor-Coarasa, A., et al., *Lyophilized kit for the preparation of the PET perfusion agent [68Ga]-MAA.* Int J Mol Imaging, 2014. **2014**.
412. Grosser, O.S., et al., *Pharmacokinetics of 99mTc-MAA-and 99mTc-HSA-Microspheres Used in Preradioembolization Dosimetry: Influence on the Liver–Lung Shunt.* Journal of Nuclear Medicine, 2016. **57**(6): p. 925-927.
413. Whinnery, J.E. and J.T. Young, *Granulomatous interstitial pneumonia in a miniature swine associated with repeated intravenous injections of Tc-99m human serum albumin: concise communication.* Journal of nuclear medicine: official publication, Society of Nuclear Medicine, 1980. **21**(3): p. 207-210.
414. Arfors, K., et al., *Temporary intestinal hypoxia induced by degradable microspheres.* Nature, 1976. **262**(5568): p. 500.
415. Sato, H., et al., *Pharmacokinetic study of taxol-loaded poly (lactic-co-glycolic acid) microspheres containing isopropyl myristate after targeted delivery to the lung in mice.* Biological and Pharmaceutical Bulletin, 1996. **19**(12): p. 1596-1601.
416. Zhang, M., et al., *The distribution and pharmacokinetics in lung of bovine serum albumin microspheres for pulmonary targeting in mice.* Hua xi yi ke da xue xue bao= Journal of West China University of Medical Sciences= Huaxi Yike Daxue Xuebao, 1994. **25**(4): p. 393-397.
417. Wang, J., et al., *Studies on lung targeting gelatin microspheres of mitoxantrone.* Yao xue xue bao= Acta pharmaceutica Sinica, 1995. **30**(7): p. 549-555.

418. Gref, R., et al., *Biodegradable long-circulating polymeric nanospheres.* Science, 1994. **263**(5153): p. 1600-1603.
419. Chen, X., et al., *Preparation of lung-targeting, emodin-loaded polylactic acid microspheres and their properties.* International Journal of Molecular Sciences, 2014. **15**(4): p. 6241-6251.
420. Dorta, M., O. Munguia, and M. Llabres, *Effects of polymerization variables on PLGA properties: molecular weight, composition and chain structure.* Int J Pharm, 1993. **100**(1-3): p. 9-14.
421. Garcia, J., *Comparative degradation study of biodegradable microspheres of poly (DL-lactide-co-glycolide) with poly (ethyleneglycol) derivates.* Journal of microencapsulation, 1999. **16**(1): p. 83-94.
422. Delgado, A., et al., *Radiolabelled biodegradable microspheres for lung imaging.* European journal of pharmaceutics and biopharmaceutics, 2000. **50**(2): p. 227-236.
423. Häfeli, U.O., et al., *Lung perfusion imaging with monosized biodegradable microspheres.* Biomacromolecules, 2010. **11**(3): p. 561-567.
424. Tsopelas, C., F. Dylan, and L. Bartholomeusz, *A potential lung perfusion imaging agent of synthetic origin.* Journal of Labelled Compounds and Radiopharmaceuticals, 2006. **49**(4): p. 367-375.
425. Tsopelas, C., *A study of radiogallium aqueous chemistry: in vitro and in vivo characterisation of 67Ga-hydrolysed-stannous fluoride particles.* Journal of Labelled Compounds and Radiopharmaceuticals, 2016. **59**(5): p. 197-204.
426. Fleer, R., et al., *Stable Multicopy Vectors for High–Level Secretion of Recombinant Human Serum Albumin by Kluyveromyces Yeasts.* Bio/Technology, 1991. **9**: p. 968.
427. Lodhi, N.A., et al., *Development of 99mTc-Labeled Human Serum Albumin with Prolonged Circulation by Chelate-then-Click Approach: A Potential Blood Pool Imaging Agent.* Molecular Pharmaceutics, 2019. **16**(4): p. 1586-1595.
428. Miroslavov, A.E., et al., *Evaluation of 99m Tc (CO) 5 I as a potential lung perfusion agent.* Nucl Med Biol, 2009. **36**(1): p. 73-79.
429. Lacoeuille, F., et al., *New starch-based radiotracer for lung perfusion scintigraphy.* Eur J Nucl Med Mol Imaging, 2010. **37**(1): p. 146.
430. Pimentel, G. and E. Estevez, *Calcium phytate: A promising lung perfusion agent without risk of biological contamination*, 2005.
431. Hsieh, W., et al., *(68) Ga-Ca-phytate particles: A potential lung perfusion agent of synthetic origin prepared in a cold kit format.* J Labelled Comp Radiopharm, 2016. **59**(12): p. 506-516.
432. Oettl, K. and R. Stauber, *Physiological and pathological changes in the redox state of human serum albumin critically influence its binding properties.* Br J Pharmacol, 2007. **151**(5): p. 580-590.
433. Ferrer-Miralles, N., et al., *Microbial factories for recombinant pharmaceuticals.* Microb Cell Fact, 2009. **8**(1): p. 17.
434. Lawn, R.M., et al., *The sequence of human serum albumin cDNA and its expression in E. coli.* Nucleic acids research, 1981. **9**(22): p. 6103-6114.
435. Salinas, G., et al., *Tuned Escherichia coli as a host for the expression of disulfide-rich proteins.* Biotechnology Journal, 2011. **6**(6): p. 686-699.
436. Sharma, A. and T.K. Chaudhuri, *Revisiting Escherichia coli as microbial factory for enhanced production of human serum albumin.* Microbial Cell Factories, 2017. **16**(1): p. 173.
437. Bushell, M., et al., *Cyclic fed-batch culture for production of human serum albumin in Pichia pastoris.* Biotechnology and bioengineering, 2003. **82**(6): p. 678-683.

438. Li, B., et al., *A novel protein expression system-PichiaPink™-and a protocol for fast and efficient recombinant protein expression.* African Journal of Biotechnology, 2011. **10**(83): p. 19464-19472.
439. Millán, F.S., et al., *A chloroplast transgenic approach to hyper-express and purify Human Serum Albumin, a protein highly susceptible to proteolytic degradation.* Plant Biotechnology Journal, 2003. **1**(2): p. 71-79.
440. Sun, Q.-Y., et al., *Improved expression and purification of recombinant human serum albumin from transgenic tobacco suspension culture.* Journal of biotechnology, 2011. **155**(2): p. 164-172.
441. Lau, O.S. and S.S. Sun, *Plant seeds as bioreactors for recombinant protein production.* Biotechnology advances, 2009. **27**(6): p. 1015-1022.
442. He, Y., et al., *Large-scale production of functional human serum albumin from transgenic rice seeds.* Proceedings of the National Academy of Sciences of the United States of America, 2011. **108**(47): p. 19078-19083.
443. Wu, X., et al., *The extremely high level expression of human serum albumin in the milk of transgenic mice.* Transgenic research, 2012. **21**(6): p. 1359-1366.
444. Shani, M., et al., *Expression of human serum albumin in the milk of transgenic mice.* Transgenic research, 1992. **1**(5): p. 195-208.
445. Barash, I., et al., *Synthesis and secretion of human serum albumin by mammary gland explants of virgin and lactating transgenic mice.* Transgenic research, 1993. **2**(5): p. 266-276.
446. LATTA, M., et al., *Tryptophan promoter derivatives on multicopy plasmids: a comparative analysis of expression potentials in Escherichia coli.* DNA and cell biology, 1990. **9**(2): p. 129-137.
447. Saunders, C.W., et al., *Secretion of human serum albumin from Bacillus subtilis.* Journal of bacteriology, 1987. **169**(7): p. 2917-2925.
448. Kang, H.-A., et al., *Expression and secretion of human serum albumin in the yeast Saccharomyces cerevisae.* Journal of microbiology and biotechnology, 1998. **8**(1): p. 42-48.
449. Quirk, A.V., et al., *Production of recombinant human serum albumin from Saccharomyces cerevisiae.* Biotechnology and applied biochemistry, 1989. **11**(3): p. 273-287.
450. Belew, M., et al., *Purification of recombinant human serum albumin (rHSA) produced by genetically modified Pichia pastoris.* Separation Science and Technology, 2008. **43**(11-12): p. 3134-3153.
451. Kobayashi, K., et al., *Addition of oleic acid increases expression of recombinant human serum albumin by the AOX2 promoter in Pichia pastoris.* Journal of bioscience and bioengineering, 2000. **89**(5): p. 479-484.
452. Blondeau, K., et al., *Physiological approach to heterologous human serum albumin production by Kluyveromyces lactis in chemostat culture.* Yeast, 1994. **10**(10): p. 1297-1303.
453. Lodi, T., B. Neglia, and C. Donnini, *Secretion of human serum albumin by Kluyveromyces lactis overexpressing KlPDI1 and KlERO1.* Applied and environmental microbiology, 2005. **71**(8): p. 4359-4363.
454. Saliola, M., et al., *Use of the KlADH4 Promoter for Ethanol-Dependent Production of Recombinant Human Serum Albumin inKluyveromyces lactis.* Applied and environmental microbiology, 1999. **65**(1): p. 53-60.
455. Hurwitz, D.R., et al., *Specific combinations of human serum albumin introns direct high level expression of albumin in transfected COS cells and in the milk of transgenic mice.* Transgenic research, 1994. **3**(6): p. 365-375.
456. Barash, I., et al., *In vivo and in vitro expression of human serum albumin genomic sequences in mammary epithelial cells with β-lactoglobulin and whey acidic protein promoters.* Molecular Reproduction and Development: Incorporating Gamete Research, 1999. **52**(3): p. 241-252.

457. Huang, Y., et al., *High expression of human serum albumin in milk of transgenic mice directed by the goat β-casein gene promoter region.* Chinese Science Bulletin, 2001. **46**(7): p. 582-585.
458. Echelard, Y., et al., *Production of recombinant albumin by a herd of cloned transgenic cattle.* Transgenic research, 2009. **18**(3): p. 361-376.
459. Ogawa, S., et al., *Generation of a transgenic silkworm that secretes recombinant proteins in the sericin layer of cocoon: production of recombinant human serum albumin.* Journal of biotechnology, 2007. **128**(3): p. 531-544.
460. Sijmons, P.C., et al., *Production of correctly processed human serum albumin in transgenic plants.* Bio/Technology, 1990. **8**(3): p. 217-221.
461. Farran, I., et al., *Targeted expression of human serum albumin to potato tubers.* Transgenic research, 2002. **11**(4): p. 337-346.
462. Huang, L.-F., et al., *Production of human serum albumin by sugar starvation induced promoter and rice cell culture.* Transgenic research, 2005. **14**(5): p. 569-581.
463. Heo, J.-H., et al., *Properties of the Hansenula polymorpha-derived constitutive GAP promoter, assessed using an HSA reporter gene.* FEMS yeast research, 2003. **4**(2): p. 175-184.
464. Cox, H., et al., *Constitutive expression of recombinant proteins in the methylotrophic yeast Hansenula polymorpha using the PMA1 promoter.* Yeast, 2000. **16**(13): p. 1191-1203.
465. Kang, H.A., et al., *Development of expression systems for the production of recombinant human serum albumin using the MOX promoter in Hansenula polymorpha DL-1.* Biotechnology and bioengineering, 2001. **76**(2): p. 175-185.
466. Kobayashi, K., *Summary of recombinant human serum albumin development.* Biologicals, 2006. **34**(1): p. 55-59.
467. Chuang, V. and M. Otagiri, *Recombinant human serum albumin.* Drugs Today, 2007. **43**(8): p. 547-561.
468. Kobayashi, K., et al., *The development of recombinant human serum albumin.* Therapeutic Apheresis and Dialysis, 1998. **2**(4): p. 257-262.
469. Bosse, D., et al., *Phase I Comparability of Recombinant Human Albumin and Human Serum Albumin.* The Journal of Clinical Pharmacology, 2005. **45**(1): p. 57-67.
470. Bain, V.G., et al., *A phase 2 study to evaluate the antiviral activity, safety, and pharmacokinetics of recombinant human albumin-interferon alfa fusion protein in genotype 1 chronic hepatitis C patients.* J Hepatol, 2006. **44**(4): p. 671-678.
471. Ohnishi, K., et al., *A Comparative Pharmacokinetic Study of Recombinant Human Serum Albumin With Plasma-derived Human Serum Albumin in Patients With Liver Cirrhosis.* The Journal of Clinical Pharmacology, 2008. **48**(2): p. 203-208.
472. Bronchud, M., et al., *Phase I/II study of recombinant human granulocyte colony-stimulating factor in patients receiving intensive chemotherapy for small cell lung cancer.* British journal of cancer, 1987. **56**(6): p. 809-813.
473. Sportès, C., et al., *Phase I study of recombinant human interleukin-7 administration in subjects with refractory malignancy.* Clinical Cancer Research, 2010. **16**(2): p. 727-735.
474. Perkins, A. and M. Frier, *Experimental biodistribution studies of 99m Tc-recombinant human serum albumin (rHSA): a new generation of radiopharmaceutical.* European Journal of Nuclear Medicine, 1994. **21**(11): p. 1231-1233.
475. Lacoeuille, F., et al., *A starch-based microparticulate system dedicated to diagnostic and therapeutic nuclear medicine applications.* Biomaterials, 2011. **32**(31): p. 7999-8009.

476. Verger, E., et al., *68Ga and 188Re Starch-Based Microparticles as Theranostic Tool for the Hepatocellular Carcinoma: Radiolabeling and Preliminary In Vivo Rat Studies.* PLoS One, 2016. **11**(10): p. e0164626.
477. Denizot, B., et al., *Compositions based on polysaccharides grafted by polyamine or polysulphurised compounds*, 2015, Google Patents.
478. Heit, J.A., *The epidemiology of venous thromboembolism in the community.* Arteriosclerosis, thrombosis, and vascular biology, 2008. **28**(3): p. 370-372.
479. Schiff, G.D., et al., *Diagnostic error in medicine: analysis of 583 physician-reported errors.* Archives of internal medicine, 2009. **169**(20): p. 1881-1887.
480. Le Gal, G. and H. Bounameaux, *Diagnosing pulmonary embolism: running after the decreasing prevalence of cases among suspected patients.* Journal of thrombosis and haemostasis, 2004. **2**(8): p. 1244-1246.
481. Lewis, C.A., S.J. Farr, and K.J. Broadley, *Development of a method for monitoring the migration of 111In-labelled eosinophils and neutrophils to the lungs of anaesthetized guinea pigs by gamma scintigraphy and bronchoalveolar lavage.* Journal of immunological methods, 1996. **190**(1): p. 51-60.
482. Hunt, A.P., et al., *Preparation of Tc-99m-macroaggregated albumin from recombinant human albumin for lung perfusion imaging.* Eur J Pharm Biopharm, 2006. **62**(1): p. 26-31.
483. Bolch, W.E., et al., *MIRD pamphlet no. 21: a generalized schema for radiopharmaceutical dosimetry—standardization of nomenclature.* Journal of Nuclear Medicine, 2009. **50**(3): p. 477-484.
484. Stabin, M.G. and J.A. Siegel, *Physical models and dose factors for use in internal dose assessment.* Health physics, 2003. **85**(3): p. 294-310.
485. Snyder, W., *" S" Absorbed Dose Per Unit Cumulated Activity for Selected Radionuclides and Organs.* MIRD Pamphlet no. 11, 1975.
486. Valentin, J., *The 2007 recommendations of the international commission on radiological protection. ICRP publication 103.* Ann iCRP, 2007. **37**(2): p. 1-332.
487. Lamesa, C., et al., *68Ga somatostatin analog radiolabelling: The radiopharmacist's point of view.* Médecine Nucléaire, 2015. **39**(1): p. 3-10.
488. Medicines, E.D.f.t.Q.o., *European pharmacopoeia 5th edition: supplement 5.2.* Strasbourg: Council of Europe, 2005.
489. Sparks, R. and B. Aydogan, *Comparison of the effectiveness of some common animal data scaling techniques in estimating human radiation dose*, 1999, Oak Ridge Associated Universities, TN (United States).
490. Valentin, J., *Radiation dose to patients from radiopharmaceuticals:(Addendum 2 to ICRP Publication 53) ICRP Publication 80 Approved by the Commission in September 1997.* Annals of the ICRP, 1998. **28**(3): p. 1-1.
491. Satin, M., *Functional properties of starches.* FAO report, 1998.
492. Zobel, H., *Molecules to granules: a comprehensive starch review.* Starch-Stärke, 1988. **40**(2): p. 44-50.
493. Davis, M., *Particulate radiopharmaceuticals for pulmonary studies*, in *Radiopharmaceuticals*1975.
494. Commission, E.P., E.D.f.t.Q.o. Medicines, and Healthcare, *European pharmacopoeia*. Vol. 1. 2010: Council of Europe.
495. Spang, P., C. Herrmann, and F. Roesch. *Bifunctional gallium-68 chelators: Past, present, and future*. in *Semin Nucl Med*. 2016. Elsevier.

496. Burke, B.P., G.S. Clemente, and S.J. Archibald, *Recent advances in chelator design and labelling methodology for 68Ga radiopharmaceuticals.* Journal of Labelled Compounds and Radiopharmaceuticals, 2014. **57**(4): p. 239-243.
497. Greenman, J., T.W. Price, and G.J. Stasiuk, *Current advances in ligand design for inorganic positron emission tomography tracers ^{68}Ga, ^{64}Cu, ^{89}Zr and ^{44}Sc.* Dalton transactions, 2016. **45**(40).
498. Velikyan, I., *Prospective of 68Ga-radiopharmaceutical development.* Theranostics, 2014. **4**(1): p. 47.
499. Zeglis, B.M., et al., *Underscoring the influence of inorganic chemistry on nuclear imaging with radiometals.* Inorganic chemistry, 2013. **53**(4): p. 1880-1899.
500. Price, T.W., et al., *Amino acid based gallium-68 chelators capable of radiolabeling at neutral pH.* Dalton transactions, 2017. **46**(48): p. 16973-16982.
501. Hsieh, W., et al., *68Ga-Ca-phytate particles: A potential lung perfusion agent of synthetic origin prepared in a cold kit format.* Journal of Labelled Compounds and Radiopharmaceuticals, 2016. **59**(12): p. 506-516.
502. Price, T.W., J. Greenman, and G.J. Stasiuk, *Current advances in ligand design for inorganic positron emission tomography tracers 68 Ga, 64 Cu, 89 Zr and 44 Sc.* Dalton transactions, 2016. **45**(40): p. 15702-15724.
503. Price, E.W. and C. Orvig, *Matching chelators to radiometals for radiopharmaceuticals.* Chemical Society Reviews, 2014. **43**(1): p. 260-290.
504. Gambhir, S.S., *Molecular imaging of cancer with positron emission tomography.* Nature Reviews Cancer, 2002. **2**(9): p. 683.
505. Lee, Y.-S. and J.M. Jeong, *Inorganic radionuclides for nuclear medicine therapy*, in *Therapeutic Nuclear Medicine*2012, Springer. p. 151-163.
506. Fani, M., J.P. Andre, and H.R. Maecke, *68Ga-PET: a powerful generator-based alternative to cyclotron-based PET radiopharmaceuticals.* Contrast media & molecular imaging, 2008. **3**(2): p. 53-63.
507. Roesch, F. and P. J Riss, *The renaissance of the 68Ge/68Ga radionuclide generator initiates new developments in 68Ga radiopharmaceutical chemistry.* Current topics in medicinal chemistry, 2010. **10**(16): p. 1633-1668.
508. Zolle, I., *Technetium-99m pharmaceuticals*. Vol. 1. 2007: Springer.
509. Veelaert, S., et al., *Chemical and physical transitions of periodate oxidized potato starch in water.* Carbohydrate polymers, 1997. **33**(2-3): p. 153-162.
510. Chia, H., *Particulate radiopharmaceuticals in nuclear medicine.* Radiopharmacy and radiopharmacology yearbook, 1987. **2**.
511. Stabin, M., J. Stubbs, and E. Watson, *Recent controversy in radiation dosimetry.* European Journal of Nuclear Medicine and Molecular Imaging, 1993. **20**(5): p. 371-372.
512. Poston, J.W., *Application of the effective dose equivalent to nuclear medicine patients. The MIRD Committee.* Journal of nuclear medicine: official publication, Society of Nuclear Medicine, 1993. **34**(4): p. 714.
513. Loevinger, R., T.F. Budinger, and E.E. Watson, *MIRD primer for absorbed dose calculations*1988: Society of Nuclear Medicine.
514. Protection, R., *ICRP publication 103.* Ann iCRP, 2007. **37**(2.4): p. 2.
515. Tang, G., et al., *Pharmacokinetics and radiation dosimetry estimation of O-(2-[18F] fluoroethyl)-L-tyrosine as oncologic PET tracer.* Applied radiation and isotopes, 2003. **58**(2): p. 219-225.

516. Moerlein, S., et al., *Radiation dosimetry of [18F](N-methyl) benperidol as determined by whole-body PET imaging of primates.* Nuclear medicine and biology, 1997. **24**(4): p. 311-318.

5.1 Annex

These two figures are the schematic representation of the experimental work of thesis.

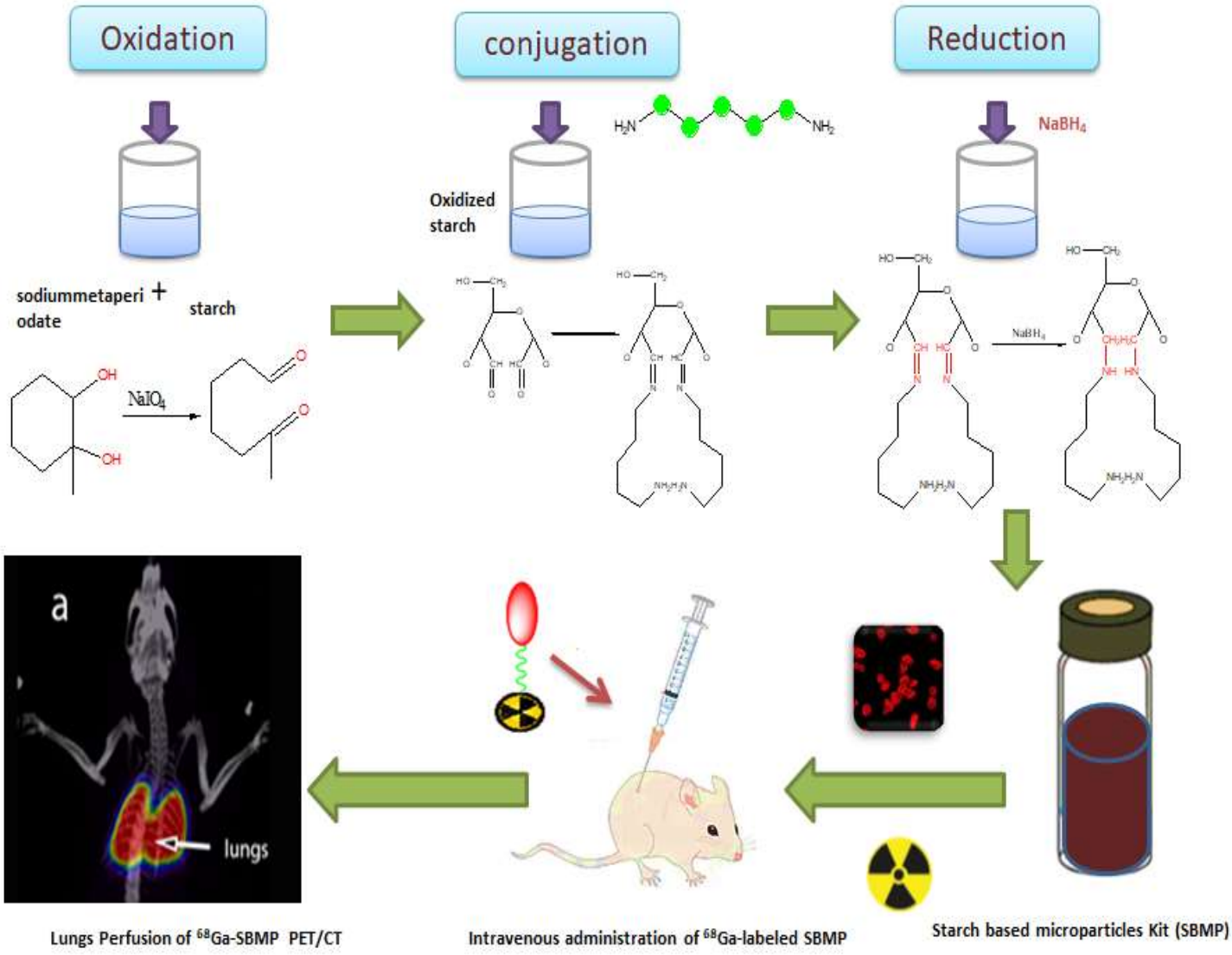

Figure 54 Schematically Representation of Lung Perfusion Studies

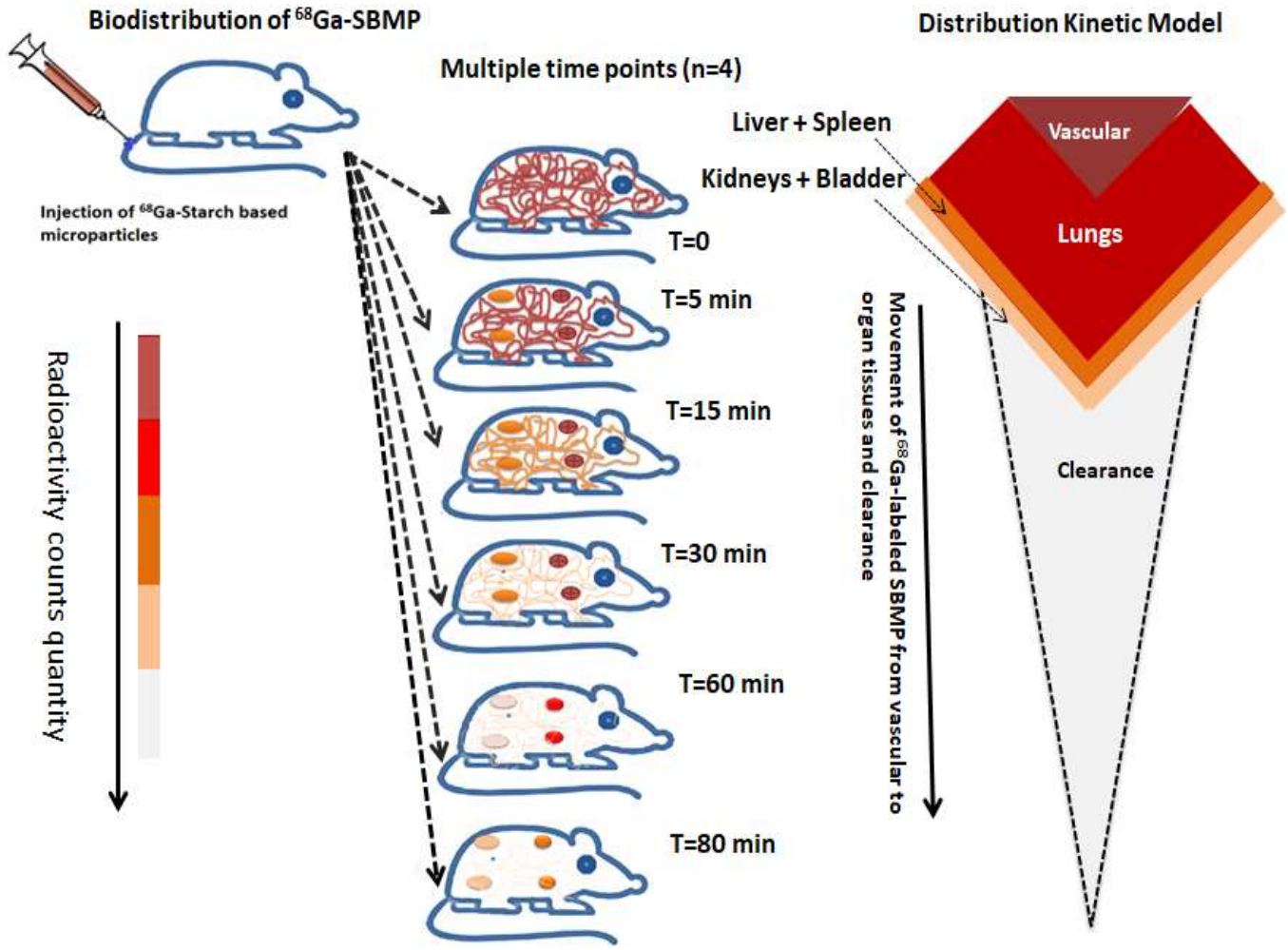

Figure 55 Schematic Illustration of Biodistribution and Clearance Kinetics of ^{68}Ga-Labeled SBMP

Abstract published: The American Congress of the Society of Nuclear Medicine (SNM New Orleans 2020, SBMMI-A-1717-2020):

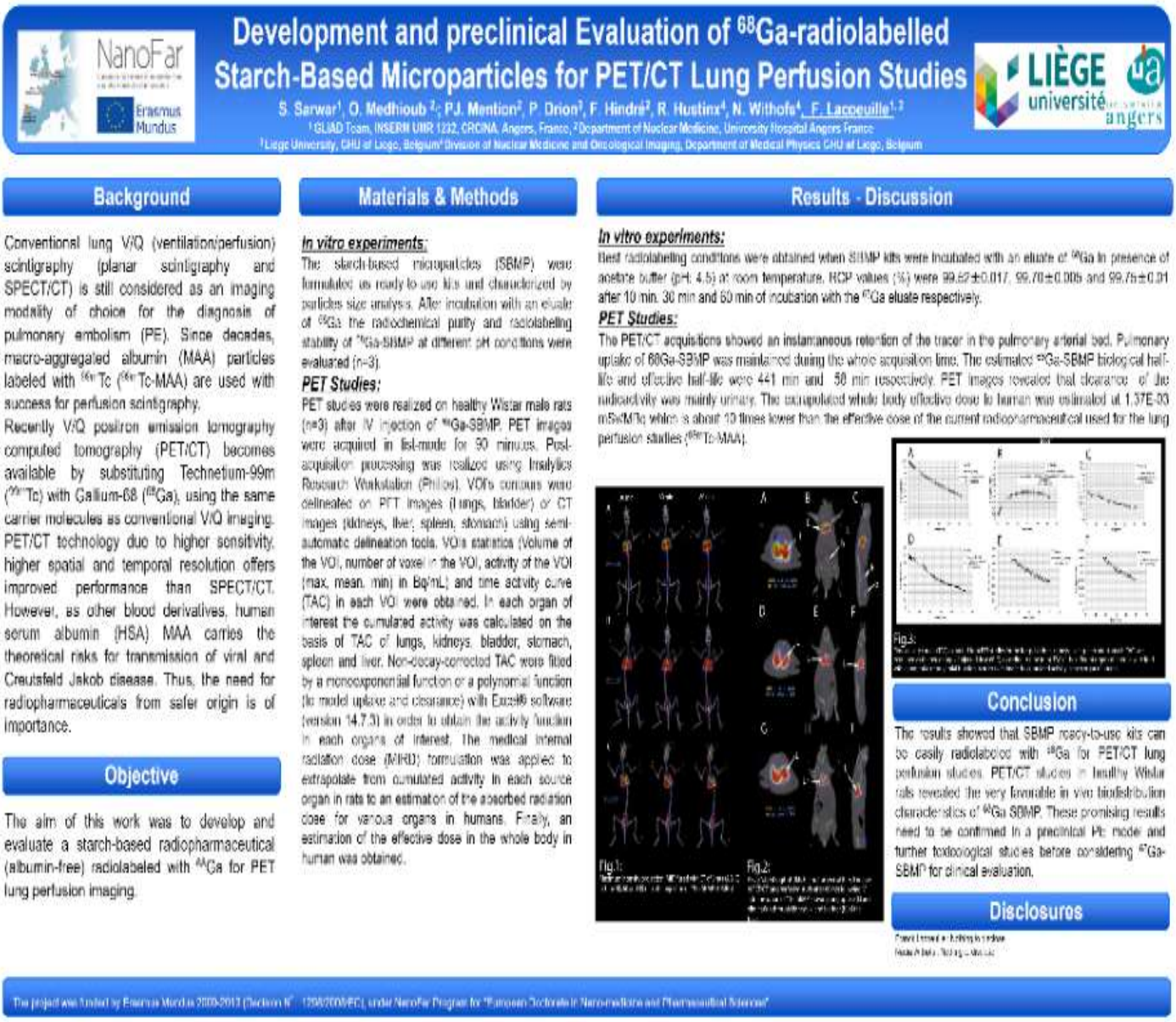

Development and preclinical Evaluation of ^{68}Ga-radiolabelled Starch-Based Microparticles for PET/CT Lung Perfusion Studies

S. Sarwar[1], O. Medhioub [2], P.J. Mention[2], P. Drion[3], F. Hindré[3], R. Hustinx[4], N. Withofs[4], F. Lacoeuille[1, 2]
[1] GLIAD Team, INSERM UMR 1232, CRCINA, Angers, France, [2] Department of Nuclear Medicine, University Hospital Angers France
[3] Liege University, CHU of Liege, Belgium [4] Division of Nuclear Medicine and Oncological Imaging, Department of Medical Physics CHU of Liege, Belgium

Background

Conventional lung V/Q (ventilation/perfusion) scintigraphy (planar scintigraphy and SPECT/CT) is still considered as an imaging modality of choice for the diagnosis of pulmonary embolism (PE). Since decades, macro-aggregated albumin (MAA) particles labeled with ^{99m}Tc (^{99m}Tc-MAA) are used with success for perfusion scintigraphy.

Recently V/Q positron emission tomography computed tomography (PET/CT) becomes available by substituting Technetium-99m (^{99m}Tc) with Gallium-68 (^{68}Ga), using the same carrier molecules as conventional V/Q imaging. PET/CT technology due to higher sensitivity, higher spatial and temporal resolution offers improved performance than SPECT/CT. However, as other blood derivatives, human serum albumin (HSA) MAA carries the theoretical risks for transmission of viral and Creutsfeld Jakob disease. Thus, the need for radiopharmaceuticals from safer origin is of importance.

Objective

The aim of this work was to develop and evaluate a starch-based radiopharmaceutical (albumin-free) radiolabeled with ^{68}Ga for PET lung perfusion imaging.

Materials & Methods

In vitro experiments:

The starch-based microparticles (SBMP) were formulated as ready to use kits and characterized by particles size analysis. After incubation with an eluate of ^{68}Ga the radiochemical purity and radiolabeling stability of ^{68}Ga-SBMP at different pH conditions were evaluated (n=3).

PET Studies:

PET studies were realized on healthy Wistar male rats (n=3) after IV injection of ^{68}Ga-SBMP. PET images were acquired in list-mode for 90 minutes. Post-acquisition processing was realized using Imalytics Research Workstation (Philips). VOIs contours were delineated on PET images (lungs, bladder) or CT images (kidneys, liver, spleen, stomach) using semi-automatic delineation tools. VOIs statistics (Volume of the VOI, number of voxel in the VOI, activity of the VOI (max, mean, min) in Bq/mL) and time activity curve (TAC) in each VOI were obtained. In each organ of interest the cumulated activity was calculated on the basis of TAC of lungs, kidneys, bladder, stomach, spleen and liver. Non-decay-corrected TAC were fitted by a monoexponential function or a polynomial function (to model uptake and clearance) with Excel® software (version 14.7.3) in order to obtain the activity function in each organs of interest. The medical internal radiation dose (MIRD) formulation was applied to extrapolate from cumulated activity in each source organ in rats to an estimation of the absorbed radiation dose for various organs in humans. Finally, an estimation of the effective dose in the whole body in human was obtained.

Results - Discussion

In vitro experiments:

Best radiolabeling conditions were obtained when SBMP kits were incubated with an eluate of ^{68}Ga in presence of acetate buffer (pH: 4.5) at room temperature. RCP values (%) were 99.62±0.017, 99.70±0.005 and 99.75±0.01 after 10 min, 30 min and 60 min of incubation with the ^{68}Ga eluate respectively.

PET Studies:

The PET/CT acquisitions showed an instantaneous retention of the tracer in the pulmonary arterial bed. Pulmonary uptake of ^{68}Ga-SBMP was maintained during the whole acquisition time. The estimated ^{68}Ga-SBMP biological half-life and effective half-life were 441 min and 58 min respectively. PET images revealed that clearance of the radioactivity was mainly urinary. The extrapolated whole body effective dose to human was estimated at 1.37E-03 mSv/MBq which is about 10 times lower than the effective dose of the current radiopharmaceutical used for the lung perfusion studies (^{99m}Tc-MAA).

Fig.1:

Fig.2:

Conclusion

The results showed that SBMP ready-to-use kits can be easily radiolabeled with ^{68}Ga for PET/CT lung perfusion studies. PET/CT studies in healthy Wistar rats revealed the very favorable in vivo biodistribution characteristics of ^{68}Ga SBMP. These promising results need to be confirmed in a preclinical PE model and further toxicological studies before considering ^{68}Ga-SBMP for clinical evaluation.

Disclosures

The project was funded by Erasmus Mundus 2009-2013 (Section N° 159/2009/EC), under NanoFar Program for "European Doctorate in Nanomedicine and Pharmaceutical Sciences"

Figure 56 Poster presented in SNM New Orleans 2020

RÉSUMÉ

La scintigraphie de ventilation/perfusion pulmonaire (V/Q), par le biais de la tomographie par émission monophotonique (TEMP/CT) et des macroagrégats d'albumine (MAA) marqués au ^{99m}Tc (^{99m}Tc-MAA) comme agent de perfusion pulmonaire, est toujours considérée comme une modalité d'imagerie de choix pour le diagnostic de l'embolie pulmonaire. Cependant, la technique TEMP/TDM présente certaines limites, comme une résolution spatiale ou une sensibilité plus faible que la tomographie par émission de positons (TEP/TDM). Avec la disponibilité récente des générateurs ^{68}Ge/^{68}Ga et le développement de produits radiopharmaceutiques marqués au ^{68}Ga qui peuvent être produits sur place et à la demande, la TEP/TDM V/Q semble désormais réalisable. Ainsi, différents groupes ont mis au point des procédures de radiomarquage des MAA pour substituer le ^{99m}Tc par du ^{68}Ga et réalisent avec succès des études de perfusion pulmonaire par TEP/CT. Cependant, les MAA, comme d'autres dérivés sanguins, comporte un risque théorique de transmission d'agents pathogènes infectieux. Pour relever ce défi, notre équipe a mis au point, il y a quelques années, un nouveau vecteur microparticulaire, d'origine végétale, sans albumine, capable de former des complexes stables avec les radiométaux pour des applications de médecine nucléaire (notamment la scintigraphie de perfusion pulmonaire). Ces microparticules à base d'amidon (SBMP) présentent des caractéristiques favorables telles qu'une taille de particule appropriée, une disponibilité sous forme de kits lyophilisés et un radiomarquage facile avec divers isotopes tels que le ^{99m}Tc, ^{68}Ga ou ^{188}Re.

Sur la base de ces résultats prometteurs, l'objectif du présent travail était d'évaluer, pour la première fois, la performance des microparticules 68Ga-SBMP comme radiopharmaceutique pour des études de TEP de perfusion pulmonaire. À cette fin, un radiomarquage, des études précliniques en TEP/CT et une estimation dosimétrique basée sur l'imagerie après injection intraveineuse de ^{68}Ga-SBMP ont été réalisés. Le ^{68}Ga étiqueté SBMP a été développé à température ambiante par la méthode simple et robuste sans conditions qui impliquent de sévères réactions produisant une pureté radiochimique très élevée (>99%) après 10 minutes d'incubation à température ambiante avec l'éluat gallium-68 ($^{68}GaCl_3$). Le radiopharmaceutique présenté visualisait clairement la zone pulmonaire et générait des images affinées de la vascularisation pulmonaire en peu de temps. Les estimations de dosimétrie basées sur l'image ont montré pour l'homme des valeurs plus faibles que la norme disponible de ^{99m}Tc-MAA (ICRP 80). D'autres études cliniques sont recommandées pour évaluer le potentiel de ^{68}Ga-SBMP dans les cliniques humaines

mots-clés: Microparticules à base d'amidon (SBMP), Gallium-68 (^{68}Ga), Perfusion pulmonaire, PET/CT, Dosimétrie

ABSTRACT

The lungs ventilation/perfusion (V/Q) scintigraphy, by the mean of Single Photon Emission Computed Tomography (SPECT/CT) and macroaggregates of albumin (MAA) labelled with ^{99m}Tc (^{99m}Tc-MAA) as lung perfusion agent, is still considered as an imaging modality of choice for the diagnosis of pulmonary embolism. However, SPECT/CT technique has some limitations such as lower spatial resolution or poor sensitivity compared to Positron Emission Tomography (PET/CT). With the recent availability of ^{68}Ge/^{68}Ga generator and the development of ^{68}Ga-labeled radiopharmaceuticals that can be produced on site and on demand, V/Q PET/CT appears now feasible. Thus, different groups have developed radiolabeling procedures of MAA with ^{68}Ga instead of ^{99m}Tc and successfully perform PET/CT lung perfusion studies. However, MAA, like other blood-derivatives, carries a theoretical risk of disease transmission. To address this challenge, few years ago, our team has developed a new microparticulate albumin-free carrier from vegetal origin, able to form complex with radiometals for nuclear medicine applications and especially for lung perfusion scintigraphy. These starch-based microparticles (SBMP) exhibit favorable characteristics such as suitable particle size, availability as freeze-dried kits and easy radiolabeling with various isotopes such as ^{99m}Tc, ^{68}Ga or ^{188}Re.

Based on those promising results, the objective of the present work was to evaluate, for the first time, the performance of the ^{68}Ga-SBMP microparticles as radiotracer for lung perfusion PET studies. To this end, radiolabeling, preclinical PET/CT studies and imaging-based dosimetry estimation following intravenous injection of ^{68}Ga-SBMP were realized. The ^{68}Ga labeled SBM has been developed at room temperature through simple, and robust method without the involvement of any severe reaction conditions producing very high radiochemical purity (>99%) after 10 minutes of room temperature incubation with gallium-68 eluate ($^{68}GaCl_3$). The presented radiopharmaceutical visualized the lungs fields clearly and generated fine-tuned images of pulmonary vasculature in a small time. Image based dosimetry estimates for humans indicated lower values than the available standard of ^{99m}Tc-MAA (ICRP 80). Further clinical studies are recommended to assess the potential of ^{68}Ga-SBMP in human clinics.

keywords: Starch based microparticles (SBMP), Gallium-68 (^{68}Ga), Lung Perfusion, PET/CT, Dosimetry